# Properties of pseudoscalar flavor singlet mesons from lattice QCD

DISSERTATION

ZUR

ERLANGUNG DES DOKTORGRADES (DR. RER. NAT.)

DER

MATHEMATISCH-NATURWISSENSCHAFTLICHEN FAKULTÄT

DER

RHEINISCHEN FRIEDRICH-WILHELMS UNIVERSITÄT BONN

VORGELEGT VON

KONSTANTIN OTTNAD

AUS

FREIBURG i.BR.

BONN 2013

# Abstract

The central topic of this work are masses and mixing parameters of the $\eta$–$\eta'$ system, which are investigated within the framework of Wilson twisted mass lattice QCD, using gauge configurations provided by the European Twisted Mass Collaboration. We present the first calculation with $N_f = 2+1+1$ dynamical quark flavors performed at three different values of the lattice spacing and multiple values of the light quark mass, corresponding to charged pion masses ranging from $\sim 230\,\text{MeV}$ to $\sim 500\,\text{MeV}$. Moreover, we use selected ensembles which differ only by the value of the strange quark mass while all other parameters are kept fixed in order to obtain information on the strange quark mass dependence of our observables. This allows us to carry out chiral and continuum extrapolations with well-controlled systematics for the mass of the $\eta$ meson. Using the standard method, the statistical error for the $\eta'$ turns out significantly larger due to the large contributions of quark disconnected diagrams and autocorrelation effects. However, employing an improved analysis method based on an excited state subtraction in the connected pieces of the correlation function matrix, it becomes feasible to obtain a result for the $\eta'$ mass with controlled systematics as well. The values for both masses $M_\eta = 551(8)_{\text{stat}}(6)_{\text{sys}}\,\text{MeV}$ and $M_{\eta'} = 1006(54)_{\text{stat}}(38)_{\text{sys}}(+64)_{\text{ex}}\,\text{MeV}$ turn out to be in excellent agreement with experiment.

Considering matrix elements in the quark-flavor basis, one expects the mixing in the $\eta$–$\eta'$ system to be described reasonably well by a single mixing angle $\phi$ and two decay constants $f_l$, $f_s$. The required accuracy of the matrix elements is again guaranteed by the aforementioned, improved analysis method, yielding a value of $\phi = 46.0(0.9)_{\text{stat}}(2.7)_{\text{sys}}^\circ$ for the mixing angle extrapolated to the physical point. In addition we obtain results for the ratios $f_l/f_{\text{PS}} = 0.859(07)_{\text{stat}}(64)_{\text{sys}}$ and $f_s/f_K = 1.166(11)_{\text{stat}}(31)_{\text{sys}}$. We find that our data is indeed described well by a single mixing angle, indicating that the $\eta'$ is mostly a flavor singlet state. Moreover, our results confirm that the charm quark does not contribute to any of the two states within errors.

Apart from the flavor singlet sector, we also perform calculations of masses for the remaining light pseudoscalar octet mesons. Matching these masses to two-flavor Wilson chiral perturbation theory allows for a determination of the low energy constants $W_6'$, $W_8'$ and their linear combination $c_2$ which controls the $\mathcal{O}\left(a^2\right)$ mass splitting between charged and neutral pion. We study the dependence of these low energy constants on the number of dynamical quark flavors and for different choices of the lattice action.

Parts of this work have been previously published in journals [1–3] and conference proceedings [4–6]; see also the list included on the next page.

# List of publications

[1] Konstantin Ottnad, Carsten Urbach, Chris Michael, and Siebren Reker. Eta and eta' meson masses from Nf=2+1+1 twisted mass lattice QCD. *PoS*, LATTICE2011:336, 2011, 1111.3596.

[2] Konstantin Ottnad et al. $\eta$ and $\eta'$ mesons from Nf=2+1+1 twisted mass lattice QCD. *JHEP*, 1211:048, 2012, 1206.6719.

[3] Krzysztof Cichy, Vincent Drach, Elena Garcia Ramos, Karl Jansen, Chris Michael, et. al. Properties of pseudoscalar flavour-singlet mesons from 2+1+1 twisted mass lattice QCD. *PoS*, LATTICE2012:151, 2012, 1211.4497.

[4] Gregorio Herdoiza, Karl Jansen, Chris Michael, Konstantin Ottnad and Carsten Urbach. Determination of Low-Energy Constants of Wilson Chiral Perturbation Theory. *JHEP*, 1305:038, 2013, 1303.3516.

[5] Chris Michael, Konstantin Ottnad and Carsten Urbach. $\eta$ and $\eta'$ mixing from Lattice QCD. *Phys. Rev. Lett.* 111, 181602, 2013, 1310.1207.

[6] Chris Michael, Konstantin Ottnad and Carsten Urbach. $\eta$ and $\eta'$ masses and decay constants from lattice QCD with 2+1+1 quark flavours. 2013, 1311.5490.

# Contents

# Introduction

The rise of modern theoretical physics is very closely tied to the concept of symmetries. In fact, quantum field theories which are based on so-called local gauge symmetries have been proven to be tremendously successful in describing elementary particle interactions and provide the theoretical foundation for the present standard model of particle physics. Besides local symmetries which are essential to the construction of quantum field theories, there are further global symmetries. These include discrete symmetries such as parity ($\mathcal{P}$), time-reversal ($\mathcal{T}$) or charge conjugation ($\mathcal{C}$), as well as continuous ones like chiral symmetry. However, while gauge symmetries are required to be exact for theoretical reasons, many other symmetries are actually broken in nature, leading to a wide range of intriguing phenomena. In principle, there are several ways of breaking symmetries. Firstly, there is *explicit* symmetry breaking which refers to a situation where a symmetry is violated (or only realized to some approximation) due to terms in the Lagrangian that do not respect the symmetry in question, while the remaining parts of the Lagrangian are indeed invariant. For instance, the presence of non-vanishing quark masses explicitly violates chiral symmetry in quantum chromodynamics (QCD), hence it is only realized as an approximate symmetry. Secondly, there is also the possibility of *spontaneous* symmetry breaking, which refers to a situation where the Lagrangian itself is invariant under a given symmetry, but the system develops a non-trivial vacuum expectation value, hence breaking the symmetry of the ground state. An example for such a mechanism is found in chiral symmetry, which is spontaneously broken by a non-vanishing quark condensate[1].

Another kind of symmetry breaking is again related to strong interactions and concerns only a specific subgroup of chiral symmetry, the so-called flavor singlet axial rotations. It was discovered in the 70s that – while this symmetry holds at the classical level of the theory – it is *anomalously* broken by quantization through the occurrence of topologically non-trivial gluon field configurations. Formally, the symmetry breaking manifests itself in the non-invariance of the fermionic integration measure of the partition function of the theory. This symmetry violation is expected to affect the observed hadron spectrum. It is believed that a prime example for its impact is given by the unnaturally large mass splitting that is experimentally observed in the nonet of the lowest-lying pseudoscalar mesons. This mass splitting between the $\eta$ and the $\eta'$ meson is also known as the $U(1)_A$ problem of QCD. Naively, one would expect these two mesons

---

[1]Note that in the standard model the non-vanishing quark masses are actually generated by spontaneous symmetry breaking as well by means of the Higgs mechanism. However, considering only QCD itself, the presence of a mass term still constitutes an example of explicit symmetry breaking.

to have approximately the same mass, taking into account only their respective quark contents. The study of the system formed by these two mesons constitutes the central topic of this work. Since QCD is nowadays commonly accepted as the fundamental theory of strong interactions, it would be very desirable to verify that this mass splitting can indeed be reproduced from *first principles* without additional model assumptions. Due to the highly non-trivial nature of the effect, this represents a crucial test case for QCD.

However, performing this calculation from first principles is not a straightforward task. Unlike quantum electrodynamics (QED), which can be treated perturbatively in its coupling constant at all relevant energies, such an approach is not valid for QCD at low energies, as the value of its coupling constant increases for decreasing energies. This peculiar feature is caused by the non-abelian structure of QCD, allowing for self-interactions among gluons, which is not the case for the gauge boson of QED, i.e. the photon. Therefore, it is necessary to use alternative methods in the low energy regime of QCD, such as effective field theories or lattice QCD (LQCD). The effective field theory of QCD is known as chiral perturbation theory ($\chi$PT) and is based on the approximate chiral symmetry for the two (or three) lightest quark flavors, leading to an expansion in small momenta and masses. However, this expansion requires a rapidly increasing number of so-called low energy constants (LECs) for each additional order. Since these constants are not known a priori, they have to be determined from experimental input. In this work we will mainly use LQCD which relies on Monte-Carlo methods to numerically calculate correlation functions from QCD in discrete Euclidean spacetime. This approach does not require any further input besides the Lagrangian of QCD itself and only a few experimentally measured quantities in order to set the scale and fix the physical parameters (i.e. quark masses). Therefore, it is suitable to study the hadron spectrum from first principles. Nevertheless, the corresponding calculations are demanding from a computational and technical point of view. This is primarily caused by large contributions of quark disconnected diagrams, which are intrinsically noisy and difficult to calculate with sufficient statistical precision. It is also reflected by the rather small set of world data from LQCD for the masses of the $\eta$ and $\eta'$ mesons which has been available prior to this work as shown in figure 1. Furthermore, the studies that lead to these results involved only one or two values of the lattice spacing and very few different quark masses, which makes a reliable estimation of systematic errors unfeasible. In particular, there are only few data available at smaller values of the pion mass and no clear picture arises concerning an extrapolation to the physical point.

For our investigations we employ $N_f = 2 + 1 + 1$ dynamical flavors of Wilson twisted mass quarks at maximal twist. This allows us to use powerful variance reduction techniques that are required to tackle the quark disconnected diagrams which are essential for the properties of the $\eta$–$\eta'$ system. We will employ simulations at several values of the lattice spacing $a$ and many different values for the quark masses, which will allow us to perform controlled continuum and chiral extrapolations, leading to a rather complete assessment of the systematic uncertainties in our study. Through special techniques we will achieve precise values for the masses of the $\eta$ and $\eta'$ mesons as well as mixing parameters, which has not been feasible in the past due to the intrinsic noise in these quantities and the resulting computational cost.

A secondary aim of this work concerns a particular feature of our lattice formulation, namely
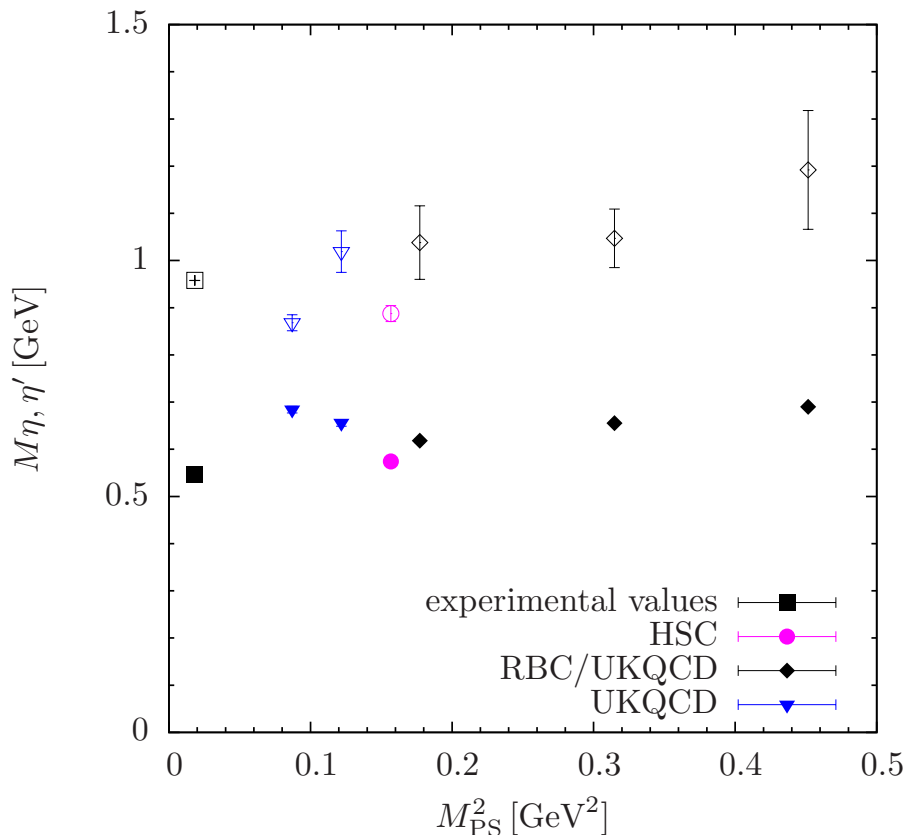
Figure 1: LQCD results for $M_\eta$ and $M_{\eta'}$ available in literature from different collaborations (RBC/UKQCD [7], HSC [8], UKQCD [9]). Only data obtained from simulations with at least $N_f = 2 + 1$ dynamical quark flavors have been included in this plot. The data are plotted as a function of the squared mass of the lightest pseudoscalar meson (i.e. the charged pion) and have been converted to physical units.

the isospin breaking through large $\mathcal{O}\left(a^2\right)$ lattice artifacts. In general, there are infinitely many different ways to formulate a certain gauge theory on a lattice, the only requirement is that they have to be equivalent in the continuum. However, aside from the continuum limit they may differ and an important criterion for the construction of lattice actions is to reduce possible artifacts occurring at finite values of the lattice spacing. This potentially allows to perform simulations at computationally cheaper (i.e. larger) values of the lattice spacings. While one of the main benefits of Wilson twisted mass fermions is its property of so-called automatic $\mathcal{O}\left(a\right)$ improvement, this does not exclude the possibility of large $\mathcal{O}\left(a^2\right)$ artifacts in certain quantities. In fact, a corresponding effect is observed in Wilson twisted mass lattice QCD (WtmLQCD) for the difference between the masses of the charged and the neutral pion. Since in the Wilson twisted mass formulation the neutral pion receives contribution from quark disconnected diagrams similar to those occurring in the $\eta$–$\eta'$ system, the precise determination of this splitting is again computationally demanding. A systematic, quantitative investigation of these kind of

lattice artifacts can be performed within the framework of Wilson chiral perturbation (W$\chi$PT). It extends the expansion of standard $\chi$PT to include powers of the lattice spacing, hence introducing additional LECs which parametrize effects induced by finite values of the lattice spacing. In this context an additional advantage of LQCD is the possibility to study the properties of further, artificial particles on the lattice, which can also be treated in the framework of W$\chi$PT, hence giving additional input for the determination of LECs. An example for such a particle is given by a neutral "connected-only" pion without the disconnected contributions which are required in our formulation. Since we obtain the required observables in the pion sector as a by-product of our study of the $\eta$–$\eta'$ system we can exploit these data to determine the low energy constants which control the mass splitting for the charged and neutral pion at leading order in the chiral expansion of W$\chi$PT. In addition, we will use data obtained in other lattice setups to explore the dependence of these LECs on the details of the actual lattice action (e.g. number of dynamical quark flavors or smearing) in order to gain some insight on how a twisted mass type action with reduced isospin breaking effects could be defined.

The work is organized as follows: the theoretical foundations are discussed in chapter 1. This includes a brief review of QCD itself and of selected topics of chiral perturbation theory which are relevant to this work. A major part of this chapter is dedicated to a general introduction to lattice QCD and the Wilson twisted mass formulation that has been employed in our investigations. Chapter 2 outlines the relevant methods for hadron spectroscopy and related technical details (e.g. definition of observables) of our studies. In addition, we include a summary of the statistical methods used for the data analysis in this work. In chapter 3 we present the results and details of our analysis. This covers the extraction of masses and decay parameters for pseudoscalar flavor singlet and non-singlet mesons as well as the required extrapolations. We give results for $\eta$ and $\eta'$ masses extrapolated to the physical point, the mixing angle and further parameters related to mixing derived from pseudoscalar matrix elements in the quark flavor basis. Moreover, we detail the results of our analysis concerning Wilson chiral perturbation theory in the pion sector and the determination of corresponding low energy constants. At the end of this work we summarize the results of our studies and give an outlook on further possible investigations and unresolved issues. The content of this work is complemented by three appendices, detailing conventions, analytical results for correlation functions and some additional, technical details of our fitting procedures.

# Chapter 1

# Theoretical Background

The purpose of this chapter is to provide an overview on the theoretical foundations for this work. Starting with an introduction to quantum chromodynamics in the continuum, as the underlying, fundamental quantum field theory describing strong interactions, some of the theoretical properties and relevant phenomenological aspects of QCD are discussed. Secondly, a brief outline of chiral perturbation theory is included, which is required for certain parts of the analysis of the results from our simulations. Next we focus on the formulation of QCD in discretized Euclidean spacetime, a nowadays well-established approach that is known as lattice QCD. In particular we shall consider Wilson twisted mass lattice QCD, which is the formulation employed in our simulations and discuss several of its properties in detail. The final part of the chapter is dedicated to meson spectroscopy on the lattice, again with particular emphasis on the twisted mass formulation.

## 1.1 Quantum Chromodynamics

Quantum Chromodynamics is a local gauge theory that is commonly believed to be the fundamental theory of strong interactions. It is part of the standard model of particle physics, which itself is a direct product of local gauge groups $SU(3) \otimes SU(2) \otimes U(1)$, incorporating also electroweak interactions.

The fermionic particle content of QCD consists of quarks, which are assumed to be pointlike particles described by Dirac fields $q_{i,A}^{\alpha}(x)$ in the fundamental representation of the gauge group $SU(N_c)$. These fields carry *color* charge denoted by the index $A = 1, ..., N_c$, where $N_c = 3$ is the number of colors realized in nature. In addition, the quark fields exhibit a Dirac spinor index $\alpha = 1, ..., 4$, which we suppress in the following by using spinor fields instead of components thereof. Finally, the lower index $i$ refers to the quark *flavor* and is also employed to label the respective quark mass $m_i$. There are $N_f = 6$ different flavors known to be realized in nature, denoted by $u$, $d$, $s$, $c$, $b$ and $t$. For many purposes it is convenient to identify $f \equiv q_{i(f)}$ for a

given flavor $f$ with index $i(f)$[1].

Considering only global $SU(N_c)$-transformations, the corresponding free fermionic Lagrangian with $N_F$ quark flavors reads

$$\mathcal{L}_{F,\text{free}} = \sum_{i=1}^{N_f} \bar{q}_i(x)\left(i\gamma^\mu\partial_\mu - m_i\right)q_i(x) , \tag{1.1}$$

where the color fields $q_{i,A}$ have been arranged in $q_i(x) = (q_{i,1}(x), ..., q_{i,N_c}(x))^T$.

The interaction between quarks is mediated by gluon fields $A_\mu^a(x)$ that belong to the adjoint representation of SU$(N_c)$. Since these are vector fields, they carry a spacetime index $\mu = 0, ..., 3$ in addition to their color index $a = 1, ..., N_c^2 - 1$. The emergence of this interaction is intrinsically tied to the concept of local gauge invariance:

Under a local gauge transformation acting on some quark field $q(x)$

$$q(x) \rightarrow \Lambda(x) q(x), \qquad \bar{q}(x) \rightarrow \bar{q}(x)\Lambda^{-1}(x), \qquad \Lambda(x) \in \text{SU}(N_c) , \tag{1.2}$$

one has

$$\bar{q}(x)\partial_\mu q(x) \rightarrow \bar{q}(x)\partial_\mu q(x) + \bar{q}(x)\Lambda^{-1}(x)\left(\partial_\mu\Lambda(x)\right)q(x) , \tag{1.3}$$

implying that the kinetic term in Eq. (1.1) needs to be modified in order to retain local gauge invariance. This is achieved by replacing the standard derivative with a gauge-covariant derivative

$$D_\mu q(x) = \left(\partial_\mu - ig_s T^a A_\mu^a\right)q(x) , \tag{1.4}$$

where $T^a$ are the $N_c^2 - 1$ generators of SU$(N_c)$ and $g_s$ the coupling constant of the theory, which determines the strength of the interaction. The generators satisfy the Lie algebra

$$[T^a, T^b] = if^{abc}T^c , \tag{1.5}$$

with SU$(N_c)$ structure constants $f^{abc}$. For the special case of SU$(3)$ a convenient representation of the generators $T^a$ is given by $T^a = \lambda^a/2$ where the $\lambda^a$ are the eight Gell-Mann matrices listed in appendix A.3. The covariant derivative $D_\mu q(x)$ is by definition required to obey a transformation rule similar to that of the quark color triplets $q(x)$ themselves

$$D_\mu q(x) \rightarrow \Lambda(x) D_\mu q(x) , \tag{1.6}$$

leading to the following transformation behavior for the fields $A_\mu = T^a A_\mu^a$

$$A_\mu \rightarrow \Lambda(x) A_\mu \Lambda^{-1}(x) - \frac{i}{g_s}\left(\partial_\mu\Lambda(x)\right)\Lambda^{-1}(x) . \tag{1.7}$$

Considering an infinitesimal gauge transformation

$$\Lambda(x) = \exp\left(-iT^a\omega^a(x)\right) \approx 1 - iT^a\omega^a(x) , \qquad \omega^a(x) \ll 1 , \tag{1.8}$$

---

[1]For general indexing conventions see appendix A.1. Indices irrelevant to the current context will be suppressed

where $\omega^a(x)$ are the parameters of SU $(N_c)$, one obtains

$$A_\mu^a \to A_\mu^a + f^{abc}\omega^b A_\mu^c - \frac{1}{g_s}\partial_\mu\omega^a \,. \tag{1.9}$$

The corresponding field strength tensor is given by

$$F_{\mu\nu}^a = \partial_\mu A_\nu^a - \partial_\nu A_\mu^a + g_s f^{abc} A_\mu^b A_\nu^c \,, \tag{1.10}$$

and transforms as

$$T^a F_{\mu\nu}^a \to \Lambda(x) T^a F_{\mu\nu}^a \Lambda^{-1}(x) \,, \tag{1.11}$$

which yields

$$F_{\mu\nu}^a \to F_{\mu\nu}^a + f^{abc}\omega^b F_{\mu\nu}^c \,, \tag{1.12}$$

for an infinitesimal gauge transformation. A gauge invariant quantity of dimension four, consisting purely of gauge fields can either be constructed using only $F_{\mu\nu}^a$ but also from its dual

$$\tilde{F}_{\mu\nu}^a = \epsilon_{\mu\nu\rho\sigma}F^{a,\rho\sigma} \,, \tag{1.13}$$

where $\epsilon_{\mu\nu\rho\sigma}$ denotes the totally antisymmetric tensor of rank four.

Arranging the $N_f$ quark flavors in $\psi = \left(q_1(x),...,q_{N_f}(x)\right)^T$ and defining the quark mass matrix $M = \text{diag}\left(m_1,...,m_{N_f}\right)$, the most general Lagrangian invariant under local $SU(N_c)$ transformations, compatible with Lorentz invariance, hermiticity and satisfying the constraints of renormalizability reads [10–12]

$$\mathcal{L}_{\text{QCD}}\left[\psi,\bar{\psi},A\right] = \underbrace{\bar{\psi}\left(i\gamma^\mu D_\mu - M\right)\psi}_{\equiv\mathcal{L}_F} \underbrace{-\frac{1}{4}F_{\mu\nu}^a F^{a,\mu\nu}}_{\equiv\mathcal{L}_G} \underbrace{-\theta_0\frac{g_s^2}{64\pi^2}F_{\mu\nu}^a \tilde{F}^{a,\mu\nu}}_{\equiv\mathcal{L}_\theta} \,. \tag{1.14}$$

For our purposes it is convenient to perform the quantization by means of the path integral formulation, which will later allow for a natural extension to discretized spacetime. To this end one defines the classical action of QCD

$$\mathcal{S}_{\text{QCD}}\left[\psi,\bar{\psi},A\right] = \int d^4x\, \mathcal{L}_{\text{QCD}}\left[\psi,\bar{\psi},A\right] \,, \tag{1.15}$$

such that the partition function (the path integral) of QCD is given by

$$\mathcal{Z} = \int \mathcal{D}\psi\mathcal{D}\bar{\psi}\mathcal{D}A \, \exp\left(i\mathcal{S}_{\text{QCD}}\left[\psi,\bar{\psi},A\right]\right) \,. \tag{1.16}$$

### 1.1.1 General properties and parameters

As a result of the non-abelian structure of the Lagrangian in Eq. (1.14), it does not only contain interactions between gauge fields and fermions via the covariant derivative but also triple and

quartic self-interactions of the gauge fields. These are induced by the additional term $g_s f^{abc} A_\mu^b A_\nu^c$ in the field strength tensor which is absent in an abelian gauge theory such as quantum electrodynamics (QED) for which the gauge fields do not carry the corresponding group charge. It is commonly assumed that these self-interactions of the gluon fields account for the fact that only color-neutral objects can be observed directly, i.e. quarks and gluons are always bound in hadrons such as mesons or baryons. This experimentally well-known, but not mathematically rigorously proven property of QCD is called (*color*) *confinement*.

Moreover, the non-abelian structure of QCD allows for a feature that is known as *asymptotic freedom* [10, 13, 14] which refers to the fact that QCD at short distances and large energies resembles a free theory. This becomes apparent in the running coupling constant of QCD, which reads to one-loop order in perturbation theory

$$g_s^2\left(\mu^2\right) = \frac{48\pi^2}{(11N_c - 2N_f)\log\left(\frac{\mu^2}{\Lambda_{\mathrm{QCD}}^2}\right)}\,, \tag{1.17}$$

for some energy scale $\mu^2$. For $N_f < \frac{11}{2}N_c$ – which is fulfilled by $N_c = 3$ and $N_f = 6$ – the coupling constant decreases for energies larger than the intrinsic scale $\Lambda_{\mathrm{QCD}}$. This particular feature of QCD implies the failure of standard perturbation theory at low energies for which $g_s \approx 1$ is not a small parameter anymore. The value of $\Lambda_{\mathrm{QCD}}$ depends on the choice of the renormalization scheme and the number of active quark flavors $n_f$, i.e. the number of quarks for which $m_i < \mu$ holds. Literature values of $\Lambda_{\mathrm{QCD}}$ in the widely used $\overline{\mathrm{MS}}$-renormalization scheme and for various values of $n_f$ are usually of order

$$\Lambda_{\mathrm{QCD},\overline{\mathrm{MS}}} \sim 200 - 400\,\mathrm{MeV}\,, \tag{1.18}$$

e.g. recent, non-perturbative determinations [15,16] for two active quark flavors quote $\Lambda_{\mathrm{QCD},\overline{\mathrm{MS}}}^{n_f=2} = 315\,(30)$ MeV and $\Lambda_{\mathrm{QCD},\overline{\mathrm{MS}}}^{n_f=2} = 310\,(20)$ MeV, respectively.

Further fundamental parameters of QCD are given by the quark masses $m_i$. As stated before, quarks cannot be observed directly, which is why their masses have to be determined indirectly from measurements of hadronic properties. Therefore, values for the quark masses are always dependent on the renormalization scheme and scale. The Particle Data Group quotes the following values [17]

$$\begin{array}{lll} m_u = 2.3_{-0.5}^{+0.7}\,\mathrm{MeV} & m_d = 4.8_{-0.3}^{+0.7}\,\mathrm{MeV} & m_s = 95(5)\,\mathrm{MeV} \\ m_c = 1.275(25)\,\mathrm{GeV} & m_b = 4.18(3)\,\mathrm{GeV} & m_t = 173.5(6)(8)\,\mathrm{GeV} \end{array}\,. \tag{1.19}$$

Apart from the top quark, these are the running masses in the $\overline{\mathrm{MS}}$-scheme defined at a scale of $\mu = 2\,\mathrm{GeV}$ for $i = u, d, s$, whereas for $i = c, b$ the scale has been chosen to match the resulting mass of the heavy quark itself, i.e. the quoted values are $m_i^{\overline{\mathrm{MS}}}(\mu = m_i^{\overline{\mathrm{MS}}})$. For the definition of the top quark mass we refer to the notes included in [17]. Besides color charge and mass, quarks also carry a fractional electric charge, which is $+3/2$ for $u, c, t$ and $-1/3$ for $d, s, b$.

In principle, there is one more fundamental parameter ($\theta_0$) in the last term $\mathcal{L}_\theta$ of the QCD Lagrangian. This term is also known as the *$\theta$-term* and gives rise to $\mathcal{P}$- and $\mathcal{CP}$-violating

interactions. Naively, one would expect the parameter $\theta_0$ to be of natural size, i.e. $\theta_0 = \mathcal{O}(1)$. However, it turns out in experiments that $\theta_0$ actually has to be very small and is even compatible with zero. For instance, the neutron electric dipole moment $d_n$, which should be non-zero only in the presence of $\mathcal{CP}$-violating interactions, has been restricted by experiment to $|d_n| < 2.9 \times 10^{-26}\, e\,\mathrm{cm}$ [18]. Combining this value with theoretical predictions for $d_n$ results in an upper bound for $\theta_0$. In [19] chiral perturbation theory with three quark flavors has been used to derive $|\theta_0| < 2.5 \times 10^{-10}$. The smallness of $\theta_0$ represents the so-called *strong $\mathcal{CP}$-problem*. Since strong $\mathcal{CP}$-violation itself is not within the scope of this work, $\mathcal{L}_\theta$ will be dropped from the full Lagrangian for the purpose of numerical simulations.

### 1.1.2 Chiral symmetry and anomaly

QCD features several exact symmetries, which include Lorentz invariance, local gauge invariance and invariance under charge conjugation ($\mathcal{C}$). In addition to these exact symmetries, it exhibits certain approximate symmetries. In order to disclose them, we consider vanishing masses for all $N_f$ quark flavors and decompose $\psi(x)$ in left- and right-handed components $\psi_L(x)$, $\psi_R(x)$

$$\psi_{L/R}(x) = P_{L/R}\psi(x) = \frac{1}{2}(1 \mp \gamma_5)\psi(x) . \tag{1.20}$$

This procedure leads to a decoupling of left- and right-handed quark fields in the fermionic Lagrangian $\mathcal{L}_F$ in Eq. (1.14)

$$\bar{\psi}_i(x)(i\gamma^\mu D_\mu - m_i)\psi_i(x) \rightarrow \bar{\psi}_{i,L}(x)\,i\gamma^\mu D_\mu\psi_{i,L}(x) + \bar{\psi}_{i,R}(x)\,i\gamma^\mu D_\mu\psi_{i,R}(x) . \tag{1.21}$$

Moreover, there is no mixing between left- and right-handed fields present in the gauge sector, such that the full QCD Lagrangian in Eq. (1.14) is now invariant under a global $\mathrm{U}(N_f)_L \otimes \mathrm{U}(N_f)_R$ symmetry. In order to further study the properties of this symmetry, it is useful to consider the decomposition into irreducible subgroups

$$\mathrm{SU}(N_f)_L \otimes \mathrm{SU}(N_f)_R \otimes \mathrm{U}(1)_V \otimes \mathrm{U}(1)_A . \tag{1.22}$$

The invariance under the $\mathrm{SU}(N_f)_L \otimes \mathrm{SU}(N_f)_R$ subgroup is known as *chiral symmetry* and the case of vanishing quark masses is called the *chiral limit*. The left- and right-handed Noether currents, that are induced by chiral symmetry read

$$J^a_{\mu,L/R} = \bar{\psi}(x)\,\gamma_\mu P_{L/R}T^a\psi(x) . \tag{1.23}$$

The vector and axial vector components of these currents can be separated, allowing us to define

$$V^a_\mu = J^a_{\mu,R} + J^a_{\mu,L} , \tag{1.24}$$

$$A^a_\mu = J^a_{\mu,R} - J^a_{\mu,L} . \tag{1.25}$$

The divergences of these currents are given by

$$\partial^\mu V^a_\mu = \bar{\psi}(x)\,[M, T^a]\,i\psi(x) , \tag{1.26}$$

$$\partial^\mu A_\mu^a = \bar{\psi}\left(x\right)\left\{M, T^a\right\} i\gamma_5 \psi\left(x\right) ,\tag{1.27}$$

implying conservation in the limit of vanishing quark masses.

Concerning the two $U\left(1\right)$ factors, the corresponding singlet vector and singlet axial vector currents are given similar to Eqs. (1.24),(1.25) by

$$V_\mu^0 = \bar{\psi}\left(x\right) T^0 \gamma_\mu \psi\left(x\right) ,\tag{1.28}$$

$$A_\mu^0 = \bar{\psi}\left(x\right) T^0 \gamma_\mu \gamma_5 \psi\left(x\right) ,\tag{1.29}$$

where $T^0 = \sqrt{1/(2N_f)}\,\mathbb{1}_{N_f \times N_f}$. This normalization is chosen such that the trace condition in Eq. (A.7) holds also for $T^0$. Unlike chiral symmetry, the invariance under global $\mathrm{U}\left(1\right)_V$ actually remains exact even for the case of massive quarks, i.e. the divergence of the corresponding current vanishes

$$\partial^\mu V_\mu^0 = 0 ,\tag{1.30}$$

implying baryon number conservation.

However, the remaining $\mathrm{U}\left(1\right)_A$ subgroup turns out to behave very differently. Although it is a symmetry of the classical theory, it is anomalously broken due to quantum effects [20, 21]. In [22] it was shown that in the path integral formalism this becomes manifest in a shift of the fermionic integration measure in the partition function in Eq. (1.16). Considering a global $\mathrm{U}\left(1\right)_A$ transformation

$$\psi \to \exp\left(i\alpha\gamma_5\right)\psi, \qquad \bar{\psi} \to \bar{\psi}\exp\left(i\alpha\gamma_5\right) ,\tag{1.31}$$

where $\alpha$ denotes the group generator, the fermionic integration measure transforms as

$$\mathcal{D}\psi\mathcal{D}\bar{\psi} \to \exp\left(-i\alpha N_f \int d^4x\, \frac{g_s^2}{32\pi^2} F_{\mu\nu}^a \tilde{F}^{a,\mu\nu}\right)\mathcal{D}\psi\mathcal{D}\bar{\psi} \equiv \exp\left(-2i\alpha N_f \int d^4x\,\omega\left(x\right)\right)\mathcal{D}\psi\mathcal{D}\bar{\psi} .\tag{1.32}$$

In this expression the *topological charge density* $\omega\left(x\right)$ has been defined, which represents a total divergence

$$\omega\left(x\right) = \frac{g_s^2}{64\pi^2} F_{\mu\nu}^a \tilde{F}^{a,\mu\nu} = \frac{g_s^2}{32\pi^2} \partial^\mu K_\mu \tag{1.33}$$

of a gauge-variant current $K_\mu$ (Chern-Simons 3-form)

$$K_\mu = 2\epsilon_{\mu\nu\rho\sigma}\left(A^{\nu,a}\partial^\rho A^{\sigma,a} - \frac{g_s}{3} f^{abc} A^{\nu,a} A^{\rho,b} A^{\sigma,c}\right) .\tag{1.34}$$

The associated topological charge (Pontryagin index)

$$Q_t = \int d^4x\,\omega\left(x\right) \tag{1.35}$$

takes integer values and is related to distinct topological sectors of QCD. Since $Q_t$ is given as an integral of a total divergence it may be rewritten as a surface integral by application of Stokes' theorem

$$Q_t \sim \int d^4x\,\partial^\mu K_\mu = \oint d\sigma^\mu K_\mu .\tag{1.36}$$

Naively, such an integral would yield zero for gauge field configurations that vanish sufficiently fast at infinity. However, it was realized by 't Hooft that QCD allows for a particular kind of field configuration, known as instantons, which cause non-zero contributions [23–25].

Furthermore, the aforementioned shift in the integration measure effectively adds a term to the QCD Lagrangian which is of the same form as $\mathcal{L}_\theta$, hence it can be considered a shift of $\theta_0$

$$\theta_0 \to \theta_0 + 2N_f \alpha \,. \tag{1.37}$$

The notion of $\theta_0$ as an angle is related to the fact that the topological contribution in the path integral

$$Z \sim \int \mathcal{D}\psi \mathcal{D}\bar{\psi} \exp i\mathcal{S}_\theta = \int \mathcal{D}\psi \, \mathcal{D}\bar{\psi} \exp i\theta_0 Q_t \tag{1.38}$$

is invariant under any shift of $\theta_0$ by integer multiples of $2\pi$. Note that in the chiral limit this implies that one can always remove the $\theta$-term by application of a global $U(1)_A$ transformation, rendering the actual value of $\theta_0$ irrelevant.

Finally, the divergence of the singlet axial vector current takes the following explicit form

$$\partial^\mu A_\mu^0 = \bar{\psi}(x) \, 2MT^0 i\gamma_5 \psi(x) + \sqrt{2N_f} \, \omega(x) \,. \tag{1.39}$$

Therefore, the anomaly is present regardless of taking the chiral limit of the theory or considering the case of massive quarks. It is only removed in the so-called large-$N_c$ limit [26], i.e. sending $N_c \to \infty$ while keeping $g_s^2 N_c = \mathrm{const}$. This behavior is caused by $\omega(x)$ being suppressed by a factor $g_s^2 = \mathcal{O}\left(N_c^{-1}\right)$. Together with the chiral limit this procedure restores the invariance of the theory under $U(1)_A$.

### 1.1.3 Spontaneous symmetry breaking and pseudoscalar mesons

From the physical values of the quark masses in Eq. (1.19) it is apparent that the quarks can be arranged in two groups consisting of three light and three heavy flavors, respectively. The scale that separates the two groups is roughly $\sim 1\,\mathrm{GeV}$, which happens to be the mass scale of the lightest baryons. Since the divergences of the vector and axial vector currents in Eqs. (1.26) and (1.27) are proportional to the quark mass matrix, one should clearly not expect chiral symmetry to hold to a reasonable level in case of the heavy quarks flavors. Nevertheless, the approximate chiral symmetry for the three light flavors proves particularly useful when dealing with QCD at low energies, hence it is worthwhile to consider for now only $u$, $d$ and $s$ quarks, i.e. setting $N_f = 3$.

In this case the approximate conservation of the currents in Eqs. (1.24) and (1.25) should result in two octets of hadrons with opposite parity. However, this parity doubling is not observed experimentally, hence chiral symmetry cannot be realized in the Wigner-Weyl mode, but has to be spontaneously broken and realized in the Goldstone mode. If we assume that the chiral group is spontaneously broken to its vector subgroup

$$\mathrm{SU}(N_f)_L \otimes \mathrm{SU}(N_f)_R \xrightarrow{SSB} SU(N_f)_V \,, \tag{1.40}$$

one expects to find $N_f^2 - 1 = 8$ pseudoscalar pseudo-Goldstone bosons, inheriting their parity assignments from the broken group generators. For the case of only the two lightest quark flavors these can be identified with the pion triplet ($\pi^\pm$, $\pi^0$), which are indeed the lightest mesons observed in nature [17]

$$
\begin{aligned}
M_{\pi^\pm}^{\text{exp}} &= 139.57018(35)\,\text{MeV}, & M_{\pi^0}^{\text{exp}} &= 134.9766(6)\,\text{MeV}, \\
M_{K^\pm}^{\text{exp}} &= 493.677(16)\,\text{MeV}, & M_{K^0}^{\text{exp}} &= M_{\bar{K}^0}^{\text{exp}} = 497.614(24)\,\text{MeV}, \\
M_{\eta}^{\text{exp}} &= 547.853(24)\,\text{MeV}.
\end{aligned}
\tag{1.41}
$$

For $N_f = 3$ the octet is completed by two charged kaons ($K^\pm$), two neutral kaons ($K^0$, $\bar{K}^0$) and the $\eta$ with heavier masses compared to the pions, which is mostly due to contributions of the strange quark.

In addition to the octet mesons, there is a flavor singlet field associated to the $U(1)_A$ which is experimentally identified with the $\eta'$ (up to mixing; see subsection 1.1.5). Naively, one would expect the mass of this field to be of the order of the other octet mesons with strange quark content. Surprisingly, it turns out that the mass found in experiment is roughly twice as large [17]

$$
M_{\eta'}^{\text{exp}} = 957.78(6)\,\text{MeV}.
\tag{1.42}
$$

This extraordinary large mass represents the so-called $U(1)_A$-problem, i.e. the absence of a ninth (pseudo-) Goldstone boson in the physical spectrum. In order to gain further insight on how the $U(1)_A$-anomaly generates an additional contribution to $M_{\eta'}$ it is useful to consider flavor singlet and octet fields $\eta_0$ and $\eta_8$. In the chiral limit, flavor symmetry becomes exact and one can identify the physical $\eta,\eta'$ with $\eta_8$ and $\eta_0$, respectively. This corresponds to ignoring any mixing in the $\eta$–$\eta'$ system which will be discussed in subsection 1.1.5. Considering the matrix element of the $\eta_0$-field with the flavor singlet axial vector current in momentum space

$$
\langle 0 |\, A_\mu^0\,(0)\, | \eta_0\,(p) \rangle = i f_0 p_\mu,
\tag{1.43}
$$

where the singlet decay constant $f_0$ has been introduced, it is possible to determine the contribution of the anomaly to the mass of the $\eta_0$. To this end, one takes the divergence of the matrix element in the chiral limit and applies Eq. (1.39), leading to

$$
\langle 0 |\, \partial^\mu A_\mu^0\,(0)\, | \eta_0\,(p) \rangle = \sqrt{6}\, \langle 0 |\, \omega\,(0)\, | \eta_0\,(p) \rangle = f_0 M_{\eta_0}^2.
\tag{1.44}
$$

Again, it is only due to non-trivial, topological effects that this matrix element yields a non-zero contribution as it vanishes to any finite order in perturbation theory. Therefore, the large mass of the $\eta'$ has to be considered a generic non-perturbative effect. From Eq. (1.43) it follows that $f_0 = \mathcal{O}\left(O\sqrt{N_c}\right)$ holds in the chiral limit, because the matrix element on the left side involves one quark loop counting as $\mathcal{O}(N_c)$ and one meson normalization factor which is of order $\mathcal{O}\left(1/\sqrt{N_c}\right)$. For additional insight into these counting rules see [27] and the discussion in the next subsection. Together with Eq. (1.44), where the topological charge density $\omega(x) \sim g_s^2$ yields another order $\mathcal{O}\left(M_C^{-1}\right)$, this leads to $M_{\eta_0}^2 = \mathcal{O}\left(N_c^{-1}\right)$. This implies, that treating QCD in the large-$N_c$ limit, the squared physical $\eta'$ mass has to vanish as $1/N_c$ [27, 28]. As will be discussed in the next subsection, this feature allows to consistently include the $\eta'$ in the framework of an effective field theory.

### 1.1.4  Chiral perturbation theory

One approach to tackle the non-perturbative regime of QCD is given by $\chi$PT [29,30], an effective field theory exploiting the approximate chiral symmetry of QCD. The formalism required to construct $\chi$PT as an effective field theory was developed in the late 60's by Callan, Coleman, Wess and Zumino and is known as "CCWZ"-formalism [31,32]. For a modern formulation of the procedure see [33]. Since we are mainly interested in applications of $\chi$PT to LQCD results as well as certain features related to the mixing in the $\eta$–$\eta'$ system, we will restrict ourselves to a discussion of the basic principles, avoiding several technical details. For the explicit inclusion of discretized spacetime in the formulation of $\chi$PT we refer to section 1.3.5.

The fundamental principle which allows to obtain actual predictions from an effective field theory relies on a conjecture by Weinberg [34]. It states that it is possible to determine $\mathcal{S}$-matrix elements in any quantum field theory perturbatively from the most general effective Lagrangian respecting all the symmetries of the underlying theory while complying with the principles of analyticity, unitarity and cluster decomposition. In general, this conjecture leads to an effective Lagrangian consisting of an infinite number of terms and parameters called low energy constants, whose numerical values cannot be fixed from the underlying symmetries alone. These LECs can be considered to parametrize the ignorance towards processes at energies beyond the low energy regime for which the effective theory is valid, hence they have to be determined from some additional (experimental, LQCD) input.

In the case of $\chi$PT the effective Lagrangian describes the dynamics of Goldstone bosons (mesons) and may also contain interactions involving further hadronic states (e.g. baryons). However, for the purposes of this work it is sufficient to restrict ourselves to the mesonic case only. In order to render $\chi$PT predictive, one first needs to introduce some counting scheme which allows to classify terms in the effective Lagrangian as well as the resulting Feynman diagrams with respect to their relative importance. To this end one employs Weinberg's power counting scheme which basically is an expansion in small momenta and masses. In this scheme one analyzes the behavior of terms in the effective Lagrangian $\mathcal{L}_{\text{eff}}$, as well as that of amplitudes under rescaling of derivatives (or momenta) and masses by a common expansion parameter $\delta$, i.e.

$$p \to \delta p, \qquad m_{\text{meson}} \to \delta M_{\text{meson}}, \qquad m_q \to \delta^2 m_q\,. \tag{1.45}$$

This allows to arrange the terms $\mathcal{L}^{(n)}$ in the effective Lagrangian according to the combined number of derivatives and meson masses

$$\mathcal{L}_{\text{eff}} = \mathcal{L}^{(0)} + \mathcal{L}^{(1)} + \mathcal{L}^{(2)} + ...\,, \tag{1.46}$$

and to assign a chiral dimension $D$ to every amplitude, given by

$$\mathcal{M} \to \delta^D \mathcal{M}\,. \tag{1.47}$$

The latter is then used to decide which diagrams contribute to a calculation of a certain order in $\chi$PT. This procedure yields the desired perturbative expansion, that allows one to consider only a finite subset of terms in the Lagrangian and diagrams contributing to the amplitude in

question. Note that for the case of purely mesonic interactions there are only terms including an even number of derivatives and meson masses in the effective Lagrangian in Eq. (1.46), because quark masses count as $\mathcal{O}(\delta)$ and all occurring Lorentz indices are contracted either by the metric tensor $g_{\mu\nu}$ or the fourth order totally antisymmetric tensor $\epsilon_{\mu\nu\rho\sigma}$.

Since we are interested in the $\eta$–$\eta'$ system we will need to include a singlet field into the effective field theory. A systematic construction of the corresponding effective Lagrangian has originally been given in by Gasser and Leutwyler in [30], although effective Lagrangians including the singlet field have already been used in [28, 35, 36]. For our purposes it is convenient to mostly stick to the formulation in [37–39], with some minor changes in notation. Furthermore we will restrict all further discussion to the isospin symmetric limit $m_u = m_d \equiv m_l$, which is sufficient for our applications.

As mentioned before, $\chi$PT describes the dynamics of Goldstone bosons, whereas QCD is formulated in terms quarks and gluons. In general, the Goldstone fields are represented by matrix-valued elements in H/G, where H is the full symmetry group of the Hamiltonian and G the symmetry group of the ground state. For now let us consider the case of the standard chiral group, i.e. $H = \mathrm{SU}(3)_L \times \mathrm{SU}(3)_R$. and choose $\mathrm{G} = \mathrm{SU}(3)_V$, which implements the pattern of spontaneous chiral symmetry breaking as given in Eq. (1.40). This implies for the coset space $\mathrm{H/G} = \mathrm{SU}(3)$ and we choose the broken operators to be $X^a = T_L^a - T_R^a$, where $T_L^a$, $T_R^a$ are the generators of $\mathrm{SU}(3)_L$ and $\mathrm{SU}(3)_R$, respectively. The unbroken generators are given by $T^a = T_L^a + T_R^a$, where again the $T^a$ are our standard generators of $\mathrm{SU}(3)$ defined in terms of the Gell-Mann matrices. A convenient choice of basis for the Goldstone field $U(x)$ is then given by

$$U(x) = \exp\left(i\varphi(x)\right), \tag{1.48}$$

where $\varphi = 2T^a\varphi^a = \lambda^a\varphi^a$ contains the $\dim(H) - \dim(G) = 8$ fields corresponding to the broken generators $X^a = T_L^a - T_R^a$. With this choice, the field $U(x)$ behaves linearly under chiral transformations $L, R \in \mathrm{U}(3)_{L,R}$

$$U(x) \to RU(x)L^\dagger, \tag{1.49}$$

whereas the octet field $\varphi$ itself transforms in a complicated, nonlinear way. In terms of meson fields we have

$$\varphi = \sqrt{2}\begin{pmatrix} \frac{1}{\sqrt{2}}\pi^0 + \frac{1}{\sqrt{6}}\eta_8 & \pi^+ & K^+ \\ \pi^- & -\frac{1}{\sqrt{2}}\pi^0 + \frac{1}{\sqrt{6}}\eta_8 & K^0 \\ K^- & \bar{K}^0 & -\frac{2}{\sqrt{6}}\eta_8 \end{pmatrix}. \tag{1.50}$$

If we extend the symmetry group of the Hamiltonian to $H = \mathrm{U}(3)_L \times \mathrm{U}(3)_R$, an additional singlet field is introduced which shows up as a phase in $U(x)$

$$U(x) = \exp\left(i\varphi(x) + \frac{i}{3}\varphi^0(x)\right). \tag{1.51}$$

For the singlet field we choose $\varphi^0 = 6T^0\eta_0$, such that its overall normalization agrees with our previous definition of $T^0$ and we end up with the same form of the kinetic term as for the octet mesons[2]. Nevertheless, pulling $\frac{1}{3}$ out of $\phi_0$ turns out to be convenient for the construction of the

---

[2]Note that this choice differs by an additional factor of $\sqrt{6}$ from the convention used by [37–39], but matches the one used in the review of $\eta, \eta'$-mixing by Feldmann [40] which we follow for the discussion in the next subsection.

effective Lagrangian because the singlet field shows up as the phase of the determinant of $U(x)$

$$\log \det U = i\varphi^0 \,, \tag{1.52}$$

without an additional numerical factor for this particular choice of normalization.

The effective Lagrangian has to be invariant under $\mathrm{U}(3)_L \times \mathrm{U}(3)_R$ transformations, which motivates the treatment of the vacuum angle $\theta_0$ as an external field $\theta(x)$, transforming under $\mathrm{U}(1)_A$ rotations according to

$$\theta \to \theta - 2N_f\alpha \,. \tag{1.53}$$

This transformation behavior is chosen in such a way that it cancels the shift in Eq. (1.37) which is introduced by the fermionic integration measure of the path integral. The field $U$ and the quark mass matrix $M$ are both required to transforms as

$$U \to RUL^\dagger \,, \qquad M \to RUL^\dagger \,, \tag{1.54}$$

where $L \in \mathrm{U}(3)_L$ and $R \in \mathrm{U}(3)_R$. In addition, for the singlet field we have

$$\log \det U \to \log \det +2N_f\alpha \,, \tag{1.55}$$

hence one can build the invariant combination

$$\bar{\theta} = \log \det U + \theta \,, \tag{1.56}$$

that turns out to be convenient for the construction of the effective Lagrangian. Furthermore one introduces the usual external fields $s(x)$, $p(x)$, $v_\mu(x)$, $a_\mu(x)$ in the QCD Lagrangian

$$\tilde{\mathcal{L}}_{\mathrm{QCD}} = \mathcal{L}^0_{\mathrm{QCD}} - \bar{\psi}(s - i\gamma_5 p)\psi + \bar{\psi}\gamma^\mu(v_\mu + \gamma_5 a_\mu)\psi - \theta(x)\omega \,, \tag{1.57}$$

where $\mathcal{L}^0_{\mathrm{QCD}}$ denotes the massless QCD Lagrangian without $\mathcal{L}_\theta$. Obviously, the original QCD Lagrangian is recovered for the choice $p = v_\mu = a_\mu = 0$ and $s = M$. Defining $l_\mu = v_\mu - a_\mu$ and $r_\mu = v_\mu + a_\mu$ one ends up with the following transformation behavior for the external currents

$$l_\mu \to Ll_\mu L^\dagger + iL\partial_\mu L^\dagger \,, \tag{1.58}$$

$$r_\mu \to Rr_\mu R^\dagger + iR\partial_\mu R^\dagger \,, \tag{1.59}$$

$$s + ip \to R(s + ip)L^\dagger \,. \tag{1.60}$$

The covariant derivative acting on the field $U$ takes the following, simple form

$$D_\mu U = \partial_\mu U + i[U, v_\mu] - i\{U, a_\mu\} = \partial_\mu U + iUl_\mu - ir_\mu U \,. \tag{1.61}$$

For the singlet field $\phi_0$ and the variable $\theta$ we have

$$D_\mu\phi_0 = \partial_\mu\phi_0 - 2\operatorname{tr}[a_\mu] \,, \qquad D_\mu\theta = \partial_\mu\theta + 2\operatorname{tr}[a_\mu] \,, \tag{1.62}$$

implying that the covariant derivative acting on the invariant variable $\bar{\theta}$ is given by $D_\mu\bar{\theta} = \partial_\mu\bar{\theta}$ as expected. The most general effective Lagrangian to second order in the derivative expansion reads [30, 37]

$$\mathcal{L}^{(0,2)}_{\mathrm{eff}} = -V_0(\bar{\theta}) + V_1(\bar{\theta})\operatorname{tr}[D_\mu U^\dagger D^\mu U] + V_2(\bar{\theta})\operatorname{tr}[(s + ip)U^\dagger] + V_2^*(\bar{\theta})\operatorname{tr}[(s - ip)U]$$

$$+ V_3 \left( \bar{\theta} \right) D_\mu \phi_0 D^\mu \phi_0 + V_4 \left( \bar{\theta} \right) D_\mu \phi_0 D^\mu \theta + V_5 \left( \bar{\theta} \right) D_\mu \theta D^\mu \theta \,, \tag{1.63}$$

where the trace is understood to be taken in flavor space. In contrast to the standard $\mathrm{SU}(3)$ case one cannot neglect the zeroth order term $\mathcal{L}_{\mathrm{eff}}^{(0)} = -V_0 \left( \bar{\theta} \right)$ in the effective Lagrangian, as it is not an irrelevant constant anymore but a function of the invariant variable $\bar{\theta}$. In fact this is true for all the potentials $V_i$ which are not LECs as in the standard $\mathrm{SU}(3)$ case but become functions of $\bar{\theta}$. They encode the dynamics of the singlet field $\phi_0$ and are not restricted by chiral symmetry, i.e. they are each represented by an infinite power series in $\bar{\theta}$. As discussed in [30], the potentials $V_i \left( \bar{\theta} \right)$ can be expanded in powers of $1/N_c$ which allows to keep only a finite amount of terms. To this end one considers a general connected $(Q+T)$-point function $G_{Q,T}$ consisting of the time-ordered product of $Q$ quark currents $J_i \left( x_i \right) = \bar{q} \left( x_i \right) \Gamma_i q \left( x_i \right)$, where $\Gamma_i$ denote matrices acting in spin and flavor space, and $T$ topological charge densities $\omega \left( x_i \right)$

$$G_{Q,T} = \langle 0 | \, T J \left( x_1 \right) \dots J \left( x_Q \right) \omega \left( x_{Q+1} \right) \dots \omega \left( x_{Q+T} \right) | 0 \rangle_{\mathrm{conn}} \,. \tag{1.64}$$

This kind of Green function has a definite order in powers of $N_c$

$$G_{Q,T} = \left\{ \begin{array}{ll} \mathcal{O}\!\left( N_c^{1-T} \right) & \text{for} \quad Q > 0 \\ \mathcal{O}\!\left( N_c^{2-T} \right) & \text{for} \quad Q = 0 \end{array} \right. \,, \tag{1.65}$$

which we exploit to reveal the large-$N_c$ dependence of the generating functional $\tilde{\mathcal{Z}}$ corresponding to the Lagrangian $\tilde{\mathcal{L}}_{\mathrm{QCD}}$ in Eq. (1.57). For this purpose one introduces $N_c$-independent functionals $f_1 \left( \theta / N_c \right)$ and $f_2 \left( s, p, v_\mu, a_\mu, \theta / N_c \right)$, such that $\tilde{\mathcal{Z}}$ takes the following form

$$\tilde{\mathcal{Z}} = N_c^2 f_1 \left( \frac{\theta}{N_c} \right) + N_c f_2 \left( s, p, v_\mu, a_\mu, \frac{\theta}{N_c} \right) + \mathcal{O} \left( N_c^0 \right) \,. \tag{1.66}$$

Plugging in an expansion of $U$ in the meson fields $\phi$, $\phi_0$ into the effective Lagrangian in Eq. (1.63) and comparing the terms which are independent of $\phi$ and $\phi_0$ with the expression for $\tilde{\mathcal{Z}}$ reveals the large-$N_c$ behavior of the potentials $V_i$

$$V_i \left( \bar{\theta} \right) = N_c^{n_i} v_i \left( \frac{\bar{\theta}}{N_c} \right) \,, \tag{1.67}$$

where $n_0 = 2$, $n_{1,2} = 1$ and $n_{3,4,5} = 0$. The functions $v_i$ in the above expression do not depend on $N_c$ anymore. Moreover, parity implies that

$$V_i \left( \bar{\theta} \right) = \sum_n V_i^{(2n)} \bar{\theta}^{2n}, \quad i = 0,1,3,4,5 \,, \tag{1.68}$$

$$V_2 \left( \bar{\theta} \right) = \sum_n V_2^{(2n+1)} \bar{\theta}^{2n+1} \,. \tag{1.69}$$

where the coefficients $V_{0,1,3,4,5}^{(2n)}$ and $V_2^{(2n+1)}$ are suppressed by increasing powers of $1/N_c$. This feature allows to introduce a unified power counting scheme

$$p = \mathcal{O} \left( \delta \right), \qquad m_q = \mathcal{O} \left( \delta^2 \right), \qquad \frac{1}{N_c} = \mathcal{O} \left( \delta^2 \right) \tag{1.70}$$

and to keep only a finite number of terms in the potentials $V_i$. The form of the potentials $V_i$ in the Lagrangian in Eq. (1.63) is not unique but can be changed by some transformation $U \to U \exp if(\bar{\theta})$ which leaves the overall structure of the Lagrangian invariant [30]. Here we follow the approach in [37] and exploit this ambiguity to remove the term $\sim V_4$. At this point we may also discard the vacuum angle by setting $\theta = 0$, as it was only required for the construction of the effective Lagrangian and not any actual physics. This additionally eliminates the last term $\sim V_5$ and implies $\bar{\theta} \to \phi_0 = \sqrt{6}\eta_0$. Keeping only the terms that survive in the large $N_c$-limit the relevant potentials read [30, 37] [3]

$$V_0 = \epsilon_0 + 3\tau\eta_0^2 + \mathcal{O}\left(N_c^{-2}\right) , \tag{1.71}$$

$$V_1 = \frac{1}{8}f^2 + \mathcal{O}\left(N_c^{-1}\right) , \tag{1.72}$$

$$V_2 = \frac{1}{4}f^2 B^2 \left(1 - i\sqrt{\frac{2}{3}}\Lambda_2\eta_0\right) + \mathcal{O}\left(N_c^{-1}\right) , \tag{1.73}$$

$$V_3 = \frac{1}{24}f^2\Lambda_1 + \mathcal{O}\left(N_c^{-2}\right) . \tag{1.74}$$

The very first term $\epsilon_0 = \mathcal{O}(N_c^2)$ in $V_0$ is just an irrelevant cosmological constant, whereas $\tau$ coincides at leading order with the topological susceptibility from pure Yang-Mills theory [27, 38], i.e. $\tau = \chi_t(0)|_{\text{YM}} + \mathcal{O}\left(N_c^{-1}\right)$, where

$$\chi_t(0)|_{\text{YM}} = \int dx^4 \langle 0| T\omega(x)\omega(0)|0\rangle|_{\text{YM}} . \tag{1.75}$$

Moreover, $f = \mathcal{O}\left(N_c^{1/2}\right)$ is identified with an universal, leading order octet (pion) decay constant in the chiral limit, c.f. Eq. (1.84), and $B_0$ is related to the non-vanishing chiral condensate $B_0 \sim \langle 0| \bar{q}q |0\rangle$ signaling the spontaneous breakdown of chiral symmetry. The latter occurs only in the combination $\chi = 2B_0(s + ip)$, which becomes

$$\chi = 2B_0 M , \tag{1.76}$$

for the choice $s = M$, $p = 0$. Finally, the parameters $\Lambda_1$, $\Lambda_2$ are again specific to the inclusion of the singlet field, they are absent in the SU(3) version of $\chi$PT. The leading order effective Lagrangian now reads

$$\mathcal{L}_{\text{eff}}^{\delta^0} = \frac{1}{8}f^2\text{tr}\left[D_\mu U^\dagger D^\mu U\right] + \frac{1}{8}f^2\text{tr}\left[\chi^\dagger U + U^\dagger\chi\right] - 3\tau\eta_0^2 , \tag{1.77}$$

where the form of the first two terms is identical to the ones in the standard SU(3) theory. For the discussion of $\eta$,$\eta'$-mixing we also include the relevant terms appearing in the Lagrangian at NLO [37, 40]

$$\mathcal{L}_{\text{eff}}^{\delta^2} = L_5\text{tr}\left[D_\mu U^\dagger D^\mu U\left(\chi^\dagger U + U^\dagger\chi\right)\right] + L_8\text{tr}\left[\chi^\dagger U\chi^\dagger U + U^\dagger\chi U^\dagger\chi\right] +$$

---

[3]Note that our normalization for the universal decay constant $f$ is given by $f = \sqrt{2}F$, where $F$ is the decay constant used by the authors of [30, 37]

$$+ \frac{f^2}{4} \Lambda_1 \partial_\mu \eta_0 \partial^\mu \eta_0 + i \frac{f^2}{4} \Lambda_2 \eta_0 \mathrm{tr} \left[ \chi^\dagger U - U^\dagger \chi \right] + \dots \, . \tag{1.78}$$

Considering only terms including octet fields in the Lagrangian in Eq. (1.77) and choosing the quark mass matrix to be diagonal and real, i.e. $s = M$ one obtains the usual leading order expressions for the masses of the corresponding mesons

$$M_\pi^2 = 2 B_0 m_l + \mathcal{O} \left( \delta^4 \right) \, , \tag{1.79}$$

$$M_{\mathrm{K}}^2 = B_0 \left( m_l + m_s \right) + \mathcal{O} \left( \delta^4 \right) \, , \tag{1.80}$$

$$M_\eta^2 = \frac{2}{3} B_0 \left( m_l + 2 m_s \right) + \mathcal{O} \left( \delta^4 \right) \, . \tag{1.81}$$

Note that to this order one identifies $M_\eta = M_{\eta_8}$ and that due to the assumption of exact isospin symmetry the pion triplet becomes mass degenerate as well as the kaons, although $M_\pi \neq M_{\mathrm{K}} \neq M_\eta$ still holds because of $m_l \neq m_s$. Combining these three expressions yields the leading order Gell-Mann Okubo (GMO) mass relation

$$3 M_\eta^2 = 4 M_{\mathrm{K}}^2 - M_\pi^2 + \mathcal{O} \left( \delta^4 \right) \, , \tag{1.82}$$

implying that

$$\frac{3 M_\eta^2}{4 M_{\mathrm{K}}^2 - M_\pi^2} \approx 1 \, , \tag{1.83}$$

which turns out to be accurate up to $\sim 6\%$ employing the values of $M_{\pi^\pm}^{\mathrm{exp}}$, $M_{K^\pm}^{\mathrm{exp}}$ and $M_\eta^{\mathrm{exp}}$ as listed in Eq. (1.41).

Before proceeding with the discussion of the mass for the $\eta_0$-field, we briefly consider its decay constant. In the chiral limit it receives two contributions from tree-level graphs, i.e. the standard one from the first term in the Lagrangian in Eq. (1.77) and an additional one from the term $\sim \Lambda_1$ in Eq. (1.78). This implies that one actually has to deal with two distinct decay constants for the octet and the singlet

$$f_0 = \sqrt{1 + \Lambda_1} f, \qquad f_8 = f \, , \tag{1.84}$$

even without taking any higher order loop graphs into account or considering massive quarks. Note that the scale dependence of $f_0$ due to its anomalous dimension is to this order absorbed into $\Lambda_1$ [37]. A dedicated discussion of mixing and decay constants is included in the next subsection.

For the singlet field, the last term in Eq. (1.77) yields a non-vanishing mass in the chiral limit

$$\mathring{M}_{\eta'}^2 = \frac{12}{f_0^2} \chi_t \left( 0 \right) |_{\mathrm{YM}} + \mathcal{O} \left( N_c^{-2} \right) \, . \tag{1.85}$$

This expression represents the famous Witten-Veneziano formula in its original form [27]. To leading order there is no mixing present and the singlet field $\eta_0$ is identified with the $\eta'$. In fact, the above mass contribution vanishes as $\mathcal{O}(N_c^{-1})$, which is the expected behavior for $M_{\eta'}^2$. However, for non-vanishing quark masses there is an additional contribution at leading order,

which is induced by the second term in Eq. (1.77) similar to the masses of the octet mesons, such that the mass of the singlet takes the form

$$M_{\eta'}^2 = \frac{12}{f_0^2}\chi_t\left(0\right)|_{\text{YM}} + \frac{2}{3}B_0\left(2m_l + m_s\right) + \mathcal{O}\left(\delta^4\right)\,. \tag{1.86}$$

Plugging in the leading order expressions for the octet meson masses in Eqs. (1.79)–(1.81) and reshuffling of terms, leads to the full Witten-Veneziano formula [41] in its standard form

$$M_{\text{U(1)}_{\text{A}}}^2 \equiv \frac{12}{f_0^2}\chi_t\left(0\right)|_{\text{YM}} = M_{\eta'}^2 + M_{\eta}^2 - 2M_{\text{K}}^2 + \mathcal{O}\left(\delta^4\right)\,, \tag{1.87}$$

where the mass contribution due to the $\text{U}\left(1\right)_{\text{A}}$ anomaly has been denoted by $M_{\text{U(1)}_{\text{A}}}$.

### 1.1.5   Mixing in the $\eta$–$\eta'$ system

In the last subsection it has been shown that even in the chiral limit there are two different decay constants $f_0$, $f_8$ required for the singlet and the octet field. Actually the situation becomes even more involved for non-vanishing quark masses and if higher orders in the chiral expansion are included, leading to mixing between octet and singlet states. In this subsection we will discuss $\eta,\eta'$-mixing starting from the general definition via matrix elements and resort to $\chi$PT only for the sake of disclosing relations and differences between mixing schemes. Since we are ultimately interested in performing non-perturbative calculations directly from lattice QCD, it should – at least in principle – be possible to access such matrix elements directly. The central aspects of the subsequent discussion are based on the comprehensive review article by Feldmann [40] and publications [42, 43]. Further relevant details, particularly on the $\chi$PT side of the subject can again be found in [30, 37].

In general, decay constants are defined for any pseudoscalar meson P from axial vector matrix elements

$$\langle 0| A_\mu^a |\text{P}\left(p\right)\rangle = if_{\text{P}}^a p_\mu\,, \tag{1.88}$$

which leads to

$$\langle 0| \partial^\mu A_\mu^a |\text{P}\left(0\right)\rangle = f_{\text{P}}^a M_{\text{P}}^2\,, \tag{1.89}$$

for projection to zero momentum. Assuming that $\eta$ and $\eta'$ are not flavor eigenstates, each of them exhibits a coupling to the singlet and octet current $A_\mu^0$ and $A_\mu^8$, respectively. Therefore, one ends up with four independent decay constants for the $\eta$–$\eta'$ system, which are commonly parametrized in terms of two decay constants $f_0$, $f_8$ and two mixing angles $\phi_0$, $\phi_8$

$$\begin{pmatrix} f_\eta^8 & f_\eta^0 \\ f_{\eta'}^8 & f_{\eta'}^0 \end{pmatrix} = \begin{pmatrix} f_8\cos\phi_8 & -f_0\sin\phi_0 \\ f_8\sin\phi_8 & f_0\cos\phi_0 \end{pmatrix} \equiv \Xi\left(\phi_8, \phi_0\right)\text{diag}\left(f_8, f_0\right)\,. \tag{1.90}$$

The choice of $A_\mu^0$, $A_\mu^8$ together with P $= \eta, \eta'$ in Eq. (1.88) defines the so-called *singlet-octet basis*, which is special in the sense that the decay constants $f_{\text{P}}^a$ defined in Eq. (1.88) relate the

singlet and octet fields $\varphi^0$, $\varphi^8$ introduced in the last section directly to the physical fields $\eta, \eta'$ via

$$\varphi^a = \left(f^a_\eta\right)^{-1} \eta + \left(f^a_{\eta'}\right)^{-1} \eta' . \tag{1.91}$$

Moreover, employing the effective Lagrangians in Eqs. (1.77),(1.78), it is possible to relate the mixing parameters in the $\eta$–$\eta'$ system to the remaining octet decay constants $f_\pi$, $f_K$ and the parameter $\Lambda_1$

$$f_0^2 = \left(f^0_\eta\right)^2 + \left(f^0_{\eta'}\right)^2 = \frac{1}{3} \left(2f_K^2 + f_\pi^2\right) + \Lambda_1 f_\pi^2 , \tag{1.92}$$

$$f_8^2 = \left(f^8_\eta\right)^2 + \left(f^8_{\eta'}\right)^2 = \frac{1}{3} \left(4f_K^2 - f_\pi^2\right) , \tag{1.93}$$

$$f_0 f_8 \sin\left(\phi_8 - \phi_0\right) = f^0_\eta f^8_\eta + f^0_{\eta'} f^8_{\eta'} \;\; = -\frac{2\sqrt{2}}{3} \left(f_K^2 - f_\pi^2\right) , \tag{1.94}$$

where the parameter $L_5$ has been expressed in terms of $f_\pi$ and $f_K$ [37]. As pointed out in [40], these expressions have certain implications concerning the mixing angles $\phi_0$, $\phi_8$. First of all, from the last relation one infers that $\phi_0 \neq \phi_8$ because the experimental values of $f_\pi$ and $f_K$ are given by [44]

$$f_\pi^{\mathrm{exp}} = 130.41(3)(20)\,\mathrm{MeV}, \qquad f_K^{\mathrm{exp}} = 156.1(2)(8)(2)\mathrm{MeV} , \tag{1.95}$$

such that $f_K \approx 1.197 f_\pi$ holds due to $\mathrm{SU}(3)_F$ breaking effects. In the chosen basis and to the given chiral order the additional, OZI-violating corrections are specific to the singlet sector, i.e. the term $\sim \Lambda_1 = \mathcal{O}\left(N_c^{-1}\right)$ affects neither $f_8$ nor the angles $\phi_0$, $\phi_8$ but only the parameter $f_0$. From the experimental values of the meson masses in Eqs. (1.41),(1.42) and the Witten-Veneziano formula in Eq. (1.87) it follows that the contribution of the $\mathrm{U}(1)_A$ anomaly clearly dominates over $\mathrm{SU}(3)_F$ violations, i.e. $M_K^2 - M_\pi^2 < M_{\mathrm{U}(1)_A}^2$, leading to the expectation that the mixing angles $\phi_0$, $\phi_8$ are rather small, hence

$$\left| \frac{\phi_0 - \phi_8}{\phi_0 + \phi_8} \right| \lll 1 . \tag{1.96}$$

Therefore, one should not expect the mixing in the singlet-octet basis to be described to any reasonable approximation by means of a single angle. The two angles only coincide for the case of unbroken $\mathrm{SU}(3)_F$ symmetry, for which they are in fact exactly zero in the chosen parametrization.

However, the fact that there are different types of contributions to the mixing, i.e. $\mathrm{SU}(3)_F$-breaking and OZI-violating effects $\sim \Lambda_1$, can be exploited in order to choose a basis in which the two resulting mixing angles do not exhibit a sizable splitting. To this end one introduces the *quark flavor basis* with the axial vector currents $A^0_\mu$ and $A^8_\mu$ replaced by the combinations

$$A^l_\mu = \frac{2}{\sqrt{3}} A^0_\mu + \sqrt{\frac{2}{3}} A^8_\mu = \frac{1}{\sqrt{2}} \left(\bar{u}\gamma_\mu\gamma_5 u + \bar{d}\gamma_\mu\gamma_5 d\right) , \tag{1.97}$$

$$A^s_\mu = \sqrt{\frac{2}{3}} A^0_\mu - \frac{2}{\sqrt{3}} A^8_\mu = \bar{s}\gamma_\mu\gamma_5 s , \tag{1.98}$$

in which the light quarks and the strange quark contributions are disentangled. This is the reason why this basis is more convenient in lattice simulations as its currents have the same structure as the standard interpolating operators; see section 2.1, which allows direct access to the corresponding matrix elements. In exact analogy to the singlet-octet basis this basis again allows for a parametrization in terms of two decay constants and two mixing angles

$$
\begin{pmatrix} f_\eta^l & f_\eta^s \\ f_{\eta'}^l & f_{\eta'}^s \end{pmatrix} = \Xi\left(\phi_l, \phi_s\right) \mathrm{diag}\left(f_l, f_s\right), \tag{1.99}
$$

where the mixing matrix $\Xi$ has the same form as the one defined in Eq. (1.90). In this basis the relations between mixing parameters in the $\eta$–$\eta'$ system and $f_\pi$, $f_K$, $\Lambda_1$ read

$$
f_l^2 = \left(f_\eta^l\right)^2 + \left(f_{\eta'}^l\right)^2 = f_\pi^2 + \frac{2}{3}\Lambda_1 f_\pi^2, \tag{1.100}
$$

$$
f_s^2 = \left(f_\eta^s\right)^2 + \left(f_{\eta'}^s\right)^2 = 2f_K^2 - f_\pi^2 + \frac{1}{3}\Lambda_1 f_\pi^2, \tag{1.101}
$$

$$
f_l f_s \sin\left(\phi_l - \phi_s\right) = f_\eta^l f_\eta^s + f_{\eta'}^l f_{\eta'}^s = \frac{\sqrt{2}}{3}\Lambda_1 f_\pi^2. \tag{1.102}
$$

The most important feature of the quark flavor basis becomes manifest in the last expression, which is now entirely given by an OZI-violating contribution $\sim \Lambda_1$, amounting to an additional suppression of $\mathcal{O}\left(\delta^2\right)$ for the difference $|\phi_l - \phi_s|$ compared to $|\phi_0 - \phi_8|$. The difference between the mixing angles in the quark flavor basis does not receive any contribution from $\mathrm{SU}\left(3\right)_F$ breaking effects to the given order in the chiral expansion. Furthermore, in a $\mathrm{SU}\left(3\right)_F$ symmetric world the angles $\phi_l \approx \phi_s$ would take a value of

$$
\phi_{\mathrm{SU}(3)_F} = \arctan\sqrt{2}, \tag{1.103}
$$

hence their numerical value is not expected to be small. Therefore, we have

$$
\left|\frac{\phi_l - \phi_s}{\phi_l + \phi_s}\right| \ll 1. \tag{1.104}
$$

motivating a simplified mixing scheme in the quark flavor basis with only one angle $\phi$

$$
\begin{pmatrix} f_\eta^l & f_\eta^s \\ f_{\eta'}^l & f_{\eta'}^s \end{pmatrix} = \Xi\left(\phi\right) \mathrm{diag}\left(f_l, f_s\right) + \mathcal{O}\left(\Lambda_1\right), \tag{1.105}
$$

where $\Xi\left(\phi\right) \equiv \Xi\left(\phi, \phi\right)$. The mixing angle $\phi$ is related to the double ratio of amplitudes

$$
\tan^2\left(\phi\right) = -\frac{f_{\eta'}^l f_\eta^s}{f_\eta^l f_{\eta'}^s}. \tag{1.106}
$$

Up to OZI-violating terms of $\mathcal{O}\left(\Lambda_1\right)$ one has the following relations between the parameters of the simplified mixing scheme in the quark flavor basis and those of the singlet-octet basis [42]

$$
\phi_0 = \phi - \arctan\left(\sqrt{2}f_l/f_s\right) + \mathcal{O}\left(\Lambda_1\right), \tag{1.107}
$$

$$\phi_8 = \phi - \arctan\left(\sqrt{2}f_s/f_l\right) + \mathcal{O}\left(\Lambda_1\right). \tag{1.108}$$

This allows to convert the mixing parameters determined in the quark flavor basis into the angles of the singlet-octet basis. However, such a conversion is again only exact up to subleading, OZI-violating contributions. In this context the $\mathrm{SU}\left(3\right)_F$ breaking becomes manifest in the decay constant ratio $f_l/f_s \neq 1$. Similarly, the decay constants in the quark flavor basis and singlet-octet basis are related up to an OZI-violating correction as well

$$f_0^2 = \frac{1}{3}\left(2f_l^2 + f_s^2\right) + \mathcal{O}\left(\Lambda_1\right), \tag{1.109}$$

$$f_8^2 = \frac{1}{3}\left(f_l^2 + 2f_s^2\right) + \mathcal{O}\left(\Lambda_1\right), \tag{1.110}$$

which completes the set of relations between both mixing schemes.

In the present discussion we have so far only considered axial vector currents, which occur in the general definition of decay constants. However, one may also consider pseudoscalar matrix elements in order to retrieve information on the mixing parameters. In principle, this is possible due to the relation between axial vector and pseudoscalar matrix elements which is given non-perturbatively by Eq. (1.39). Nonetheless, this relation itself is not sufficient for any practical purposes, e.g. relating the mixing parameters defined from axial vector matrix elements to pseudoscalar ones, mainly because it requires knowledge of the additional matrix element involving the topological charge density. Therefore, one needs to gain further, detailed insight on how the pseudoscalar matrix elements are linked to the mixing parameters, which can again be achieved by the use of $\chi$PT. To this end it is most convenient to consider pseudoscalar currents in the quark flavor basis in analogy to Eqs. (1.97),(1.98).

$$P^l = \frac{1}{\sqrt{2}}\left(\bar{u}\gamma_5 u + \bar{d}\gamma_5 d\right), \tag{1.111}$$

$$P^s = \bar{s}i\gamma_5 s, \tag{1.112}$$

such that the matrix elements for pseudoscalar mesons P are given by

$$h_{\mathrm{P}}^i = 2m_i \left\langle 0\right| P^i \left|\mathrm{P}\right\rangle. \tag{1.113}$$

In order to make contact with the quark flavor basis parametrization for axial vector matrix elements in Eq. (1.99) one can use the effective Lagrangians in Eqs. (1.77),(1.78), leading to expressions for the matrix elements $h_{\mathrm{P}}^i$ in terms of decay constants $f_l$, $f_s$, the mixing angle $\phi$ and the parameters $B_0$, $L_8$, $\Lambda_2$. Again, terms of $\mathcal{O}\left(\Lambda_1\right)$ and $\mathcal{O}\left(\Lambda_2\right)$ are only subleading corrections and hence dropped to the order in the chiral expansion at which only one mixing angle is required in the quark flavor basis. The parameters, $B_0$ and $L_8$ can be treated for expressions involving meson masses and decay constants, such that they do not explicitly appear in the final result either, which reads [40]

$$\begin{pmatrix} h_\eta^l & h_\eta^s \\ h_{\eta'}^l & h_{\eta'}^s \end{pmatrix} = \Xi\left(\phi\right) \mathrm{diag}\left(M_\pi^2 f_l, \left(2M_{\mathrm{K}}^2 - M_\pi^2\right)f_s\right) + \mathcal{O}\left(\Lambda_1, \Lambda_2\right). \tag{1.114}$$

A crucial feature of this mixing scheme is given by the fact that it is intrinsically dependent on $\chi$PT. Unlike in the axial vector case, it is not straightforward to obtain two different angles, because this requires to take higher orders in the chiral expansion into account. While for the axial vector currents this is trivially achieved by simply not employing $\chi$PT at all, one has explicitly to take terms of $\mathcal{O}\left(\Lambda_1, \Lambda_2\right)$ into account in the case of pseudoscalar currents, hence introducing additional dependence on a priori unknown low energy constants. The intrinsic dependence on effective field theory is a drawback which cannot be avoided if one wants to consider pseudoscalar matrix elements instead of their axial vector counterparts. However, the angle $\phi$ itself can still be determined in exact analogy to Eq. (1.106) by simply replacing the axial vector matrix elements by their respective pseudoscalar counterparts

$$\tan\left(\phi\right) = \sqrt{-\frac{h^l_{\eta'} h^s_\eta}{h^l_\eta h^s_{\eta'}}}, \tag{1.115}$$

because the terms involving meson masses and decay constant parameters on the right hand side of Eq. (1.114) cancel exactly in this ratio.

Concerning the foregoing discussion of $\eta,\eta'$-mixing, a few concluding remarks are in order with respect to our lattice simulations. First of all, one should be aware that avoiding the isospin limit for light quarks introduces some additional mixing with the neutral pion, which would lead to a more complicated mixing pattern. Although our simulations do in fact involve isospin breaking of a very different kind, they are carried out for $m_u = m_d$, hence there is no mixing present between $\eta,\eta'$ and the neutral pion and the corresponding matrix elements are zero by definition. This is why we do not need to consider the neutral pion in this particular context.

Secondly, one might probe gluonic contributions to the $\eta,\eta'$ by including a matrix element of the topological charge density

$$A^g_{\mathrm{P}} = \langle 0 | 2\omega | \mathrm{P} \rangle \,. \tag{1.116}$$

This allows for an additional mixing angle related to the gluonic content of the states which is given by

$$\tan\phi_g = -\frac{A^g_\eta}{A^g_{\eta'}}\,, \tag{1.117}$$

However, we will consider only fermionic operators, hence such matrix elements are beyond the scope of this work. The same applies for possible mixing with glueballs, which would require implementation of gluonic operators as well. Nonetheless, the aforementioned gluonic mixing angle enters also implicitly in an extension of the mixing scheme to include possible effects of the charm quark.

This represents the third and last issue, i.e. one might question whether there really is no impact of the charm quark on the $\eta$–$\eta'$ system. This scenario can be covered by an extended mixing scheme, which includes the physical $\eta_c$ as a third state. Again, such an extension is conveniently discussed in the quark flavor basis [40]. To this end we consider an additional axial vector and pseudoscalar current for the charm quark to the quark flavor basis

$$A^c_\mu = \bar{c}\gamma_\mu\gamma_5 c \qquad P^c = \bar{c}\gamma_5 c \,, \tag{1.118}$$

such that the resulting $f_\mathrm{P}^i$, $h_\mathrm{P}^i$ for the two currents each yield a $3 \times 3$-matrix which we denote by $\left(f_\mathrm{P}^i\right)$, $\left(h_\mathrm{P}^i\right)$, now including flavor indices $i = l, s, c$ and physical states $\mathrm{P} = \eta, \eta', \eta_c$. The extended mixing scheme for axial vector and pseudoscalar matrix elements is then given by

$$\left(f_\mathrm{P}^i\right) = \Xi\left(\phi, \phi_g, \phi_c\right) \operatorname{diag}\left(f_l, f_s, f_c\right) + \mathcal{O}\left(\Lambda_1, 1/m_c^2\right) , \tag{1.119}$$

$$\left(h_\mathrm{P}^i\right) = \Xi\left(\phi, \phi_g, \phi_c\right) \operatorname{diag}\left(M_\pi^2 f_l, \left(2M_\mathrm{K}^2 - M_\pi^2\right) f_s, M_{\eta_c}^2 f_c\right) + \mathcal{O}\left(\Lambda_1, \Lambda_2, 1/m_c^2\right) , \tag{1.120}$$

employing the same single-angle mixing pattern for $u$, $d$ and $s$ that has already been introduced for the case of the $\mathrm{SU}\left(3\right)_F$ quark flavor basis and neglecting terms that are suppressed in the $1/m_c$ expansion. The mixing matrix reads

$$\Xi\left(\phi, \phi_c, \phi_g\right) = \begin{pmatrix} \cos\phi & -\sin\phi & -\phi_c \sin\phi_g \\ \sin\phi & \cos\phi & \phi_c \cos\phi_g \\ \phi_c \sin\left(\phi_g - \phi\right) & -\phi_c \cos\left(\phi_g - \phi\right) & 1 \end{pmatrix} , \tag{1.121}$$

implementing the additional assumption that the angle $\phi_c$ which parametrizes the charm admixture to the two light states is a small quantity. Since there is a dynamic charm quark included in our simulations it is in principle possible to investigate whether we observe a non-vanishing charm quark contribution to $\eta, \eta'$.

## 1.2   Lattice QCD

In this section we introduce the formulation of QCD in discrete Euclidean spacetime, which ultimately allows one to perform numerical simulations by means of Monte-Carlo methods. The original approach of quantizing a gauge theory on a Euclidean spacetime lattice was established in a paper by Wilson [45] which dates back to 1974. Since these days the procedure has become a common tool to treat the non-perturbative regime of QCD, thus large parts of the following presentation are based on standard textbooks [46–48].

### 1.2.1   QCD in Euclidean spacetime

Starting from the partition function of QCD in Eq. (1.16), the expectation value of any observable $O\left[\psi, \bar{\psi}, A\right]$ is given by

$$\langle O \rangle = \frac{1}{\mathcal{Z}} \int \mathcal{D}\psi \mathcal{D}\bar{\psi} \mathcal{D}A \, O\left[\psi, \bar{\psi}, A\right] \exp\left(i\mathcal{S}_\mathrm{QCD}\left[\psi, \bar{\psi}, A\right]\right) . \tag{1.122}$$

However, this expression itself is not yet suitable for numerical calculations. This is caused on the one hand by the oscillating behavior of the functional $\sim \exp\left(iS_\mathrm{QCD}\right)$ and on the other hand by the fermion fields being represented by anti-commuting Grassmann variables which cannot easily be implemented numerically. The first issue is resolved by applying a *Wick rotation* $x_0 \to -ix_0$, which transforms the Minkowski product into an Euclidean product

$$x^2 = x_0^2 - |\vec{x}|^2 \to -|x_E|^2 = -x_0^2 - |\vec{x}|^2 . \tag{1.123}$$

For the action this implies

$$i\mathcal{S}_{\mathrm{QCD}} \to -\mathcal{S}_{\mathrm{QCD},E} \,, \tag{1.124}$$

such that the integrands in the expression for the expectation value $\langle O \rangle$ and the partition function $\mathcal{Z}$ itself are each replaced by a real and exponentially damped, functional. From now on we work solely in Euclidean spacetime, hence it is convenient to identify $t \equiv x_0$ and suppress the index $E$ which has been used to label quantities in Euclidean spacetime.

The second obstacle can be circumvented by integrating out the fermionic fields analytically, which is possible as $\mathcal{Z}$ is formulated in terms of classical fields $\psi$, $\bar{\psi}$, $A_\mu$ only and does not involve any operators. For the partition function this leads to

$$\mathcal{Z} = \int \mathcal{D}A \det D \exp\left(-\mathcal{S}_G\left[A\right]\right) \,, \tag{1.125}$$

where $D = \gamma^\mu D_\mu - M$ denotes the Euclidean Dirac operator and $S_G$ the pure gauge part of the QCD action. Provided that $\det D$ is a real and positive definite quantity, the exponential factor in $\mathcal{Z}$ now simply represents a Boltzmann weight factor because the action $\mathcal{S}_G\left[A\right]$ is real as well and bounded from below. The functional determinant of the Dirac operator is given by the sum of vacuum diagrams and encodes the dynamics due to fermionic degrees of freedom. Moreover, it is also possible to integrate out the fermions in the expression for the expectation value $\langle O \rangle$. However, this requires the application of Wick's theorem to replace the time ordered product of fermion fields in the observable $O$ by a product of propagators $D^{-1}$. Defining the effective action

$$\mathcal{S}_{\mathrm{eff}}\left[A\right] = \int d^4x \left(-\log \det D + \mathcal{L}_G\right) \,, \tag{1.126}$$

one ends up with an expression for $\langle O \rangle$

$$\langle O \rangle = \frac{1}{\mathcal{Z}} \int \mathcal{D}A\, O\left[A, D^{-1}\right] \exp\left(-\mathcal{S}_{\mathrm{eff}}\left[A\right]\right) \,, \tag{1.127}$$

for which the integration measure depends only on the gauge fields. Albeit formulated in continuous Euclidean spacetime, this expression has a form which allows one to treat it numerically for a given lattice formulation. Nonetheless, there is an additional subtlety which is related to the fact that we are no longer working in Minkowski spacetime. This concerns the property of Hilbert space positivity and the existence of a non-negative, hermitian Hamiltonian, which are not guaranteed to hold in the Euclidean formulation. As it was shown by Osterwalder and Schrader [49, 50], these two properties have to be replaced by a condition which is called *reflection positivity* in order to be able to retain the full quantum field theory from a particular formulation in Euclidean spacetime.

Another complication is introduced by the fermionic determinant that arises as a consequence of integrating out the Grassmann fields. The numerical treatment of this determinant in lattice simulations turns out to be very expensive as it is a highly non-local object. Therefore, in the early days of lattice QCD it was common practice to employ the choice $\det D \equiv 1$ which is also known as the *quenched approximation*. This is equivalent to the use of a pure Yang-Mills action in the sea quark sector, i.e. setting the number of sea quarks $N_s$ to zero. Obviously, for this

$$C\left(p^2\right) \qquad\qquad D_0\left(p^2\right) \qquad\qquad D_1\left(p^2\right)$$
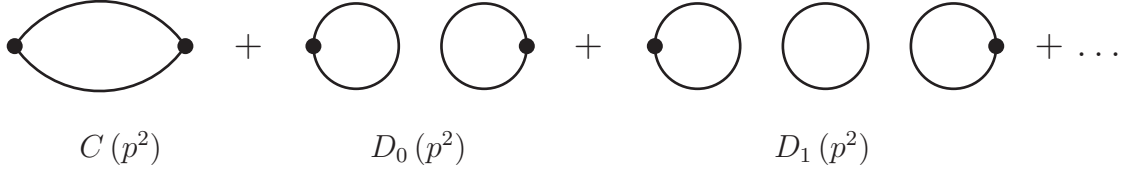
Figure 1.1: Sum of quark connected and disconnected diagrams contributing to the $\eta'$ propagator

constraint any dynamical effects mediated by sea quarks are neglected. In modern days, it has become feasible to include dynamical fermions, which turns out to be a crucial requirement to tackle the $\eta$–$\eta'$ system. The reason for this lies in a significant sea quark contribution to the propagator $G_{\eta'}\left(p^2\right)$ of the $\eta'$. This propagator can be decomposed in a connected diagram $C\left(p^2\right)$ and an infinite sum of disconnected loop graphs $D_i\left(p^2\right)$, with $i = 0, 1, 2, ...$ internal fermion loops as depicted in Fig. (1.1). The connected piece is just the usual Goldstone propagator which is given by

$$C\left(p^2\right) = \frac{1}{p^2 + M_\pi^2} . \tag{1.128}$$

Following the presentation in [46], the zeroth order *hairpin* insertion $D_0\left(p^2\right)$ can be expressed in the large-$N_c$ limit by

$$D_0\left(p^2\right) = -C\left(p^2\right) \frac{N_v \lambda^2}{N_c} C\left(p^2\right) , \tag{1.129}$$

where $\lambda^2/N_c$ is a contribution induced by the anomaly and $N_v$ denotes the number of valence quarks. Each further loop insertion yields an additional factor of $-N_s \lambda^2/N_c C\left(p^2\right)$, leading to a geometric series for the $\eta'$-propagator

$$G_{\eta'}\left(p^2\right) = C\left(p^2\right)\left(1 - \frac{N_v}{N_s}\right) + \frac{N_v}{N_c}\tilde{C}\left(p^2\right) , \quad \tilde{C}\left(p^2\right) = \frac{1}{p^2 + M_\pi^2 + \lambda^2 N_s/N_c} . \tag{1.130}$$

In the unquenched case $N_s = N_v = N_f > 0$ the first term in $G_{\eta'}\left(p^2\right)$ vanishes and the remaining expression yields a massive propagator, which becomes massless only in the limit $N_c \to \infty$, as expected. For partial quenching $N_v > N_s > 0$ there is still a massive $\eta'$-propagator but also an additional Goldstone mode occurs by virtue of the first term in $G_{\eta'}\left(p^2\right)$. However, in the quenched case $N_s = 0$ the situation is fundamentally different, because only the very first disconnected diagram in the bubble sum survives

$$G_{\eta'}\left(p^2\right)^{N_s=0} = C\left(p^2\right) - C\left(p^2\right) \frac{N_v}{N_c} \lambda^2 C\left(p^2\right) . \tag{1.131}$$

Besides the Goldstone propagator there is now a second state present which contains two poles and that has negative norm. Apart from the fact that the latter violates the constraints of a valid quantum field theory, this implies that there is no $\eta'$ meson present in quenched QCD regardless of the actual choice of $N_v$ and $N_c$.

### 1.2.2 Lattice regularization

As a next step towards a lattice regularized version of QCD we formally redefine the covariant derivative in terms of a limiting procedure

$$D_\mu = \lim_{a \to 0} \frac{1}{a} \left( \mathcal{U}(x; x + a\hat{\mu})\psi\left(x + a\hat{\mu}\right) - \psi\left(x\right) \right) , \qquad (1.132)$$

where $\mathcal{U}(x; y)$ is a SU $(3)$ matrix in color space, which is called a *parallel transporter* and that is required to transforms under local SU $(3)$ transformations as

$$\mathcal{U}(x; y) \to \Lambda\left(x\right)\mathcal{U}(x; y)\Lambda^{-1}\left(y\right) . \qquad (1.133)$$

The notation $\hat{\mu}$ refers to the unit vector in $\mu$-direction and $\mathcal{U}(x; y)$ itself is given by

$$\mathcal{U}(x; y) = \exp\left( -iag_sT^a \int\limits_x^y dz^\mu A_\mu^a\left(z\right) \right) . \qquad (1.134)$$

It is convenient to introduce a shorthand notation for the parallel transporter

$$\mathcal{U}_\mu(x) \equiv \mathcal{U}(x; x + a\hat{\mu}) , \qquad (1.135)$$

such that the argument $x$ refers to its position in spacetime and the index $\mu$ to its direction. Note that the transformation law in Eq. (1.133) implies that $\mathcal{U}(x + a\hat{\mu}; x) = \mathcal{U}_\mu(x)^\dagger$ holds. The parameter $a$ will later be identified with the lattice spacing of the discretized theory. For infinitesimal $a$ one can replace the integral in Eq. (1.134) by a linear approximation

$$\mathcal{U}_\mu(x) = \exp\left( -iag_sT^a A_\mu^a\left(x + \frac{a\hat{\mu}}{2}\right) + \mathcal{O}\left(a^3\right) \right) . \qquad (1.136)$$

Plugging this expression into Eq. (1.132) and taking the continuum limit $a \to 0$ reproduces the standard covariant derivative as introduced in Eq. (1.4).



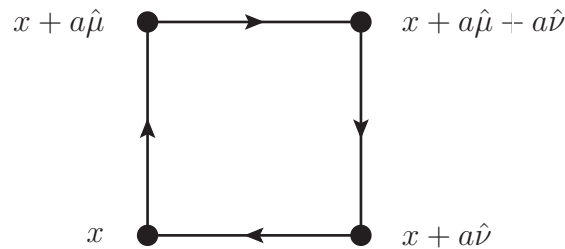Figure 1.2: Graphic depiction of a plaquette with arrows denoting the orientation of the parallel transporters. The origin of the first $\mathcal{U}_\mu(x)$ in Eq. (1.137) is positioned in the lower left corner.

Keeping $a$ finite in the expression for $D_\mu$, it is rather straightforward to formulate a naive discretization for the fermionic part $\mathcal{L}_F$ of the QCD Lagrangian. For the purely gluonic part

$\mathcal{L}_G$ we still need to construct a suitable, gauge-invariant expression. To this end we introduce the so-called *plaquette* $\mathcal{U}_{x,\mu\nu}^{1\times1}$ as the product of four parallel transporters with arguments chosen in such a way that they describe a unit lattice square in spacetime

$$\mathcal{U}_{x,\mu\nu}^{1\times1} = \mathcal{U}_\mu(x)\,\mathcal{U}_\nu(x+a\hat{\mu})\,\mathcal{U}_\mu(x+a\hat{\nu})^\dagger\,\mathcal{U}_\nu(x)^\dagger \, , \tag{1.137}$$

The plaquette itself is not yet gauge-invariant, but this can be cured by taking its trace, which we expand in $a$ to obtain

$$\mathrm{tr}\left[\mathcal{U}_{x,\mu\nu}^{1\times1}\right] = \mathrm{tr}\left[\mathbb{1}_{3\times3}\right] - \frac{1}{4}a^2 g_s^2 F_{\mu\nu}^a F^{a,\mu\nu} + \mathcal{O}\left(a^6\right) \, . \tag{1.138}$$

Besides the occurrence of an additional factor of $g^2 a^4$, the second term on the right-hand side exhibits the structure of $\mathcal{L}_G$.

In order to regularize QCD, one replaces the continuous Euclidean spacetime by a hyper-cubic lattice with spacing $a$. Furthermore, any actual simulation requires a finite number of lattice sites, hence one has to work in a finite volume specified by the extensions of the lattice in spatial and time direction, which we denote by $aT$ and $aL$, respectively. This requires some kind of boundary conditions, which are chosen periodic in our simulations with exception of the quark fields that are provided with anti-periodic boundary conditions in time direction. The latter choice is a necessary condition to obtain reflection positivity.

While the quark fields $\psi(x)$ are defined on the lattices sites themselves, the gauge fields are incorporated by the so-called *gauge links* which are given by the linear approximation of the parallel transporters as defined in Eq. (1.136) for finite (though still small) values of $a$. In this context one introduces the notion of a *gauge configuration* $\mathcal{U}$, which refers to the set of all gauge links on a given lattice

$$\mathcal{U} \equiv \{\mathcal{U}_\mu(x)\} \, . \tag{1.139}$$

In lattice simulations one first generates $n$ such gauge configurations $\{\mathcal{U}_\mu(x)\}_i$, by some Markov process

$$\{\mathcal{U}_\mu(x)\}_1 \xrightarrow{W} \{\mathcal{U}_\mu(x)\}_2 \xrightarrow{W} \ldots \xrightarrow{W} \{\mathcal{U}_\mu(x)\}_n \, , \tag{1.140}$$

such that they are distributed according to the weight

$$W\left[\mathcal{U}\right] = \det D \exp\left(-\mathcal{S}_G\left[\mathcal{U}\right]\right) \, . \tag{1.141}$$

For the stochastic estimation $\langle O \rangle_n$ of the expectation value $\langle O \rangle$ this yields

$$\langle O \rangle_n = \frac{1}{n} \sum_{i=1}^{n} O\left(\{\mathcal{U}_\mu(x)\}_i\right) \, , \tag{1.142}$$

with an error of $\mathcal{O}\left(1/\sqrt{n}\right)$, assuming statistically independent gauge configurations.

In the regularized theory the measure $\mathcal{D}A$ of the functional integral in the partition function is replaced by a product over gauge links

$$\int \mathcal{D}A \to \int \prod_{x,\mu} d\mathcal{U}_\mu(x) \, , \tag{1.143}$$

where on the right-hand side the gauge invariant *Haar measure* is employed for the integration over the link variables, which are matrix-valued elements of the compact group SU (3); see most standard textbooks for further details, e.g. [46, 47]. Similarly, the functional integration over fermionic degrees of freedom changes to

$$\int \mathcal{D}\psi \mathcal{D}\bar{\psi} \to \int d\psi\left(x\right) d\bar{\psi}\left(x\right) . \tag{1.144}$$

Furthermore, the integration in the action is replaced by a finite sum over lattice sites and links.

Finally we remark that the notion of "lattice regularization" refers to the fact that the introduction of discrete Euclidean spacetime imposes an ultra-violet cutoff $\sim a^{-1}$ to all momenta. As long as the volume is kept finite, the momenta $p$ take discrete values, given by

$$p = \pm\frac{2\pi n}{aL} , \quad n = 1, ..., L/2 . \tag{1.145}$$

### 1.2.3 Lattice actions

In this subsection we turn to the actual discretization of the QCD action. We will focus on the fermionic part of the action and restrict ourselves to a very brief introduction of lattice gauge actions as the latter are only of indirect relevance to this work.

Let us start by defining the covariant forward and backward difference operators $\nabla_\mu$ and $\nabla_\mu^*$ by

$$\nabla_\mu \psi\left(x\right) = \frac{1}{a}\left(\mathcal{U}_\mu(x)\psi\left(x + a\hat{\mu}\right) - \psi\left(x\right)\right) , \tag{1.146}$$

$$\nabla_\mu^* \psi\left(x\right) = \frac{1}{a}\left(\psi\left(x\right) - \mathcal{U}_\mu(x - a\mu)^\dagger \psi\left(x - a\hat{\mu}\right)\right) , \tag{1.147}$$

such that

$$D_\mu^{\text{naive}} = \frac{1}{2}\left(\nabla_\mu + \nabla_\mu^*\right) , \tag{1.148}$$

reproduces the covariant derivative in Eq. (1.132) in the naive continuum limit (i.e. formally sending $a \to 0$). The resulting fermionic lattice action reads

$$\mathcal{S}_F^{\text{naive}}\left[\psi, \bar{\psi}, \mathcal{U}\right] = a^4 \sum \bar{\psi}\left(x\right)\left(D_{\text{naive}} + m_0\right)\psi\left(x\right) . \tag{1.149}$$

where $D_{\text{naive}} = \gamma_\mu D_\mu^{\text{naive}}$ denotes the naive Dirac operator in Euclidean spacetime and $m_0$ is the bare quark mass. Although this action appears to be a valid choice, it is labeled naive as it suffers from a major deficiency known as *fermion doubling*. This refers to the occurrence of a multiplicity $m = 2^d$ in the fermionic spectrum, which is related to the spacetime dimension $d$. To understand the origin of this multiplicity consider the naive Dirac operator in momentum space

$$D_{\text{naive}}\left(p\right) = \frac{i}{a}\gamma_\mu \sin\left(ap_\mu\right) = i\gamma_\mu p_\mu + \mathcal{O}\left(a^2\right) , \tag{1.150}$$

which has zeros for $p_\mu = 0$, $\pi/a$. This yields $2^d - 1$ additional poles in the corresponding quark propagator, which represent the doublers in the spectrum. In order to cure this problem, Wilson introduced a modified version of the Dirac operator

$$D_{\mathrm{W}} = \frac{1}{2}\gamma_\mu \left( \nabla_\mu + \nabla_\mu^* \right) - \frac{1}{2}ar\nabla_\mu\nabla_\mu^* \,, \qquad (1.151)$$

which differs by a term of $\mathcal{O}(a)$ from the naive discretization, such that the covariant derivative is still retained in the continuum. Valid choices for the parameter $r$ are subject to the constraint $-1 \leq r \leq +1$. Although the *Wilson term* vanishes in the continuum, it affects the spectrum at finite values of the lattice spacing. This is again apparent from the momentum space representation of the Wilson Dirac operator

$$D_{\mathrm{W}}(p) = \frac{i}{a}\gamma_\mu \sin(ap_\mu) + \frac{2r}{a}\sin^2(ap_\mu) \,, \qquad (1.152)$$

where the second term yields an additional contribution of $\mathcal{O}(r/a)$ to the mass of the doublers in the corresponding propagator, hence shifting them to the cutoff scale and effectively removing them from the spectrum. However, the removal of doublers comes at a price as the Wilson term explicitly breaks chiral symmetry at finite values of the lattice spacing. This issue will be addressed in more detail in the next subsection. The breaking of chiral symmetry introduces lattice artifacts of $\mathcal{O}(a)$, whereas the naive action exhibits only artifacts of $\mathcal{O}(a^2)$. This represents a serious drawback in numerical simulations as the computational cost increases for smaller values of lattice spacing. Another complication concerns the renormalization of the bare quark mass, which is no longer purely multiplicative but receives an additive contribution. Therefore, it is convenient to introduce a subtracted bare quark mass

$$m_q = m_0 - m_{\mathrm{crit}} \,, \qquad (1.153)$$

where the *critical mass parameter* $m_{\mathrm{crit}}$ has to be properly determined such that a well-defined chiral limit is obtained, e.g such that the mass of the lightest pseudoscalar state vanishes in this limit.

The full Wilson action reads

$$\mathcal{S}^{\mathrm{W}} \left[ \psi, \bar{\psi}, \mathcal{U} \right] = a^4 \sum_x \bar{\psi} \left( D_W + m_0 \right) \psi + \mathcal{S}_G^{\mathrm{W}} \left[ \mathcal{U} \right] \,, \qquad (1.154)$$

where $\mathcal{S}_G^{\mathrm{W}}$ denotes the Wilson plaquette action

$$\mathcal{S}_G^{\mathrm{W}} \left[ \mathcal{U} \right] = \beta \sum_x \sum_{1 \leq \mu < \nu} \left( 1 - \frac{1}{3}\mathrm{Re}\,\mathrm{tr} \left[ \mathcal{U}_{x,\mu\nu}^{1 \times 1} \right] \right) \,. \qquad (1.155)$$

The parameter $\beta = 6/g_s^2$ is related to the bare coupling constant of QCD and for $\beta > 0$ the action is real and positive. In lattice simulations this action is usually rewritten by introducing the *hopping parameter*

$$\kappa \equiv \frac{1}{2am_0 + 8r} \,, \qquad (1.156)$$

which is employed in a rescaling of the fermion fields

$$\psi(x) \rightarrow \sqrt{\frac{2\kappa}{a^3}} \psi(x) \ , \qquad \bar{\psi}(x) \rightarrow \sqrt{\frac{2\kappa}{a^3}} \bar{\psi}(x) \ . \tag{1.157}$$

such that the resulting hopping parameter representation of the fermionic action takes the form

$$\mathcal{S}_F^{\mathrm{W}}\left[\psi, \bar{\psi}, \mathcal{U}\right] = \sum_x \Bigg( \bar{\psi}(x)\psi(x) - \kappa\bar{\psi}(x) \sum_\mu \Big( \mathcal{U}_\mu(x)(r + \gamma_\mu)\psi(x + a\hat{\mu})$$
$$+ \mathcal{U}_\mu(x - a\hat{\mu})^\dagger(r - \gamma_\mu)\psi(x - a\hat{\mu})\Big)\Bigg) \ . \tag{1.158}$$

We remark that the Wilson action complies with reflection positivity, provided that the value of the hopping parameter respects the constraint [51]

$$|\kappa| < \frac{1}{6} \ . \tag{1.159}$$

Before closing this subsection, we briefly mention that there are several ways to implement improvement with respect to cut-off effects of a given lattice formulation. As the computational cost of lattice simulations increases significantly for smaller values of $a$, such improvements help to avoid large corrections towards the continuum limit. A very general way to achieve such an improvement has been introduced by Symanzik [52–54] and is therefore known as *Symanzik improvement program*. It basically amounts to adding suitable counter terms $c_i O_i$ to the action $\mathcal{S}^{\mathrm{W}}\left[\psi, \bar{\psi}, \mathcal{U}\right]$, i.e.

$$\mathcal{S}^{\mathrm{W}}\left[\psi, \bar{\psi}, \mathcal{U}\right] \rightarrow \mathcal{S}^{\mathrm{W}}\left[\psi, \bar{\psi}, \mathcal{U}\right] + \sum_i c_i O_i\left[\psi, \bar{\psi}, \mathcal{U}\right] \ , \tag{1.160}$$

where $O_i\left[\psi, \bar{\psi}, \mathcal{U}\right]$ are operators restricted by the symmetries of the theory and the $c_i$ are coefficients that may be tuned to cancel discretization effects. For the fermionic part of the action it is possible add the so-called *Sheikholeslami-Wohlert term* $\delta\mathcal{S}_{\mathrm{sw}}\left[\psi, \bar{\psi}, \mathcal{U}\right]$ (also known as *clover term*) [55] to the action, which is basically given by a single dimension-five operator

$$\delta\mathcal{S}_{\mathrm{sw}}\left[\psi, \bar{\psi}, \mathcal{U}\right] = a^5 c_{\mathrm{sw}} \sum_x \bar{\psi}(x)\frac{i}{4}\sigma_{\mu\nu}\hat{F}_{\mu\nu}\left[\mathcal{U}\right]\psi(x) \ . \tag{1.161}$$

where $\hat{F}_{\mu\nu}\left[\mathcal{U}\right]$ denotes some lattice representation of the field strength tensor built from gauge links. However, it is in general not sufficient to simply tune the coefficient $c_{\mathrm{sw}}$ to obtain $\mathcal{O}(a)$-improved results using this action. Instead there may be further, operator-specific coefficients depending on the observable in question. The reason for this is that the occurrence of discretization effects is not solely tied to the action itself, but they may also be introduced by certain field combinations that are used to build observables, e.g. interpolating operators [56]. An $\mathcal{O}(a)$-improved fermionic action that does only require to tune a single parameter is obtained in the Wilson twisted mass formulation of lattice QCD which will be detailed in the next section.

Avoiding the discussion of any further technical details, we finally introduce two improved versions of the Wilson plaquette action which are relevant to this work and that can be obtained from the following generic gauge action

$$\mathcal{S}_G^{\text{generic}} = \frac{\beta}{3} \sum_x \left( b_0 \sum_{1 \le \mu < \nu} \left(1 - \operatorname{Re} \operatorname{tr} \left[\mathcal{U}_{x,\mu\nu}^{1\times 1}\right]\right) + b_1 \sum_{\mu \ne \nu} \left(1 - \operatorname{Re} \operatorname{tr} \left[\mathcal{U}_{x,\mu\nu}^{1\times 2}\right]\right) \right) , \qquad (1.162)$$

for suitable choices of the parameters $b_0$ and $b_1$, which are subject to the normalization condition $b_0 = 1 - 8b_1$. In this expression $\mathcal{U}_{x,\mu\nu}^{1\times 2}$ denotes rectangular $(1 \times 2)$ Wilson loops defined in analogy to the plaquette in Eq. (1.137). For the choice $b_1 = 0$ these rectangular loops do not contribute and the original, unimproved Wilson plaquette action $\mathcal{S}_G^{\text{W}}$ is recovered up to some physically irrelevant constant. Choosing $b_1 = -1/12$ yields the *tree-level Symanzik improved action* $\mathcal{S}_G^{\text{tlSym}}$ [57, 58] which has been used in simulations by the European Twisted Mass Collaboration (ETMC) with two dynamical quark flavors. Finally, the gauge configurations used in the computations for this work have been generated employing the even further improved *Iwasaki action* $\mathcal{S}_G^{\text{Iwa}}$, which is obtained for $b_1 = -0.331$ [59–61].

## 1.2.4   Symmetries on the lattice

While the standard Wilson action explicitly breaks chiral symmetry, it still shares the ordinary, discrete symmetries of QCD. First of all we have invariance under charge conjugation, which for our choice of representation of the Dirac matrices is defined by

$$\mathcal{C} : \begin{cases} \psi(x) & \to & i\gamma_0\gamma_2\bar{\psi}(x)^T \\ \bar{\psi}(x) & \to & -\psi(x)^T i\gamma_0\gamma_2 \\ \mathcal{U}_\mu(x) & \to & \mathcal{U}_\mu(x)^* \end{cases} . \qquad (1.163)$$

Similarly, the regularized theory is invariant under parity and time-reversal, which are given by

$$\mathcal{P} : \begin{cases} \psi(x_0, \vec{x}) & \to & \gamma_0 \psi(x_0, -\vec{x}) \\ \bar{\psi}(x_0, \vec{x}) & \to & \bar{\psi}(x_0, -\vec{x})\gamma_0 \\ \mathcal{U}_0(x_0, \vec{x}) & \to & \mathcal{U}_0(x_0, -\vec{x})^\dagger \\ \mathcal{U}_k(x_0, \vec{x}) & \to & \mathcal{U}_k(x_0, -\vec{x} - a\hat{k})^\dagger, \quad k = 1, 2, 3 \end{cases} , \qquad (1.164)$$

and

$$\mathcal{T} : \begin{cases} \psi(x_0, \vec{x}) & \to & i\gamma_0\gamma_5 \psi(-x_0, \vec{x}) \\ \bar{\psi}(x_0, \vec{x}) & \to & \bar{\psi}(-x_0, \vec{x}) i\gamma_0\gamma_5 \\ \mathcal{U}_0(x_0, \vec{x}) & \to & \mathcal{U}_0(-x_0 - a, \vec{x})^\dagger \\ \mathcal{U}_k(x_0, \vec{x}) & \to & \mathcal{U}_k(-x_0, \vec{x}), \quad k = 1, 2, 3 \end{cases} , \qquad (1.165)$$

respectively. Besides the fact that invariance under the combined symmetries $\mathcal{CPT}$ is required for any valid quantum field theory, it is in principle possible to violate discrete symmetries of continuum QCD at finite values of the lattice spacing. Nonetheless, it is favorable to retain as many such symmetries as possible in the regularized theory, as they are – for example –

required to classify interpolating operators with respect to their quantum numbers. If such regularization-dependent symmetry violations are present, they may introduce additional mixing between states, which renders a reliable extraction more difficult. As we will see this is the case for Wilson twisted mass fermions, which will be discussed in the next section.

Concerning the aforementioned explicit breaking of chiral symmetry by the Wilson term at finite values of the lattice spacing, we remark that there is a no-go theorem by Nielsen and Ninomiya [62–64] stating that it is impossible to construct a lattice action $\mathcal{S}_{\mathrm{latt}}$ simultaneously satisfying all of the following properties

1. $\mathcal{S}_{\mathrm{latt}}$ is hermitian and local (to be more precise, by "local" we mean that the Dirac operator has to be exponentially bounded).

2. $\mathcal{S}_{\mathrm{latt}}$ is chirally symmetric in the limit of vanishing quark masses.

3. $\mathcal{S}_{\mathrm{latt}}$ has the correct continuum limit.

4. There are no massless fermion doublers present in the spectrum.

In principle, this still allows for several ways to circumvent the occurrence of massless doublers. However, many modern formulations either explicitly break chiral symmetry (Wilson type fermions), or replace it by a different property that reproduces the correct chiral symmetry in the continuum, i.e. the Ginsparg-Wilson relation [65]

$$\{\gamma_5, D\} = aD\gamma_5 D \,, \tag{1.166}$$

where $D$ denotes the corresponding Dirac operator. This relation is fulfilled by the *overlap* formulation [66,67] sacrificing strict locality of the Dirac operator and the *domain wall* formulation [68] which is based on the introduction of an additional spacetime dimension. Although these exactly chiral formulations have advantages such as a well-defined topological charge, they come at a price, i.e. they are numerically much more expensive. For overlap fermions this results from being not local in the strict sense as – for example – Wilson fermions are, whereas for domain wall fermions this is simply caused by the additional spacetime dimension.

Another issue that needs to be addressed concerns once again global $\mathrm{U}(1)_A$ transformations. The reason for this is that one might question if and how the anomaly is realized in a lattice regularized theory. In continuum QCD, the anomaly arises as a result of the integration measure of the partition function requiring regularization and it is possible to derive the anomaly equation of QCD directly from the famous triangle graph. In the latter case one needs to introduce some regularization as well, because the corresponding diagrams exhibit a linear divergence. However, in a lattice regularized theory, such as the Wilson formulation, the regularization is already implemented at the level of the path integral, which explicitly breaks chiral symmetry and effectively removes the anomalous term in Eq. (1.39) at finite values of the lattice spacing. Although the correct anomaly may in principle be recovered in the continuum limit, it is not obvious that this actually holds for any such lattice formulation.

For Wilson fermions the subject has first been studied in [69], where it was shown that the correct anomaly is indeed reproduced for Wilson fermions in the continuum limit as a residual effect of the chiral symmetry breaking at finite values of the lattice spacing. Moreover, it was shown that the flavor non-singlet currents are conserved in the chiral continuum limit, just as it is the case for the chiral limit of standard QCD. Finally, we remark that one can actually prove that the anomaly is reproduced in the continuum limit for a rather general class of lattice actions subject to the following constraints [70]:

1. $\mathcal{S}_{\text{latt}}$ respects gauge invariance and has the correct continuum limit.

2. Its Dirac operator is local.

3. There are no massless fermion doublers present in the spectrum.

Leaving aside the fact that the existence of the correct continuum limit has not strictly been proven for any formulation, these conditions are fulfilled by Wilson type fermions and apply also to the other formulations that have been previously mentioned, with the exception of naive fermions that obviously do not exhibit the last required property.

## 1.3   Wilson twisted mass formulation

In this section we introduce the Wilson twisted mass (Wtm) formulation of LQCD which is used in our numerical studies. To illustrate the basic concept and features of this formulation we first consider the case of a mass degenerate doublet of light quarks. In a second step we proceed with the introduction of a non-degenerate doublet which is required to describe strange and charm quarks. The implementation of a non-degenerate quark doublet leads to a somewhat more complicated structure with respect to symmetries and renormalization. For a comprehensive review of the subject we refer to [71].

### 1.3.1   Light sector

Starting from the action of continuum QCD in Eq. (1.15) for a light, mass-degenerate quark doublet we consider an axial transformation of the corresponding doublet fields $\psi_l$, $\bar{\psi}_l$

$$\psi_l = \exp\left(\frac{i}{2}\omega_l\gamma_5\tau^3\right)\chi_l \,, \qquad \bar{\psi}_l = \bar{\chi}_l \exp\left(\frac{i}{2}\omega_l\gamma_5\tau^3\right) \,, \tag{1.167}$$

where the parameter $\omega_l$ denotes the *twist angle* in the light quark sector and $\chi_l$, $\bar{\chi}_l$ are the light quark doublet fields in the *twisted basis* as opposed to the *physical basis*, which is given in terms of the original fields $\psi_l$, $\bar{\psi}_l$. Single quarks in the twisted basis will be denoted by $\chi_u$, $\chi_d$ to distinguish them from the ones in the physical basis whenever necessary. Applying such axial transformations leaves the form of the action invariant, but the mass term picks up a phase factor

$$M \to M \exp\left(i\omega_l\gamma_5\tau^3\right) \,. \tag{1.168}$$

This allows us to write down the resulting continuum action of QCD in the twisted mass basis

$$\mathcal{S}_{F,l}^{\text{tm}}\left[\chi_l, \bar{\chi}_l, A_\mu\right] = \int d^4 x \bar{\chi}_l \left(\gamma_\mu D_\mu + m_q + i\mu_l\tau^3\right) \chi_l \, , \tag{1.169}$$

where the bare untwisted quark mass $m_q$ and the bare twisted mass $\mu_l$ are related to $M$ and $\omega_l$ via

$$M^2 = m_q^2 + \mu_l^2 \, , \qquad \tan\omega_l = \frac{\mu_l}{m_q} \, . \tag{1.170}$$

The index of the bare twisted mass $\mu_l$ is chosen in anticipation of this action being used for the light quark doublet, as it does not yet include a mass splitting term for the two quarks. Note that the choice of the Pauli-matrix for the twist-rotation is in principal arbitrary, although in the present case of a mass degenerate doublet it is convenient to choose $\tau^3$ as it leads to a flavor-diagonal lattice formulation. However, there is an additional constraint concerning the form of a twisted mass term which is given by the demand that the fermionic integration measure in the path integral has to be invariant under axial rotations

$$\chi_l \to \exp\left(\frac{i}{2}\omega_l\gamma_5\tau^3\right)\chi_l \, , \qquad \bar{\chi}_l \to \bar{\chi}_l \exp\left(\frac{i}{2}\omega_l\gamma_5\tau^3\right) \, , \tag{1.171}$$

similar to the ones that relate the twisted mass basis to the standard basis of QCD. Otherwise one would introduce additional, anomalous effects, altering the resulting physics. In practice, this implies that the relevant transformations as given in Eq. (1.167) have to be traceless, which is satisfied by the choice of $\tau^3$ (or any other Pauli matrix).

For the lattice regularized theory one applies the transformations in Eq. (1.167) to the Wilson action in Eq. (1.154), which yields the Wilson twisted mass action for light quarks [72]

$$\mathcal{S}_{F,l}^{\text{Wtm}}\left[\chi_l, \bar{\chi}_l, \mathcal{U}\right] = a^4 \sum_x \bar{\chi}_l \left(D_{\text{W}} + m_0 + i\mu_l\gamma_5\tau^3\right)\chi_l \, . \tag{1.172}$$

Again, the bare quark mass $m_0$ is related to the subtracted bare quark mass $m_q$ as defined in Eq. (1.153). Similar to the case of the pure Wilson action, one obtains a hopping parameter representation of the Wilson twisted mass action by applying the transformations in Eq. (1.157). For later purposes we define the Wilson twisted mass Dirac operator for a light, degenerate quark doublet by

$$D_l = D_{\text{W}} + m_0 + i\mu_l\gamma_5\tau^3 \, . \tag{1.173}$$

The crucial difference between the Wtm formulation and the continuum twisted mass formulation lies in their respective transformation behavior under axial rotations as defined in Eq. (1.171). Although these transformation leave the continuum twisted mass action invariant, this does not hold for the lattice regularized version, because the Wilson term $\sim ar\nabla_\mu\nabla_\mu^*$ is not invariant under such transformations. Therefore, the transition from the standard Wilson formulation to the Wilson twisted mass formulation yields a different lattice regularization and is not just a change of basis as for the case of the continuum action. Depending on the value of the twist angle $\omega_l$ this leads to different lattice artifacts for observables compared to the

standard Wilson formulation. We will discuss further implications of this property in the next subsection.

To gain further insights into the Wtm formulation it is instructive to consider the relation between currents in the physical and the twisted basis for all possible flavor structures of light quarks. For the (pseudo-)scalar and (axial) vector currents the relation reads

$$S_l^a = \bar{\psi}_l \frac{\tau^a}{2} \psi_l \quad \rightarrow \quad \begin{cases} \tilde{S}_l^a \cos \omega_l + i \tilde{P}_l^a \sin \omega_l \,, & a = 0, 3 \\ \tilde{S}_l^a \,, & a = 1, 2 \end{cases} \,, \tag{1.174}$$

$$P_l^a = \bar{\psi}_l \gamma_5 \frac{\tau^a}{2} \psi_l \quad \rightarrow \quad \begin{cases} \tilde{P}_l^a \cos \omega_l + i \tilde{S}_l^a \sin \omega_l \,, & a = 0, 3 \\ \tilde{P}_l^a \,, & a = 1, 2 \end{cases} \,, \tag{1.175}$$

$$V_{l,\mu}^a = \bar{\psi}_l \gamma_\mu \frac{\tau^a}{2} \psi_l \quad \rightarrow \quad \begin{cases} \tilde{V}_{l,\mu}^a \,, & a = 0, 3 \\ \tilde{V}_{l,\mu}^a \cos \omega_l + \tilde{A}_{l,\mu}^b \epsilon^{3ab} \sin \omega_l \,, & a = 1, 2 \end{cases} \,, \tag{1.176}$$

$$A_{l,\mu}^a = \bar{\psi}_l \gamma_\mu \gamma_5 \frac{\tau^a}{2} \psi_l \quad \rightarrow \quad \begin{cases} \tilde{A}_{l,\mu}^a \,, & a = 0, 3 \\ \tilde{A}_{l,\mu}^a \cos \omega_l + \tilde{V}_{l,\mu}^b \epsilon^{3ab} \sin \omega_l \,, & a = 1, 2 \end{cases} \,. \tag{1.177}$$

In these relations $S_l^a$, $P_l^a$, $V_{l,\mu}^a$ and $A_{l,\mu}^a$ on the left-hand side denote the light quark currents in the physical basis, whereas $\tilde{S}_l^a$, $\tilde{P}_l^a$, $\tilde{V}_\mu^a$ and $\tilde{A}_\mu^a$ on the right-hand side refer to currents in the twisted mass basis, assuming the same form of the currents in both cases apart from the replacements $\psi_l \leftrightarrow \chi_l$ and $\bar{\psi}_l \leftrightarrow \bar{\chi}_l$. In the above list the currents with flavor-singlet structure $\frac{\tau^0}{2} = \frac{1}{2} \mathbb{1}_{2 \times 2}$ have been included explicitly, as they are relevant for our purposes concerning $\eta$ and $\eta'$ mesons. In general, rotating to the twisted basis does not only change the spin structure but may also lead to mixing between currents with different $\gamma$-matrices depending on their respective flavor structure. However, the above transformation rules are greatly simplified for a particular choice of the twist angle, namely choosing $\omega_l = \pm \pi/2$ which is known as *maximal twist*. This corresponds to tuning $m_0$ to its critical value $m_{\text{crit}}$, such that $m_q = 0$. In this case there is no mixing present between different spin structures for the twisted currents on the right hand side, which is favorable as it leads to a much simpler pattern of renormalization.

As an example for Ward identities in the twisted basis, we briefly consider the partially conserved vector current (PCVC) and the partially conserved axial vector current (PCAC) relations, which differ from the standard identities

$$\partial_\mu \tilde{V}_{l,\mu}^a = -2\mu_l \tilde{P}_l^b \epsilon^{3ab} \,, \tag{1.178}$$

$$\partial_\mu \tilde{A}_{l,\mu}^a = 2m_q \tilde{P}_l^a + 2i\mu_l \left( \tilde{S}_l^0 \delta^{3a} + \tilde{S}_l^3 \delta^{0a} \right) + \sqrt{2N_f} \omega(x) \delta^{0a} \,. \tag{1.179}$$

From the PCVC relation one infers that the twisted quark mass (PCVC quark mass) renormalizes multiplicatively with $Z_\mu = 1/Z_P$, where $Z_P$ denotes the pseudoscalar flavor non-singlet renormalization constant. This incidentally implies that at maximal twist the light quark mass $m_l$ renormalizes only multiplicatively as well

$$m_l^R \equiv \mu_l^R = \frac{1}{Z_P} \mu_l \,, \tag{1.180}$$

as it is entirely given by the twisted mass $\mu_l$ for this special case. Clearly, this behavior is favorable for practical purposes compared to Wilson fermions, for which the light quark mass (i.e. the PCAC quark mass) is subject to additional, additive renormalization.

## 1.3.2 Properties and symmetries

The twisted mass formulation exhibits further advantages over the standard Wilson formulation besides the aforementioned, multiplicative renormalization of the light quark mass at maximal twist. Historically, the motivation to introduce the formulation was related to the occurrence of exceptional gauge configurations in quenched simulations which lead to very small eigenvalues for the Dirac operator. It can be shown that this is cured by introducing a twist term with non-zero $\mu_l$ acting as an infrared cutoff on the eigenvalues [73]. However, the most prominent advantage is the so-called *automatic $\mathcal{O}(a)$ improvement* which is obtained at maximal twist [74]. The denotation "$\mathcal{O}(a)$ improvement" refers to the absence of $\mathcal{O}(a)$ terms in a certain class of observables namely those of even parity, i.e. such an observable in the regularized theory differs at most by $\mathcal{O}(a^2)$ terms from the one in the continuum

$$\left\langle O\left[\psi_l, \bar{\psi}_l, \mathcal{U}\right]\right\rangle^{cont} + \mathcal{O}\left(a^2\right) = \left\langle O\left[\chi_l, \bar{\chi}_l, \mathcal{U}\right]\right\rangle^{latt} . \tag{1.181}$$

where the superscripts "*cont*" and "*latt*" indicate that the corresponding expectation values are to be evaluated employing continuum and lattice action, respectively. The term "automatic" adverts to the fact that the improvement is achieved for all parity-even observables simultaneously by tuning only a single parameter, unlike the case of the usual Symanzik improvement program that may involve the tuning of further, operator-dependent improvement coefficients. It was first shown in [75, 76] for the quenched approximation that this way to obtain $\mathcal{O}(a)$ improvement works in practice, i.e. it indeed leads to improved scaling properties compared to standard Wilson fermions. Similarly for $N_f = 2$ dynamical quark flavors this was shown in [77, 78] and there are strong indications that also for $N_f = 2 + 1 + 1$ simulations the scaling behavior at maximal twist is improved [79]. For the details on how to tune to maximal twist in actual simulations we refer to [79, 80], here we only briefly outline the basic idea. Taking renormalization into account, the twist angle is given by the relation

$$\tan \omega_l = \frac{\mu_l^R}{m_q^R} , \tag{1.182}$$

where the renormalized masses are given by $\mu_l^R = \mu_l/Z_P$ and $m_q^R = Z_m(m_0 - m_{\text{crit}})$ with $Z_m$ denoting the corresponding quark mass renormalization constant. From the lattice version of the PCAC relation in Eq. (1.179) it is possible to define the PCAC quark mass

$$am_{\text{PCAC}} = \frac{\sum_{\vec{x}} \langle 0| \nabla_0^* \tilde{A}_{l,0}^a(x) \tilde{P}_l^a(0) |0\rangle}{2\sum_{\vec{x}} \langle 0| \tilde{P}_l^a(x) \tilde{P}_l^a(0) |0\rangle} , \quad a = 1, 2 \tag{1.183}$$

where in any actual simulation the right-hand side has to be evaluated at sufficiently large Euclidean times; see also the dedicated discussion of correlation functions in section 2.2. The

PCAC quark mass is related to $m_q^R$ by

$$m_q^R = \frac{Z_A}{Z_P} m_{\text{PCAC}}, \tag{1.184}$$

where $Z_A$ denotes the axial vector flavor non-singlet renormalization constant. Therefore, the critical line can be determined by tuning the PCAC quark mass to zero, as Eq. (1.182) now takes the form

$$\tan \omega_l = \frac{\mu_l}{Z_A m_{\text{PCAC}}}. \tag{1.185}$$

For all further considerations we will assume maximal twist unless stated otherwise.

A drawback of the twisted mass formulation arises from the fact that the twisted mass term explicitly breaks parity and time reversal as defined in Eqs. (1.164),(1.165) as well as the flavor symmetry $\mathcal{F}^a$ of the action at finite values of the lattice spacing. This in principle allows for additional mixing between states in the regularized theory as these broken symmetries are not good quantum numbers anymore. However, although neither flavor symmetry nor $\mathcal{P}$, $\mathcal{T}$ alone are symmetries of the twisted mass action, the combination of any two of them remains a symmetry. Invariance under $\mathcal{PT}$ is fulfilled because $\mathcal{C}$ and $\mathcal{CPT}$ are symmetries of the action. In fact, successive application of $\mathcal{P}$, $\mathcal{T}$ flips the sign of the twisted mass term twice, hence leaving it invariant. Combining a discrete flavor rotation $\mathcal{F}^a$ with either $\mathcal{P}$ or $\mathcal{T}$ leads to the following modified fermionic symmetries at maximal twist

$$\mathcal{P}^a : \begin{cases} \chi_l\left(x_0, \vec{x}\right) & \rightarrow & i\gamma_0 \tau^a \chi_l\left(x_0, -\vec{x}\right) \\ \bar{\chi}_l\left(x_0, \vec{x}\right) & \rightarrow & -\bar{\chi}_l\left(x_0, -\vec{x}\right) i\tau^a \gamma_0 \end{cases} , \quad a = 1, 2, \tag{1.186}$$

$$\mathcal{T}^a : \begin{cases} \chi_l\left(x_0, \vec{x}\right) & \rightarrow & i\gamma_0 \gamma_5 \tau^a \chi_l\left(-x_0, \vec{x}\right) \\ \bar{\chi}_l\left(x_0, \vec{x}\right) & \rightarrow & \bar{\chi}_l\left(-x_0, \vec{x}\right) i\gamma_0 \gamma_5 \tau^a \end{cases} , \quad a = 1, 2, \tag{1.187}$$

which may be used in order to classify states in place of the standard symmetries. Note that the additional flavor rotation is equivalent to a sign change of the twisted mass term.

The fact that the twisted mass term breaks flavor symmetry can also be exploited to obtain a relation for the Dirac operator and its inverse, which proves useful in actual lattice simulations. While the standard Wilson operator exhibits a property known as $\gamma_5$-hermiticity, i.e.

$$D_{\text{W}} = \gamma_5 D_{\text{W}}^\dagger \gamma_5, \tag{1.188}$$

the hermitian conjugate of the twisted mass term picks up a sign, which effectively exchanges the flavor components, leading to

$$D_{uu}^{xy} = \gamma_5 \left(D_{dd}^{yx}\right)^\dagger \gamma_5, \qquad D_{dd}^{xy} = \gamma_5 \left(D_{uu}^{yx}\right)^\dagger \gamma_5, \tag{1.189}$$

where $D_{uu}^{xy} = \frac{1+\tau^3}{2} D_l^{xy}$ and $D_{dd}^{xy} = \frac{1-\tau^3}{2} D_l^{xy}$ refer to the up ($\chi_u$) and down ($\chi_d$) quark components of the twisted mass Dirac operator. Here the double flavor index notation has been used in anticipation of the case of a non-degenerate doublet, which will be discussed in the next subsection. The spacetime index structure is relevant for applications to correlation functions.

Since the light quark sector is flavor diagonal, the relation for the Dirac operator implies a similar one for the corresponding propagators $G_{uu}^{xy} = \left(D_{uu}^{xy}\right)^{-1}$ and $G_{dd}^{xy} = \left(D_{dd}^{xy}\right)^{-1}$

$$G_{uu}^{xy} = \gamma_5 \left(G_{dd}^{yx}\right)^{\dagger}\gamma_5\,, \qquad G_{dd}^{xy} = \gamma_5 \left(G_{uu}^{yx}\right)^{\dagger}\gamma_5\,. \tag{1.190}$$

This relation between up and down propagators simplifies the evaluation of certain correlation functions and it is one of the essential ingredients of a very powerful variance reduction technique exclusive to the twisted mass formulation of LQCD; see subsection 2.2.1 for further details.

Concerning the breaking of chiral symmetry at maximal twist, the situation is somewhat different compared to standard Wilson fermions. While both formulations share the invariance under $\mathrm{U}(1)_V$ symmetry they exhibit a different breaking pattern of $\mathrm{SU}(2)_V$ and $\mathrm{SU}(2)_A$ symmetries. To gain further insight, one considers the following twisted transformations

$$\mathrm{U}(1)_V^a : \begin{cases} \chi_l\left(x\right) & \rightarrow & \frac{1-i\gamma_5\tau^3}{\sqrt{2}}\exp\left(\frac{i}{2}\alpha_V^a\tau^a\right)\frac{1+i\gamma_5\tau^3}{\sqrt{2}}\chi_l\left(x\right) \\ \bar{\chi}_l\left(x\right) & \rightarrow & \bar{\chi}_l\left(x\right)\frac{1+i\gamma_5\tau^3}{\sqrt{2}}\exp\left(\frac{i}{2}\alpha_V^a\tau^a\right)\frac{1-i\gamma_5\tau^3}{\sqrt{2}} \end{cases}, \tag{1.191}$$

$$\mathrm{U}(1)_A^a : \begin{cases} \chi_l\left(x\right) & \rightarrow & \frac{1-i\gamma_5\tau^3}{\sqrt{2}}\exp\left(\frac{i}{2}\alpha_A^a\gamma_5\tau^a\right)\frac{1+i\gamma_5\tau^3}{\sqrt{2}}\chi_l\left(x\right) \\ \bar{\chi}_l\left(x\right) & \rightarrow & \bar{\chi}_l\left(x\right)\frac{1+i\gamma_5\tau^3}{\sqrt{2}}\exp\left(\frac{i}{2}\alpha_A^a\gamma_5\tau^a\right)\frac{1-i\gamma_5\tau^3}{\sqrt{2}} \end{cases}, \tag{1.192}$$

which correspond to the vector and axial vector subgroups $\mathrm{U}(1)_V^a$ and $\mathrm{U}(1)_A^a$ of the twisted $\mathrm{SU}(2)_V$ and $\mathrm{SU}(2)_A$. The group parameters are denoted by $\alpha_V^a$ and $\alpha_A^a$, respectively and there is no summation over group indices implied on the right-hand side. The ordinary Wilson and Wilson twisted mass formulation are both invariant under $\mathrm{U}(1)_V^3$ but for the charged subgroups given by $a = 1, 2$, it turns out that the twisted mass term is actually invariant under $\mathrm{U}(1)_V^1\otimes \mathrm{U}(1)_V^2\otimes \mathrm{U}(1)_V^3$, whereas the pure Wilson formulation is invariant under $\mathrm{U}(1)_A^1\otimes \mathrm{U}(1)_A^2\otimes \mathrm{U}(1)_V^3$. This implies that in the twisted mass formulation the charged vector current does not receive renormalization and that in the massless case the theory exhibits an exact charged axial vector symmetry. The former result can be used to show that the charged pion decay constant does not require any renormalization [75,81,82] (see also the discussion of observables in subsection 2.2.3), whereas the latter one is the reason why the charged pion is not affected by $\mathcal{O}\left(a^2\right)$ cutoff effects in the chiral limit unlike the neutral pion, as will be discussed in the subsection 1.3.5 in more detail.

### 1.3.3 Heavy sector

For the inclusion of the strange degree of freedom, which is essential to study the $\eta$–$\eta'$ system, it is necessary to introduce another doublet in the twisted mass formulation. In fact, it is an intrinsic feature of WtmLQCD that quark fields can only be implemented in doublets due to the required structure of the twisted mass term in flavor space. Again, we start form the standard continuum action of QCD as given in Eq. (1.15), considering a doublet of heavy quarks, denoted by $\psi_h$, $\bar{\psi}_h$. However, for technical reasons it is convenient to rewrite the general mass matrix $M$ in the following form

$$M \rightarrow M\tau^0 + \mu_\delta\tau^3\,, \tag{1.193}$$

such that the mass splitting is explicitly given by the term $\sim \mu_\delta \tau^3$, whereas the scalar $M$ on the right-hand side will be identified with the polar mass in the twisted basis. The bare masses for strange and charm are then given by

$$m_{c,s} = M \pm \mu_\delta \,. \tag{1.194}$$

Similar to the case of the light doublet, the continuum WtmLQCD action is related to the standard QCD action by an axial transformation of the form

$$\psi_h = \exp\left(\frac{i}{2}\omega_h\gamma_5\tau^1\right)\chi_h \,, \qquad \bar{\psi}_h = \bar{\chi}_h \exp\left(\frac{i}{2}\omega_h\gamma_5\tau^1\right) \,, \tag{1.195}$$

where $\chi_h$, $\bar{\chi}_h$ denote the heavy quark doublet in the twisted basis and the choice of $\tau^1$ is what has been used in actual simulations of ETMC [79]. We assume the twisted charm quark $\chi_c$ to be the upper component of $\chi_h$ whereas the strange quark $\chi_s$ is the lower one. The resulting action and its lattice regularized equivalent read [83]

$$\mathcal{S}_{F,h}^{\mathrm{tm}}\left[\chi_h, \bar{\chi}_h, A_\mu\right] = \int d^4x \bar{\chi}_h \left(\gamma^\mu D_\mu + m_q + i\mu_\sigma\gamma_5\tau^1 + \mu_\delta\tau^3\right)\chi_h \,, \tag{1.196}$$

and

$$\mathcal{S}_{F,h}^{\mathrm{Wtm}}\left[\chi_h, \bar{\chi}_h, \mathcal{U}\right] = a^4 \sum_x \bar{\chi}_h \left(D_{\mathrm{W}} + m_0 + i\mu_\sigma\gamma_5\tau^1 + \mu_\delta\tau^3\right)\chi_h \,, \tag{1.197}$$

respectively, such that the twisted mass Dirac operator for the heavy doublet takes the form

$$D_h = D_{\mathrm{W}} + m_0 + i\mu_\sigma\gamma_5\tau^1 + \mu_\delta\tau^3 \,, \tag{1.198}$$

where now again the term $\mu_\delta\tau^3$ is responsible for the mass splitting. In exact analogy to the light sector, the polar mass $M$ may be expressed in terms of $m_q$ and $\mu_\sigma$ via $M^2 = m_q^2 + \mu_\sigma^2$ and the relation for the heavy twist angle $\omega_h$

$$\tan\omega_h = \frac{\mu_\sigma}{m_q} \,, \tag{1.199}$$

implies that at maximal twist also $M = \mu_\sigma$ holds. For the resulting quark masses at $\omega_h = \pi/2$ a complication arises due to the different spin structure of the mass splitting term $\sim \mu_\delta$ compared to the twist term $\sim \mu_\sigma$. While $\mu_\sigma$ obtains a factor $Z_P^{-1}$ similar to $\mu_l$ before, the mass splitting $\mu_\delta$ renormalizes with the inverse of the flavor non-singlet scalar renormalization factor $Z_S$ such that the renormalized strange and charm quark mass are given by

$$m_{c,s}^R = Z_P^{-1}\mu_\sigma \pm Z_S^{-1}\mu_\delta = Z_P^{-1}\left(\mu_\sigma \pm Z\mu_\delta\right) \,, \tag{1.200}$$

where the ratio

$$Z = Z_P/Z_S \tag{1.201}$$

has been defined. As can be inferred from the second equality by dropping the overall factor $Z_P^{-1}$, the ratio $Z$ is required even for the bare quark masses. The possible values of the bare parameters $\mu_\sigma$ and $\mu_\delta$ are constrained by the demand of positivity for the fermionic determinant,

i.e. $\mu_\sigma > \mu_\delta$, which together with the above definition of $m_s^R$, $m_c^R$ yields a constraint on the ratio of pseudoscalar and scalar flavor non-singlet renormalization constants

$$Z = \frac{\mu_\sigma^R}{\mu_\delta^R} < \frac{m_c^R - m_s^R}{m_c^R + m_s^R} < 1 \,, \tag{1.202}$$

assuming $m_s^R < m_c^R$.

Applying the twist rotations in Eq. (1.195) to physical currents yields

$$S_h^a = \bar{\psi}_h \frac{\tau^a}{2} \psi_h \quad \rightarrow \quad \begin{cases} \tilde{S}_h^a \cos\omega_h + i\tilde{P}_h^a \sin\omega_h \,, & a = 0, 1 \\ \tilde{S}_h^a \,, & a = 2, 3 \end{cases} \,, \tag{1.203}$$

$$P_h^a = \bar{\psi}_h \gamma_5 \frac{\tau^a}{2} \psi_h \quad \rightarrow \quad \begin{cases} \tilde{P}_h^a \cos\omega_h + i\tilde{S}_h^a \sin\omega_h \,, & a = 0, 1 \\ \tilde{P}_h^a \,, & a = 2, 3 \end{cases} \,, \tag{1.204}$$

$$V_{h,\mu}^a = \bar{\psi}_h \gamma_\mu \frac{\tau^a}{2} \psi_h \quad \rightarrow \quad \begin{cases} \tilde{V}_{h,\mu}^a \,, & a = 0, 1 \\ \tilde{V}_{h,\mu}^a \cos\omega_h + \epsilon^{1ab} \tilde{A}_{h,\mu}^b \sin\omega_h \,, & a = 2, 3 \end{cases} \,, \tag{1.205}$$

$$A_{h,\mu}^a = \bar{\psi}_h \gamma_\mu \gamma_5 \frac{\tau^a}{2} \psi_h \quad \rightarrow \quad \begin{cases} \tilde{A}_{h,\mu}^a \,, & a = 0, 1 \\ \tilde{A}_{h,\mu}^a \cos\omega_h + \epsilon^{1ab} \tilde{V}_{h,\mu}^b \sin\omega_h \,, & a = 2, 3 \end{cases} \,. \tag{1.206}$$

where again the twisted currents $\tilde{S}_h^a$, $\tilde{P}_h^a$, $\tilde{V}_{h,\mu}^a$, $\tilde{A}_{h,\mu}^a$ are assumed to have the same form as the ones in the physical basis apart from the required replacements for the quark doublet fields $\psi_l \leftrightarrow \chi_l$ and $\bar{\psi}_l \leftrightarrow \bar{\chi}_l$.

Before turning to the discussion of maximal twist on the lattice, we briefly consider the PCVC and PCAC relations in the twisted mass basis for heavy quarks

$$\partial_\mu \tilde{V}_{h,\mu}^a = -2\mu_\sigma \epsilon^{1ab} P^b + 2i\mu_\delta \epsilon^{3ab} S^b \,, \tag{1.207}$$

$$\partial_\mu \tilde{A}_{h,\mu}^a = 2m_q \tilde{P}_h^a + 2i\mu_\sigma \left( \delta^{1a} \tilde{S}_h^0 + \delta^{0a} \tilde{S}_h^1 \right) + 2\mu_\delta \left( \delta^{3a} \tilde{P}_h^0 + \delta^{0a} \tilde{P}_h^3 \right) + \sqrt{2N_f} \omega(x) \delta^{0a} \,. \tag{1.208}$$

Apparently, the structure of these relations is more complicated than for a degenerate quark doublet, e.g. only the second component of the PCAC relation corresponds to the standard QCD case, whereas now all other components receive additional contributions.

As discussed in the previous subsection an important advantage of the twisted mass formulation is the feature of automatic $\mathcal{O}(a)$ improvement. For the case of a non-degenerate doublet this is achieved in a similar manner as for the degenerate doublet. However, in principle, one might have different bare untwisted quark masses $m_{l,0}$, $m_{h,0}$ for the light and the heavy sector instead of a common mass $m_0$ as used in Eqs. (1.172),(1.197). Nonetheless, it is possible and very convenient to demand $m_{l,0} = m_{h,0} \equiv m_0$ and tune only the light PCAC quark mass to zero to obtain automatic $\mathcal{O}(a)$ improvement in both sectors simultaneously [80,83]. In fact, the PCAC relation for the non-degenerate doublet in Eq. (1.208) allows to define a heavy PCAC quark mass on the lattice in analogy to Eq. (1.183)

$$am_{h,\text{PCAC}} = \frac{\sum_{\vec{x}} \langle 0 | \nabla_0^* \tilde{A}_{h,0}^2(x) \tilde{P}_h^2(0) | 0 \rangle}{2 \sum_{\vec{x}} \langle 0 | \tilde{P}_h^2(x) \tilde{P}_h^2(0) | 0 \rangle} \,, \tag{1.209}$$

which one might tune to zero separately, i.e. without making the choice $m_{l,0} = m_{h,0}$. Note that for any other component than $a = 2$ one needs to insert factors $Z_A^{-1}$ for the additional terms in the PCAC relation for consistency with the renormalization of the PCAC quark mass as defined in Eq. (1.183); see also the discussion in [80]. However, apart from the additional effort of tuning a second parameter, such a method suffers from a very serious drawback, which is the occurrence of quark disconnected diagrams in the correlation functions defining the PCAC quark mass in Eq. (1.209) that are notoriously noisy and difficult to calculate. The reason for this is the mass splitting term in the lattice action for the non-degenerate doublet, which renders the heavy quark sector non-diagonal in flavor space, i.e. $D_h$ exhibits off-diagonal components $D_{sc}^{xy}$, $D_{cs}^{xy}$. These allow for explicitly flavor violating propagators $G_{sc}^{xy}$ $G_{cs}^{xy}$ between strange and charm quarks, which are related to the flavor space components of the Dirac operator by the relation

$$\begin{pmatrix} G_{cc}^{xy} & G_{sc}^{xy} \\ G_{cs}^{xy} & G_{ss}^{xy} \end{pmatrix} = \begin{pmatrix} D_{cc}^{xy} & D_{sc}^{xy} \\ D_{cs}^{xy} & D_{ss}^{xy} \end{pmatrix}^{-1} . \tag{1.210}$$

The crucial point here is that the components on both sides are not directly related, e.g. $(D_{cc}^{xy})^{-1} \neq G_{cc}^{xy}$. Consequently, the $\gamma_5$-trick for the non-degenerate doublet takes a non-diagonal form as well

$$\begin{pmatrix} G_{cc}^{xy} & G_{sc}^{xy} \\ G_{cs}^{xy} & G_{ss}^{xy} \end{pmatrix} = \begin{pmatrix} \gamma_5 \left(G_{cc}^{yx}\right)^{\dagger} \gamma_5 & -\gamma_5 \left(G_{cs}^{yx}\right)^{\dagger} \gamma_5 \\ -\gamma_5 \left(G_{sc}^{yx}\right)^{\dagger} \gamma_5 & \gamma_5 \left(G_{ss}^{yx}\right)^{\dagger} \gamma_5 \end{pmatrix} . \tag{1.211}$$

Further implications of the flavor structure for the heavy quark doublet will be addressed in the context of interpolating operators and correlation functions; see also the next chapter and appendix B. In the following we shall restrict ourselves again to the case of maximal twist $\omega_l = \omega_h = \pi/2$, which is also assumed to be fulfilled in any actual numerical study discussed in this work.

### 1.3.4  Symmetries in the heavy sector

Due to the requirement of a mass splitting term for the heavy doublet, it is impossible to define a flavor-diagonal action in this case. Some relevant implications concerning the resulting currents in the twisted basis and renormalization have already been discussed in the last subsection. However, this feature also affects the symmetries of the action, which in general is less symmetric than the one for the degenerate doublet. In this subsection we include a dedicated discussion of the symmetries for the case of a non-degenerate quark doublet in the twisted mass formulation.

Again we start by considering $\mathcal{P}$ and $\mathcal{T}$, which are both violated in the twisted mass formulation and need to be combined with a discrete rotation in flavor space $\mathcal{F}^a$ to retain a symmetry of the action. In the light sector it was possible to use $\tau^1$ and $\tau^2$, but in the heavy sector the only possible choice leading to the required invariance of the action behavior is given by $\tau^3$. The resulting fermionic symmetries $\mathcal{P}^3 = \mathcal{P} \times \mathcal{F}^3$ and $\mathcal{T}^3 = \mathcal{T} \times \mathcal{F}^3$ of the twisted mass action read

$$\mathcal{P}^3 : \begin{cases} \chi_l(x_0, \vec{x}) & \to & i\gamma_0 \tau^3 \chi_l(x_0, -\vec{x}) \\ \bar{\chi}_l(x_0, \vec{x}) & \to & -\bar{\chi}_l(x_0, -\vec{x}) \, i\tau^3 \gamma_0 \end{cases} , \tag{1.212}$$

$$\mathcal{T}^3 : \begin{cases} \chi_l\left(x_0, \vec{x}\right) & \rightarrow & i\gamma_0\gamma_5\tau^3\chi_l\left(-x_0, \vec{x}\right) \\ \bar{\chi}_l\left(x_0, \vec{x}\right) & \rightarrow & \bar{\chi}_l\left(-x_0, \vec{x}\right)i\gamma_0\gamma_5\tau^3 \end{cases} , \tag{1.213}$$

Similar to the case of the degenerate doublet the flavor rotation corresponds to a sign flip for the twisted mass term $\mu_\delta \rightarrow -\mu_\delta$ and standard charge conjugation as defined in $\mathcal{C}$ in Eq. (1.163) remains a symmetry of WtmLQCD as well. Further effects of the reduced number of symmetries in the heavy quark sector concern the structure and mixing of interpolating operators which will be discussed in detail in subsection 2.1.

Finally, we remark that the remnant chiral symmetry of the action is also reduced by the mass splitting term, which is – for example – reflected by the occurrence of additional terms in the PCAC and PCVC relations as we saw in the last subsection. The transformations corresponding to the twisted versions of the $\mathrm{U}\left(1\right)_{A,V}^a$ subgroups for the heavy sector are given similar to Eqs. (1.191), but with $\tau^3$ replaced by $\tau^1$ in the twist rotations

$$\mathrm{U}\left(1\right)_V^a : \begin{cases} \chi_l\left(x\right) & \rightarrow & \frac{1-i\gamma_5\tau^1}{\sqrt{2}}\exp\left(\frac{i}{2}\alpha_V^a\tau^a\right)\frac{1+i\gamma_5\tau^1}{\sqrt{2}}\chi_l\left(x\right) \\ \bar{\chi}_l\left(x\right) & \rightarrow & \bar{\chi}_l\left(x\right)\frac{1+i\gamma_5\tau^1}{\sqrt{2}}\exp\left(\frac{i}{2}\alpha_V^a\tau^a\right)\frac{1-i\gamma_5\tau^1}{\sqrt{2}} \end{cases} , \tag{1.214}$$

$$\mathrm{U}\left(1\right)_A^a : \begin{cases} \chi_L\left(x\right) & \rightarrow & \frac{1-i\gamma_5\tau^1}{\sqrt{2}}\exp\left(\frac{i}{2}\alpha_A^a\gamma_5\tau^a\right)\frac{1+i\gamma_5\tau^1}{\sqrt{2}}\chi_l\left(x\right) \\ \bar{\chi}_l\left(x\right) & \rightarrow & \bar{\chi}_l\left(x\right)\frac{1+i\gamma_5\tau^1}{\sqrt{2}}\exp\left(\frac{i}{2}\alpha_A^a\gamma_5\tau^a\right)\frac{1-i\gamma_5\tau^1}{\sqrt{2}} \end{cases} , \tag{1.215}$$

Considering the flavor non-singlet symmetries, a brief calculation reveals that the twist term $i\mu_\sigma\gamma_5\tau^1$ is still invariant under $\mathrm{U}\left(1\right)_V^1 \otimes \mathrm{U}\left(1\right)_V^2 \otimes \mathrm{U}\left(1\right)_V^3$, whereas the mass splitting term is only invariant under $\mathrm{U}\left(1\right)_V^3$, such that at maximal twist the symmetry of the sum of both terms is reduced to $\mathrm{U}\left(1\right)_V^3$ as well. However, the singlet $\mathrm{U}\left(1\right)_V$ factor remains unbroken for both terms as expected.

## 1.3.5 Wilson chiral perturbation theory

Nowadays, lattice QCD simulations based on the Wilson discretization of the Dirac operator are performed with light dynamical quarks [79,84–90]. For decreasing values of the light quark mass at a fixed value of the lattice spacing the explicit breaking of chiral symmetry by the Wilson term causes a subtle interplay between mass and discretization effects. Therefore it is important to obtain an understanding of the size of these discretization effects, which in general depend on the observables in question. For sufficiently small values of the light quark mass and close to the continuum limit, the discretization effects can be described by Wilson chiral perturbation theory, which represents an extension of continuum $\chi$PT to include powers of the lattice spacing [91]. The following presentation of W$\chi$PT including the expressions relevant to this work is based on the one given in the publication of our results [2]. For a recent review on applications of $\chi$PT in the context of LQCD we also refer to [92].

First of all, we remark that the inclusion of terms proportional to powers of the lattice spacing in the chiral expansion leads to an extended counting scheme, which is given by

$$p = \mathcal{O}\left(\delta\right) , \quad m_q = \mathcal{O}\left(\delta^2\right) , \quad a = \mathcal{O}\left(\delta\right) . \tag{1.216}$$

Note that in the context of W$\chi$PT we do not employ large-$N_c$ counting rules. In general, this extension leads to the occurrence of additional, numerically unknown LECs, compared to standard $\chi$PT. These LECs depend on the choice of the lattice action and need to be determined from suitable, numerical simulations. Since the W$\chi$PT-related part of this work relies on the computation of light, pseudoscalar meson masses (i.e. the pion masses $M_{\text{PS}} \equiv M_{\pi^\pm}$ , $M_{\pi^0}$ and the so-called *connected neutral pion mass* $M_{\pi^0,c}$, which is calculated from the quark connected contributions to the neutral pion correlator) from Wilson twisted mass fermions, we may restrict ourselves to the case of SU$(2)_f$ symmetry and do neither include strange nor charm quarks explicitly. The resulting, partially quenched chiral Lagrangian depends on the renormalized version of the twisted quark mass matrix, which we denote by $M = m_0^{\text{R}} + i\mu_l^{\text{R}}\tau^3$ and must not be confused with the polar mass in previous subsections. After removing a term of $\mathcal{O}(a)$ by a suitable shift of the quark mass, the leading order Lagrangian reads [91, 93]

$$
\begin{aligned}
\mathcal{L}_{\text{W}\chi\text{PT}}^{\delta^2} = & + \frac{1}{8}f^2\,\text{tr}\big[\partial_\mu\Sigma\partial_\mu\Sigma^\dagger\big] - \frac{1}{4}f^2\,B_0\,\text{tr}\big[M^\dagger\Sigma + \Sigma^\dagger M\big] \\
& - \hat{a}^2 W_6'\,\Big(\text{tr}\big[\Sigma + \Sigma^\dagger\big]\Big)^2 - \hat{a}^2 W_7'\,\Big(\text{tr}\big[\Sigma - \Sigma^\dagger\big]\Big)^2 - \hat{a}^2 W_8'\,\text{tr}\big[\Sigma^2 + (\Sigma^\dagger)^2\big] ,
\end{aligned}
\tag{1.217}
$$

where the field $\Sigma$ collects the Goldstone bosons arising from the spontaneous breakdown of the chiral group SU$(2)_L \times$ SU$(2)_R$, in analogy to the field $U$ defined in Eqs. (1.50),(1.51). Again, the trace is understood to be taken in flavor space and we introduced the convenient abbreviation $\hat{a} = 2aW_0$ in the above expression. Compared to continuum two flavor $\chi$PT, the leading order effective Lagrangian exhibits four additional LECs $W_0$, $W_6'$, $W_7'$ and $W_8'$, which are specific to Wilson $\chi$PT and hence related to discretization effects.

Since W$\chi$PT predicts a non-trivial phase structure for Wilson type fermions in the lattice spacing and quark mass plane [91, 94, 95], it is interesting to determine the numerical values of these additional LECs. In fact, it can be shown that the sign of a certain combination of Wilson LECs determines if either the so-called *Aoki-scenario* [94] or the *Sharpe-Singleton-scenario* [91] is realized for a particular lattice formulation. The relevant combination of LECs is denoted by $c_2 \sim -(2W_6' + W_8')$ and the Aoki-scenario is indicated by positive values of this combination, whereas the Sharpe-Singleton-scenario is expected for negative values. There is evidence for both scenarios in LQCD investigations and the corresponding phase diagram has been studied by several groups [80, 96–106]. The Aoki-scenario was found to be realized in quenched simulations and the Sharpe-Singleton-scenario has been observed in dynamical simulations employing the Wilson twisted mass formulation at maximal twist [103–106]. In the twisted mass formulation, the sign of $c_2$ becomes manifest in the splitting of squared masses for the neutral pion and the charged pion, which is directly proportional to $c_2$ at leading order. A negative sign results in a lighter neutral pion mass $M_{\pi^0}$ compared to the charged one, $M_{\text{PS}}$. Therefore, measuring the mass-splitting allows to determine $c_2$ in the Wilson twisted mass formulation and gives access to the involved LECs of W$\chi$PT. However, this method is rather challenging due to the disconnected contributions that have to be evaluated for the neutral pion.

Before discussing the approach that is actually used in this work, we briefly mention that there are other ways to extract the LECs of W$\chi$PT. One possibility is given by matching analytical predictions for the spectrum of the Dirac operator in finite volume and with fixed index [107–113]

to lattice data, which has been done in [113–116]. Furthermore, it is possible to compute the LECs from the spectral density of the hermitian Wilson-Dirac operator [117–119] or from the lattice calculations of the pion scattering length [120,121], which has been extended to a partially quenched formulation in [122]. Considering a Wilson-type action for sea quarks and a different, chirally invariant one for valence quarks it is possible to construct a corresponding mixed action chiral effective Lagrangian [93, 123]. Such a mixed action setup has been studied in [124] for overlap fermions on a Wilson twisted mass sea, which again allowed to determine the relevant LECs.

In the present work we aim at calculating the LECs implementing an approach which has recently been proposed in [125]. This method is also based on the computation of pseudoscalar mesons masses employing Wilson twisted mass fermions. However, it does not require the neutral pion mass to determine the LEC $W_8'$, but only the splitting between the charged pion mass $M_{\mathrm{PS}}$ and the connected neutral pion mass $M_{\pi^0,c}$. Since for both of these quantities quark disconnected diagrams are absent, such a determination is expected to have a much more favorable signal-to-noise ratio compared to one that involves the full neutral pion correlator, allowing for an extraction of $W_8'$ with much better statistical precision. Nonetheless, the full neutral pion mass $M_{\pi^0}$ is required for the determination of $W_6'$, which is related to the mass-splitting $M_{\pi^0,c}^2 - M_{\pi^0}^2$ between the connected and the full neutral pion. Within our study we will also consider higher order corrections in the mass and lattice spacing to the splittings that determine the LECs. In the following we shall discuss some technical details of the method and introduce the relevant expressions from partially quenched W$\chi$PT which we match to the results of our lattice QCD calculations.

As already discussed, our simulations employ Wilson twisted mass fermions at maximal twist in order to obtain automatic $\mathcal{O}\left(a\right)$ improvement. This has to be taken into account at the level of the effective theory by setting $m_0 = 0$ in the effective Lagrangian in Eq. (1.217). The $\mathcal{O}\left(a^2\right)$ splitting between $M_{\mathrm{PS}}$ and $M_{\pi^0}$ is reproduced at finite values of the lattice spacing by the flavor symmetry breaking twisted mass term in Eq. (1.172). Similarly, $M_{\mathrm{PS}}$ also differs from $M_{\pi^0,c}$ and the corresponding, leading order expressions in partially quenched W$\chi$PT for the three masses are given by [125–128]

$$
\begin{aligned}
M_{\mathrm{PS}}^2 &= 2B_0\mu_l \,, \\
M_{\pi^0}^2 &= 2B_0\mu_\ell - 8a^2\left(2w_6' + w_8'\right), \\
M_{\pi^0,c}^2 &= 2B_0\mu_\ell - 8a^2\, w_8' \,,
\end{aligned}
\tag{1.218}
$$

where the notation

$$
w_i' = \frac{16W_0^2\, W_i'}{f^2}\,, \qquad i = 6, 8\,,
\tag{1.219}
$$

has been introduced. In the mass splittings

$$
M_{\mathrm{PS}}^2 - M_{\pi^0,c}^2 = 8a^2\, w_8'\,,
\tag{1.220}
$$

$$
\frac{1}{2}\left(M_{\pi^0,c}^2 - M_{\pi^0}^2\right) = 8a^2\, w_6'\,,
\tag{1.221}
$$

the LECs are disentangled such that it is possible to determine them individually. Moreover, from the expression for $M_{\pi^0}$ in Eq. (1.218) it can be inferred that the mass-splitting between the charged and the neutral pion is controlled by the previously mentioned combination

$$c_2 = -\frac{32W_0^2}{f^2}(2W_6' + W_8')\,.$$  (1.222)

Using Eqs. (1.218),(1.219) this expression can be rewritten in terms of masses or the parameters $w_i'$

$$c_2 = \frac{1}{4a^2}\left(M_{\pi^0}^2 - M_{\rm PS}^2\right) = -2\left(2w_6' + w_8'\right)\,.$$  (1.223)

As already mentioned, these W$\chi$PT expressions are partially quenched for the case of $N_f = 2 + 1 + 1$ dynamical quark flavors which we use in our simulations. Assuming that the strange and the charm quark decouple from the light sector in these quantities they can be used for $N_f = 2 + 1 + 1$ as well. The residual effects of the strange and the charm quark will then introduce an additional dependence of the LECs on the corresponding heavy quark masses.

For higher order W$\chi$PT expressions of the pion mass and its decay constant, we refer to [129–131] and [132] for the case of $N_f = 2$ and $N_f = 2 + 1 + 1$ dynamical quarks, respectively.

# Chapter 2

# Spectroscopy and analysis methods

The focus of this chapter lies on methods that are commonly employed in lattice calculations and relevant to this work. Large parts of it are dedicated to hadron spectroscopy, comprising its theoretical foundations, as well as the interpolating operators, correlation functions and observables that have actually been investigated in our studies. The most important tool reviewed in the context of the extraction of observables is the variational approach, leading to a generalized eigenvalue problem for the determination of energies and amplitudes of the desired states. Moreover, we discuss renormalization that has to be performed at the level of correlation functions and how we set the scale in our simulations as well as the the required extrapolations (i.e. chiral extrapolation, finite size effects and continuum limit) to obtain physical results for our observables.

Furthermore, we include a section on data analysis, which deals mainly with the methods of error estimation and fitting used in our investigations. Besides these more general aspects, we also briefly describe the factorizing fit model that we employ for certain parts of the analysis in addition to the generalized eigenvalue problem.

## 2.1 Interpolating operators

As we are interested in the lightest pseudoscalar mesons (i.e. the octet mesons and the $\eta'$) which are classified by quantum numbers $J^{P(C)} = 0^{P(C)}$, the simplest possible operators are given by local bilinears

$$\mathcal{O}\left(x\right) = c_\Gamma \bar{\psi}\left(x\right)\Gamma\psi\left(x\right) \ , \tag{2.1}$$

where again $\psi\left(x\right)$, $\bar{\psi}\left(x\right)$ denote quark fields in the physical basis and $\Gamma$ contains a spin and flavor structure composed of Dirac and Pauli matrices. The factor $c_\Gamma$ has been introduced for reasons of computational convenience and takes a value of either $1$ or $i$ such that the resulting operator is hermitean. From a theoretical point of view it is possible to allow for anti-hermitean operators as well, but this would yield purely imaginary correlators in addition to the real ones, leading to certain avoidable complications for the further analysis. Now the flavor and spin structure of

| $\Gamma$ | $(\mathcal{C}, \mathcal{P}, \mathcal{T})$ | $(\mathcal{P}^1, \mathcal{T}^1)$ | $(\mathcal{P}^2, \mathcal{T}^2)$ | $(\mathcal{P}^3, \mathcal{T}^3)$ |
|---|---|---|---|---|
| $(\mathbb{1}_s \tau^0)$ | $(+, +, +)$ | $(+, +)$ | $(+, +)$ | $(+, +)$ |
| $(\mathbb{1}_s \tau^1)$ | $(+, +, +)$ | $(+, +)$ | $(-, -)$ | $(-, -)$ |
| $(\mathbb{1}_s \tau^2)$ | $(+, +, +)$ | $(-, -)$ | $(+, +)$ | $(-, -)$ |
| $(\mathbb{1}_s \tau^3)$ | $(+, +, +)$ | $(-, -)$ | $(-, -)$ | $(+, +)$ |
| $(\gamma_5 \tau^0)$ | $(+, -, -)$ | $(-, -)$ | $(-, -)$ | $(-, -)$ |
| $(\gamma_5 \tau^1)$ | $(+, -, -)$ | $(-, -)$ | $(+, +)$ | $(+, +)$ |
| $(\gamma_5 \tau^2)$ | $(+, -, -)$ | $(+, +)$ | $(-, -)$ | $(+, +)$ |
| $(\gamma_5 \tau^3)$ | $(+, -, -)$ | $(+, +)$ | $(+, +)$ | $(-, -)$ |
| $(\gamma_0 \tau^0)$ | $(-, +, -)$ | $(+, -)$ | $(+, -)$ | $(+, -)$ |
| $(\gamma_0 \tau^1)$ | $(-, +, -)$ | $(+, -)$ | $(-, +)$ | $(-, +)$ |
| $(\gamma_0 \tau^2)$ | $(-, +, -)$ | $(-, +)$ | $(+, -)$ | $(-, +)$ |
| $(\gamma_0 \tau^3)$ | $(-, +, -)$ | $(-, +)$ | $(-, +)$ | $(+, -)$ |
| $(\gamma_0 \gamma_5 \tau^0)$ | $(-, -, +)$ | $(-, +)$ | $(-, +)$ | $(-, +)$ |
| $(\gamma_0 \gamma_5 \tau^1)$ | $(-, -, +)$ | $(-, +)$ | $(+, -)$ | $(-, +)$ |
| $(\gamma_0 \gamma_5 \tau^2)$ | $(-, -, +)$ | $(+, -)$ | $(-, +)$ | $(-, +)$ |
| $(\gamma_0 \gamma_5 \tau^3)$ | $(-, -, +)$ | $(+, -)$ | $(+, -)$ | $(-, +)$ |

Table 2.1: Quantum numbers $(\mathcal{C}, \mathcal{P}, \mathcal{T}, \mathcal{P}^{1,2,3}, \mathcal{T}^{1,2,3})$ for operators in the physical and twisted basis involving all four Dirac and flavor structures. The twisted mass symmetries $\mathcal{P}^{1,2,3}, \mathcal{T}^{1,2,3}$ are also symmetries in the physical basis and equivalent to standard $\mathcal{P}$ and $\mathcal{T}$ with respect to the resulting quantum numbers in this case. Note that any further normalization factors of actual interpolating operators do not affect the quantum numbers.

$\Gamma$ has to be chosen in such a way that it reproduces the (valence) flavor structure and quantum numbers of the desired states, i.e. the correct behavior under $\mathcal{P}$ and $\mathcal{C}$; cf. table (2.1) where the quantum numbers from physical $(\mathcal{C}, \mathcal{P}, \mathcal{T})$ and twisted mass symmetries in the light $(\mathcal{P}, \mathcal{T})$ and heavy sector $(\mathcal{P}, \mathcal{T})$ have been listed for all four flavor and spin structures. Within this work we restrict ourselves to scalar, pseudoscalar, vector and axial vector operators build from $\mathbb{1}_s$, $\gamma_0$ and $\gamma_5$, which means that we will not consider any operators involving factors of $\gamma_i$. The constraint $J = 0$ is satisfied by projecting to zero momentum and using only local operators.

After choosing the operators in the physical basis one has to apply the twist rotation using $\omega_l = \omega_h = \pi/2$ to obtain the operators that are actually used in our lattice simulations at maximal twist. Considering operators made solely of light quarks the operators used in our numerical simulation are in principle very similar to the currents discussed in subsections 1.3.1 and 1.3.3, besides some normalization factors. As mentioned before, the twisted mass formulation requires to introduce quark fields in doublets, implying that if one wants to use particular flavor components separately, one needs to introduce an additional flavor projector. However, such projections have not been considered at the level of the currents in Eqs. (1.203)–(1.206). In general, this is the case for any operator involving the non-degenerate doublet and as we will see, this procedure introduces additional mixing between operators of different spin in the twisted

basis. For the pion sector such complications do not occur as the corresponding interpolating operators consist solely of light quarks.

### 2.1.1 Pion sector

For the charged pion with quantum numbers $0^-$ there are two spin structures available in the physical basis which exhibit the correct quantum numbers i.e. pseudoscalar and vector currents as can be inferred from table (2.1). In addition, one may also consider the physical axial vector, because it is already known from the relations for the currents in Eqs. (1.205),(1.206) that in the twisted basis the flavor non-diagonal components of the vector and axial vector current mix at $\mathcal{O}(a)$ if the tuning to maximal twist is not assumed to be perfect, which one expects to be the case in any actual simulation. The resulting interpolating operators in the twisted basis are then given by

$$\frac{1}{\sqrt{2}}\bar{\psi}_l i\gamma_5\tau^a\psi_l \to \frac{1}{\sqrt{2}}\bar{\chi}_l i\gamma_5\tau^a\chi \qquad \equiv \mathcal{P}_l^a\,, \quad a=1,2\,, \tag{2.2}$$

$$\frac{1}{\sqrt{2}}\bar{\psi}_l\gamma_0\tau^a\psi_l \to \frac{1}{\sqrt{2}}\bar{\chi}_l i\gamma_0\gamma_5 i\epsilon^{3ab}\tau^b\chi \equiv \mathcal{A}_l^a\,, \quad a=1,2\,, \tag{2.3}$$

$$\frac{1}{\sqrt{2}}\bar{\psi}_l i\gamma_0\gamma_5\tau^a\psi_l \to \frac{1}{\sqrt{2}}\bar{\chi}_l\gamma_0 i\epsilon^{3ab}\tau^b\chi \qquad \equiv \mathcal{A}_l^a\,, \quad a=1,2\,, \tag{2.4}$$

where we used calligraphic symbols to denote the interpolating operators in the twisted basis such that they are distinguishable from the currents defined before. The index $l$ refers to the light sector to avoid any further ambiguities. In principle, any combination of these operators can be used to build correlation functions, although varying only the flavor structure does not yield any additional information, e.g. replacing $P^1$ by $P^2$. This is due to the residual $\mathrm{U}(1)_V^3$ symmetry of the twisted mass formulation which implies that the two charged pions are exactly mass degenerate.

In practice it is most convenient to exploit this ambiguity stemming from the flavor structure by using eigenstates of $\mathcal{C}$ which correspond to the flavor projectors $\tau^\pm = (\tau^1 \pm i\tau^2)/2$ instead of employing $\tau^1$ and $\tau^2$ separately, as it simplifies the formal structure of the operators and the resulting correlation functions; see also the following the subsection. The corresponding operators are then given by

$$\frac{1}{\sqrt{2}}\bar{\psi}_l i\gamma_5\tau^\pm\psi_l \to \frac{1}{\sqrt{2}}\bar{\chi}_l i\gamma_5\tau^\pm\chi \qquad \equiv \mathcal{P}_l^\pm\,, \tag{2.5}$$

$$\frac{1}{\sqrt{2}}\bar{\psi}_l\gamma_0\tau^\pm\psi_l \to \frac{1}{\sqrt{2}} \pm \bar{\chi}_l i\gamma_0\gamma_5\tau^\pm\chi \equiv \mathcal{A}_l^\pm\,, \tag{2.6}$$

$$\frac{1}{\sqrt{2}}\bar{\psi}_l i\gamma_0\gamma_5\tau^\pm\psi_l \to \frac{1}{\sqrt{2}} \pm \bar{\chi}_l\gamma_0\tau^\pm\chi \qquad \equiv \mathcal{A}_l^\pm\,. \tag{2.7}$$

Finally, we remark that in our study we restrict ourselves to the use of pseudoscalar and axial vector operators in the twisted basis. The reason for this is simply that the twisted mass vector

current turns out to be too noisy, such that it does not give any improvement for the signal quality. Besides, it is not explicitly needed for any particular observable we are interested in.

Concerning the interpolating operators in the physical basis the situation for the neutral pion is rather similar to the one for the charged pion, besides the fact that the flavor structure has to be replaced by the third component and that only pseudoscalar and axial vector currents may contribute. In fact, any further mixing is ruled out by twisted mass symmetries or flavor symmetry even if not considering maximal twist at all. The interpolating operators in the physical and the twisted basis are given by

$$\frac{1}{\sqrt{2}}\bar{\psi}_l i\gamma_5\tau^3\psi_l \rightarrow -\frac{1}{\sqrt{2}}\bar{\chi}_l\chi \qquad \equiv \mathcal{S}_l^0\,, \tag{2.8}$$

$$\frac{1}{\sqrt{2}}\bar{\psi}_l i\gamma_0\gamma_5\tau^3\psi_l \rightarrow \frac{1}{\sqrt{2}}\bar{\chi}_l i\gamma_0\gamma_5\tau^3\chi \equiv \mathcal{A}_l^3\,. \tag{2.9}$$

### 2.1.2   Kaon sector

Unlike the pions, the kaons are all mass degenerate states in the twisted mass formulation. However, a complication arises from the fact that one of the quark doublets is non-degenerate, which requires the use of an additional flavor projector to separate strange and charm quarks in the operators in the physical basis, leading to a more involved mixing structure in the twisted basis. This is the reason why it is in principle more convenient to use a mixed action setup with a flavor diagonal action in the valence sector to calculate kaon related quantities. In such a setup one does not need to deal with explicit flavor symmetry violation for strange and charm quarks, avoiding a complicated mixing structure in the twisted basis and unphysical transitions between states. Such an analysis was performed in [133]. Nonetheless, in our study we want to work with the unitary action for consistency reasons. We remark that since the kaon itself is not in the main focus of this work we did not include a dedicated discussion of the heavy-light currents in the previous section and for any further technical details concerning the kaon and $D$-meson sector we refer to [80,134]. Here we will only illustrate the basic ideas that lead to the interpolating fields that have actually been used in our studies.

In principle it is possible to employ all four available spin structures in the physical basis, i.e. $S$, $P$, $V$ and $A$, however, for our purposes it is sufficient to restrict ourselves to scalar and pseudoscalar sector, which can be treated separately from vector and axial vector sector, as mixing only occurs within each of these two groups. Furthermore, the vector and axial vector case can be treated in exact analogy and also it turns out that the additional operators do not improve the signal quality for any of the observables that are relevant to our investigations. Therefore, starting in the physical basis we consider the following operators

$$\mathcal{S}_{neutral}^{\pm,phys} = \bar{\psi}_l\left(\frac{1\pm\tau^3}{2}\right)\psi_h \qquad = \begin{cases} \bar{u}c \\ \bar{d}s \end{cases}\,, \tag{2.10}$$

$$\mathcal{S}_{charged}^{\pm,phys} = \bar{\psi}_l\left(\frac{\tau^1\pm i\tau^2}{2}\right)\psi_h \qquad = \begin{cases} \bar{u}s \\ \bar{d}c \end{cases}\,, \tag{2.11}$$

$$\mathcal{P}_{neutral}^{\pm,\,phys} = \bar{\psi}_l i\gamma_5 \left(\frac{1 \pm \tau^3}{2}\right)\psi_h \;=\; \begin{cases} \bar{u}i\gamma_5 c \\ \bar{d}i\gamma_5 s \end{cases}, \tag{2.12}$$

$$\mathcal{P}_{charged}^{\pm,\,phys} = \bar{\psi}_l i\gamma_5 \left(\frac{\tau^1 \pm i\tau^2}{2}\right)\psi_h = \begin{cases} \bar{u}i\gamma_5 s \\ \bar{d}i\gamma_5 c \end{cases}. \tag{2.13}$$

$$\tag{2.14}$$

Assuming again maximal twist and applying the twist rotations as defined in Eqs. (1.167),(1.195) one obtains the corresponding operators in the twisted basis

$$\mathcal{S}_{neutral}^{\pm,\,phys} \rightarrow \frac{1}{2}\begin{cases} +\bar{\chi}_u\chi_c - \bar{\chi}_u\chi_s + \bar{\chi}_u i\gamma_5\chi_c + \bar{\chi}_u i\gamma_5\chi_s \\ +\bar{\chi}_d\chi_c + \bar{\chi}_d\chi_s + \bar{\chi}_d i\gamma_5\chi_c - \bar{\chi}_d i\gamma_5\chi_s \end{cases} \equiv \mathcal{S}_{neutral}^{\pm,\,tm}, \tag{2.15}$$

$$\mathcal{S}_{charged}^{\pm,\,phys} \rightarrow \frac{1}{2}\begin{cases} -\bar{\chi}_u\chi_c + \bar{\chi}_u\chi_s + \bar{\chi}_u i\gamma_5\chi_c + \bar{\chi}_u i\gamma_5\chi_s \\ +\bar{\chi}_d\chi_c + \bar{\chi}_d\chi_s - \bar{\chi}_d i\gamma_5\chi_c + \bar{\chi}_d i\gamma_5\chi_s \end{cases} \equiv \mathcal{S}_{charged}^{\pm,\,tm}, \tag{2.16}$$

$$\mathcal{P}_{neutral}^{\pm,\,phys} \rightarrow \frac{1}{2}\begin{cases} +\bar{\chi}_u\chi_c - \bar{\chi}_u\chi_s - \bar{\chi}_u i\gamma_5\chi_c - \bar{\chi}_u i\gamma_5\chi_s \\ +\bar{\chi}_d\chi_c + \bar{\chi}_d\chi_s - \bar{\chi}_d i\gamma_5\chi_c + \bar{\chi}_d i\gamma_5\chi_s \end{cases} \equiv \mathcal{P}_{neutral}^{\pm,\,tm}, \tag{2.17}$$

$$\mathcal{P}_{charged}^{\pm,\,phys} \rightarrow \frac{1}{2}\begin{cases} -\bar{\chi}_u\chi_c + \bar{\chi}_u\chi_s - \bar{\chi}_u i\gamma_5\chi_c - \bar{\chi}_u i\gamma_5\chi_s \\ +\bar{\chi}_d\chi_c + \bar{\chi}_d\chi_s + \bar{\chi}_d i\gamma_5\chi_c - \bar{\chi}_d i\gamma_5\chi_s \end{cases} \equiv \mathcal{P}_{charged}^{\pm,\,tm}, \tag{2.18}$$

where we denoted single quarks in the twisted basis by $\chi_f, \bar{\chi}_f$ with $f = u, d, s, c$. The superscript $tm$ has been introduced to distinguish the present operators from the final ones and to indicate that the spin structure implied by the operator symbol ($\mathcal{S}$, $\mathcal{P}$) actually still refers to the physical basis. Although we had to keep the doublet structure in the light sector in order to apply the twist rotations, we can now drop all operators involving the up quark as they do not contain additional information. This effectively reduces the numbers of operators by a factor of two and is a direct consequence of the $\mathcal{P}^{1,2}$ and $\mathcal{P}^3$ symmetries in the light and heavy sector, respectively. Furthermore, it is convenient to disentangle the different spin and flavor combinations because this greatly simplifies the resulting correlation functions. Besides, it has the advantage that renormalization factors are avoided at the level of building the correlation function, such that they only need to added later in the analysis. The disentanglement can be achieved by applying a rotation $R_K \in SO(4)$ to the original vector of operators in the twisted basis, i.e.

$$(\mathcal{S}_{lh}^c, \mathcal{S}_{lh}^s, \mathcal{P}_{lh}^c, \mathcal{P}_{lh}^s)^T = R_K \left(\mathcal{S}_{neutral}^{\pm,\,tm}, \mathcal{S}_{charged}^{\pm,\,tm}, \mathcal{P}_{neutral}^{\pm,\,tm}, \mathcal{P}_{charged}^{\pm,\,tm}\right)^T \tag{2.19}$$

where the subscript $lh$ of the final interpolating operators refers to the light and heavy quarks that occur in each bilinear. The index $K$ for the rotation matrix has been introduced in anticipation of a similar matrix occurring for the case of the $\eta$–$\eta'$ system and $R_K$ has the following form

$$R_K = \frac{1}{2}\begin{pmatrix} +1 & +1 & -1 & +1 \\ +1 & +1 & +1 & -1 \\ +1 & -1 & +1 & +1 \\ -1 & +1 & +1 & +1 \end{pmatrix}. \tag{2.20}$$

The final set of interpolating operators read

$$\mathcal{S}_{lh}^c = \bar{\chi}_d\chi_c, \qquad \mathcal{S}_{lh}^s = \bar{\chi}_d\chi_s, \qquad \mathcal{P}_{lh}^c = \bar{\chi}_d i\gamma_5\chi_c, \qquad \mathcal{P}_{lh}^s = \bar{\chi}_d i\gamma_5\chi_s. \tag{2.21}$$

### 2.1.3 Flavor singlet sector

In the flavor singlet sector one needs to consider operators exclusively consisting of either light or heavy quarks, but no mixed operators as for the kaon. Again, for the heavy quarks an additional flavor structure is required to project out the non-degenerate strange and charm components. Concerning the spin structure, we restrict ourselves to pseudoscalar currents in the physical basis. In principle, it would be very useful to be able to study axial vector matrix elements as well, because they are required for a determination of mixing parameters without resorting to chiral perturbation theory for the case of the decay constant parameters $f_l$, $f_s$. However, in practice they turn out to be to noisy to allow for any meaningful analysis. Here we quote the axial vector operators solely for the sake of completeness and because they have not been discussed elsewhere for the case of heavy quarks in the twisted basis. For all further technical discussions we will restrict ourselves to the pseudoscalar case. In the light sector there are two operators in the physical basis, which are given by

$$\mathcal{P}_l^{0,phys} = \frac{1}{\sqrt{2}}\bar{\psi}_l i\gamma_5 \psi_l \,, \tag{2.22}$$

$$\mathcal{A}_l^{0,phys} = \frac{1}{\sqrt{2}}\bar{\psi}_l i\gamma_0\gamma_5 \psi_l \,, \tag{2.23}$$

while in the heavy sector we have two operators for each spin structure corresponding to charm ("+") and strange ("-") components

$$\mathcal{P}_h^{\pm,phys} = \bar{\psi}_h i\gamma_5 \frac{1 \pm \tau^3}{2} \psi_h \,, \tag{2.24}$$

$$\mathcal{A}_h^{\pm,phys} = \bar{\psi}_h i\gamma_0\gamma_5 \frac{1 \pm \tau^3}{2} \psi_h \,. \tag{2.25}$$

In the light sector it is straightforward to obtain the final operators similar to the case of the neutral pion by applying the twist rotation in Eq. (1.167) at maximal twist, which yields

$$\mathcal{P}_l^{0,phys} \to -\frac{1}{\sqrt{2}}\bar{\chi}_h \tau^3 \chi_h \ \equiv \mathcal{S}_l^3 \,, \tag{2.26}$$

$$\mathcal{A}_l^{0,phys} \to \frac{1}{\sqrt{2}}\bar{\chi}_h i\gamma_0\gamma_5 \chi_h \equiv \mathcal{A}_l^0 \,. \tag{2.27}$$

For the heavy sector the application of Eq. (1.195) at maximal twist leads to a mixing between spin structures, i.e. a mixing of scalar and pseudoscalar currents on the one hand and vector and axial vector currents on the other hand

$$\mathcal{P}_h^{\pm,phys} \to \bar{\chi}_h \left(-\tau^1 \pm i\gamma_5\tau^3\right) \chi_h \ \equiv \mathcal{P}_h^{\pm,tm} \,, \tag{2.28}$$

$$\mathcal{A}_h^{\pm,phys} \to \bar{\chi}_h \left(i\gamma_0\gamma_5 \mp i\gamma_0\tau^2\right) \chi_h \equiv \mathcal{A}_h^{\pm,tm} \,, \tag{2.29}$$

where the superscript $tm$ is employed similar to the case of the kaon to distinguish the present operators from the final ones. Besides, the spin structure indicated by the operator symbol still refers to the physical basis. In fact, the mixing in the heavy sector is maximal in the sense

that even for the case of non-maximally twisted quarks no further mixing occurs, which can also be inferred from table (2.1). For the further discussion we can now restrict ourselves to the case of the (physical) pseudoscalar operators because the remaining steps can be performed in exact analogy for the axial vector. In order to disentangle the contributions of different spin one applies a rotation in flavor space $R_{\eta,\eta'} \in \mathrm{SO}(3)$ to the vector of interpolating operators

$$\left(\mathcal{S}_l^3, \mathcal{S}_h^1, \mathcal{P}_h^3\right)^T = R_{\eta,\eta'} \left(\mathcal{S}_l^3, \mathcal{P}_h^{+,tm}, \mathcal{P}_h^{-,tm}\right)^T , \qquad (2.30)$$

where

$$R_{\eta,\eta'} = \begin{pmatrix} +1 & 0 & 0 \\ 0 & -\frac{1}{\sqrt{2}} & -\frac{1}{\sqrt{2}} \\ 0 & +\frac{1}{\sqrt{2}} & -\frac{1}{\sqrt{2}} \end{pmatrix} . \qquad (2.31)$$

In principle, it is not required to include the light sector in the rotation as it is not affected, however, including it will allow for a more compact notation in following discussions. The final set of interpolating operators in the heavy sector reads

$$\mathcal{S}_h^1 = \frac{1}{\sqrt{2}}\bar{\chi}_h \tau^1 \chi_h \qquad = \frac{1}{\sqrt{2}}\left(\bar{\chi}_c\chi_s + \bar{\chi}_s\chi_c\right) , \qquad (2.32)$$

$$\mathcal{P}_h^3 = \frac{1}{\sqrt{2}}\bar{\chi}_h \tau i\gamma_5 \tau^3 \chi_h = \frac{1}{\sqrt{2}}\left(\bar{\chi}_c i\gamma_5 \chi_c - \bar{\chi}_s i\gamma_5 \chi_s\right) . \qquad (2.33)$$

Before closing this section, we remark that in addition to the local operator discussed here, we also employ fuzzing which allows to create spatially non-local operators that can be used to increase our operators basis in many applications. Further details about this technique can be found in [135, 136].

## 2.2 Correlation functions and extraction of observables

In Eq. (1.127) we defined the expectation value of an arbitrary observable in LQCD after performing a Wick rotation to Euclidean spacetime and integrating out the Grassmann fields to allow for numerical treatment. Considering hadron spectroscopy one usually studies $n$-point functions of suitable interpolating operators, which for mesons made up of two valence quarks simplifies to the special case of 2-point functions (or matrices thereof), which are formally given in continuous Euclidean spacetime by

$$\mathcal{C}_{\mathcal{O}_i\mathcal{O}_j}(x,y) = \langle 0| T\mathcal{O}_i(x)\mathcal{O}_j(y)|0\rangle = \frac{1}{\mathcal{Z}} \int \mathcal{D}A\, \mathcal{O}_i(x)\mathcal{O}_j(y) \exp\left(-\mathcal{S}_{\mathrm{eff}}[A]\right) , \qquad (2.34)$$

where $\mathcal{O}_i$, $\mathcal{O}_j$ in the time-ordered product denote operators at source and sink that in practice have to be appropriately chosen to couple to the desired states. We remark that for our purposes it is sufficient to consider operators projected to zero momentum by summation over spatial components, which is why we restrict ourselves to the time dependence $x_0$, $y_0$ for the operators $\mathcal{O}_i(x)\,\mathcal{O}_j(y)$ in the following discussion.

Since we are interested in the particle spectrum of our lattice theory we need to establish a relation between correlation functions and the eigenvalues of the corresponding Hamiltonian $H$. For this we start by rewriting the above expression using the *transfer matrix* $\exp(aH)$

$$\mathcal{C}_{\mathcal{O}_i \mathcal{O}_j}(x_0, y_0) = \frac{1}{\mathcal{Z}} \text{tr} \left[ \mathcal{O}_i(x_0) \mathcal{O}_j(y_0) \exp(-HT) \right] \tag{2.35}$$

with

$$\mathcal{Z} = \text{tr} \left[ \exp(-HT) \right] . \tag{2.36}$$

In these expressions $T/a$ denotes the lattice size in time direction. Furthermore, we separated the time dependence of the operators by means of appropriate factors of the transfer matrix, i.e. $\mathcal{O}_i(x_0) = \exp(Hx_0) \mathcal{O}_i \exp(-Hx_0)$ and use the cyclic property of the trace to obtain

$$\mathcal{C}_{\mathcal{O}_i \mathcal{O}_j}(x_0, y_0) = \frac{1}{\mathcal{Z}} \text{tr} \left[ \mathcal{O}_i \exp(-H(x_0 - y_0)) \mathcal{O}_j \exp(H(x_0 - y_0 - T)) \right] . \tag{2.37}$$

Finally, defining $t = x_0 - y_0$ and inserting a complete set of eigenstates $|m\rangle$, $H|m\rangle = E_m|m\rangle$ yields

$$\mathcal{C}_{\mathcal{O}_i \mathcal{O}_j}(t) = \frac{1}{\sum_n \exp(-E_n T)} \sum_{m,n} \langle n| \mathcal{O}_i |m\rangle \exp(-E_m t) \langle m| \mathcal{O}_j |n\rangle \exp(E_n(t - T)) \tag{2.38}$$

For sufficiently large values of $T$ and $E_1 - E_0 > 0$ we may write

$$\mathcal{Z} = \sum_n \exp(-E_n T) = \exp(-E_0 T) \left( 1 + \mathcal{O}(\exp(-E_1 T)) \right) . \tag{2.39}$$

At this point it is instructive to consider the two possible cases $i = j$ and $i \neq j$ separately to gain further insight into the analytic structure of the correlation functions. First we will restrict ourselves to the choice of equal operators at source and sink $i = j$. Keeping only the lowest lying state and defining its mass by $m^{(1)} = E_1 - E_0$ we are left with

$$\mathcal{C}_{\mathcal{O}_i \mathcal{O}_i}(t) = |\langle 0| \mathcal{O}_i |0\rangle|^2 + |\langle 0| \mathcal{O}_i |1\rangle|^2 \left( \exp\left(-m^{(1)} t\right) + \exp\left(m^{(1)} t - m^{(1)} T\right) \right) . \tag{2.40}$$

The very first term is only present if the operator $\mathcal{O}_i$ exhibits a non-vanishing vacuum expectation value. In general this will be the case unless it is explicitly ruled out by any symmetry, i.e. a non-zero vacuum expectation value arises only if the operator is even under all discrete symmetries of the theory (e.g. $\mathcal{T}^{1,2,3}, \mathcal{P}^{1,2,3}$), which in practice turns out to be a very restrictive condition. In fact, for the interpolating operators that have been discussed in the previous subsection, a vacuum expectation value occurs only for one of the operators relevant to the neutral pion, i.e. the scalar operator $\mathcal{S}_l^0$ in Eq. (2.8) which is relevant to the neutral pion and that transforms even under all symmetries, c.f. table 2.1. The correlation functions that are actually used in our analysis are defined without this first term, which means that one has to subtract it before sewing together the disconnected graphs for the neutral pion.

The remaining two terms show a cosh-like behavior in time, i.e.

$$\mathcal{C}_{\mathcal{O}_i \mathcal{O}_i}(t) \sim 2 |\langle 0| O_i |1\rangle|^2 \exp\left(m^{(1)} \frac{T}{2}\right) \cosh\left(m^{(1)} \left(\frac{T}{2} - t\right)\right) , \tag{2.41}$$

which allows to extract the mass of the ground state by fitting the correlation at large Euclidean times $t$. A complementary method is given by the *effective mass*

$$m_{\text{eff}} = \log\left(\frac{\mathcal{C}_{\mathcal{O}_i\mathcal{O}_i}(t)}{\mathcal{C}_{\mathcal{O}_i\mathcal{O}_i}(t+1)}\right) \tag{2.42}$$

that for large Euclidean times $t$ asymptotically approaches a plateau from which one can determine the mass of the ground state as well. Moreover, we remark that one may exploit the symmetry of the correlation function to further improve the signal quality by shifting the origin in time to $T/2$, i.e. replacing $t \to t - T/2$ and average over positive an negative times to improve the signal quality. However, the correlation between data at positive and negative times usually tends to be very large, such that this yields only a rather moderate improvement in practice.

For the case of cross-correlators, i.e. different operators at source and sink $i \neq j$, the situation is slightly more complicated, because instead of Eq. (2.40) one obtains

$$\mathcal{C}_{\mathcal{O}_i\mathcal{O}_j}(t) = \langle 0|\,\mathcal{O}_i\,|0\rangle\,\langle 0|\,\mathcal{O}_j\,|0\rangle + \langle 0|\,\mathcal{O}_i\,|1\rangle\,\langle 0|\,\mathcal{O}_j\,|1\rangle^*\exp\left(-m^{(1)}t\right)$$
$$+ \langle 0|\,\mathcal{O}_i\,|1\rangle^*\,\langle 0|\,\mathcal{O}_j\,|1\rangle\exp\left(m^{(1)}(t-T)\right). \tag{2.43}$$

First of all we remark that again a non-vanishing vacuum expectation value may be present if is not prohibited by symmetries for any of the two operators $\mathcal{O}_i$, $\mathcal{O}_j$. To reveal further details of the functional dependence on Euclidean time one rewrites this expression in terms of real $R_{i,j} = \text{Re}\,\langle 0|\,\mathcal{O}_{i,j}\,|1\rangle$ and imaginary parts $I_{i,j} = \text{Im}\,\langle 0|\,\mathcal{O}_{i,j}\,|1\rangle$ of the amplitudes, performs the shift $t \to t - T/2$ and removes its vacuum expectation value, resulting in

$$\mathcal{C}_{\mathcal{O}_i\mathcal{O}_j}(t) = \exp\left(-m^{(1)}\frac{T}{2}\right)\left((R_iR_j + I_iI_j)\cosh\left(m^{(1)}t\right) + i\,(R_iI_j - I_iR_j)\sinh\left(m^{(1)}t\right)\right). \tag{2.44}$$

Depending on the behavior of the operators under $\mathcal{T}^{1,2,3}$ symmetry as listed in table 2.1 (or standard time reversal for operators in the physical basis), either the cosh-like or the sinh-like contributions survive. For example, the operators $\mathcal{S}_l^3$, $\mathcal{S}_h^1$ and $\mathcal{P}_h^3$ that are relevant to the flavor singlet sector and correspond to pseudoscalar operators in the physical basis transform odd under $\mathcal{T}^{1,2}$ or $\mathcal{T}^3$, respectively, which is why all resulting cross-correlators are cosh-like. Note that the actual form of the correlators is also affected by the choice of boundary conditions, which in our simulations are antiperiodic in time for the quark fields (and periodic in the spatial components). This has to be taken into account when averaging over positive and negative $t$-values.

Before we discuss how correlation functions are calculated numerically in the next subsection, we briefly consider the correlation functions resulting from the interpolating operators that have been used in this work. For the charged pion as well as the kaon sector, these correlation functions take a particularly simple form, i.e. they consist only of a single quark connected contribution. In general, on the lattice we will consider two-point correlation function matrices of the form

$$\mathcal{C}(t) = a^3\sum_{\vec{x}}\langle 0|\,\vec{\mathcal{O}}(0)\otimes\vec{\mathcal{O}}(x)^\dagger\,|0\rangle, \tag{2.45}$$

where $\vec{\mathcal{O}}$ denotes a suitable vector of interpolating operators, occurring at source $(0)$ and sink $(x)$. Note that here the hermitean conjugate is understood to be taken element-wise on the vector of interpolating operators $\vec{\mathcal{O}}(x)$. For the charged pion only light quarks contribute and the full correlation function matrix in the above equation, involving all operators defined in Eqs. (2.5)–(2.7), can be written as

$$\mathcal{C}^{\pi^\pm} = a^3 \sum_{\vec{x}} \langle 0 | T \vec{\mathcal{O}}^- (0) \otimes \vec{\mathcal{O}}^+ (x) | 0 \rangle \ , \qquad (2.46)$$

where we defined $\vec{\mathcal{O}}^\pm = \left( \mathcal{P}_l^\pm , \mathcal{A}_l^\pm , \mathcal{V}_l^\pm \right)^T$ and applied the relation $\mathcal{O}_i^+ = \left( \mathcal{O}_i^- \right)^\dagger$, which holds for any of the operators labeled by $i = 1, 2, 3$. A single matrix element is described by the following generic expression

$$\mathcal{C}^{\pi^\pm}_{\mathcal{O}_i^+ \mathcal{O}_j^-} (t) = -a^3 \sum_{\vec{x}} \mathrm{tr} \left[ \gamma_5 \left( G_{uu}^{0x} \right)^\dagger \gamma_5 \Gamma_i G_{uu}^{0x} \Gamma_j \right] \ , \qquad (2.47)$$

where $\Gamma_{i,j}$ denotes the Dirac structure of the operators $\mathcal{O}_{i,j}^\pm$. Note that in the above expressions translational invariance on the lattice has been exploited to put one of the operators at the origin and the sum indicates the projection to zero momentum by summation over spatial components. Moreover, $\gamma_5$-hermiticity has been used to replace a down quark propagator by an up quark propagator. In fact, we also apply $\gamma_5$-hermiticity in exactly the same way for any other correlation function to allow for a unified implementation of certain routines in our codes.

In the kaon sector the vector of interpolating operators in Eq. (2.45) is given by the operators in Eq. (2.21), i.e.

$$\vec{\mathcal{O}}^K = \left( \mathcal{S}_{lh}^c , \mathcal{S}_{lh}^c , \mathcal{S}_{lh}^c , \mathcal{S}_{lh}^c \right)^T \ . \qquad (2.48)$$

Again it is possible to describe all resulting correlation functions by a single, generic expression

$$\mathcal{C}_{ij}^K (t) = -a^3 \sum_{\vec{x}} \mathrm{tr} \left[ \gamma_5 \left( G_{uu}^{0x} \right)^\dagger \gamma_5 \Gamma_i G_{f_i f_j}^{0x} \Gamma_j \right] \ , \qquad (2.49)$$

where $f_{i,j} = s, c$ denotes the heavy quark flavor in each operator and $\Gamma_{i,j}$ again the Dirac structure at source and sink. Note that in the above expression we introduced the simplified notation $\mathcal{C}_{ij}^K (t) \equiv \mathcal{C}_{\mathcal{O}_i^K \mathcal{O}_j^K}^K (t)$ which is unambiguous, if the same vector of interpolating operators is used at source and sink.

For the case of the neutral pion and the flavor singlet sector the resulting correlation functions involve disconnected diagrams leading to a more complicated structure, which is why they have been listed explicitly in appendix B. In particular they contain relative signs and factors and non-trivial structures in flavor space for the heavy quark operators occurring for $\eta$, $\eta'$.

Finally, we remark that the size of the resulting correlation matrices may be increased by the additional use of fuzzed operators as mentioned before. In this case every matrix element $\mathcal{C}_{\mathcal{O}_i \mathcal{O}_j}$ is replaced by a $2 \times 2$ submatrix

$$\mathcal{C}_{ij}^{LF} (t) = a^3 \sum_{\vec{x}} \langle 0 | T \vec{\mathcal{O}}_i^{LF} (0) \otimes \vec{\mathcal{O}}_j^{LF} (x)^\dagger | 0 \rangle \ , \qquad \vec{\mathcal{O}}_{i,j}^{LF} = \left( \mathcal{O}_{i,j}^L , \mathcal{O}_{i,j}^F \right)^T \ , \qquad (2.50)$$

which is built from local and fuzzed operators $\mathcal{O}_{i,j}^L$ and $\mathcal{O}_{i,j}^F$, respectively. However, this has no influence on the flavor structure, i.e. these submatrices are diagonal in flavor space and hence all further analysis steps, e.g. rotations in flavor space, can be trivially extended to cover this case as well.

### 2.2.1 Calculation of correlation functions

For the numerical evaluation of correlation functions we resort to stochastic methods as described in [136], which allow to extract the information contained in the gauge configurations more efficiently than by the use of simple point sources, which are non-zero only for a single spin-color component. Before detailing the actual procedures, we remark that any inversions that are required to calculate correlation functions within this work have been performed using the open source tmLQCD suite [137]. The basic idea behind any stochastic method is the introduction of randomly generated sources $\xi_{A,\alpha}^{x,r}$, where the index $r = 1, ..., R$ denotes different samples for each gauge configuration. The indices $A$ and $\alpha$ label color and spin. Since most of the following discussion is independent of flavor structures we will suppress flavor indices in this context unless explicitly needed. In the limit of a large number of samples $R \to \infty$ we demand the following relations

$$\lim_{R\to\infty} \frac{1}{R} \sum_{r=1}^{R} \left( \xi_{A,\alpha}^{x,r} \right)^* \xi_{B,\beta}^{y,r} = \delta_{AB} \, \delta_{\alpha\beta} \, \delta^{xy} \tag{2.51}$$

and

$$\lim_{R\to\infty} \frac{1}{R} \sum_{r=1}^{R} \xi_{A,\alpha}^{x,r} \xi_{B,\beta}^{y,r} = 0 \,. \tag{2.52}$$

Note that these relations are independent of the actual form of the noise that is used for the generation of the sources. In order to estimate the desired correlation function one needs to invert the lattice Dirac operator $D = D_l, D_h$ on every sample for each gauge configuration

$$\phi_{A,\alpha}^{x,r} = \left( D_{AB,\alpha\beta}^{xy,r} \right)^{-1} \xi_{B,\beta}^r \,, \tag{2.53}$$

such that in the limit of a large number of samples $R$ the propagator $\left( D_{AB,\alpha\beta}^{xy} \right)^{-1}$ is recovered from the following unbiased estimator

$$\lim_{R\to\infty} \frac{1}{R} \sum_{r=1}^{R} \left( \xi_{B\beta}^{y,r} \right)^* \phi_{A,\alpha}^{x,r} = \lim_{R\to\infty} \frac{1}{R} \sum_{r=1}^{R} \left( \xi_{B,\beta}^{y,r} \right)^* \left( D_{AC,\alpha\gamma}^z \right)^{-1} \xi_{C,\gamma}^{z,r} = \left( D_{AB,\alpha\beta}^{xy} \right)^{-1} \,. \tag{2.54}$$

Of course, in actual calculations one uses a finite number of sources, which introduces some remnant stochastic noise. Usually, one demands that $R$ has to be chosen large enough, such that the remaining stochastic noise is of similar size as the gauge noise. Denoting the total number of source degrees of freedom ("volume") by $V$ (i.e. spin, color and spacetime), the noise scales as $\sqrt{V}/\sqrt{R}$, whereas the signal is of $\mathcal{O}(1)$. This is the reason why the direct use

of Eq. (2.54) is still rather inefficient and more sophisticated methods of variance reduction are applied in most actual simulations.

For the evaluation of connected diagrams we employ stochastic timeslice sources using the so-called *one-end-trick* [136, 138, 139], which allows for much better variance reduction. Instead of applying Eq. (2.54) one considers the product $\left(\phi_{A,\alpha}^{x,r}\right)^* \phi_{B,\beta}^{y,r}$, where the $\phi_{A,\alpha}^{x,r}$ are obtained similar to what has been described before, besides that the stochastic sources used for the inversion are now non-zero for only one particular timeslice $t_0$ (which is why they are called "time-slice source"). The time-slice is chosen randomly for every gauge configuration to avoid introducing unnecessary autocorrelation while retaining translational invariance for sufficiently large sets of gauge configurations. Averaging over a large number of samples $R$ yields an unbiased estimator for the product of two propagators, i.e.

$$\lim_{R\to\infty} \frac{1}{R} \sum_{r=1}^{R} \left(\phi_{A,\alpha}^{x,r}\right)^* \phi_{B,\beta}^{y,r} = \lim_{R\to\infty} \frac{1}{R} \sum_{r=1}^{R} \left(\left(D_{AC,\alpha\gamma}^{xz}\right)^{-1} \xi_{C,\gamma}^{z,r}\right)^* \left(D_{BD,\beta\delta}^{yw}\right)^{-1} \xi_{D,\delta}^{w,r}$$

$$= \left(\left(D_{AC,\alpha\gamma}^{xz}\right)^\dagger\right)^{-1} \left(D_{BC,\beta\gamma}^{yz}\right)^{-1} . \tag{2.55}$$

From this expression it is possible to obtain the connected, zero-momentum correlation function by summation over the spatial components and taking the trace over the remaining open indices. As discussed in [136], this leads to a favorable signal-to-noise ratio of $\mathcal{O}(1)$ even for using only a single sample, compared to $\mathcal{O}(\sqrt{R}/\sqrt{V})$ for the approach that has been considered first. Despite the improved variance reduction, Eq. (2.55) does not yet allow for arbitrary Dirac structure at the source, which is why an additional extension to the method is required. Such an extension is provided by introducing so-called *linked sources*

$$\xi_{A,\alpha\beta}^{x_0 y_0,\vec{x},r} = \delta_{\alpha\beta}\delta^{x_0 y_0}\zeta_A^{\vec{x},r} , \tag{2.56}$$

which share an identical stochastic noise field $\zeta_A^{\vec{x},r}$ for the four possible values $\beta = 0, 1, 2, 3$ of the Dirac index. Again, these sources are non-zero only on a certain time-slice $y_0$. The use of two linked sources in the evaluation of Eq. (2.55) instead of standard time-slice sources allows to introduce an arbitrary Dirac structure $\Gamma$ at source $y_0$, requiring now four instead of one inversion. Moreover, it is even possible to evaluate connected pieces of correlators involving spatially non-local operators (like those generated by application of fuzzing or other smearing techniques) employing only a minor modification to the sources and at the prize of three additional inversions. The modified linked sources are of the form $F\xi_{A,\alpha\beta}^{x_0 y_0,\vec{x},r}$ where $F$ denotes a suitable product of links, implementing the required spatial structure. These sources are often referred to as "fuzzed" or "smeared" sources, depending on the actual technique that is used to implement spatially non-local operators. The aforementioned, additional inversions of the Dirac operator are then performed on these sources and together with the inversions on the standard linked sources this ultimately allows to build correlations functions with any desired spatial and Dirac structure at source an sink as discussed in [136].

Although the preceding considerations are equally valid for a degenerate and a non-degenerate doublet, we remark that in order to invert the heavy doublet one projects out the single, non-

degenerate flavors, i.e. one solves[1]

$$
\begin{pmatrix} \phi_{cc} \\ \phi_{cs} \end{pmatrix} = D_h^{-1} \begin{pmatrix} 1 \\ 0 \end{pmatrix} , \qquad \begin{pmatrix} \phi_{sc} \\ \phi_{ss} \end{pmatrix} = D_h^{-1} \begin{pmatrix} 0 \\ 1 \end{pmatrix} . \tag{2.57}
$$

For the evaluation of disconnected diagrams we use stochastic volume sources with complex Gaussian noise [136]. Although the corresponding calculations rely on exactly the same basic identities for stochastic sources which have just been discussed, one usually has to take additional care with respect to variance reduction. This is because disconnected diagrams are significantly noisier than the connected ones and in fact, using the naive stochastic estimate for a single loop with Dirac structure $\Gamma$

$$
\lim_{R \to \infty} \frac{1}{R} \sum_{r=1}^{R} (\xi^r)^* \Gamma \phi^r = \text{tr} \left[ D^{-1} \Gamma \right] \tag{2.58}
$$

turns out to be insufficient for almost any practical purposes. Note that having established the basic principles of the stochastic method in the preceding discussion, we may now again suppress color, spin and spacetime indices for further considerations, as it has been done in the above equation. The trace on both sides of the equation acts on color, spin and spacetime.

A very powerful method of variance reduction, which is exclusive to the case of a degenerate quark doublet in the twisted mass formulation, is again based on the application of the one-end-trick [140]. The method relies on the following identity relating the $u$ and $d$ components $D_u = D_l \left( 1 + \tau^3 \right) / 2$, $D_d = D_l \left( 1 - \tau^3 \right) / 2$ of the twisted mass Dirac operator for light quarks $D_l$

$$
D_u - D_d = 2i\mu_l\gamma_5 , \tag{2.59}
$$

which can easily be inferred from the definition in Eq. (1.173). Together with the identity

$$
D_d^{-1} \left( D_d - D_u \right) D_u^{-1} = D_u^{-1} - D_d^{-1} , \tag{2.60}
$$

one obtains a corresponding expression for the propagators

$$
\Gamma \left( D_u^{-1} - D_d^{-1} \right) = -2i\mu_l\Gamma D_d\gamma_5 D_u , \tag{2.61}
$$

where again an additional Dirac structure $\Gamma$ has been added to allow for the different types of interpolating operators in our simulations. Application of the $\gamma_5$-trick in Eq. (1.190) on the right-hand side allows to transform the $d$ propagator into an $u$ propagator, leading to

$$
-2i\mu_l\Gamma\gamma_5 \left( D_u^{-1} \right)^\dagger D_u^{-1} = \Gamma \left( D_u^{-1} - D_d^{-1} \right) , \tag{2.62}
$$

The left-hand side of this relation can be evaluated efficiently using the one-end-trick

$$
\lim_{R \to \infty} \frac{1}{R} \sum_{r=1}^{R} \phi^r \Gamma\gamma_5 \left( \phi^r \right)^* = \left( D_u^{-1} - D_d^{-1} \right) \Gamma , \tag{2.63}
$$

---

[1]Note that in the actual implementation of the tmLQCD suite, the two components of the doublets are exchanged, i.e. the strange quark is the upper component and the charm the lower one, such that one has to make the replacements $\phi_{cc} \leftrightarrow \phi_{ss}$ and $\phi_{cs} \leftrightarrow \phi_{sc}$ to match with the actual code. However, for reasons of consistency we kept the notation that is used throughout this work.

with a signal-to-noise ratio of $\mathcal{O}(1)$. This improved behavior compared to Eq. (2.58) is caused by the additional, implicit sum over spacetime indices of the stochastic sources used for $\phi^r$, $(\phi^r)^*$ and the fact that the stochastic estimation of a rather large constant is avoided due to considering the difference of the two propagators on the right-hand side instead of estimating them separately. However, the fact that we need the difference of propagators on the right hand side is also the reason why this method is restricted to operators that exhibit a matching flavor structure, i.e. $\tau^3$ in the twisted basis. Moreover, it is not applicable in the heavy quark sector due to the off-diagonal components of $D_h$, $D_h^{-1}$ in flavor space.

Another more general, though less effective method is given by the *hopping parameter expansion* [136, 141], which we apply in all those cases for which the one-end-trick cannot be used. The idea behind this method is to rewrite the Dirac operator $D = D_l, D_h$ by

$$D_h^{-1} = B - BHB + B(HB)^2 - B(HB)^3 + D_h^{-1}(HB)^4 , \qquad (2.64)$$

with $D_h = (1 + HB)A$, $B = 1/A$ and $H$ the so-called two flavor hopping matrix. The last term in this representation can be estimated stochastically for any Dirac structure $\Gamma$ by

$$\Gamma D_h^{-1}(HB)^4 = \lim_{R \to \infty} \frac{1}{R} \sum_{r=1}^{R} (\xi^r)^* (BH) \Gamma \phi^r , \qquad (2.65)$$

whereas the other terms can be calculated directly without the need for any inversions. This method yields an improvement of a factor $\gtrsim 1.5$ compared to Eq. (2.58) at a fixed number of stochastic samples $R$. For further details we refer to [136] and references therein.

### 2.2.2 Generalized eigenvalue problem

In the first part of this section it has been discussed how the ground state can be extracted from a single correlation function. However, if one wants to deal with higher lying states systematically, it is necessary to consider matrices of correlation function as defined in Eq. (2.45) instead of a single correlator. The reason for this is that any element of the correlation function matrix involves an infinite number of states, i.e.

$$\mathcal{C}_{ij}(t) = \sum_{n=1}^{N} \hat{A}_i^{(n)} \left(\hat{A}_j^{(n)}\right)^* \left(\exp\left(-E^{(n)}t\right) \pm \exp\left(E^{(n)}(t-T)\right)\right) \qquad (2.66)$$

where $\hat{A}_i^{(n)} = \langle 0| \mathcal{O}_i |n\rangle$ denote matrix elements, which are related to the physical amplitudes $A_i^{(n)}$ via $A_i^{(n)} = \sqrt{2E^{(n)}}\hat{A}_i^{(n)}$. Note that in our applications these matrix elements are real by definition, i.e. one might as well drop the complex conjugation in the above expression. For our purposes we will identify $E^{(n)}$ with the mass $m^{(n)}$ of the $n$-th state. The basic idea behind using a matrix of correlation functions is to employ a variational approach on a finite subset of states $|n\rangle$, $n = 1, ..., N$ where $N$ corresponds to the number of interpolating operators, leading to a *generalized eigenvalue problem* (GEVP) [142–144]

$$\mathcal{C}(t) v^{(n)}(t, t_0) = \lambda^{(n)}(t, t_0) \mathcal{C}(t_0) v^{(n)}(t, t_0) , \qquad t_0 < t , \qquad (2.67)$$

where $\lambda^{(n)}(t, t_0)$, $v^{(n)}(t, t_0)$ denote eigenvalues (also referred to as *principal correlators*) and eigenvectors, respectively. Since our correlation function matrices are symmetric and positive definite by definition, such a GEVP can be reduced to a standard eigenvalue problem by applying a Cholesky decomposition $\mathcal{C}(t_0) = LL^T$ on the right-hand side, where $L$ is a triangular matrix, allowing us to rewrite Eq. (2.67)

$$\left(L^{-1}\mathcal{C}(t)\left(L^{-1}\right)^T\right)L^T v^{(n)}(t, t_0) = \lambda^{(n)}(t, t_0)L^T v^{(n)}(t, t_0) \qquad (2.68)$$

which may be treated numerically by any standard solver.

Taking into account the periodic boundary conditions for mesons, masses are obtained from solving

$$\frac{\lambda^{(n)}(t, t_0)}{\lambda^{(n)}(t+1, t_0)} = \frac{\exp\left(-m^{(n)}t\right) + \exp\left(-m^{(n)}(T-t)\right)}{\exp\left(-m^{(n)}(t+1)\right) + \exp\left(-m^{(n)}(T-(t+1))\right)}, \qquad (2.69)$$

for $m^{(n)}$. For the case of the $\eta$–$\eta'$ system the state with lowest mass should correspond to the $\eta$ and the second one to the $\eta'$. All other mesons ($\pi^\pm$, $\pi^0$ and $K$) that are considered in this work are given by the ground states of the corresponding correlation function matrices. Note that the resulting masses are independent of the actual choice of basis, as SO$(N)$ rotations in flavor space leave the eigenvalues invariant and affect only the eigenvectors, i.e. one may use any linear combinations of interpolating operators as long as the rank of the matrix remains unaffected. Moreover, masses are invariant under renormalization, which is why one does need not take care of renormalization as long as we are only interested in masses and avoid linear combinations of operators that require relative renormalization factors. This is one of the reasons why we introduced the rotations in flavor space in Eqs. (2.20),(2.31) for kaon and flavor singlet sector, respectively.

As already mentioned, the time extend of the lattice $T$ should be chosen sufficiently large to avoid pollution due to additional excited state contributions. Concerning the choice of values for $t$, we remark that they should be as large as possible, because the extracted eigenvalues receive corrections of $\mathcal{O}\left(\exp\left(-\Delta E^{(n)}t\right)\right)$ compared to the ones corresponding to the "true" eigenstates of the Hamiltonian. Here $\Delta E^{(n)}$ denotes the distance to the nearest energy level. However, in [144] it was shown that the first order corrections in perturbation theory to any energy level $E^{(n)}$ with $n \leq N$ are in fact given by $\mathcal{O}\left(\exp\left(-\left(E^{(N+1)} - E^{(n)}\right)t\right)\right)$ which usually exhibits much better convergence in $t$ compared to the aforementioned corrections, due to the larger splitting $\left(E^{(N+1)} - E^{(n)}\right) > \Delta E^{(n)}$. In this paper it is also discussed how to minimize the higher order corrections, i.e. how to recover the improved $t$-behavior of the first order corrections, which leads to a condition for $t_0$, namely to choose $t_0 > t/2$ (and both sufficiently large). The reason for this that the mixing occurring can be shown to be exponentially suppressed in $t_0$. Moreover, the form of the first order corrections also implies that the lowest lying states converge fastest in $t$ and that it is generally favorable to use as many operators as possible, as this leads to larger splittings $E^{(N+1)} - E^{(n)}$. However, in numerical simulations the possible choices for $t_0$ are often strongly restricted by the noise increasing in $t$, such that there is always a trade-off between systematic effects and statistical errors. This is particularly true for the flavor singlet sector where large disconnected contributions occur, although in general it depends on the channel

that is investigated. For the actual choice of parameters that have been used in our simulation and some further discussion on the subject we refer to appendix C.

In addition to the masses of the states it is possible to retain the corresponding amplitudes $A_i^{(n)}$ from the eigenvectors in Eq. (2.67). To this end one defines dual vectors $u^{(n)}$ to the vectors of matrix elements $\hat{A}^{(n)}$ satisfying

$$\left( u^{(n)}, \hat{A}^{(n)} \right) = \sum_{i=1}^{N} \left( u_i^{(n)} \right)^* \hat{A}_i^{(n)} = \delta^{nm} , \qquad 0 \le n, m < N . \tag{2.70}$$

The dual vectors fulfill Eq. (2.67), i.e.

$$\mathcal{C}\left( t \right) u^{(n)} = \lambda^{(n)}(t, t_0) \mathcal{C}\left( t_0 \right) u^{(n)} , \tag{2.71}$$

implying that the original eigenvectors $v^{(n)}\left( t, t_0 \right)$ and the vectors $u^{(n)}$ are related by a simple coefficient $c$

$$u^{(n)} = c v^{(n)}\left( t, t_0 \right) . \tag{2.72}$$

From the relation

$$\left( u^{(m)}, \mathcal{C}\left( t \right) u^{(n)} \right) = \delta^{mn} \left( \exp\left( -m^{(n)} t \right) \pm \exp\left( m^{(n)}\left( t - T \right) \right) \right) , \tag{2.73}$$

it is possible to determine the coefficients $c$

$$c = \pm \sqrt{ \frac{ \left( \exp\left( -m^{(n)} t \right) \pm \exp\left( m^{(n)}\left( t - T \right) \right) \right) }{ \left( v^{(n)}\left( t, t_0 \right), \mathcal{C}\left( t \right) v^{(n)}\left( t, t_0 \right) \right) } } , \tag{2.74}$$

where the sign ambiguity arises from taking the square root. In fact, the overall sign of the amplitudes is just a convention and for our purposes we choose the positive branch. The final result for the single amplitudes is obtained by plugging Eqs. (2.72),(2.74) into the relation

$$\mathcal{C}\left( t \right) u^{(n)} = \left( \exp\left( -m^{(n)} t \right) \pm \exp\left( m^{(n)}\left( t - T \right) \right) \right) \hat{A}^{(n)} , \tag{2.75}$$

and by adding the normalization factor relating matrix elements and amplitudes, which yields

$$A_i^{(n)} = \frac{ \sum_{j=1}^{N} \mathcal{C}_{ij}\left( t \right) v_j^{(n)}\left( t, t_0 \right) }{ \sqrt{ \left( v^{(n)}\left( t, t_0 \right), \mathcal{C}\left( t \right) v^{(n)}\left( t, t_0 \right) \right) \left( \exp\left( -m^{(n)} t \right) \pm \exp\left( m^{(n)}\left( t - T \right) \right) \right) } } . \tag{2.76}$$

Note that unlike masses, the extraction of amplitudes crucially depends on the choice of the linear combinations for interpolating operators in flavor space and on possible renormalization factors. This issue will be discussed in more detail in the next subsection.

### 2.2.3 Observables and renormalization

Within our studies the central observables comprise masses as well as decay constants and mixing parameters (if applicable). Whereas the extraction of the meson masses we are interested in (i.e. $M_{\mathrm{PS}}$, $M_{\pi^0}$, $M_{\pi^0,c}$, $M_K$, $M_\eta$, $M_{\eta'}$) is rather straightforward from the generalized eigenvalue problem in Eq. (2.67), the remaining observables require some additional care with respect to renormalization. In fact, all of the interpolating operators that have been introduced in subsection 2.1 require renormalization to obtain physical matrix elements and amplitudes. In addition it is necessary to ensure that the operators used for the determination of the matrix elements correspond to the correct currents in the physical basis. If we were always to use directly the corresponding operators in the twisted basis this would not be an issue, however, for the kaon and the flavor singlet sector we employ an additional change of basis for practical reasons which has to be reversed to retain the correct matrix elements. Besides, we remark that for the determination of quantities related to matrix element it is required to use matrix elements from local operators only, although further operators may be present in the correlation function matrix in order to increase the basis in this case as well.

However, for this work we need to take renormalization factors explicitly into account only for the kaon and flavor singlet sector, because we do not consider any quantities related to matrix element for the neutral pion and the decay constant $f_{\mathrm{PS}}$ of the charged pion can be determined without the need for any renormalization. The latter is a consequence of the twisted mass symmetries which have been discussed in section 1.3. Here, we briefly illustrate how the expression is obtained that we actually use to extract $f_{\mathrm{PS}}$ in our simulations. Starting from the general definition of decay constants in Eq. (1.88) and applying the axial rotations at maximal twist, one obtains in the twisted basis

$$f_{\mathrm{PS}} = \frac{\langle 0 | \, \tilde{V}_l^{2,R} \, | \pi^\pm \rangle}{M_{\mathrm{PS}}^2} = \frac{\langle 0 | \, \tilde{V}_l^{2,R} \tilde{P}_l^{1,R} \, | 0 \rangle}{\sqrt{2} M_{\mathrm{PS}}^{3/2}} \, , \tag{2.77}$$

where we introduced the superscript $R$ to denote renormalized currents. Note that the vector current in the twisted basis does not require any actual renormalization. The flavor index for the axial vector current in the physical basis has been fixed to $a = 1$ for the sake of clarity, implying that in the twisted basis we are left with the $a = 2$ component of the twisted vector current. However, the following considerations similarly apply to the case $a = 2$ and can easily be extended to matrix elements obtained from the interpolating operators defined in Eq. (2.5) that are linear combinations of the flavor components $a = 1, 2$ and which we use in practice in our analysis. Applying the PCVC relation in Eq.(1.178) it is possible to trade the vector current for a pseudoscalar current [75, 81, 82], which leads to the following expression

$$f_{\mathrm{PS}} = 2\mu_l \frac{\langle 0 | \, \tilde{P}_l^1 \, | \pi^\pm \rangle}{M_{\mathrm{PS}}^2} \, . \tag{2.78}$$

Note that in this expression the pseudoscalar flavor non-singlet renormalization factors $Z_P$ of the light quark mass $m_l^R = Z_P^{-1} \mu_l$ and the current $P_l^{1,R} = Z_P P_l^1$ cancel such that no renormalization is required at all. The occurrence of the quark mass due to the use of the PCVC relation in the

definition of the decay constants is the reason why it is convenient to use interpolation operators renormalized only up to a factor of $Z_P$, implying that our correlation function matrices need to be renormalized only up to an factor $Z_P^2$. For any other quantities that we calculate (i.e. mixing angles in the $\eta$–$\eta'$ system) only ratios of matrix elements are required, hence any global normalization factors can be ignored for them as well. Therefore, we omitted this factor in all of our actual calculations although we kept it in the following discussion for consistency reasons only. On the lattice we determine $f_{\mathrm{PS}}$ from the amplitude $A_{\mathcal{P}_l^+}^{\left(\pi^\pm\right)} = \langle 0| \mathcal{P}_l^+ |\pi^\pm\rangle = \sqrt{2M_{\mathrm{PS}}} \langle 0| \mathcal{P}_l^+ \mathcal{P}_l^- |0\rangle$, which is obtained directly from the GEVP as described in the previous section.

In principle, similar considerations apply for the kaon sector, although a complication arises from the fact that one has to employ interpolating operators made of light and heavy quarks. The corresponding relation for the kaon decay constant $f_K$ in the twisted mass formulation is given by

$$f_K = (\mu_l + \mu_s) \frac{\langle 0| \mathcal{P}_{neutral}^{+,tm} |K\rangle}{M_K^2} \,, \tag{2.79}$$

where $\mu_s =$ denotes the bare strange quark mass at maximal twist, which requires the ratio of pseudoscalar and scalar flavor non-singlet renormalization constants $Z$ defined in Eq. (1.201). Again a factor $Z_P^{-1}$ stemming from the renormalized light and strange quark mass (c.f. Eq. (1.200)) cancels with a factor pulled out of the matrix element in the twisted mass formulation. Therefore, we only need the ratio $Z$ for the renormalization of the interpolating operators in Eq. (2.21), i.e. only the scalar operators obtain a factor $Z^{-1}$ and the pseudoscalar ones remain unaffected. However, the above relation does not actually require a matrix element with the interpolating operator $\bar{d}i\gamma_5 s$ in Eq. (2.21) but with the composite interpolating operator $\mathcal{P}_{neutral}^{+,tm}$ in the "original" twisted basis. The reason to introduce the operator basis in Eq. (2.21) was on the one hand to allow for a significant simplification of the resulting correlation function and on the other hand to avoid any renormalization at the level of building correlation functions. The missing factors of $Z$ can now easily be included while rotating back to the original basis before solving the GEVP, which gives access to the amplitude required in the above equation.

The correlation function matrix that we calculate is given by

$$\mathcal{C}^K(t) = a^3 \sum_{\vec{x}} \langle 0| T\vec{\mathcal{O}}^K(0) \otimes \left(\vec{\mathcal{O}}^K(x)\right)^\dagger |0\rangle \,, \tag{2.80}$$

whereas the one we actually need as input for the GEVP reads

$$\mathcal{C}_{tm}^K(t) = a^3 \sum_{\vec{x}} \langle 0| T\left(R_K^T \vec{\mathcal{O}}^K(0)\right) \otimes \left(R_K^T \left(\vec{\mathcal{O}}^K(x)\right)^\dagger\right) |0\rangle \,, \tag{2.81}$$

where $\vec{\mathcal{O}}^K$ is the vector of interpolating operators in Eq. (2.21) and the subscript $tm$ refers to the original twisted basis. Note that in the above expression the hermitean conjugate is to be taken element-wise on the vector $\vec{\mathcal{O}}^K$. This implies that we can obtain the latter matrix simply by reversing the rotation in flavor space, i.e.

$$\mathcal{C}_{tm}^K(t) = R_K^T \mathcal{C}^K(t) R_K \,. \tag{2.82}$$

Considering the required renormalization factor this reads

$$
\begin{aligned}
\mathcal{C}_{tm}^{K,R}(t) &= Z_P^2 R_K^T \mathrm{diag}\left(Z^{-1}, Z^{-1}, 1, 1\right) \mathcal{C}^K(t) \, \mathrm{diag}\left(Z^{-1}, Z^{-1}, 1, 1\right) R_K \\
&= \left(R_K^R\right)^T \mathcal{C}^K(t) \, R_K^R \,,
\end{aligned}
\tag{2.83}
$$

where in the second line we defined the renormalized rotation matrix

$$
R_K = \frac{1}{2}\begin{pmatrix} +Z^{-1} & +Z^{-1} & -Z^{-1} & +Z^{-1} \\ +Z^{-1} & +Z^{-1} & +Z^{-1} & -Z^{-1} \\ +1 & -1 & +1 & +1 \\ -1 & +1 & +1 & +1 \end{pmatrix}.
\tag{2.84}
$$

Applying the GEVP to this matrix one finally obtains the required amplitude for the calculation of $f_K$.

In the flavor singlet sector we want to determine the mixing parameters $f_l$, $f_s$ and $\phi$ in the quark flavor basis from Eq. (1.114), i.e. using pseudoscalar matrix elements in the physical basis as given in Eq. (1.113). On the lattice this implies that we need to calculate the corresponding amplitudes in the twisted basis to obtain the matrix elements $h_P^i$ as defined in Eq. (1.113), i.e.

$$
A_l^{(\mathrm{P})} = \langle 0| \,\mathcal{S}_l^3\, |\mathrm{P}\rangle \,, \qquad A_{c,s}^{(\mathrm{P})} = \langle 0| \,\mathcal{P}_h^{\pm,tm}\, |\mathrm{P}\rangle \,, \qquad \mathrm{P} = \eta, \eta' \,,
\tag{2.85}
$$

where we included the charm quark only for the sake of completeness. For the definition of the interpolating fields $\mathcal{S}_l^3$ and $\mathcal{P}_h^{\pm,tm}$ see Eqs. (2.26),(2.28), respectively. Similar to the case of the kaon this requires to reverse the rotation in flavor space that had been used to simplify the structure of the correlation functions before solving the GEVP. The correlation matrix that we actually build is given by

$$
\mathcal{C}^{\eta,\eta'}(t) = a^3 \sum_{\vec{x}} \langle 0| \, T\vec{\mathcal{O}}^{\eta,\eta'}(0) \otimes \left(\vec{\mathcal{O}}^{\eta,\eta'}(x)\right)^\dagger |0\rangle \,,
\tag{2.86}
$$

where $\vec{\mathcal{O}}^{\eta,\eta'} = \left(\mathcal{S}_l^3, \mathcal{P}_h^{-,tm}, \mathcal{P}_h^{+,tm}\right)^T$. It is related to the correlation function matrix in the original basis by

$$
\begin{aligned}
\mathcal{C}_{tm}^{\eta,\eta'}(t) &= a^3 \sum_{\vec{x}} \langle 0| \, T\left(R_{\eta,\eta'}^T \vec{\mathcal{O}}^{\eta,\eta'}(0)\right) \otimes \left(R_{\eta,\eta'}^T \left(\vec{\mathcal{O}}^{\eta,\eta'}(x)\right)^\dagger\right) |0\rangle \\
&= R_{\eta,\eta'}^T \mathcal{C}^{\eta,\eta'}(t) \, R_{\eta,\eta'} \,.
\end{aligned}
\tag{2.87}
$$

Pulling out a global factor of $Z_P$ from the vector of interpolating operators, the renormalized correlation function matrix is given by

$$
\mathcal{C}_{tm}^{\eta,\eta',R}(t) = Z_P^2 \left(R_{\eta,\eta'}^R\right)^T \mathcal{C}_{tm}^{\eta,\eta',R}(t) \, R_{\eta,\eta'}^R \,,
\tag{2.88}
$$

where we defined

$$
R_{\eta,\eta'}^R = \begin{pmatrix} +Z^{-1} & 0 & 0 \\ 0 & -\frac{1}{\sqrt{2}Z} & -\frac{1}{\sqrt{2}Z} \\ 0 & +\frac{1}{\sqrt{2}} & -\frac{1}{\sqrt{2}} \end{pmatrix}.
\tag{2.89}
$$

As a technical aside we remark that is also possible to exchange the order of interpolating operators after building the matrix by an additional rotation in flavor space, which is useful if one wants to analyze only a particular submatrix. Moreover, it is worthwhile to mention that in the twisted basis only the scalar flavor non-singlet renormalization constant $Z_S$ occurs but not its flavor singlet counterpart $Z_{S^0}$ . This is an important feature as $Z_S$ and $Z_{S^0}$ differ at two loop order in perturbation theory [145], unlike pseudoscalar flavor non-singlet $Z_P$ and flavor singlet $Z_{P^0}$ renormalization constants which are identical to all orders. This can be considered an intrinsic advantage of the twisted mass formulation.

Finally, we mention that the mixing angle $\phi$ can be calculated directly from Eq. (1.115) on the lattice using the corresponding amplitudes from the GEVP applied to the correlation function matrix $\mathcal{C}_{tm}^{\eta,\eta',R}(t)$, i.e.

$$\tan(\phi) = \sqrt{-\frac{A_l^{(\eta')} A_s^{(\eta)}}{A_l^{(\eta)} A_s^{(\eta')}}} \,. \tag{2.90}$$

Note that in order to check for the validity of the assumptions that led to the definition of a single mixing angle in the quark flavor basis we will also calculate $\phi_l$ and $\phi_s$ separately, which are given as single ratios of the amplitudes corresponding to pseudoscalar matrix elements in the physical basis, i.e.

$$\tan(\phi_l) = \frac{A_l^{(\eta')}}{A_l^{(\eta)}} \,, \qquad \tan(\phi_s) = -\frac{A_s^{(\eta)}}{A_s^{(\eta')}} \,. \tag{2.91}$$

### 2.2.4   Scale setting and extrapolations

Up to this point we have discussed how to extract observables from lattice simulations. However, in order to make contact with actual physics, there are additional steps required. First of all, it is necessary to set the scale in our simulations to obtain observables in physical units instead of the lattice spacing $a$. This requires to fix a single, dimension-full quantity which can be measured on the lattice. Although in principle any dimension-full quantity could be used it is favorable to choose one that can be measured precisely at moderate computational cost. Within this work, we employ the *Sommer parameter* $r_0$, which represents a hadronic length scale that is implicitly defined from the following relation involving the force $F(r)$ between to static quarks [146]

$$r^2 F(r)\big|_{r=r(x)} = x \,, \tag{2.92}$$

by setting $x = 1.65$, i.e. $r_0 = r(1.65)$. Measuring this parameter on a given ensemble of gauge configurations yields a result in terms of lattice units, i.e. $r_0/a$. In practice, we then perform separate chiral extrapolations for each value of the lattice spacing and use the resulting $r_0^\chi/a$ to obtain dimensionless quantities at the each value of the the corresponding lattice spacing. After performing all further extrapolations for a given observable (i.e. chiral extrapolations, continuum extrapolation and taking care of possible finite size effects) one may use the continuum extrapolated value $r_0 \equiv r_0^\chi$ to convert the final results to physical units. For numerical values used in our investigations we refer to the general discussion of our setup included at the beginning of chapter 3.

As just mentioned, besides setting the scale it is also necessary to take care of the dependence on further input parameters of our simulations, i.e. the quarks masses which in general are not a priori set to their physical values. To this end one has to run simulations at different values of the corresponding parameters and to perform chiral extrapolations to the physical point, employing a suitable proxy for each quark mass, e.g. $M_{\mathrm{PS}}^2$ and $M_K^2$ for $m_l$ and $m_s$. Note that in our simulations we do not measure any quantities that are expected to depend significantly on the value of the charm quark mass which is why we can safely neglect any such dependence for all practical purposes. However, observables may also exhibit lattice artifacts, i.e. a residual dependence on the lattice spacing $a$ which should be of $\mathcal{O}\left(a^2\right)$ in our simulations at maximal twist. Still, they may be sizable as it is the case for the neutral pion, which has already been discussed in detail in subsection 1.3.5. In principle the required extrapolations can be performed simultaneously, provided that sufficient theoretical input is available, e.g. corresponding formulas from W$\chi$PT. However, for the $\eta$–$\eta'$ system the corresponding formulas are not available in the literature, which is why we will perform a separate scaling test, including any residual lattice spacing dependence in a systematic error. For the required chiral extrapolations it turns out to be sufficient for our applications to consider the leading order dependence on $M_{\mathrm{PS}}$ and $M_K$ as given by standard $\chi$PT, c.f. Eqs. (1.79)–(1.81) and Eq. (1.87).

Finally we mention that also finite size effects may occur, which can be investigated by varying the spatial lattice size $L/a$ while keeping the remaining parameters fixed. Typically, one expects the resulting corrections for pseudoscalar mesons to scale with the mass of the lightest pseudoscalar $M_{\mathrm{PS}}^{light}$, i.e. they should be of order $\mathcal{O}(\exp(-M_{\mathrm{PS}}^{light}L))$. For many cases one has $M_{\mathrm{PS}}^{light} = M_{\mathrm{PS}}$, although, due to the mass splitting between charged and neutral pion in WtmLQCD and the fact that $M_{\pi^0} < M_{\mathrm{PS}}$ holds, one expects the corrections in some applications rather to be of order $\mathcal{O}\left(\exp\left(-M_{\pi^0}L\right)\right)$. However, for our purposes finite size effects will turn out to be negligible within errors, which is why we do not go into further detail regarding this particular subject. We only mention that it is also possible to systematically include finite size corrections in dedicated chiral fits employing W$\chi$PT [129, 147, 148], however, this is clearly beyond the scope of this work.

## 2.3 Data analysis

The previous sections of this chapter focused on the technical details of building correlation functions and extracting observables from lattice simulations. However, for meaningful physical pre- and postdictions also a careful statistical analysis is required, because all of our calculations are based on Monte-Carlo methods. Besides systematic errors, which are usually hard to quantify, statistical errors themselves an be evaluated and treated in a systematic way. In this section we include a brief overview on the methods of statistical error analysis and fitting that have been used in this work. Most of these methods are nowadays considered standard techniques and for further reading we refer to any standard textbook, e.g. [46].

The statistical errors in Monte-Carlo simulations arise from the fact that one can only use a finite number of samples $N$ (i.e. number of gauge configurations) in any actual simulation.

A simple estimate for the error introduced by this restriction for any primary observable $O$ is related to the samples variance $\sigma_N^2$, which is defined by

$$\sigma_N^2 = \frac{1}{N-1} \sum_{n=1}^{N} \left( (O^n)^2 - \langle O \rangle^2 \right), \qquad \langle O \rangle = \frac{1}{N} \sum_{n=1}^{N} O^n. \tag{2.93}$$

where $O^n$ denotes the $n$-th measurement of $O$. Note that in this expression the factor $1/(N-1)$ (instead of $1/N$) is required to obtain an unbiased estimator, because the expectation value of $O$ has been estimated by the measured mean value. The standard error is then given by $\sigma_N/\sqrt{N}$. However, this error estimate exhibits a significant drawback as it requires the all measurements of $O$ to be uncorrelated, which one may not expect to be fulfilled in any actual computation. Therefore, it is often referred to as *naive error*. In the following we will discuss what kind of correlations may occur and how they can be dealt with in order to obtain a reliable error estimate.

### 2.3.1 Autocorrelation

One important source of correlation in the data is given by *autocorrelation*, i.e. correlation in simulation time. In order to treat these correlations one introduces the autocorrelation function

$$\Gamma(n-m) = \langle (O^n - \langle O \rangle)(O^m - \langle O \rangle) \rangle, \tag{2.94}$$

where $\tau = n - m$ denotes "Monte-Carlo time" to distinguish it from Euclidean time $t$. A measure for the autocorrelation is then given by the integrated autocorrelation time $\tau_{\text{int}}$ which is defined as

$$\tau_{\text{int}} = \frac{1}{2} \sum_{\tau=-\infty}^{\infty} \frac{\Gamma(|\tau|)}{\Gamma(0)}. \tag{2.95}$$

Another possibility is to consider the exponential decay of the autocorrelation function

$$\Gamma(n-m) \sim \exp{-\tau/\tau_c}, \tag{2.96}$$

which yields an autocorrelation time $\tau_c$ that is typically of the same order as $\tau_{\text{int}}$. In practice, one considers two measurements $O^n$, $O^m$ to be independent in simulation time if they satisfy $|n - m| \geq \tau_{\text{int}}$. However, one should stress that actual simulations always include only a finite number of measurements such that correlations at time scales similar or even larger than the length of our sample of measurements cannot be detected.

There are several ways that allow to incorporate the effects of autocorrelation into an error estimate. The most simple method is to use only gauge configurations which are separated by at least $\tau_{\text{int}}$ in simulation time. However, this has two major disadvantages. The first one is given by the fact that $\tau$ is not a priori known for a given observable such that one may have to perform more measurements than actually needed. The second disadvantage is the loss of residual information contained in the gauge configurations that lie in between every pair of independent configurations. Since the generation of configurations with dynamical quarks is

numerically very expensive this is something one would like to avoid as well. One possibility to take all available measurements into account is given by a modification to the naive error estimate $\sigma_N$ which involves the computation of $\tau_{\text{int}}$. In general, the resulting estimate for the full error $\sigma_N^{\text{corr}}$ (i.e. taking correlations into account) will be larger and one can show that $\sigma_N^{\text{corr}}$ is given by [149]

$$(\sigma_N^{\text{corr}})^2 = 2\tau_{\text{int}}\sigma_N^2 \, . \tag{2.97}$$

However, this estimate requires a precise determination of $\tau_{\text{int}}$, which can only be achieved from a sufficiently large sample size. Besides, estimating the error of $\tau_{\text{int}}$ is technically rather involved [150]. The particular method of error estimation described in [150] is also referred to as the "Γ-method".

Another simple but effective technique to deal with autocorrelation is given by *blocking*, which refers to the data being arranged in blocks of a given block length $N_b$ before performing the actual analysis using the $B = N/N_b$ block averages $B^n$ instead of the single measurements. Note that this blocks are required to contain only successive measurements, i.e. the order of the data sequence should not be affected. Then the error can be estimated from

$$\sigma_{O,N,N_b}^2 = \frac{1}{B\,(B-1)} \sum_{n=1}^{B} \left( B^n - \frac{1}{B} \sum_{m=1}^{B} B^m \right)^2 \, . \tag{2.98}$$

For a sufficiently large block size $N_b$ – i.e. $N_b$ should be of the order of $\tau_{\text{int}}$ in units of Monte-Carlo time – the blocks are statistically independent and the resulting error estimate is no longer affected by correlations. In practice one usually varies the block length until the error stays constant, i.e. fluctuation occur from further increasing the block size. This procedure allows to avoid the calculation of $\tau_{\text{int}}$, although the latter can still provide a useful cross-check. Throughout this work we rely on blocking in our error analysis, while the Γ-method is used only for cross-checks.

## 2.3.2 $\chi^2$-fitting

Apart from the correlations in simulations time that have just been discussed, further correlations may also arise among observables depending on some lattice parameter. In lattice QCD one usually considers correlation functions $\mathcal{C}_{ij}(t)$ as discussed in the previous section which depend on the Euclidean time $t$. For such functions correlations are not restricted to correlations between measurements on different gauge configurations but may also occur for measurements at different values of $t$. This has to be taken into account when fitting some model function $f(t, \vec{\chi})$ to the data, where $\vec{\chi}$ denotes a vector of fit parameters.

To this end, one considers the gauge average $\langle \mathcal{C}_{ij}(t) \rangle$ over $N$ independent configurations (or blocks). In order to determine the correlations between averages at different $t$ and to estimate the statistical uncertainty on each average one defines the *correlation matrix*

$$C_{t_1 t_2} = \frac{1}{N\,(N-1)} \sum_{n=1}^{N} \left( \mathcal{C}_{ij}^n(t_1) - \langle \mathcal{C}_{ij}(t_1) \rangle \right) \left( \mathcal{C}_{ij}^n(t_2) - \langle \mathcal{C}_{ij}(t_2) \rangle \right) \, . \tag{2.99}$$

The inverse of this correlation matrix occurs in the definition of the *correlated* $\chi^2$

$$\chi^2_{\mathrm{corr}} = \sum_{t_1, t_2} \left( \langle \mathcal{C}_{ij}(t_1) \rangle - f(t_1, \vec{\chi}) \right) \left( C^{-1} \right)_{t_1 t_2} \left( \langle \mathcal{C}_{ij}(t_2) \rangle - f(t_2, \vec{\chi}) \right) , \qquad (2.100)$$

which one needs to minimize in order to find the best fit, i.e. the optimal values the elements for the parameter vector $\vec{\chi}$. The argument that leads to the minimization condition for $\chi^2_{\mathrm{corr}}$ is that the probability distribution of $\langle \mathcal{C}_{ij}(t) \rangle$ which yields the observed correlation should be maximal. Note that for the uncorrelated case the matrix $C_{t_1 t_2}$ becomes diagonal and the usual, uncorrelated $\chi^2$ is recovered as the diagonal elements of $C_{t_1 t_2}$ simply reproduce the standard variances. For further details we refer to any textbook on statistics.

Besides simple linear fits that are used at various occasions in our analysis, a non-trivial example for such a fit is given by the following factorizing fit model

$$\mathcal{C}_{ij}(t) = \sum_n \frac{A_i^{(n)} A_j^{(n)}}{2m^{(n)}} \left[ \exp(-m^{(n)} t) + \exp(-m^{(n)}(T-t)) \right] \qquad (2.101)$$

which we apply to the correlation matrices $\mathcal{C}_{ij}$ to complement or cross-check our GEVP analysis in certain cases. Note, however, that in any actual application in our studies of $\eta$, $\eta'$ we restrict ourselves to the use of the uncorrelated $\chi^2$, because the correlation matrix turns out much too noisy to allow for a meaningful numerical inversion of the correlation matrix. This approach is justified, because we use the bootstrap method discussed in the next subsection to calculate the errors on all relevant fit parameters and do not employ the resulting $\chi^2$ in other applications or to make any statistical statements. We remark that in principle one could also use some truncation method (e.g. a singular value decomposition together with a cut in the resulting singular values) to invert the correlation matrix, however, this would introduce some additional model dependence, which we would like to avoid.

### 2.3.3  Bootstrap method

A very powerful tool to deal with correlations in the context of error analysis is given by the *bootstrap* method. It is based on resampling, i.e. starting from $N$ independent gauge configurations (or blocks) one randomly chooses $N_B$ new samples. This is done by sampling with replacement, such that single gauge configurations may enter the new sample multiple times or even not at all. In our applications we will always choose each bootstrap sample to be of the same size as the original sample. The analysis is then performed on every sample and the resulting errors can be estimated from the variance in the bootstrap means.

This method has a significant advantage over other methods to deal with correlations, which is that errors are without much ado propagated trough all stages of the analysis by simply performing all required operations on every bootstrap sample. It also allows to easily include known errors of further quantities that enter the analysis by resampling. Moreover it can be trivially combined with blocking by replacing simple measurements with blocks in the generation of bootstrap samples. For these reasons we employ bootstrapping for the determination of statistical errors throughout this work.

# Chapter 3

# Analysis and results

In this third and final chapter we present the details of our analysis and discuss the physical results obtained from our simulations. The first section details our lattice setup for $N_f = 2+1+1$ dynamical quark flavors which has been used for all $\eta,\eta'$ related investigations and which is also a major part of the setup that has been used in the determination of low energy constants for W$\chi$PT. The next four sections are devoted to our study of $\eta$ and $\eta'$ mesons. In section 3.2 we discuss the extraction of masses for flavor singlet and non-singlet mesons as well as the determination of the decay constants for the flavor non-singlets which are needed for certain parts of our analysis. In the third section we present the details of the chiral extrapolation in the light quark mass for the $M_\eta$ as well as the correction for mistuned values of the strange quark mass in our simulations. We also perform scaling tests and perform a continuum extrapolation. At this stage, corresponding extrapolations for the $\eta'$ are still omitted due to large errors of $M_{\eta'}$. The discussion of mixing in the $\eta$–$\eta'$ system is postponed until section 3.5, where the results for the mixing angle from the standard analysis method is presented together with the more comprehensive results of mixing parameters obtained from an improved analysis method.

Most of the results presented in sections 3.2, 3.3 and some parts of section 3.5 have been published in [1, 4, 5]. However, we point out that the actual numbers presented here may differ within errors from the ones in the aforementioned publications, which is due to minor improvements in statistics for certain ensembles and the inclusion of additional data points. Moreover, for the presentation in this work we have enforced consistent statistics throughout all of our investigations. We stress that none of this has any impact on the physical results as the resulting deviations lie all within errors of the originally published values. In fact, most deviations are much smaller than the respective error itself.

The results from an improved analysis method for the flavor singlet sector as discussed in section 3.4 have been partially published in [3, 6], which is also true for some parts of the results for the mixing parameters of the $\eta,\eta'$ system, that are discussed in section 3.5. Using this improved analysis method it becomes feasible to perform extrapolations for $M_{\eta'}$ as well and to determine further mixing parameters beside the angle $\phi$. The two sections 3.4 and 3.5 contain the most central physical results of our investigations, i.e. the final values for $M_\eta$, $M_{\eta'}$ and the

mixing angle $\phi$.

The last section of this chapter is dedicated to our analysis of low energy constants, which is based on our calculations of masses in the pion sector. All of the results in this section have been published in [2].

## 3.1   Lattice action and parameters

In this work we use gauge configurations produced by the European Twisted Mass Collaboration [79, 134, 151] with the fermionic action described by Eqs. (1.172),(1.197) and the Iwasaki gauge action that is given by the generic gauge action in Eq. (1.162) for a particular choice of parameters as discussed in the text. Further details of these configurations are described in [79]. A summary of the ensembles that are used in this investigation can be found in table 3.1. The first letters $A$, $B$ and $D$ used to denote the ensembles refer to the different values of the lattice spacing $a_A = 0.0863(4)$fm, $a_B = 0.0779(4)$fm and $a_D = 0.0607(2)$fm, corresponding to $\beta_A = 1.90$, $\beta_B = 1.95$ and $\beta_D = 2.10$, respectively [151]. In this table we have also listed the number of gauge configurations $N$, and the number of stochastic samples per gauge configurations $N_s$ used to estimate the disconnected contributions as described in subsection 2.2.1. We remark that the physical volumes of these ensembles are mostly larger than 3 fm with only a few exceptions and they correspond to values of $M_{\mathrm{PS}}L$ larger than 3.3. The physical spatial volumes range from $(1.9\,\mathrm{fm})^3$ to $(2.8\,\mathrm{fm})^3$.

As discussed in subsection 2.2.4 we will use the Sommer parameter $r_0$ [146] to study the scaling behavior of our results. We use the values of $r_0^\chi/a$ extrapolated to the chiral limit at each $\beta$-value separately. For the $A$ and $B$ ensembles we employ the values given in [79]. For the ensembles at the finest lattice spacings these values have not bee yet available which is why we performed the extrapolation by ourselves. The three values for $r_0^\chi/a$ are listed in table 3.2. For setting the physical scale one could in principle use the results of [151], where the scale has been set from a chiral fit to data for $f_{\mathrm{PS}}$ and $m_{\mathrm{PS}}$ and the physical value of $f_\pi$. However, this involves only two data points at $\beta = 2.10$, hence has to be considered rather preliminary. Therefore, we prefer to set the scale in our investigation using a value of $r_0 = 0.45(2)$ fm. The 5% error covers the statistical uncertainty and spread quoted [151], allowing room for systematic uncertainties. Besides, this method allows to update our results as soon as an update of the scale setting becomes available.

In order to fix the light and strange quark masses to their physical values we employ the experimental values of $M_{\pi^0,\mathrm{exp}} \approx 135\,\mathrm{MeV}$ and $M_{\mathrm{K}^0,\mathrm{exp}} \approx 498\,\mathrm{MeV}$. The motivation for using the masses of the neutral mesons results from the fact that our simulations do not incorporate electromagnetic effects. Using the masses of the neutral mesons one may expect to reduce uncertainties related to this approximation. For further discussion on this subject we refer to [152] and references therein.

Concerning heavy quark mass dependence we remark that for our ensembles the bare values of $a\mu_\sigma$ and $a\mu_\delta$ were kept fixed at each value of $\beta$, and only the value of the light twisted

| ensemble | $\beta$ | $a\mu_\ell$ | $a\mu_\sigma$ | $a\mu_\delta$ | $L/a$ | $N$ | $N_s$ | $N_b$ |
|---|---|---|---|---|---|---|---|---|
| $A30.32$ | 1.90 | 0.0030 | 0.150 | 0.190 | 32 | 1367 | 24 | 5 |
| $A40.24$ | 1.90 | 0.0040 | 0.150 | 0.190 | 24 | 2630 | 32 | 10 |
| $A40.32$ | 1.90 | 0.0040 | 0.150 | 0.190 | 32 | 863 | 24 | 4 |
| $A60.24$ | 1.90 | 0.0060 | 0.150 | 0.190 | 24 | 1251 | 32 | 5 |
| $A80.24$ | 1.90 | 0.0080 | 0.150 | 0.190 | 24 | 2449 | 32 | 10 |
| $A100.24$ | 1.90 | 0.0100 | 0.150 | 0.190 | 24 | 2493 | 32 | 10 |
| $A80.24s$ | 1.90 | 0.0080 | 0.150 | 0.197 | 24 | 2517 | 32 | 10 |
| $A100.24s$ | 1.90 | 0.0100 | 0.150 | 0.197 | 24 | 2312 | 32 | 10 |
| $B25.32$ | 1.95 | 0.0025 | 0.135 | 0.170 | 32 | 1484 | 24 | 5 |
| $B35.32$ | 1.95 | 0.0035 | 0.135 | 0.170 | 32 | 1251 | 24 | 5 |
| $B55.32$ | 1.95 | 0.0055 | 0.135 | 0.170 | 32 | 1545 | 24 | 5 |
| $B75.32$ | 1.95 | 0.0075 | 0.135 | 0.170 | 32 | 922 | 24 | 4 |
| $B85.24$ | 1.95 | 0.0085 | 0.135 | 0.170 | 24 | 573 | 32 | 2 |
| $D15.48$ | 2.10 | 0.0015 | 0.120 | 0.1385 | 48 | 1045 | 24 | 10 |
| $D20.48$ | 2.10 | 0.0020 | 0.120 | 0.1385 | 48 | 434 | 24 | 5 |
| $D30.48$ | 2.10 | 0.0030 | 0.120 | 0.1385 | 48 | 474 | 24 | 3 |
| $D45.32sc$ | 2.10 | 0.0045 | 0.0937 | 0.1077 | 32 | 1887 | 24 | 10 |

Table 3.1: The ensembles which are included in our investigations. The notation that is used to label the ensembles is the same as in [79]. In addition we give the number of configurations $N$, the number of stochastic samples $N_s$ for all ensembles and the bootstrap block length $N_b$.

| $\beta$ | 1.90 | 1.95 | 2.10 |
|---|---|---|---|
| $r_0^\chi/a$ | 5.231(38) | 5.710(41) | 7.538(58) |

Table 3.2: Values of the chirally extrapolated Sommer parameter $r_0^\chi/a$ for the three values of $\beta$.

mass parameter $a\mu_l$ is varied. The resulting kaon masses on these ensembles are rather close to the physical value although deviations of up to 10% [79] occur, which is particularly the case for the $A$ and $D$ ensembles. In addition, one may consider the $D$-meson masses whose values exhibit a large uncertainty. Nevertheless, they are also close to physical [79], implying that the resulting values of the charm quark mass lie in a reasonable range as well. In order to estimate effects of different value of the strange quark mass we will use ensembles $A80.24$ and $A100.24$ for which additional ensembles with re-tuned values of $a\mu_\sigma$ and $a\mu_\delta$ are available. In table 3.1 these ensembles are denoted by $A80.24s$ and $A100.24s$, where the suffix "$s$" refers to the re-tuning with respect to the strange quark mass, i.e. they reproduce the physical kaon mass value more accurately than the original $A80.24$ and $A100.24$ ensembles; see also the left panel of figure 3.4. In particular, these ensembles will be used to estimate the strange quark mass dependence of $M_\eta$. Further details on this will be discussed in section 3.3 in more detail.

| $\beta$ | 1.90 | 1.95 | 2.10 |
|---|---|---|---|
| $Z$ | 0.6703(8) | 0.6859(9) | 0.7493(11) |

Table 3.3: Values for $Z$ from matching mixed action (Osterwalder-Seiler) to unitary approach.

As discussed in sections 2.1 and 2.2, we need the ratio $Z$ of pseudoscalar and scalar flavor non-singlet renormalization constants for several purposes, i.e. the calculation of $f_K$ and the mixing parameters in the flavor singlet sector. The chirally extrapolated values of $Z$ at each value of the lattice spacing have been evaluated non-perturbatively for our situation in [153] and can be found in table 3.3.

## 3.2   Masses and flavor non-singlet decay constants

This section is dedicated to the extraction of masses for the light pseudoscalar flavor singlet and non-singlet mesons. First we give an overview on our results for flavor non-singlet masses and decay constants which are required for various purposes in our analysis concerning the flavor singlet states as well as the determination of low energy constants from W$\chi$PT. Since the masses of $\eta$ and $\eta$ are in the main focus of this work we dedicate a separate subsection to discuss the extraction of them in more detail. Moreover, we also include the results for the neutral pion masses, because the corresponding analysis is very similar (though simpler) to the one in the flavor singlet sector.

### 3.2.1   Charged pion and kaon

For the charged pion as well as the kaon the determination of masses is straightforward as both are the ground states of their respective correlation function matrices. Moreover, the resulting statistical errors are small (typically $\ll 1\%$), because the required correlation functions in Eqs. (2.47),(2.49) involve only quark connected diagrams. In both cases we use fuzzing to increase our operator basis by a factor of two, such that a plateau in the effective mass is reached for smaller values of $t$, which further decreases the statistical errors. For the charged pion this leads to a $4 \times 4$ correlation matrix from pseudoscalar and axial vector operators $\mathcal{P}_l^{\pm}$ and $\mathcal{A}_l^{\pm}$. For the kaon we end up with an $8 \times 8$ matrix using the interpolating operators in Eq. (2.21). Both, masses and the amplitudes that are required for the decay constants $f_{\mathrm{PS}}$ , $f_K$ are calculated by solving the GEVP and performing a single-state fit to the resulting eigenvalues at sufficiently large $t$. The details of our GEVP and fitting procedures are explained in appendix C, together with fit ranges, $\chi^2$ values and further technical details.

Our results are listed in table 3.4. However, we remark that most of the values for $M_{\mathrm{PS}}$, $f_{\mathrm{PS}}$ have been published before [79]. Nonetheless, we have recalculated the pion mass values with our statistics to allow for a more consistent analysis. Moreover, we have added the missing values

| ensemble | $aM_{\mathrm{PS}}$ | $aM_{\mathrm{K}}$ | $af_{\mathrm{PS}}$ | $af_{K}$ |
|---|---|---|---|---|
| $A30.32$ | 0.12358(30) | 0.25150(29) | 0.06452(21) | 0.07236(45) |
| $A40.24$ | 0.14484(44) | 0.25884(43) | 0.06577(24) | 0.07432(57) |
| $A40.32$ | 0.14140(30) | 0.25666(23) | 0.06839(18) | 0.07429(36) |
| $A60.24$ | 0.17277(48) | 0.26695(52) | 0.07209(20) | 0.07699(46) |
| $A80.24$ | 0.19870(35) | 0.27706(61) | 0.07581(13) | 0.07886(46) |
| $A100.24$ | 0.22127(32) | 0.28807(34) | 0.07936(14) | 0.08050(51) |
| $A80.24s$ | 0.19822(33) | 0.25503(33) | 0.07845(16) | 0.07639(18) |
| $A100.24s$ | 0.22118(33) | 0.26490(74) | 0.07857(14) | 0.07780(45) |
| $B25.32$ | 0.10685(43) | 0.21240(50) | 0.05728(21) | 0.06489(37) |
| $B35.32$ | 0.12496(45) | 0.21840(28) | 0.06105(17) | 0.06771(41) |
| $B55.32$ | 0.15396(31) | 0.22799(34) | 0.06545(11) | 0.07001(35) |
| $B75.32$ | 0.18036(39) | 0.23753(32) | 0.06908(14) | 0.07176(30) |
| $B85.24$ | 0.19373(64) | 0.24392(59) | 0.07039(26) | 0.07226(42) |
| $D15.48$ | 0.06954(26) | 0.16897(85) | 0.04373(19) | 0.04818(33) |
| $D20.48$ | 0.08000(36) | 0.17273(38) | 0.04486(19) | 0.04833(17) |
| $D30.48$ | 0.09801(25) | 0.17760(23) | 0.04735(15) | 0.05026(16) |
| $D45.32sc$ | 0.11991(37) | 0.17570(84) | 0.04825(14) | 0.04584(37) |

Table 3.4: Results of $aM_{\mathrm{PS}}$, $aM_K$ for all ensembles and the corresponding values for the charged pion decay constant $af_{\mathrm{PS}}$ and the kaon decay constant $af_{\mathrm{K}}$. Most of the pion and kaon mass values as well as the pion decay constants have been published already in [79]. However, we have recomputed the pion related observables as well as the missing kaon masses with our statistics. The values for $f_K$ have not been determined from the unitary action before.

for $M_K$ and $f_K$. The values for the kaon decay constant have not been previously calculated using the unitary action. It should be noted that the numbers of gauge configurations used for the missing kaon quantities are usually smaller than those that have been used for the pion and flavor singlet sector as detailed in table 3.1. The reason for this is that we did not recalculate all of kaon masses but only the missing ones and used resampling whenever the corresponding errors enter our analysis. Since the required accuracy for $M_K$ and $f_K$ can be reached with (much) smaller numbers of configurations than one needs in the flavor singlet sector, this helps to save a substantial amount of computation time.

All errors quoted in table 3.4 are purely statistical and have been calculated using the bootstrap method with 1000 bootstrap samples. Neither the pion related quantities nor those for the kaon show any sizable autocorrelation effects. However, for consistency reasons we have employed the same blocking as in the analysis of the flavor singlet sector; see next subsection for details.

### 3.2.2    Flavor singlet and neutral pion masses

In the flavor singlet sector we have calculated all the contractions required to build the correlation function matrix in the rotated twisted basis as given in Eq. (2.86). The numerical techniques for the evaluation of the connected and disconnected diagrams can be found in subsection 2.2.1. For the latter we used the same numbers of stochastic samples $N_s$ in the light and heavy sector and the actual values of $N_s$ for each ensemble are listed in table 3.1. In order to check that the stochastic noise introduced by our methods is of the same order (or even smaller) than the gauge noise we have increased $N_s$ from 24 to 64 for ensemble $B25.32$. This increase in $N_s$ did not further reduce the error of the masses.

Again, we use local and fuzzed operators to enlarge our correlation matrix by a factor two. Besides the interpolating operators in Eqs. (2.26),(2.32) and (2.33), one corresponding operators involving the $\gamma$-matrix combination $i\gamma_0\gamma_5$, which would further increase the correlation matrix. However, the corresponding correlation functions turn out to be too noisy to give any further improvement. In fact in the heavy sector the resulting signal is indistinguishable from zero within errors for certain matrix elements. The values for the number of gauge configurations $N$ investigated per ensemble are the ones listed in table 3.1.

The error analysis is again performed using the bootstrap method and in order to compensate for autocorrelation we employ blocking with blocks of length $N_b$. The values of $N_b$ are given in table 3.1 and have been chosen in such a way that the blocks are statistically independent. In general, autocorrelation appears to be relevant for the flavor singlet sector and particularly for $M_{\eta'}$ it seems to be significant, which is why we have computed the integrated autocorrelation time $\tau_{\text{int}}$ in units of Monte-Carlo trajectories of length 1 (see also subsection 2.3.1) for the elements of the correlation matrix $\mathcal{C}^{\eta,\eta'}(t)$ at fixed Euclidean time $t/a = 3$ on several ensembles. It turns out that the matrix elements involving light quarks are the ones most strongly affected by autocorrelation. For all other elements of the correlation function matrix we observe only mild effects. For instance, for ensemble $D15.48$ the matrix element with only light quark content yields $\tau_{\text{int}} = 9(2)$, while the elements without any light quark content have at most $\tau_{\text{int}} = 1.3(2)$. Note that our normalization in the definition of the integrated autocorrelation time in Eq. (2.95) is such that $\tau_{\text{int}} = 0.5$ corresponds to the absence of any autocorrelation. However, for the calculation of the actual errors we have varied the length of the blocks used in the bootstrap analysis and found that for a block length of $N_b \geq 10$ the error for all elements of $\mathcal{C}^{\eta,\eta'}(t)$ for ensemble $D15.48$ remains constant within error. The latter method gives $\tau_{\text{int}} = 7(2)$ for the matrix elements with light quark content, which is consistent with the result from the $\Gamma$-method. The choice $N_b = 10$ corresponds for $D15.48$ to 20 Monte-Carlo trajectories of length 1; see [154] for a description of the hybrid Monte-Carlo (HMC) algorithm that has been used for the generation of the gauge configurations.

Moreover, the observed autocorrelation depends on the lattice spacing, i.e. for increasing values of the lattice spacing the autocorrelation decreases. For example, the matrix element $\mathcal{C}^{\eta,\eta'}(t)_{\mathcal{S}_l^3\mathcal{S}_l^3}$, involving only light quarks, exhibits an integrated autocorrelation time of $\tau_{\text{int}} = 6(1)$ for $B25.32$ and $\tau_{\text{int}} = 4(1)$ for $A30.32$, compared to the aforementioned $\tau_{\text{int}} = 9(2)$ for $D15.48$. A significant dependence on the quark mass has not been observed.

| ensemble | $aM_{\pi^0}$ | $aM_{\pi^0,c}$ | $aM_\eta$ | $aM_{\eta'}$ |
|---|---|---|---|---|
| $A30.32$ | 0.061(04) | 0.2111(33) | 0.286(15) | 0.49(06) |
| $A40.24$ | 0.069(07) | 0.2375(25) | 0.281(18) | 0.39(06) |
| $A40.32$ | 0.081(05) | 0.2275(31) | 0.281(11) | 0.49(09) |
| $A60.24$ | 0.101(11) | 0.2544(26) | 0.290(07) | 0.59(09) |
| $A80.24$ | 0.122(16) | 0.2659(25) | 0.302(07) | 0.60(08) |
| $A100.24$ | 0.157(18) | 0.2883(14) | 0.315(10) | 0.50(07) |
| $A80.24s$ | 0.151(12) | 0.2649(16) | 0.270(10) | 0.54(09) |
| $A100.24s$ | 0.186(14) | 0.2841(16) | 0.280(05) | 0.66(12) |
| $B25.32$ | 0.060(04) | 0.1836(21) | 0.234(20) | 0.50(08) |
| $B35.32$ | 0.071(06) | 0.1919(17) | 0.237(10) | 0.59(09) |
| $B55.32$ | 0.132(08) | 0.2177(19) | 0.249(09) | 0.60(10) |
| $B75.32$ | 0.156(13) | 0.2360(12) | 0.253(14) | 0.44(07) |
| $B85.24$ | 0.119(18) | 0.2480(11) | 0.260(13) | 0.51(12) |
| $D15.48$ | 0.056(03) | 0.1124(15) | 0.192(15) | 0.37(07) |
| $D20.48$ | 0.065(04) | 0.1170(16) | N/A | N/A |
| $D30.48$ | 0.086(05) | 0.1296(15) | 0.205(16) | 0.38(04) |
| $D45.32sc$ | 0.089(09) | 0.1480(09) | 0.201(09) | 0.30(04) |

Table 3.5: Results of $aM_{\pi^0}$, $aM_{\pi^0,c}$, $aM_\eta$, $aM_{\eta'}$ for all ensembles. For $D20.48$ we were not able to extract reliable values for $aM_\eta$ and $aM_{\eta'}$ within the statistics we used, due to bad plateaux in both relevant principal correlators.

For the details of the GEVP and fitting procedures used to extract $M_\eta$, $M'_\eta$ as well as further technical details we again refer to appendix C. For the masses we solely used the bootstrap method combined with blocking to analyze effects of autocorrelation. We found that the $\eta$ is only mildly affected by autocorrelation, whereas the $\eta'$ state shows significant effects. The latter is in agreement with what has been found earlier in the $N_f = 2$ setup [140]. Again, for ensemble $D15.48$ a block size of $N_b = 10$ seems to result in statistically independent blocks. However, we stress that with the numbers of configurations used in our investigations we can not use $N_b > 20$, because the number of blocks becomes too small. Therefore, we cannot exclude autocorrelation occurring on longer scales.

An overview of the masses together with their respective errors can be found in table (3.5). In addition we have listed the results for the neutral pion which also involves the calculation of disconnected diagrams. The analysis for the $\pi^0$ is performed in exactly the same way as the one for the flavor singlet mesons, however, autocorrelation is a much less significant factor compared to the $\eta'$ and rather comparable to the case of the $\eta$. For the neutral pion we have calculated the $4 \times 4$ correlation function matrix built from the interpolating operators $\mathcal{S}_l^0$ and $\mathcal{A}_l^3$ in Eqs. (2.8),(2.9) and again using local and fuzzed operators. Since only light quarks contribute no further rotation is required and the GEVP is applied to the resulting correlation function matrix. We refrained from calculating the corresponding decay constant as it is not required for
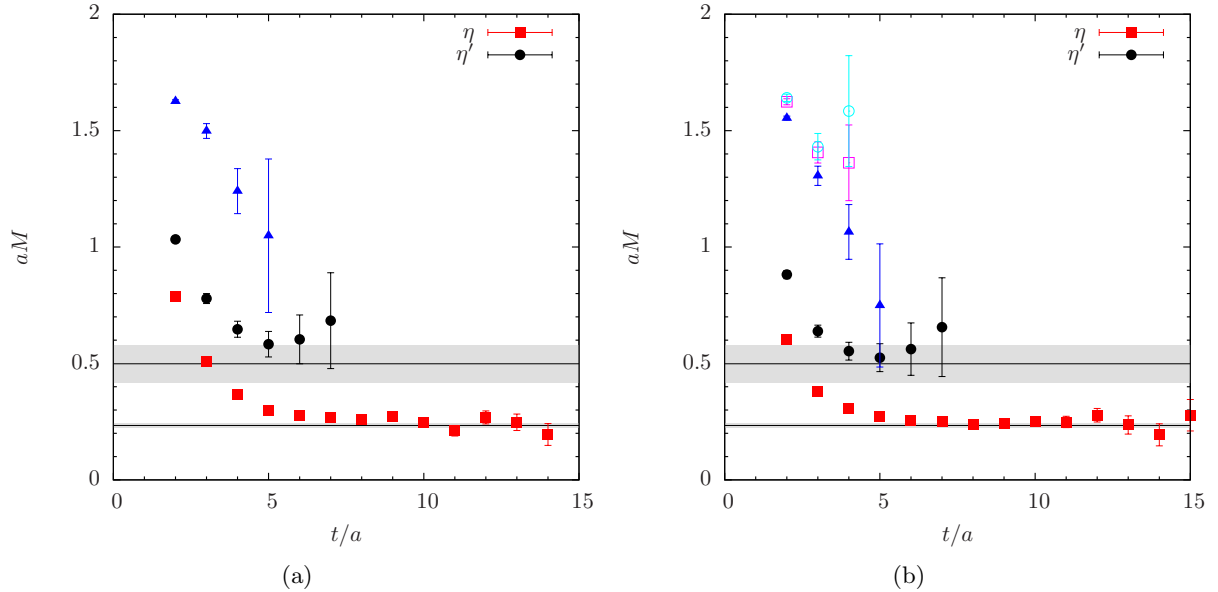
Figure 3.1: (a) Effective masses in lattice units determined from solving the GEVP for a $3 \times 3$ matrix with $t_0/a = 1$ for ensemble $B25.32$. (b) The same as in the left panel, but for a $6 \times 6$ matrix. For comparison also the fit results (see text) for the two lowest states are shown (cf. table 3.5).

any of our purposes. Besides, it is expected to exhibit rather large statistical errors.

In the left panel of figure 3.1, we show the effective masses determined from solving the GEVP on a $3 \times 3$ matrix for ensemble $B25.32$ built from local operators only. Note that only for the purpose of this plot, we kept $t_0/a = 1$ fixed. One observes that the ground state is very well determined, such that it can be extracted from a simple plateau fit. For the he second state, i.e. the $\eta'$, the situation is very different as it is much more noisy and any attempt of a mass determination seems questionable, at least from a $3 \times 3$ matrix. As previously discussed in subsection 2.2.2, enlarging the operator basis of the correlation function matrix may significantly reduce the contributions of excited states to the lowest lying states and an extraction of $M_{\eta'}$ may become feasible due to the generally smaller statistical errors at smaller values of $t$.

This effect can be observed for the $6 \times 6$ matrix that is shown in the right panel of figure 3.1 and for which fuzzed operators have been used in addition to the local ones. The final fit results and errors for the masses are indicated by the horizontal bands in figure 3.1. For the $\eta'$ we do not determine them directly from a constant fit to the plateau, but from a three state cosh fit to the eigenvalues, possibly also using larger values of $t_0$ when solving the GEVP, see appendix C. As shown in the plot, the procedure yields very good agreement with a plateau fit for the $\eta$, but gives slightly lower values for the $\eta'$. From this one may conclude that the extraction of the $\eta'$ mass is affected by non-negligible systematic uncertainties.

The third state in the left panel of figure 3.1 appears to be in the region where one would
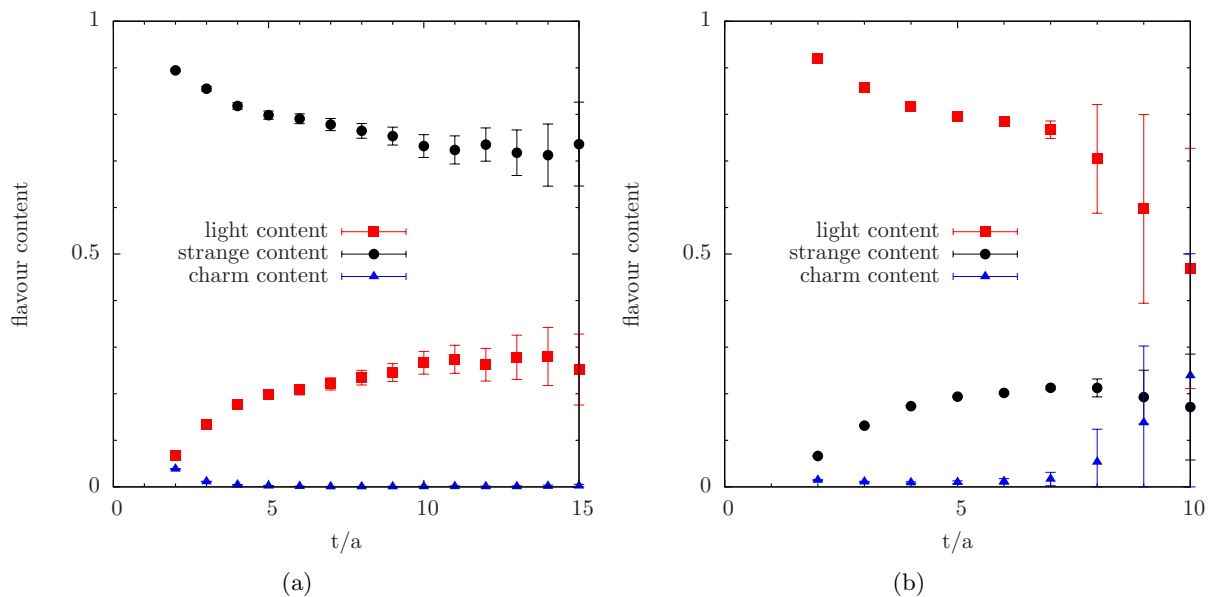
Figure 3.2: (a) Squared flavor content of $\eta$ for B25.32 from $3 \times 3$ matrix using local operators only. (b) Squared flavor content of $\eta'$ for B25.32.

expect the $\eta_c$ mass value. Unfortunately, the signal is lost at $t/a = 5$, which renders a reliable extraction impossible. Note that qualitatively the two plots in figure 3.1 are rather independent of the particular choice of the ensemble.

In order to gain further confidence in the identification of the $\eta$ and $\eta'$ states, we also determine the flavor content of the two states, which are given by the elements of the eigenvectors $v_i^{(n)}(t, t_0)$ obtained from solving the GEVP for the renormalized correlation function matrix in the original twisted basis which is given in Eq. (2.88). The index $i = l, s, c$ labeling the elements of the eigenvector corresponds to the flavors entering the interpolating operators in the physical basis. Note that for this definition we assumed the eigenvectors to be appropriately normalized, i.e. $\left|v^{(n)}(t, t_0)\right|^2 = 1$. In the left panel of figure 3.2 we exemplarily show the flavor content of the $\eta$ for ensemble $B25.32$. Indeed, as one would expect from phenomenology, the $\eta$ is dominated by strange quark content, while the second state, that is shown in the right panel of figure 3.2 is dominated by light quarks, which one expects for the $\eta'$. It should be noted though that since we do not include a gluonic operator in our analysis we only obtain information on the relative quark content. Clearly, for both states the charm contribution is compatible with zero.

Figure 3.3 shows the results for $M_\eta$ (filled symbols) and $M_{\eta'}$ (open symbols) for all our ensembles as a function of the squared pion mass. For this plot we expressed all quantities in units of $r_0$. All the masses shown in this plot are listed in table 3.5 and have been obtained from solving the GEVP for a $6 \times 6$ matrix, for further details we refer to appendix C. The results of this procedure have been independently cross-checked using the factorizing fit model in Eq. (2.101). From figure 3.3 one infers that the $\eta$ meson mass can be extracted with high statistical precision,

while the $\eta'$ meson mass is more noisy. This behavior can be understood as in the $\mathrm{SU}(3)_F$ symmetric limit the $\eta$ meson is a flavor octet with all disconnected contributions vanishing, while the $\eta'$ is the flavor singlet with non-vanishing disconnected contributions.
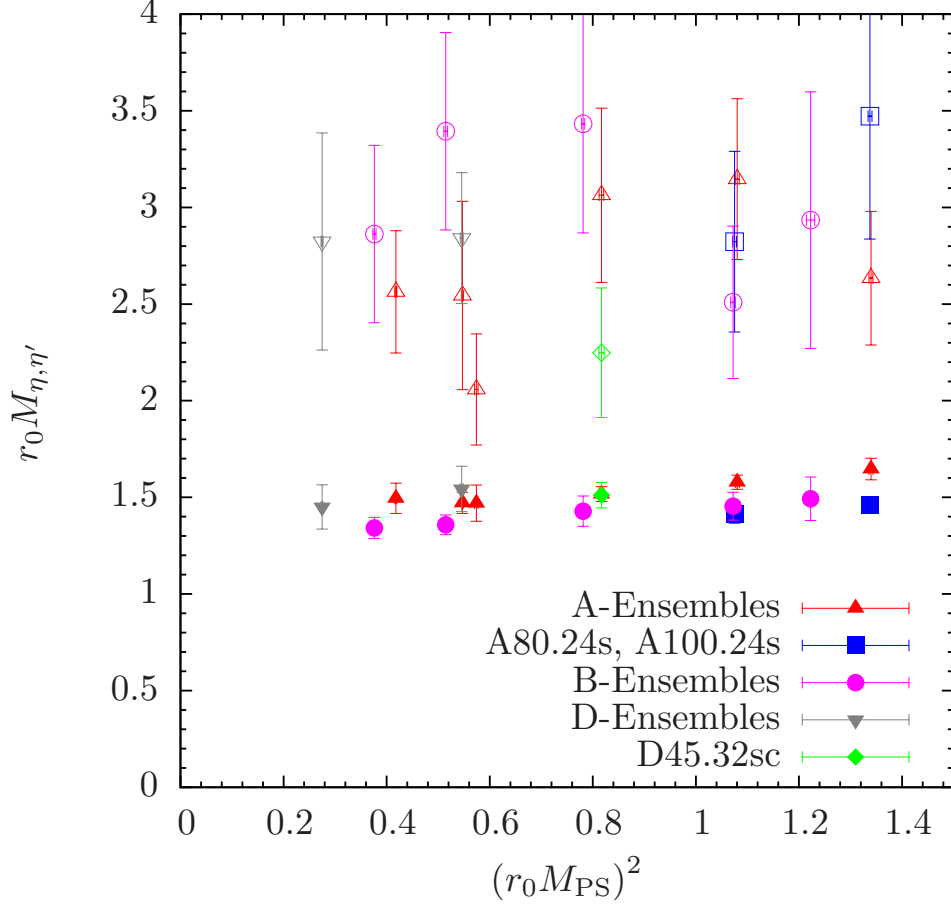


Figure 3.3: Masses for $\eta$ (filled symbols) and $\eta'$ (open symbols) in units of chirally extrapolated $r_0$ (listed in table 3.2) as a function of $(r_0 M_{\mathrm{PS}})^2$.

Finally, before turning to the discussion of the quark mass dependence, we mention that as some of our ensembles have a value of $M_{\mathrm{PS}}L < 3.5$ it is interesting to estimate possible finite size corrections to $M_\eta$ and $M_{\eta'}$. In our investigations we have included two ensembles which differ only in $L/a$, i.e. $A40.24$ and $A40.32$ which have $M_{\mathrm{PS}}L = 3.5$ and $M_{\mathrm{PS}}L = 4.5$, respectively. On these two ensembles both masses agree within their respective errors. From table 3.5 it is obvious that the values for $M_\eta$ agree particularly precisely. Furthermore, for the kaon mass the finite size corrections turn out to be below 1% on these ensembles. As a consequence of this, we conclude that the finite size corrections to $M_\eta$ and $M_{\eta'}$ will not significantly impact our analysis at the current level of precision, which is why we neglect them for all further considerations. However, we are aware that for a really definite conclusion more ensembles with different $L/a$-values are needed.

## 3.3   Chiral extrapolations and scaling artifacts for $\eta,\eta'$

The lattice calculations described in the previous section have all been carried out for unphysical values of the quark masses. Therefore, it is necessary to perform a careful chiral extrapolation in order to obtain physical results for $M_\eta$. Moreover, every lattice simulation employs a finite value of the lattice spacing, hence it is also required to perform an extrapolation in the lattice spacing to reach the continuum limit. In this section we first discuss the strange quark mass dependence for the mass of the $\eta$ and perform a scaling test after shifting the relevant ensembles to a common strange quark mass value. In a second step we correct all our ensembles for the mistuning in the strange quark mass value and perform the extrapolation to the physical point. Finally, we discuss the results of this analysis.

Concerning the $\eta'$, we remark that its mass in figure 3.3 mass shows rather large fluctuations and no consistent picture regarding quark mass dependence and lattice artifacts. This is mainly caused by the large noise in the $\eta'$ state, which has the effect that the signal for the extracted mass is lost at rather small $t$-values. Therefore, the values of the mass for the $\eta'$ are likely to be affected by non-negligible systematic uncertainties for most of our ensembles and have to be considered only as an upper bound, because a plateau in the mass is not reached. For this reason we will postpone dealing with the issue of performing an extrapolation in the light quark mass for $M_{\eta'}$ until the next section.

### 3.3.1   Strange quark mass dependence and scaling test

The results displayed in figure 3.3 have been obtained using the bare values of $a\mu_\sigma$ and $a\mu_\delta$ as used for the production of the ensembles. However, these values did not reproduce the physical values of the kaon and D-meson masses as discussed in [79, 134]. In the left panel of figure 3.4 we show the kaon mass as a function of the squared pion mass for all ensembles at the coarsest lattice spacing. From this plot it is evident that the two ensembles $A80.24s$ and $A100.24s$ with a re-tuned value of the strange quark mass yield values for the kaon mass that are much closer to the physical one; see also [79, 151]. The right panel of figure 3.4 contains a corresponding plot for $r_0 M_\eta$ which exhibits a very similar pattern as the one observed for the kaon mass. Besides the fact that the strange quark mass has been re-tuned for two of the $A$-ensembles, we remark that the physical strange and charm quark mass values differ also among the $A$, $B$ and $D$ ensembles. Therefore, one cannot draw any definite conclusion from figure 3.3 regarding lattice artifacts and the extrapolation to the physical points. However, one can infer from this plot that the light quark mass dependence of the $\eta$ mass is rather weak.

Before we actually carry out an extrapolation of all our data, we can perform a scaling test for $M_\eta$. To this end, one has to compare $M_\eta$ at the three available values of the lattice spacing for fixed values of the renormalized quark masses (e.g. by demanding $r_0 M_{\mathrm{PS}}$, $r_0 M_{\mathrm{K}}$, $r_0 M_{\mathrm{D}}$) and the physical volume. As stated before, we do not expect the volume to have any sizable effect and also the charm quark mass value should have only little influence given our uncertainties. Therefore, we disregard effects from slightly different physical volumes at the different $\beta$-values and the differences in the charm quark mass for the following considerations. Since we do not
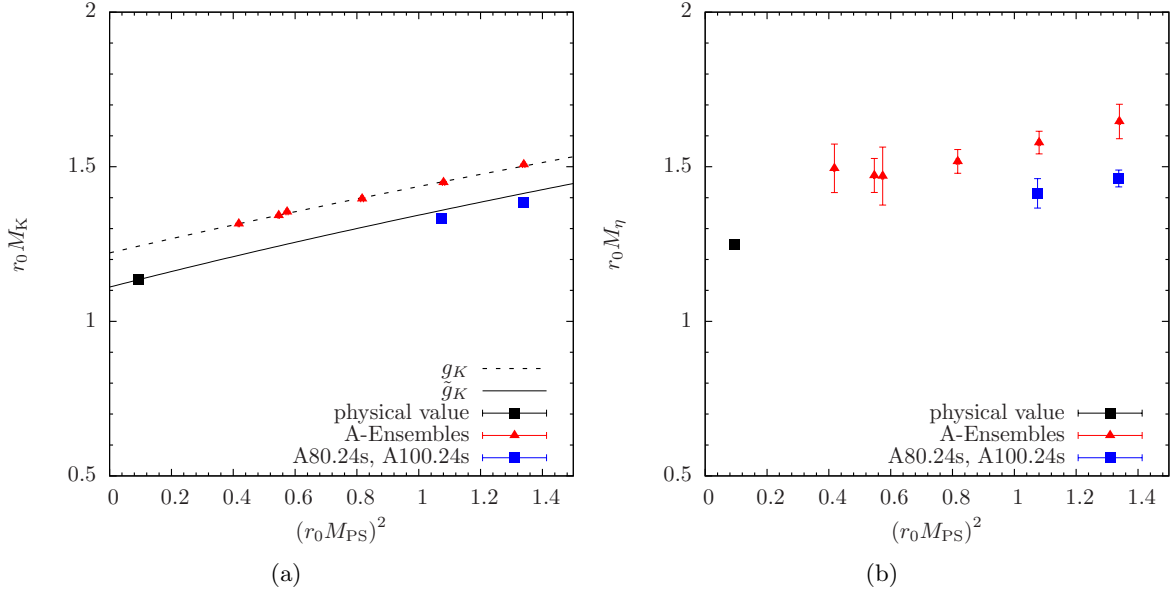
Figure 3.4: (a) The kaon mass in units of $r_0$ and (b) $r_0 M_\eta$ as a function of $(r_0 M_{\mathrm{PS}})^2$ for all $A$ ensembles. The dotted and solid curves in (a) represent the fitted $g_K$ in Eq. (3.4) and the shifted $\tilde{g}_K$ (see text), respectively.

have simulations at the three values of the lattice spacing with matched values of the strange quark mass, we need to perform an interpolation in $M_K$ for a scaling test. For this purpose we have to rely on the two pairs of $A$ ensembles for which the strange quark mass has been varied, i.e. ($A80.24$, $A80.24s$) and ($A100.24$, $A100.24s$). To be more precise, the two ensembles within each pair differ in the values of $a\mu_\sigma$ and $a\mu_\delta$, whereas $a\mu_l$ is identical, but different for the two pairs. From these ensembles we can estimate the derivative $D_\eta$ of $M_\eta^2$ with respect to $M_K^2$ and use it to correct for the mismatch in $r_0 M_K$. However, we stress that using this estimate for all our ensembles one neglects any possible dependence of $D_\eta$ on the light, strange and charm quark masses as well as on the lattice spacing.

The idea behind this interpolation is to treat the masses of the kaon and the $\eta$ as functions $M^2 = M^2[M_{\mathrm{PS}}^2, M_K^2]$ which is motivated from leading order $\chi$PT (c.f. Eqs. (1.80),(1.81)) and to define the dimensionless quantity

$$D_\eta(\mu_l, \mu_\sigma, \mu_\delta, \beta) \equiv \frac{d(aM_\eta)^2}{d(aM_K)^2} \, . \tag{3.1}$$

Within errors the estimates obtained from ($A80.24$, $A80.24s$) and ($A100.24$ $A100.24s$) agree and for the average over the two pairs of ensembles we obtain $D_\eta = 1.60(18)_{\mathrm{stat}}$. Assuming that the value of $D_\eta$ is independent of the quark mass values $\mu_l, \mu_\sigma, \mu_\delta$ and the lattice spacing, we can use $D_\eta$ to correct two sets of ensembles $S_1$, $S_2$, namely $S_1 = \{A40.32, B35.32, D30.48\}$ and $S_2 = \{A60.24, B55.24, D45.24\}$ to a common value of of $r_0 M_K \approx 1.34$ using

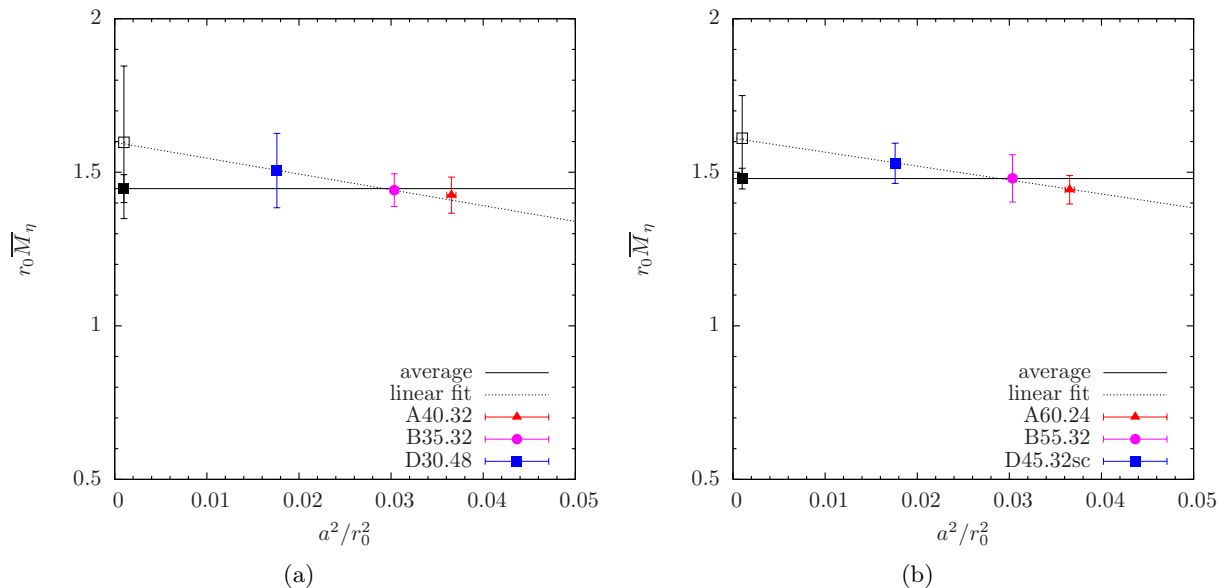$$(r_0 \overline{M}_\eta)^2 = (r_0 M_\eta)^2 + D_\eta \, \Delta_{\mathrm{K}} \, , \tag{3.2}$$

Figure 3.5: (a) $r_0\overline{M}_\eta$ as a function of $(a/r_0)^2$ for the ensembles $A40.32$, $B35.32$ and $D30.46$ (b) The same as in the left panel, but for the ensembles $A60.24$, $B55.32$ and $D45.32sc$. The continuum extrapolated values $r_0 M_\eta^{a\to 0}$ are horizontally displaced for legibility.

where $\Delta_\mathrm{K}$ is the difference in the squared kaon mass values in units of $r_0$. Note that for each set the three points have approximately equal values of $r_0 M_\mathrm{PS}$, i.e. $r_0 M_\mathrm{PS} \approx 0.73$ and $r_0 M_\mathrm{PS} \approx 0.90$ for $S_1$ and $S_2$, respectively.

The resulting values of $r_0\overline{M}_\eta$ for the sets $S_1$, $S_2$ are plotted as a function of $(a/r_0)^2$ in the left and right panel of figure 3.5, respectively. Both data sets are compatible with a constant continuum extrapolation giving $r_0 M_{\eta,S_1,\mathrm{const}}^{a\to 0} = 1.447(45)_\mathrm{stat}$ and $r_0 M_{\eta,S_2,\mathrm{const}}^{a\to 0} = 1.480(34)$. In figure 3.5 these results are indicated by the horizontal lines. In addition, we can perform a linear extrapolation, resulting in $r_0 M_{\eta,S_1,\mathrm{lin}}^{a\to 0} = 1.60(25)_\mathrm{stat}$ and $r_0 M_{\eta,S_2,\mathrm{lin}}^{a\to 0} = 1.61(14)_\mathrm{stat}$, which is also shown in the figure. The differences in between the two values from constant and linear extrapolations for each set are

$$r_0\Delta M_{\eta,S_1}^{a\to 0} = 0.15(25)_\mathrm{stat}\,, \qquad r_0\Delta M_{\eta,S_2}^{a\to 0} = 0.13(13)_\mathrm{stat}\,. \qquad (3.3)$$

In the following we will use them to estimate the systematic uncertainty related to the continuum extrapolation. Both results agree well, although the one for $S_1$ exhibits twice the error, which is mainly due to the smaller set of configurations used for $D30.48$. Therefore, we will quote an 8% relative error from $\Delta M_{\eta,S_2}^{a\to 0}/M_{\eta,S_2,\mathrm{const}}^{a\to 0}$ for our mass estimates, which we assume to be a conservative figure.

In order to obtain a more complete picture, we also attempt to correct all our ensembles for the slightly mistuned value of the strange quark mass. To this end, we first perform a linear fit to

the values of $(r_0 M_K)^2$ for the $A$-ensembles, leaving out $A80.24s$ and $A100.24s$, i.e.

$$g_{\mathrm{K}}[(r_0 M_{\mathrm{PS}})^2, a, b] = a + b\,(r_0 M_{\mathrm{PS}})^2 \,. \tag{3.4}$$

The resulting curve is then shifted such that $(r_0 M_{\mathrm{K}}^{\mathrm{exp}})^2 = g_{\mathrm{K}}[(r_0 M_\pi)^2, \tilde{a}, b]$ and we denote this new function by $\tilde{g}_{\mathrm{K}} = g_{\mathrm{K}}[(r_0 M_{\mathrm{PS}})^2, \tilde{a}, b]$. From this procedure we obtain $\tilde{a} = 1.24(11)_{\mathrm{stat}}$ and $b = 0.564(8)_{\mathrm{stat}}$[1]. In the left panel of figure 3.4 we show the two curves corresponding to $g_K$ and $\tilde{g}_K$. As it turns out, the kaon masses for the two re-tuned ensembles $A80.24s$ and $A100.24s$ are already very close to $\tilde{g}_K$.

The next step is to compute the difference of the squared kaon mass values to $\tilde{g}$ for all our ensembles, i.e.

$$\delta_{\mathrm{K}}[(r_0 M_{\mathrm{PS}})^2] = (r_0 M_{\mathrm{K}})^2[(r_0 M_{\mathrm{PS}})^2] - \tilde{g}_{\mathrm{K}}[(r_0 M_{\mathrm{PS}})^2]\,, \tag{3.5}$$

which is then used correct the measured $M_\eta^2[(r_0 M_{\mathrm{PS}})^2]$ by virtue of the following relation

$$(r_0\overline{M}_\eta)^2[(r_0 M_{\mathrm{PS}})^2] = (r_0 M_\eta)^2[(r_0 M_{\mathrm{PS}})^2] + D_\eta \cdot \delta_{\mathrm{K}}[(r_0 M_{\mathrm{PS}})^2]\,. \tag{3.6}$$

In the left panel of figure 3.6 we show the resulting values of $r_0\overline{M}_\eta$ for all our ensembles as a function of $(r_0 M_{\mathrm{PS}})^2$ and it is evident that all the data fall on a single curve within statistical uncertainties. This confirms that $M_\eta$ is not affected by large lattice artifacts. Again, we point out that we ignored the $\mu_l$, $\mu_\sigma$, $\mu_\delta$ and $\beta$ dependence of the derivative $D_\eta$ and that with the present set of data we are not able to estimate the systematic uncertainties stemming from this approximation. Moreover, we remark that the errors of the data points in this plot are highly correlated because they include the error of the derivative $D_\eta\,(\mu_l, \mu_\sigma, \mu_\delta, \beta)$. This large correlation of the point errors is also reflected by the error band displayed in the left panel of figure 3.6. However, the nice result appears to confirm the validity of our assumptions.

### 3.3.2   Extrapolation to the physical point

Having corrected our data for the mismatch of the strange quark masses by fixing of $M_K$ to its physical value $M_K^{\mathrm{exp}}$ and correcting $M_\eta$ as described in the previous subsection, we can now perform the extrapolation to the physical point, i.e. apply a linear fit to all corrected data points for $(r_0\overline{M}_\eta)^2[(r_0 M_{\mathrm{PS}})^2]$. Using $r_0 = 0.45(2)\,\mathrm{fm}$ as discussed in section 3.1, the fit yields $r_0 M_\eta\left[r_0^2 M_\pi^2\right] = 1.26(9)_{\mathrm{stat}}(10)_{\mathrm{sys}}$ and converted to physical units

$$M_\eta(M_\pi) = 551(30)_{\mathrm{stat}}(44)_{\mathrm{sys}}\,\mathrm{MeV}\,, \tag{3.7}$$

where we employed the experimental value of the neutral pion mass in Eq. (1.41) for $M_\pi$. Taking the SU (2) chiral limit we obtain $r_0 \mathring{M}_\eta^{\mathrm{SU}(2)} = 1.24(10)_{\mathrm{stat}}(10)_{\mathrm{sys}}$ or

$$\mathring{M}_\eta^{\mathrm{SU}(2)} = 542(32)_{\mathrm{stat}}(43)_{\mathrm{sys}}\,\mathrm{MeV}\,. \tag{3.8}$$

---

[1]Note that here we decided to include the error on $r_0^\chi/a$ in the error of the fit parameters, which has not been done in the original publication [1]. Moreover, at the time of the aforementioned publication less ensembles and partly lower statistics were available. However, these changes have no significant effect on further results.
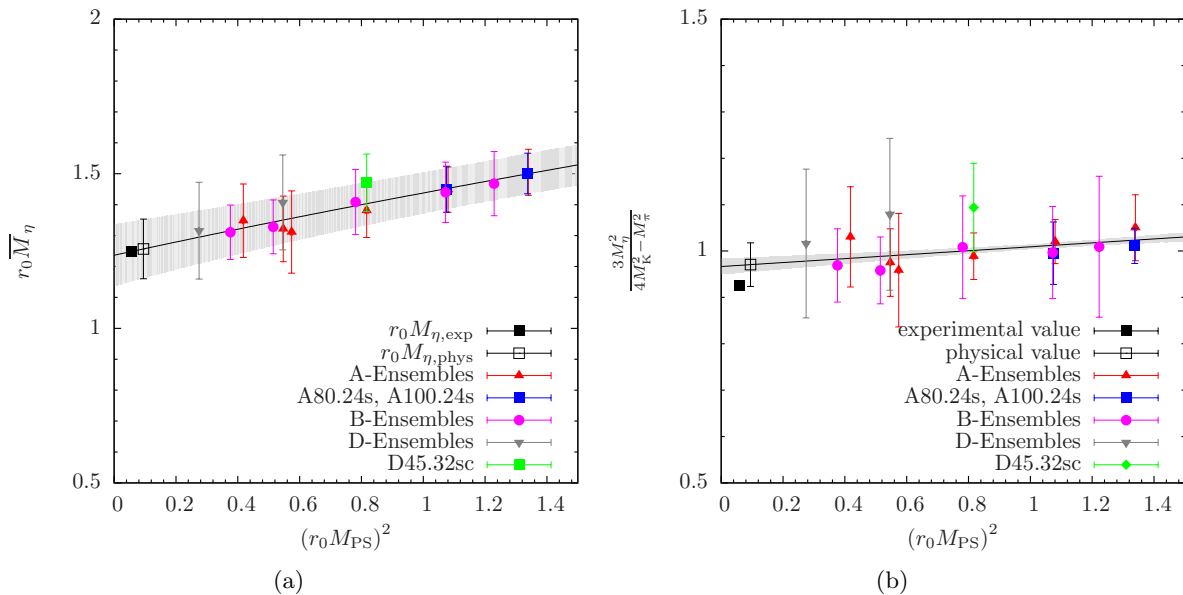
Figure 3.6:   (a) Values of $r_0\overline{M}_\eta$ as a function of $(r_0 M_{\mathrm{PS}})^2$ as explained in the text. (b) GMO ratio from Eq. (1.83) as a function of $(r_0 M_{\mathrm{PS}})^2$ for all available ensembles. Experimental values are horizontally displaced for legibility. Note that the errors of the data points in (a) are highly correlated as they include the error of the derivative $D_\eta\left(\mu_l,\mu_\sigma,\mu_\delta,\beta\right)$.

For the estimation of the systematic error we used the ratio $\Delta M_\eta^{a\to 0}/M_{\eta,\mathrm{const}}^{a\to 0}$ as discussed in the previous subsection. We remark that for the results in physical units the error on $r_0 = 0.45(2)$ yields a very significant contribution.

Since the procedure that has been applied to deal with the mistuning of the strange quark mass relies on the assumption that the derivative $D_\eta$ is independent on the bare quark mass parameters $\mu_l$, $\mu_\sigma$, $\mu_\delta$ and the lattice spacing, it is be desirable to perform a cross-check. To this end we employ two approaches which are both based on an attempt to build quantities for which most of the strange quark mass dependence is canceled. As a first possible approach, we study the ratio obtained from the Gell-Mann-Okubo relation as given in Eq. (1.83), which becomes rigorous in the SU (3) symmetric case and is violated only by a few percent for physical values of the corresponding meson masses. Therefore, one expects the strange quark mass dependence of the ratio $3M_\eta^2/(4M_\mathrm{K}^2 - M_\pi^2)$ to be weak. In the right panel of figure 3.6 we show the GMO ratio as a function of $(r_0 M_{\mathrm{PS}})^2$ together with a linear extrapolation, indicated by the solid line and the shaded error band. It is interesting to see that the data points for the ratio from $A80.24$ and $A80.24s$ as well as $A100.24$ and $A100.24s$ agree within errors, which confirms that a large part of the strange quark mass dependence is canceled in the GMO ratio. Furthermore, all the data points align onto a single curve within errors, independent of the value of the lattice spacing, as well as the strange and the charm quark mass. The linear fit in $(r_0 M_{\mathrm{PS}})^2$ to our data for the ratio yields

$$\left(3M_\eta^2/(4M_\mathrm{K}^2 - M_\pi^2)\right)_{M_\pi} = 0.970(47)_{\mathrm{stat}}\,, \qquad (3.9)$$

for the physical value of the (neutral) pion mass. The result is in agreement with the experimental value $(3M_\eta^2/(4M_K^2 - M_\pi^2))^{\exp} = 0.925$, and again, we can obtain an estimate for the physical mass of $M_\eta$ using the experimental values of $M_{\pi^0}$ and $M_{K^0}$, i.e.

$$M_\eta = 559(14)_{\rm stat}(45)_{\rm sys} \text{ MeV} , \tag{3.10}$$

which is also in good agreement with experiment. Besides, we remark that our value for $D_\eta = 1.60(18)_{\rm stat}$ is in rather good agreement to the value $4/3$ that one would naively expect from Eq. (1.82).

Secondly, from figure 3.4 it appears that $M_\eta$ and $M_K$ have a similar strange quark mass dependence, which motivates to study the ratio $M_\eta/M_K$. In the left panel of figure 3.7 we show this ratio as a function of $(r_0 M_{\rm PS})^2$ for all available ensembles. It is evident that all data points data points fall on the same curve withing errors and in particular the points within two pairs of $A$ ensembles with re-tuned strange quark mass, i.e. ($A80.24s$, $A80.24s$) and ($A100.24$, $A100.24s$), agree well within errors. This confirms that indeed most of the strange quark mass dependence cancels in the ratio $M_\eta/M_K$. In the right panel of figure 3.7 we also show the ratio $\overline{M}_\eta/M_K$ as a function of $(r_0 M_{\rm PS})^2$ and indeed there appears to be no significant correction within the present errors compared to the plot shown in the left panel. However, note that for $\overline{M}_\eta/M_K$ the derivative $D_\eta(\mu_l, \mu_\sigma, \mu_\delta, \beta)$ has again been used, which leads to correlated and thus slightly larger errors. Performing a linear extrapolation of the ratio $(M_\eta/M_K)^2$ in $(r_0 M_{\rm PS})^2$ to the physical pion mass point for all available data gives

$$(M_\eta/M_K)_{M_\pi} = 1.123(26)_{\rm stat} , \tag{3.11}$$

which agrees well with the experimental value $(M_\eta/M_K)^{\exp} = 1.100$. The result of this fit is indicated by the solid line and the shaded error band in the left panel of figure 3.7, where also the extrapolated value is shown together with the experimental one. Using the experimental value of $M_{K^0} = 498$ MeV to convert to physical units we obtain

$$M_\eta = 559(13)_{\rm stat}(45)_{\rm sys} \text{ MeV} . \tag{3.12}$$

where the systematic error has been estimated as discussed in the previous subsection. Note that in this analysis the scale $r_0 = 0.45(2)$ fm enters the final result only through the determination of the physical pion mass point. Since the slope of the extrapolation in $(r_0 M_{\rm PS})^2$ is rather small, the statistical uncertainty in $M_\eta$ turns out significantly smaller than the one obtained for the direct extrapolation of $(r_0 M_\eta)^2$. Moreover, we remark that we have performed the same extrapolation also for the corrected ratio $\overline{M}_\eta/M_K$, yielding

$$(M_\eta/M_K)_{M_\pi} = 1.110(49)_{\rm stat} \tag{3.13}$$

and

$$M_\eta = 0.547(25)_{\rm stat}(44)_{\rm sys} \text{ MeV} , \tag{3.14}$$

respectively, which is indeed in excellent agreement with the direct extrapolation of $(M_\eta/M_K)^2$, again confirming that most of the strange quark mass dependence cancels in the ratio $(M_\eta/M_K)^2$.
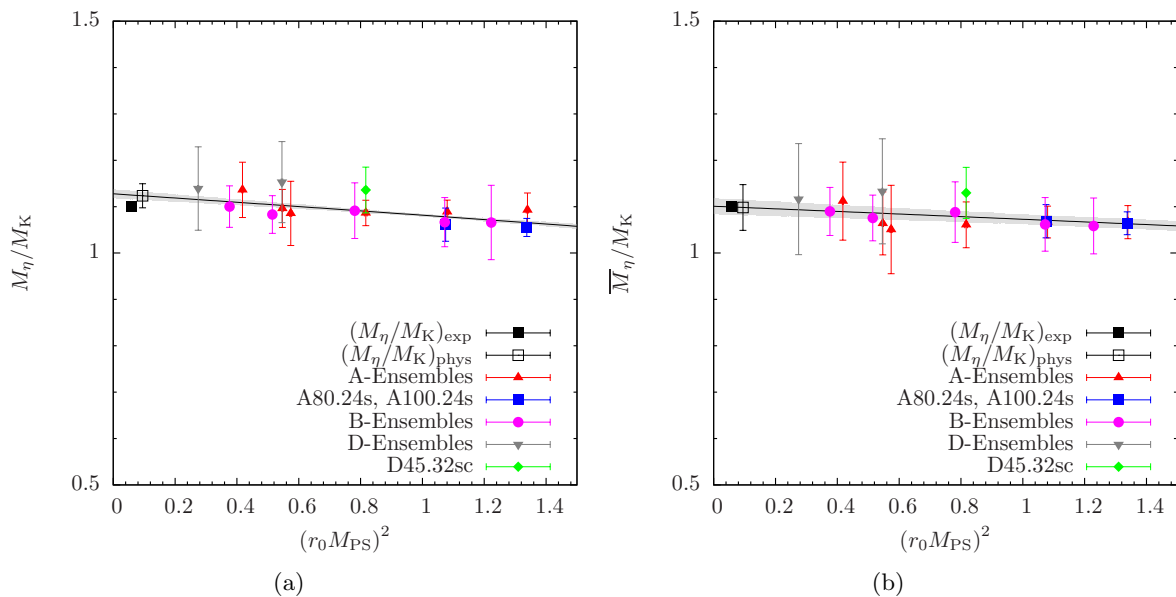
Figure 3.7: (a) $M_\eta/M_K$ as a function of $(r_0 M_{PS})^2$ for all available ensembles. (b) The same as in the left panel, but determined from the $m_s$-corrected $r_0 \overline{M}_\eta$ values and the corresponding values of the kaon mass (see text). Experimental values are horizontally displaced for legibility. The larger errors in (b) are highly correlated as they are dominated by the error of the derivative $D_\eta (\mu_l, \mu_\sigma, \mu_\delta, \beta)$.

At the very end of section 3.2 we discussed finite size corrections to $M_\eta$ and concluded that they are negligible for any of our purposes. Nevertheless, one might still ask how finite size corrections to $M_K$ and $M_{PS}$ influence our extrapolations. However, it turns out that also this influence is smaller than our statistical uncertainty for several reasons. First of all, the observed pion mass dependence of $M_\eta$ is very weak, such that any finite size effects entering $M_{PS}$ are not expected to have significant impact on the extrapolation of $M_\eta$. Secondly, the corrections entering $M_K$ appear to be small, e.g. for the two ensembles $A40.24$, $A40.32$ we have $aM_K = 0.25884(43)_{stat}$ and $aM_K = 0.25666(23)_{stat}$, respectively, see also table 3.4. Finally, only a few ensembles have small $M_{PS}L$, thus a small change due to finite size effects for these ensembles is not expected to affect the fit result significantly.

## 3.4 Removal of excited states for $\eta$, $\eta'$

From the analysis that has been detailed in the previous two sections it was not possible to obtain a sufficient signal-to-noise ratio for the mass of the $\eta'$ meson to allow for a reliable extrapolation. As stated before, the large statistical errors for this state as shown in figure 3.3 include also systematic effects due to the use of a three state cosh-fit to its eigenvalues, which is required because for most ensembles the effective mass does not reach a plateau (c.f. the left

panels of figures 3.1,3.9). Therefore, we considered the values for $M_{\eta'}$ only as an upper bound. Clearly, it would be desirable to improve this situation to be able to make physical statements about the $\eta'$ as well. One rather obvious possibility to achieve the required improvement is to increase the operator basis by including additional, suitable interpolating operators, i.e. those corresponding to the physical axial vector current. Unfortunately, it turns out that this does not help in practice, because the resulting correlation functions are much noisier than those obtained for the physical pseudoscalar current. In fact, for the heavy sector many of the resulting quark disconnected contributions give only noise and no signal at all. Moreover, it is not possible to apply the very efficient twisted mass variance reduction method based on the one-end-trick for the corresponding quark disconnected diagrams in the light sector.

However, there is another possibility to obtain a significant improvement for the extraction of $\eta'$ mass (and further observables) using a powerful method to separate ground and excited states which has first been proposed in [155] and that has already been successfully employed for the case of the $\eta_2$ for two dynamical quark flavors in [140]. In the following we will describe this method and apply it to our data.

The method is based on the assumption that the quark disconnected diagrams give a sizable contribution only to the $\eta$ and $\eta'$ states but are negligible for any heavier state with the same quantum numbers. Considering the fluctuations of the topological charge which are expected to give a dominant contribution to the mass of the $\eta'$, this assumption would be valid if these fluctuation mainly couple to the $\eta$ and $\eta'$ states. Still, the validity of this assumption needs to be carefully checked from our data and may introduce systematic uncertainties.

Since the quark connected contributions exhibit a constant signal-to-noise ratio, it is in principle possible to determine the respective ground states at sufficiently large $t/a$ with very high statistical accuracy and without any significant contamination from higher states. After fitting the respective ground states of the connected correlators, we can use it to subtract the excited state contributions such that the full connected correlators are replaced by correlators that contain only the ground state. This procedure is shown for one of our ensembles in the left panel of figure 3.8, where the original connected correlator is given by the curve consisting of red squares and the ground state without excited states subtracted is depicted by black circles. It is also clearly visible that the statistical errors are extremely small, i.e. they are covered by the data symbols over the entire range in $t/a$. In a second step we add the disconnected contributions in the usual way to obtain the full correlation functions, which is shown in the right panel of figure 3.8. Note that for sufficiently large $t/a$ this reproduces the original ground state very well by construction, i.e. the modified correlator asymptotically approaches the original one and they agree within errors for $t \gtrsim 8$.

However, we remark that using a unitary action this procedure is in practice restricted to the connected correlation functions corresponding to physical light and strange quarks. This is due to the violation of flavor symmetry in the heavy sector of the twisted mass formulation, implying that the four connected contribution in the heavy sector will all yield the same ground state. This ground state corresponds to an artificial particle, i.e. a connected-only, neutral pion-like particle made out of strange quarks. Therefore, we will restrict ourselves in the following
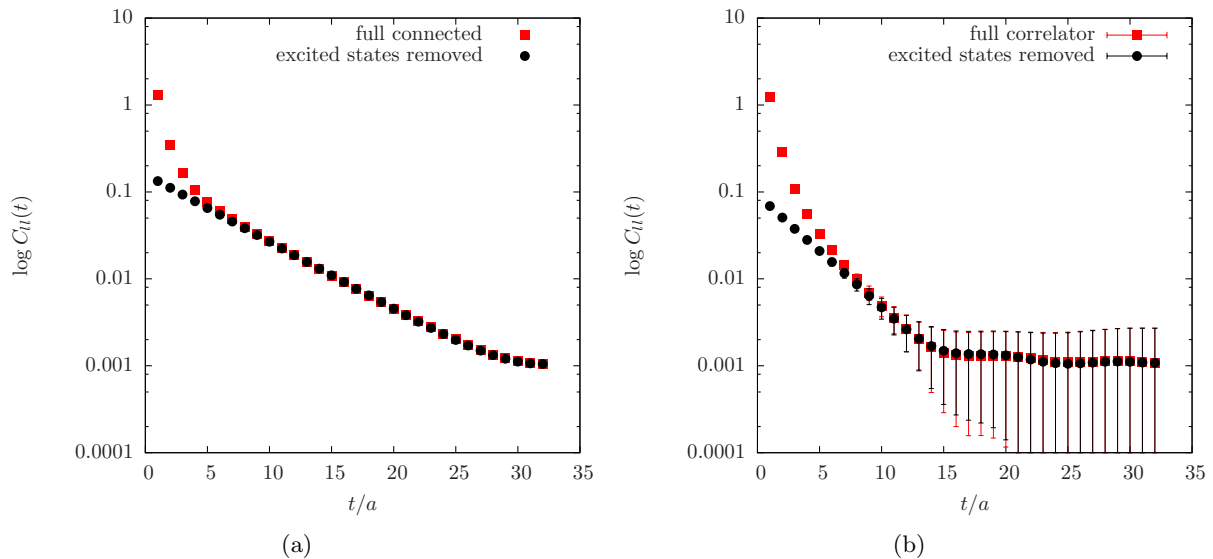
Figure 3.8: (a) Connected contribution to $\mathcal{C}_{ll}(t) \equiv \mathcal{C}_{\mathcal{S}_l^3 \mathcal{S}_l^3}^{\eta, \eta'}(t)$ from local light quark operators with and without excited states subtracted for ensemble $B25.32$. (b) The same as in the left panel, but for the full correlator.

discussion to the analysis of a $2 \times 2$ correlation function matrix corresponding to (local) physical operators made of light and strange quarks, although one should note that it is still necessary to first build the full matrix in order to apply the rotations and renormalization as discussed in section 2.2.

Now, if the aforementioned assumption holds, i.e. the disconnected diagrams are relevant only to the two lowest states $\eta$, $\eta'$ one should obtain a plateau in the effective mass at very low values of $t/a$ after solving the GEVP. The result of the procedure is shown in the right panel of figure 3.9 for the ensemble $A100.24$. Indeed, one observes a plateau for both states starting basically at the lowest possible value of $t/a$. Furthermore, a comparison with the effective masses from the standard $6 \times 6$ matrix in the left panel of figure 3.9 reveals that the plateau values agree very well within their respective errors. However, the data in the right panel allows for a much better accuracy in the determination of both masses as the point errors are much smaller at such low values of $t/a$.

We have applied this procedure to built the correlation function matrices with the excited states removed in the connected pieces for all our ensembles listed in table 3.1. The remaining analysis is performed basically along the same line as described in the previous subsections, only that now we can use a plateau fit for the $\eta'$ as well. Of course, one also needs to adjust fit ranges for both states, which is detailed in appendix C. The results for the masses are given in table 3.6. In addition we have included the corresponding values for $M_{\mathrm{U(1)_A}}$, i.e. the contribution of the anomaly to the $\eta'$ mass as given by the square root of the left-hand side of the Veneziano Witten formula in Eq. (1.87).
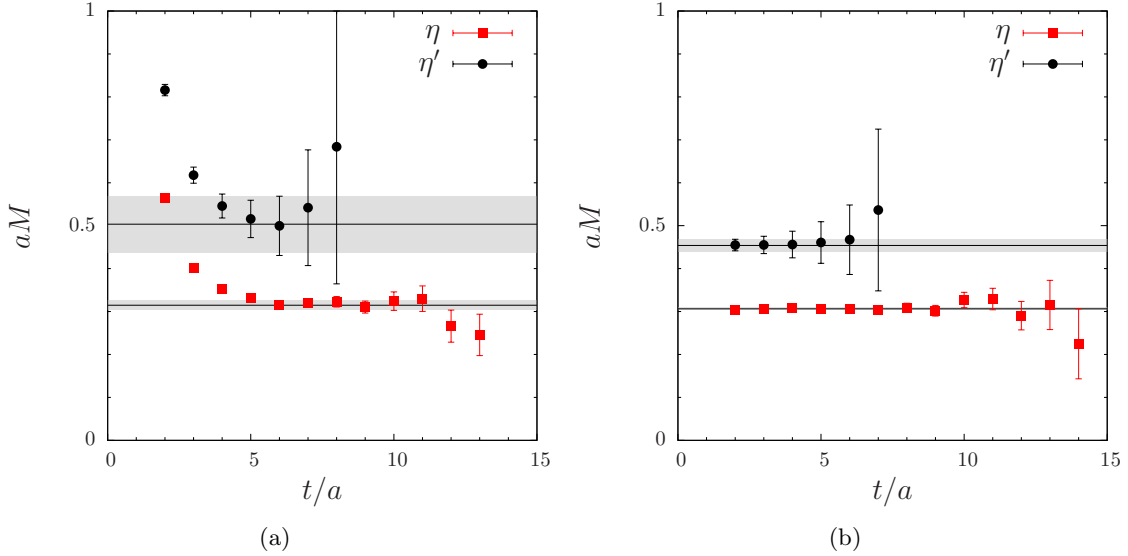
Figure 3.9: Effective masses for ensemble $A100.24$ from (a) a $6 \times 6$ matrix using local and fuzzed operators and (b) a $2 \times 2$ matrix with excited states removed in quark connected contributions.

In figure 3.4 we show an overview of the masses for for all ensembles. Most remarkably, the errors on the $\eta'$ masses are decreased by roughly a factor $\sim 5$ compared to what was shown in figure 3.3 from the standard method. In addition, the errors on the ground state masses are substantially improved, allowing us to perform an even more precise analysis for the $\eta$ mass as well. Concerning possible finite size corrections to the mass of the $\eta$ we remark that they again appear to be negligible as the values for $A40.24$ and $A40.32$ in table 3.6 still agree within statistical errors. Similarly, no significant deviations are observed for the $\eta'$, although the larger fluctuations for this state render any definite statement difficult.

### 3.4.1   Scaling behavior and strange quark mass dependence

In order to perform a scaling test for the mass of the $\eta$ we proceed in exactly the same way as described in the previous section. First we calculate the derivative $D_\eta$ using the two pairs of ensembles ($A80.24$, $A80.24s$) and ($A100.24$, $A100.24s$) while making the same assumptions as before, i.e. we neglect any dependence of $D_\eta$ on $\mu_l$, $\mu_\sigma$, $\mu_\delta$ and the lattice spacing. We find $D_\eta = 1.47(11)_{\text{stat}}$, which is in agreement with the result obtained previously using masses obtained from solving the GEVP for $6 \times 6$ matrix. In a second step we use this value to shift the three ensembles in each of the two sets $S_1$, $S_2$ with fixed $M_{\text{PS}}$ to a common value of the kaon mass $r_0 M_{\text{K}} \approx 1.34$. The results for the two sets of ensembles $S_1$ and $S_2$ are shown in the left and right panels of figure 3.11, respectively. It is apparent from these two plots that the data are perfectly compatible with a constant extrapolation which yields $r_0 M_{\eta,S_1,\text{const}}^{\to 0} = 1.433(13)_{\text{stat}}$ and $r_0 M_{\eta,S_2,\text{const}}^{\to 0} = 1.456(13)$ in agreement with the results from the full correlation function matrix. Performing linear extrapolations gives $r_0 M_{\eta,S_1,\text{lin}}^{a \to 0} = 1.47(9)_{\text{stat}}$ and $r_0 M_{\eta,S_2,\text{lin}}^{a \to 0} = 1.44(5)_{\text{stat}}$,
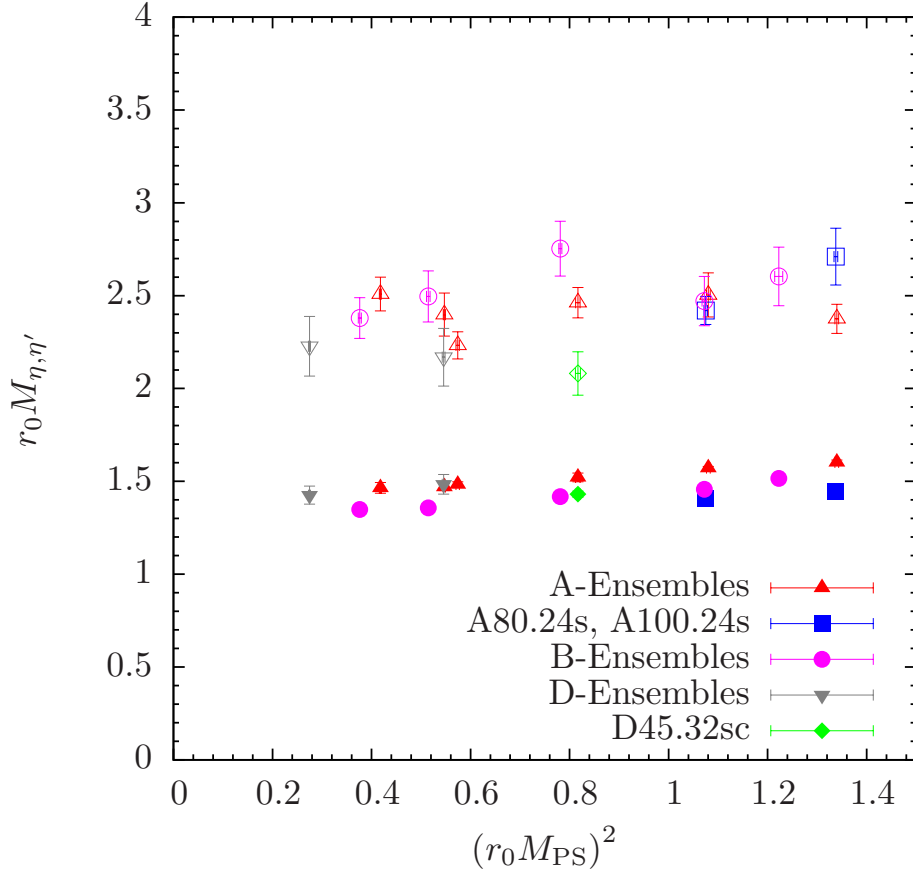
Figure 3.10: Masses for $\eta$ (filled symbols) and $\eta'$ (open symbols) in units of chirally extrapolated $r_0$ (listed in table 3.2) as a function of $(r_0 M_{\mathrm{PS}})^2$ determined from the improved analysis method, i.e. solving the GEVP for a $2 \times 2$ correlation function matrix build from local operators corresponding to physical light and strange quarks only and with excited states removed in the quark connected pieces.

| ensemble | $aM_\eta$ | $aM_{\eta'}$ | $aM_{\mathrm{U(1)}_{\mathrm{A}}}$ |
|---|---|---|---|
| $A$30.32 | 0.2800(55) | 0.480(17) | 0.426(21) |
| $A$40.24 | 0.2834(35) | 0.427(14) | 0.358(18) |
| $A$40.32 | 0.2809(28) | 0.458(22) | 0.396(28) |
| $A$60.24 | 0.2908(46) | 0.471(16) | 0.405(20) |
| $A$80.24 | 0.3004(17) | 0.479(23) | 0.408(28) |
| $A$100.24 | 0.3063(24) | 0.454(15) | 0.366(19) |
| $A$80.24$s$ | 0.2686(30) | 0.463(14) | 0.395(17) |
| $A$100.24$s$ | 0.2763(13) | 0.518(30) | 0.452(33) |
| $B$25.32 | 0.2348(41) | 0.414(19) | 0.369(23) |
| $B$35.32 | 0.2363(23) | 0.435(24) | 0.386(29) |
| $B$55.32 | 0.2469(28) | 0.480(26) | 0.433(29) |
| $B$75.32 | 0.2537(23) | 0.430(23) | 0.369(28) |
| $B$85.24 | 0.2640(28) | 0.453(28) | 0.395(33) |
| $D$15.48 | 0.1891(64) | 0.295(21) | 0.257(30) |
| $D$30.48 | 0.1969(70) | 0.288(21) | 0.242(27) |
| $D$45.32$sc$ | 0.1898(22) | 0.276(15) | 0.223(20) |

Table 3.6: Results of $aM_\eta$, $aM_{\eta'}$ for all ensembles from a $2 \times 2$-correlation function matrix (only local operators) with excited states removed. In addition we list the resulting values for $aM_{\mathrm{U(1)}_{\mathrm{A}}}$ as defined in Eq. (1.87). Again, for $D$20.48 we were not able to extract reliable values for $aM_\eta$ and $aM_{\eta'}$ within the statistics we used.

respectively, also in agreement with the previous results within errors. Note that the errors are now decreased by roughly a factor of three. In figure 3.11 the results from the constant and linear extrapolations are indicated by solid and dotted lines. For the absolute differences between the two extrapolations we obtain

$$r_0 \Delta M_{\eta,S_1}^{a \to 0} = 0.04(8)_{\mathrm{stat}} , \qquad r_0 \Delta M_{\eta,S_2}^{a \to 0} = 0.02(5)_{\mathrm{stat}} , \tag{3.15}$$

indicating that any lattice artifacts are indeed very small. Note that for $S_1$ and $S_2$ the differences have actually even opposite, relative sign, unlike what has been observed from the standard method (although within much larger errors). Considering again the ratio $\Delta M_{\eta,S_2}^{a \to 0}/M_{\eta,S_2,\mathrm{const}}^{a \to 0}$ yields an relative deviation of $\sim 2.6\%$. However, in the following analysis we will always determine the systematic uncertainties from fitting the data at different values of the lattice spacing separately and quote the maximal spread for the systematic error, which is also consistent with our approach for dealing with the systematic uncertainties for further quantities for which we cannot perform such a scaling test.

Although the data for the mass of the $\eta'$ have now much smaller errors compared to the previous analysis, we cannot proceed in the same manner as for the $\eta$ to make a definite statement about scaling effects. The reason for this is that there is no obvious way to disentangle the effects of different values of the strange quark mass from those of different values of the lattice spacings
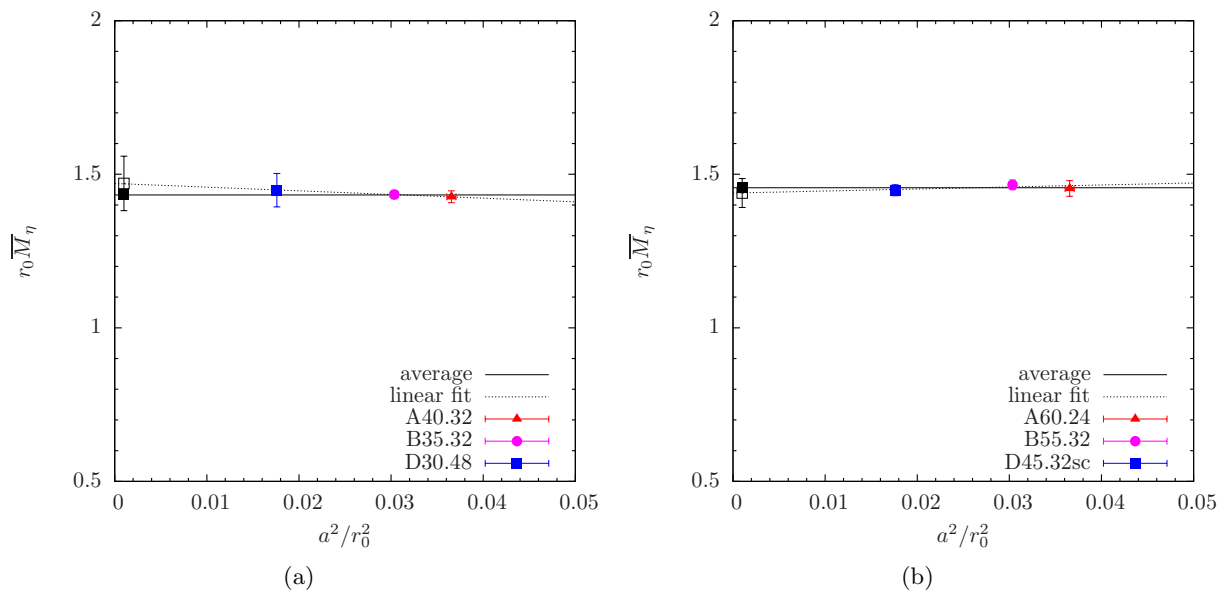
Figure 3.11: (a) $r_0\overline{M}_\eta$ from a $2\times2$ matrix with excited states removed as a function of $(a/r_0)^2$ for the ensembles $A40.32$, $B35.32$ and $D30.48$ (b) The same as in the left panel, but for the ensembles $A60.24$, $B55.32$ and $D45.32sc$. The continuum extrapolated values $r_0M_\eta^{a\to0}$ are horizontally displaced for legibility.

for this state. From figure 3.4 no clear picture arises regarding the influence of the strange quark mass on the value of $M_{\eta'}$ for the two pairs of ensembles ($A80.24$, $A80.24s$) and ($A100.24$, $A100.24s$). Moreover, comparing the data points for $M_{\eta'}$ in figure 3.4 corresponding to $A$- and $B$-ensembles, one might conclude that within statistical errors no significant dependence on the strange quark mass can be observed, although it is also not possible to exclude that there are more subtle cancellations taking place between effects stemming from different values of the strange quark mass and different values of the lattice spacing. Therefore, we are not able to correct for any mistuning of the strange quark mass, as it was the case for $M_\eta$. On the other hand, comparing the data at the coarsest and the finest lattice spacing there appears to be a trend indicating some dependence on the lattice spacing, as the points for the $D$-ensembles lie systematically lower than those for for the $A$-ensembles. In order to include these uncertainties in our analysis, we will again perform the corresponding extrapolations for each value of the lattice spacing separately. A more sophisticated approach might be given by the use of a chiral fit, however, this would require the explicit inclusion of the $\eta'$ field within the framework of three flavor W$\chi$PT to obtain the relevant formulas which to our knowledge has not been done so far. We remark that the corresponding derivative $D_{\eta'}$ might also as well exhibit a dependence on the light and strange quark mass, hence it would be desirable to have more ensembles with re-tuned values of the strange quark mass, possibly also at different values of the lattice spacing to be able to disentangle and estimate the systematic effects.

### 3.4.2    Extrapolation to the physical point

Considering the negligibility of lattice artifacts for the mass of the $\eta$ it is straightforward to perform the extrapolation to the physical point by simply repeating the steps of the analysis described in the previous section. Therefore we will restrict ourselves to a brief presentation of the corresponding results. First, we correct again all values of $M_\eta$ for the mismatch of the strange quark mass by fixing $M_K$ to its physical value $M_K^{\mathrm{exp}}$ and performing a corresponding shift of $M_\eta$ by virtue of Eq. (3.6) employing the value of $D_\eta$ determined in the last subsection. The linear fit to the corrected values $(r_0\overline{M}_\eta)^2[(r_0M_{\mathrm{PS}})^2]$ which is shown in the left panel of figure 3.12 leads to $r_0M_\eta\left[r_0^2M_\pi^2\right] = 1.26(7)_{\mathrm{stat}}(1)_{\mathrm{sys}}$ using again $r_0 = 0.45(2)\,\mathrm{fm}$ and $M_\pi = M_{\pi^0}^{\mathrm{exp}}$ for the physical value of the pion mass. Converting to physical units gives

$$M_\eta(M_\pi) = 551(11)_{\mathrm{stat}}(6)_{\mathrm{sys}}\,\mathrm{MeV}\,, \tag{3.16}$$

where the systematic error has been estimated from fitting the data at each value of the lattice spacing separately. Note that the value for the physical $\eta$ mass is in very good agreement with the result previously given in Eq. (3.3.2) as well as with the experimental value $M_\eta^{\mathrm{exp}}$ in Eq. (1.41). In addition, for the SU (2) chiral limit we have $r_0\mathring{M}_\eta^{\mathrm{SU}(2)} = 1.24(7)_{\mathrm{stat}}(2)_{\mathrm{sys}}$, which yields

$$\mathring{M}_\eta^{\mathrm{SU}(2)} = 543(11)_{\mathrm{stat}}(7)_{\mathrm{sys}}\,\mathrm{MeV}\,, \tag{3.17}$$

converting to physical units. As expected, this result agrees nicely with the one obtained from the full correlation function matrix.

Again, we may extrapolate further quantities in order to check the validity of our correction procedure for mistuned values of the strange quark mass. First, we consider the GMO ratio defined in Eq. (1.83) determined directly from the data for together with and perform an extrapolation in $(r_0M_{\mathrm{PS}})^2$. However, it turns out that taking the uncorrected values of $M_\eta$ the extrapolation misses the experimental value $(3M_\eta^2/(4M_{\mathrm{K}}^2 - M_\pi^2))^{\mathrm{exp}} = 0.925$ considering only the statistical error by more than $2\sigma$, i.e. we obtain $\left(3M_\eta^2/(4M_{\mathrm{K}}^2 - M_\pi^2)\right)_{M_\pi} = 0.963(15)_{\mathrm{stat}}(35)_{\mathrm{sys}}$. This may be seen as a hint that the significantly increased statistical precision of the improved analysis strategy allows to resolve a residual strange quark mass dependence which is not canceled in the ratio. Note that compared to the direct extrapolation the statistical precision is even further enhanced for the case of dimensionless ratios because the physical value of $r_0$ is only required for fixing the physical point but not for the conversion to physical units. In fact, considering only the $B$ ensembles for which the value of the strange quark mass is close to physical yields $\left(3M_\eta^2/(4M_{\mathrm{K}}^2 - M_\pi^2)\right)_{M_\pi}^{B} = 0.928(27)_{\mathrm{stat}}$, indicating that the systematic error is mainly caused by such a residual effect. Indeed, using the corrected values $\bar{M}_\eta$ and the corresponding values of the kaon mass to calculate the GMO ratio the extrapolation gives $\left(3M_\eta^2/(4M_{\mathrm{K}}^2 - M_\pi^2)\right)_{M_\pi} = 0.946(26)_{\mathrm{stat}}(22)_{\mathrm{sys}}$, which agrees nicely with the experimental value and exhibits a smaller systematic error compared to the result obtained from using the uncorrected values of $M_\eta$. For the physical value of the $\eta$ mass we find

$$M_\eta = 554(8)_{\mathrm{stat}}(7)_{\mathrm{sys}}\,\mathrm{MeV}\,, \tag{3.18}$$
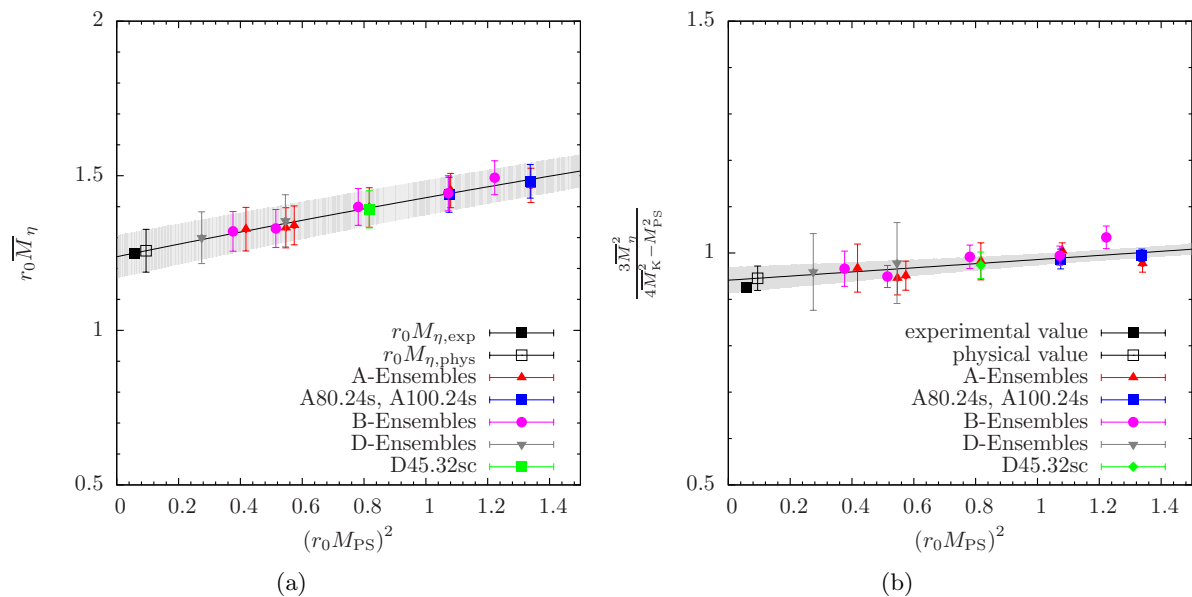
Figure 3.12: (a) Values of $r_0\overline{M}_\eta$ as a function of $(r_0 M_{\mathrm{PS}})^2$. (b) GMO ratio from Eq. (1.83) as a function of $(r_0 M_{\mathrm{PS}})^2$ for all available ensembles using the $m_s$-corrected $r_0\overline{M}_\eta$ values and the corresponding values of the kaon mass. Experimental values are horizontally displaced for legibility. Note that the errors of the data points are highly correlated as they include the error of the derivative $D_\eta(\mu_l, \mu_\sigma, \mu_\delta, \beta)$.

in agreement with the result from the direct extrapolation and the experimental value. The extrapolation for the corrected $\eta$ masses is shown in the right panel of figure 3.12. Note that the (correlated) point errors and the error band stemming from this procedure are affected by the error on the derivative $D_\eta$ which has been used to correct for the mistuning of the strange quark mass. However, they are still significantly smaller than the ones we from the analysis of the standard $6 \times 6$ correlation function matrix in the right panel of figure 3.6.

A similar picture arises from the light quark mass extrapolation of the ratio $M_\eta/M_K$ which is shown in figure 3.13. In the left panel we show the extrapolation using the uncorrected values of $M_\eta$ which yields $(M_\eta/M_{\mathrm{K}})_{M_\pi} = 1.117(8)_{\mathrm{stat}}(23)_{\mathrm{sys}}$, missing the experimental value $(M_\eta/M_{\mathrm{K}})^{\mathrm{exp}} = 1.100$ again by roughly $2\sigma$ if taking only the statistical error into account. However, note the extremely small errors in this plot, which lead to a relative statistical uncertainty for the extrapolated value lying well below the 1% level. Like for the case of the GMO ratio taking only the $B$ ensembles into account gives nice agreement with the experimental value, i.e. $(M_\eta/M_{\mathrm{K}})^B_{M_\pi} = 1.117(8)_{\mathrm{stat}}$, whereas $A$ and $D$ ensembles give significantly larger values. Therefore, we have also repeated the extrapolation using the corrected values $\bar{M}_\eta$ and the corresponding kaon masses, which is shown in the right panel of figure for comparison. Within the slightly larger statistical errors one again obtains excellent agreement, i.e. $(\overline{M}_\eta/\overline{M}_{\mathrm{K}})_{M_\pi} = 1.099(16)_{\mathrm{stat}}(19)_{\mathrm{sys}}$, which results in

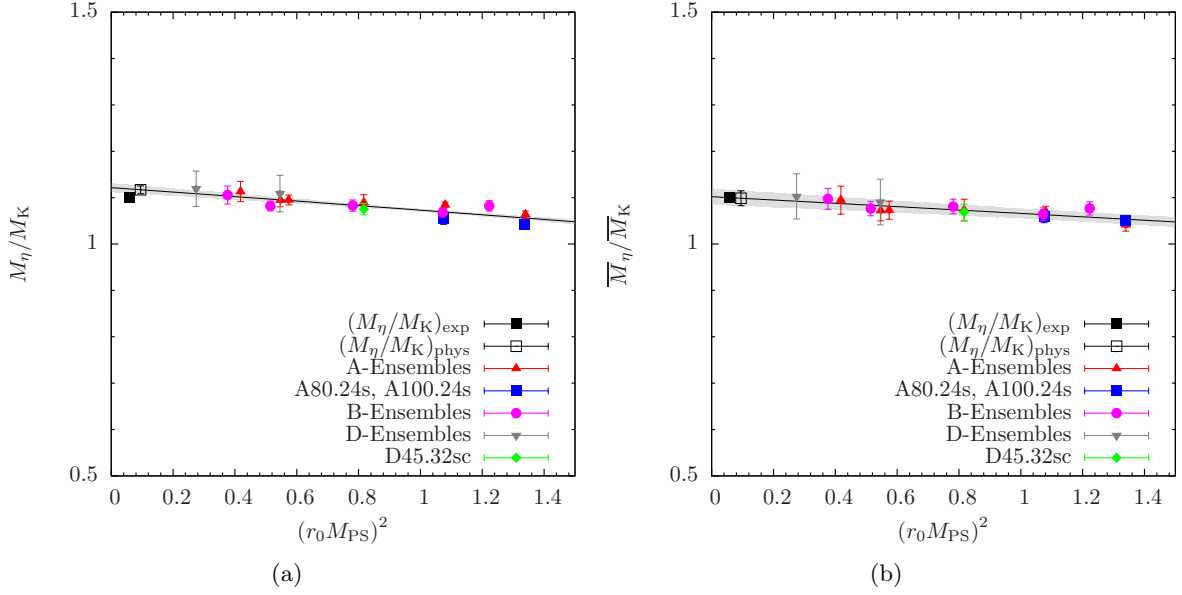$$M_\eta = 0.547(8)_{\mathrm{stat}}(9)_{\mathrm{sys}} \,\mathrm{MeV}\,, \tag{3.19}$$

Figure 3.13: (a) $M_\eta/M_K$ as a function of $(r_0 M_{PS})^2$ for all available ensembles. (b) The same as in the left panel, but determined from the $m_s$-corrected $r_0\overline{M}_\eta$ values and the corresponding values of the kaon mass. Experimental values are horizontally displaced for legibility. The larger errors in (b) are highly correlated as they are dominated by the error of the derivative $D_\eta\left(\mu_l, \mu_\sigma, \mu_\delta, \beta\right)$.

compatible with the results from direct and GMO ratio extrapolations.

In order to obtain our final result for the physical mass of the $\eta$ we take the weighted average from the three previously discussed methods used for the extrapolation in the light quark mass. Accounting for any correlations, this yields

$$M_\eta = 551(8)_{\text{stat}}(6)_{\text{sys}} \, \text{MeV} \, . \tag{3.20}$$

which is in excellent agreement with experiment and exhibits substantially smaller errors compared to any result obtained from the standard method.

As discussed in the previous subsection it is not clear how to disentangle effects of the strange quark mass (if any) from those of different values of the lattice spacing for the $\eta'$. Therefore, we rely on a direct linear fit to the data for $\left(r_0 M_{\eta'}\right)^2$ as a function of $(r_0 M_{PS})^2$ to extrapolate to the physical value of the pion mass. The result of this fit is shown in together with the direct extrapolation for the $\eta$ mass. Numerically, we obtain

$$M_{\eta'} = 1006(54)_{\text{stat}}(38)_{\text{sys}}(+61)_{\text{ex}} \, \text{MeV} \, , \tag{3.21}$$

which represents our final result for physical mass of the $\eta'$ state. In order to quantify a possible error introduced by the excited state removal in the connected contributions, we quote the difference between the extrapolations with and without excited state removal as an additional
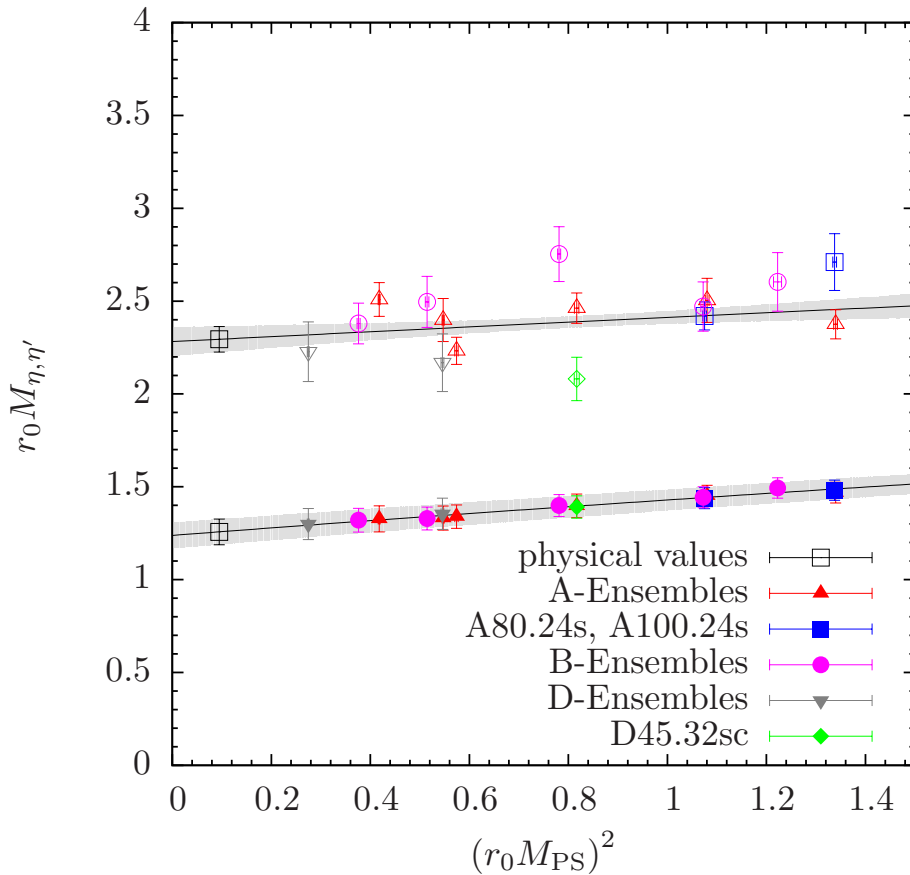
Figure 3.14: Our results for $r_0\overline{M}_\eta$ (filled symbols) (corrected for the mismatch in $r_0M_\mathrm{K}$ as discussed in subsection 3.3.1) and $r_0M_{\eta'}$ (open symbols). The fitted curves are linear functions in $(r_0M_\mathrm{PS})^2$ as discussed in the text.

systematic error. Again, the standard systematic error has been determined from fits to the data at single values of the lattice spacing and it is interesting to note that it actually turns out to be the smallest of the three errors. Within the larger errors this result is again in very good agreement with experiment, confirming that QCD indeed accounts for the significantly larger mass of the $\eta'$ that is observed experimentally.

### 3.4.3 Discussion of results

In figure 3.15 we have included a compilation of our results for $\eta$ and $\eta'$ masses obtained from the standard (left panel) and excited state removal method (right panel), together with results available in the literature for $N_f = 2+1$ flavor lattice QCD. For $M_\eta$ we show the values corrected for the mismatch in $M_\mathrm{K}$. We remark that in [156] $\eta$ and $\eta'$ meson masses have been computed using $N_f = 2+1$ flavors of overlap quarks at one value of the lattice spacing and large values
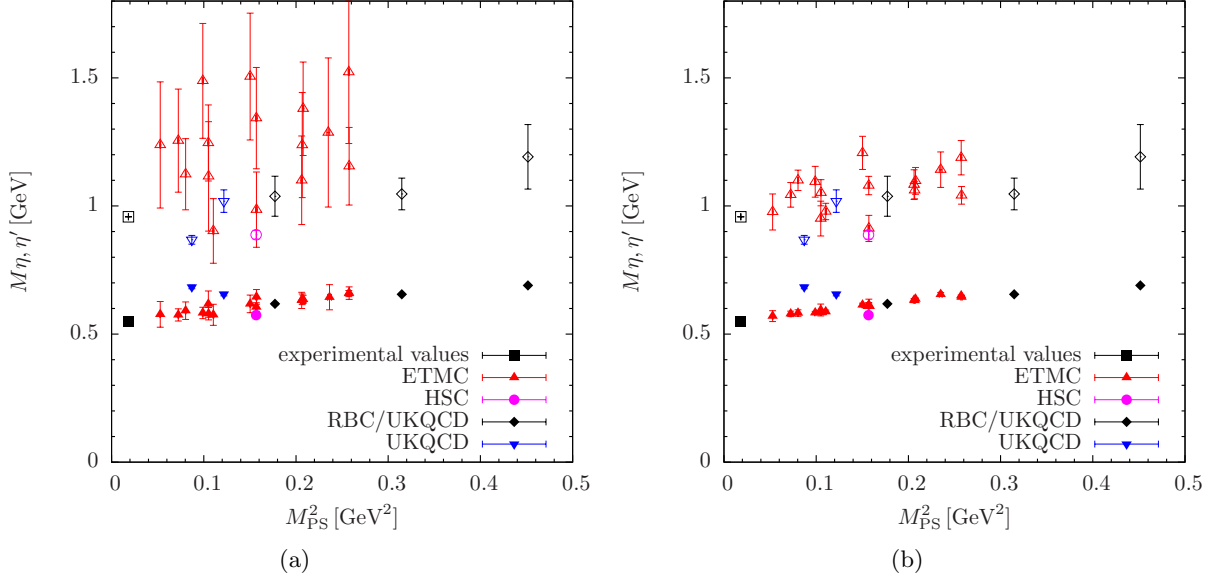
Figure 3.15: Comparison of our results for $\overline{M}_\eta$ (filled symbols) (corrected for the mismatch in $M_K$ as discussed in the text) and $M_{\eta'}$ (open symbols) in physical units for all three values of the lattice spacing to results from the literature (RBC/UKQCD [7], HSC [8], UKQCD [9]). (a) shows our results from the standard method and (b) the results from the excited state removal method. The scale for our points was set using $r_0 = 0.45(2)$ fm.

of the pion mass, however, in this reference not enough details are given to be included in our comparison figure 3.15. The results in [7] have been obtained using $N_f = 2 + 1$ flavors of domain wall fermions and again for a single value of the lattice spacing $a \approx 0.1$ fm but for three values of the pion mass in a range from $\sim 400$ MeV to $\sim 700$ MeV. The corresponding data points in figure 3.15 are labeled "RBC/UKQCD". Another single data point is added from [8] by the Hadron Spectrum Collaboration (HSC) for which Wilson fermions have been employed. Again, it was not possible to include more recent results by the HSC [157] due to the lack of explicit, numerical values in this reference for the relevant masses. Finally, in [9] data from staggered fermions is presented for two different values of the lattice spacing with each of them also at a different value value of the pion mass. In figure 3.15 the corresponding data points are labeled "UKQCD".

First of all, figure 3.15 shows that the results presented in this work increase the available world data for $\eta$ and $\eta'$ masses from lattice QCD with more than two dynamical quark flavors by almost a factor of four (c.f. figure 1). In particular, our results are obtained at significantly lower values of the pion mass than any other data available before. Moreover, our results agree nicely with those obtained from domain wall and Wilson fermions, despite the fact that no systematic uncertainties have been taken into account for this plot and also that we used $N_f = 2 + 1 + 1$ dynamical quark flavors. Only for the mass of the $\eta$ a significant tension is observed when comparing to the results computed from staggered quarks, however, for the $\eta'$

no such deviation is observed.

Moreover, figure 3.15 allows for a comparison of the statistical uncertainties in the different studies. The plot in the left panel shows that our errors for $M_{\eta'}$ determined from the full $6 \times 6$ correlation function matrix are much larger than those quoted by the other collaborations. For the error on the mass of the $\eta$ a similar, though less severe trend is observed. In the following we discuss several possible causes that in principle might contribute to this discrepancy. One source for the larger error on the $\eta'$ mass is the significant autocorrelation that we observe for this state, c.f. subsection 3.2.2. At least this is the reason why the error on the data for the $\eta'$ is larger than that for the $\eta$ when comparing to results by other collaborations. For the results by RBC/UKQCD [7] 300 configurations separated by 20 HMC trajectories have been investigated and no autocorrelation among these configurations has been observed for the investigated quantities. Similarly, the (HSC) [8] used 479 configurations also separated by 20 HMC trajectories. However, these two investigations were performed at a lattice spacing of $\sim 0.12\,\mathrm{fm}$, which is significantly larger than our coarsest value. Compared to both studies we have hence investigated a similar number of independent configurations per ensemble, but at smaller values of the lattice spacing. Furthermore, our methods to compute quark disconnected contributions are based on the use of stochastic noise, which is not the case for the methods used by the two aforementioned collaborations. However, we have explicitly checked that the stochastic noise is not dominantly contributing to the errors on our results, it is at most of the size of the gauge noise or smaller. Compared to the HSC study we have used a much smaller number of inversion per independent gauge configurations while RBC/UKQCD used a similar number. Besides, the large operator basis employed by the HSC clearly allows for higher precision in the extraction of the relevant states. The smaller errors found by RBC/UKQCD might be caused by the better chiral properties of the domain wall formulation, the larger value of the lattice spacing or the smaller volume in lattice units. Finally, we remark that the study using staggered quarks by UKQCD [9] employs a similar method to deal with the disconnected contributions but involves are significantly larger number of independent configurations. Additionally, we would like to point out again that for the standard method the large error on our data for $M_{\eta'}$ also reflects the systematic uncertainty in identifying a plateau in its effective mass, as discussed earlier.

The situation concerning the errors changes drastically when comparing to our results from the excited state removal method, which is shown in the right panel of figure 3.15. Since for this method we are able to perform fits at much smaller values of Euclidean time, the errors are of the same size or even smaller than those quoted by the other collaborations, depending on the statistics used and the values of the light quark mass and the lattice spacing. In particular, one observes a nice agreement within the much smaller errors for the $\eta'$ masses among the different collaborations and excellent agreement of our data for the $\eta$ masses with those obtained from domain wall fermions by RBC/UKQCD and also the single data point by HSC seems more or less compatible. The tension with the two data points computed from staggered fermions by UKQCD remains and is now even more pronounced by the smaller errors. It is not clear to us what kind of systematic effect is responsible for this latter observation.

## 3.5   $\eta$, $\eta'$-mixing

The previous sections of this chapter have been mainly concerned with the extraction and extrapolation of masses for the light pseudoscalar, flavor singlet mesons. In this section we will focus on the extraction of the mixing parameters for the $\eta$–$\eta'$ system defined for the quark flavor basis introduced in Eqs. (1.97),(1.98). Since we do not have direct access to the axial-vector matrix elements, we have to employ the simplified mixing scheme in Eq. (1.105) which relies on additional theoretical input from $\chi$PT, as detailed in subsection 1.1.5. In principle, it is possible to calculate the relevant amplitudes either directly from the GEVP as discussed in subsections 2.2.2 and 2.2.3 or from the factorizing fit model in Eq. (2.101). For consistency reasons with respect to the previous analysis, it would be desirable to stick with the GEVP approach, however, using the standard $6 \times 6$ correlation function matrix it turns out that this approach does not allow to extract the relevant amplitudes for the first excited state with any reasonable precision, as the signal for them is lost as very early values of $t/a$. Therefore, we employ the factorizing fit model together with suitable priors for the masses of the first two states as obtained from the GEVP analysis in order to compute these amplitudes. For the factorizing fit we first rotate the the correlation function matrix back to the original twisted basis as discussed in subsection 2.2.3 and for the further analysis we consider only light and strange degrees of freedom (both, local and fuzzed), as the charm quark does not contribute within errors. In fact, we checked explicitly that the results from fitting to a full $6 \times 6$ matrix are in excellent agreement with those from a $4 \times 4$ matrix, i.e. the resulting deviations (if any) are much smaller than the average errors. Again, we would like to point out that the determination of the mixing parameters requires the ratio of renormalization constants $Z$ as input, for which we use the values listed in table 3.3. The details of our fitting procedure can be found in appendix C.2.

The results for the mixing angle $\phi$ defined from the double ratio of amplitudes in Eq. 2.90 are given in table 3.7 for local ($\phi^L$) and fuzzed amplitudes ($\phi^F$) calculated from the standard $4 \times 4$ correlation function matrix without the charm sector. In addition, we have included corresponding results for the two angles $\phi_l$, $\phi_s$ in Eq. 2.91. The errors for the angles are more or less of similar relative size compared to those obtained for the values of $M_{\eta'}$ determined from the standard method. For the angle $\phi$ we will see that it is possible to perform an extrapolation in the light quark mass to the physical point which will be discussed in the next subsection. However, it is already obvious from the values in table 3.7 that no clear picture arises for $\phi_l$ and $\phi_s$, which we attribute to large systematic uncertainties in these quantities. Apparently, some of these systematic effects cancel in the double ratio of amplitudes for the single angle $\phi$, which is not the case for the simple ratios of amplitudes required to obtain the values for the angles $\phi_l$ and $\phi_s$. Therefore, we will not consider them in the subsequent analysis and restrict any further study of these quantities to the corresponding results from the excited state removal method. Similarly, we refrain from computing the decay constant parameters $f_l$ and $f_s$ using the standard method as this does not allow for any reliable extrapolations either.

For the case of the flavor singlet masses we obtained substantial improvement on the error of our results from the application of the excited state removal method. The same method can also be

| ensemble | $\phi_l^L$ | $\phi_s^L$ | $\phi^L$ | $\phi_l^F$ | $\phi_s^F$ | $\phi^F$ |
|---|---|---|---|---|---|---|
| $A$30.32 | 57(15) | 49(13) | 56(15) | 36(09) | 53(13) | 46(11) |
| $A$40.24 | 39(16) | 41(11) | 39(16) | 43(11) | 40(12) | 41(13) |
| $A$40.32 | 56(18) | 33(11) | 54(18) | 33(11) | 44(11) | 44(11) |
| $A$60.24 | 66(15) | 29(13) | 66(15) | 30(13) | 49(08) | 49(08) |
| $A$80.24 | 73(07) | 20(10) | 73(07) | 24(10) | 48(06) | 50(06) |
| $A$100.24 | 62(10) | 37(10) | 62(10) | 39(09) | 50(05) | 51(05) |
| $A$80.24$s$ | 59(16) | 36(16) | 59(16) | 41(16) | 48(12) | 50(12) |
| $A$100.24$s$ | 75(13) | 20(16) | 76(12) | 25(16) | 50(07) | 54(07) |
| $B$25.32 | 74(13) | 25(10) | 73(13) | 28(10) | 52(06) | 53(06) |
| $B$35.32 | 67(14) | 19(07) | 63(15) | 22(08) | 42(06) | 41(07) |
| $B$55.32 | 74(11) | 14(06) | 73(11) | 18(07) | 43(06) | 46(06) |
| $B$75.32 | 50(14) | 52(15) | 50(14) | 52(15) | 51(11) | 51(11) |
| $B$85.24 | 60(16) | 47(20) | 61(16) | 46(19) | 54(13) | 54(13) |
| $D$15.48 | 59(14) | 25(09) | 57(14) | 29(09) | 41(10) | 42(10) |
| $D$30.48 | 65(11) | 39(14) | 64(11) | 47(15) | 53(12) | 56(12) |
| $D$45.32$sc$ | 60(19) | 57(15) | 59(19) | 58(15) | 59(15) | 58(15) |

Table 3.7: Results for the mixing angles in Eqs. (2.91),(2.90) from a $4 \times 4$-correlation function matrix using local (L) and fuzzed (F) operators for all ensembles. For $D$20.48 it was not possible to extract reliable results within the statistics we used.

used to compute the mixing parameters. Note that for this procedure we are a priori restricted to the use of a $2 \times 2$ matrix and we employ only local operators. Since the method allows to perform fits to the principal correlators and also the corresponding eigenvectors at very small values of $t/a$ it enables us to determine the amplitudes directly from the GEVP in line with our previous analysis for the masses. The parameters used for the GEVP analysis are the same that have been used for the computation of the masses and can be found in appendix C.1. The numerical results are given in table 3.8, where we have now included the decay constant parameters $f_l$, $f_s$ and again values for all three angles $\phi_l$, $\phi_s$ and $\phi$. For the statistical errors on the angles the method yields an impressive improvement of about an order of magnitude. The relative errors on the angles are typically $\lesssim 4\%$ for $A$ and $B$-ensembles, while for the $D$-ensembles one observes large errors up to $\sim 10\%$ for the lightest quark mass. Furthermore, the values for all three angles are now very close to each other and actually agree within errors on many ensembles. We will discuss this observation in more detail in the next subsection. Similarly, the determination of the remaining decay constant parameters appears to give consistent results with even smaller relative errors of typically $\lesssim 2\%$. The only relevant exception is given by the ensemble $D$30.48 for which significantly fewer gauge configuration have been used.

| ensemble | $af_l$ | $af_s$ | $\phi$ | $\phi_l$ | $\phi_s$ |
|----------|--------|--------|--------|----------|----------|
| $A$30.32 | 0.0544(09) | 0.0851(13) | 49.2(1.5) | 51.3(1.9) | 47.0(1.4) |
| $A$40.24 | 0.0561(06) | 0.0841(11) | 45.7(1.4) | 46.2(1.7) | 44.9(1.2) |
| $A$40.32 | 0.0573(07) | 0.0863(11) | 45.6(1.7) | 47.5(2.3) | 43.9(1.4) |
| $A$60.24 | 0.0625(08) | 0.0880(12) | 49.1(1.8) | 51.0(2.0) | 47.2(1.7) |
| $A$80.24 | 0.0657(06) | 0.0897(08) | 49.9(1.1) | 51.2(1.8) | 48.5(0.7) |
| $A$100.24 | 0.0705(07) | 0.0885(07) | 50.0(0.9) | 50.4(1.2) | 49.5(0.8) |
| $A$80.24$s$ | 0.0680(07) | 0.0825(08) | 51.6(1.2) | 53.3(1.1) | 49.9(1.6) |
| $A$100.24$s$ | 0.0679(05) | 0.0842(08) | 53.7(0.5) | 56.7(1.0) | 50.6(1.2) |
| $B$25.32 | 0.0484(06) | 0.0743(10) | 49.3(2.0) | 51.2(2.4) | 47.4(1.8) |
| $B$35.32 | 0.0536(07) | 0.0752(07) | 49.7(1.3) | 52.5(2.0) | 46.8(1.1) |
| $B$55.32 | 0.0604(08) | 0.0764(08) | 51.7(1.0) | 54.8(1.8) | 48.5(0.9) |
| $B$75.32 | 0.0638(09) | 0.0779(07) | 51.1(1.0) | 52.5(1.5) | 49.8(1.2) |
| $B$85.24 | 0.0656(11) | 0.0784(10) | 52.9(1.2) | 54.1(1.7) | 51.6(1.5) |
| $D$15.48 | 0.0402(10) | 0.0574(13) | 41.6(4.9) | 42.1(5.3) | 41.1(4.5) |
| $D$30.48 | 0.0524(68) | 0.0513(25) | 53.9(6.8) | 51.7(4.7) | 55.9(9.0) |
| $D$45.32$sc$ | 0.0439(05) | 0.0501(07) | 44.8(3.1) | 44.1(3.5) | 45.5(2.7) |

Table 3.8: Results for the $\eta,\eta'$-mixing parameters $af_l$, $af_s$ and $\phi$ in the quark-flavor basis from pseudoscalar matrix elements as given in Eq. (1.114). These values are obtained from a $2 \times 2$-correlation function matrix with removed excited states. For comparison we also included the results obtained using two individual angles $\phi_l$, $\phi_s$ in Eq. (1.114), although to the given order only a single mixing angle is predicted by the effective field theory. For $D$20.48 it was not possible to extract reliable results within the statistics we used.

### 3.5.1   Chiral extrapolations

In the left panel of figure 3.16 we have plotted the values for the mixing angle in the quark flavor basis determined from local amplitudes of a $4 \times 4$ correlation function matrix as a function of $(r_0 M_{\text{PS}})^2$. This is again motivated from continuum three flavor $\chi$PT. In order to distinguish the result from local amplitudes from that derived from their fuzzed counterparts the angle is denoted by $\phi^L$ in this plot. In addition, we show results from the full $6 \times 6$ matrix using amplitudes corresponding to fuzzed operators in the right panel. As stated in the previous subsection, these results are in agreement with the ones determined from local amplitudes, and in both cases we do neither observe a dependence on the lattice spacing nor on $(r_0 M_{\text{K}})^2$, at least within the relatively large errors. Therefore, we perform a linear fit in $(r_0 M_{\text{PS}})^2$ which is also shown in the two plots in figure together with the resulting error bands and the respective values for $\phi^{L,F}$ at the physical pion mass. The two extrapolations are in good agreement and we quote the value from a combined fit to local an fuzzed data as our result for the physical mixing angle, i.e.

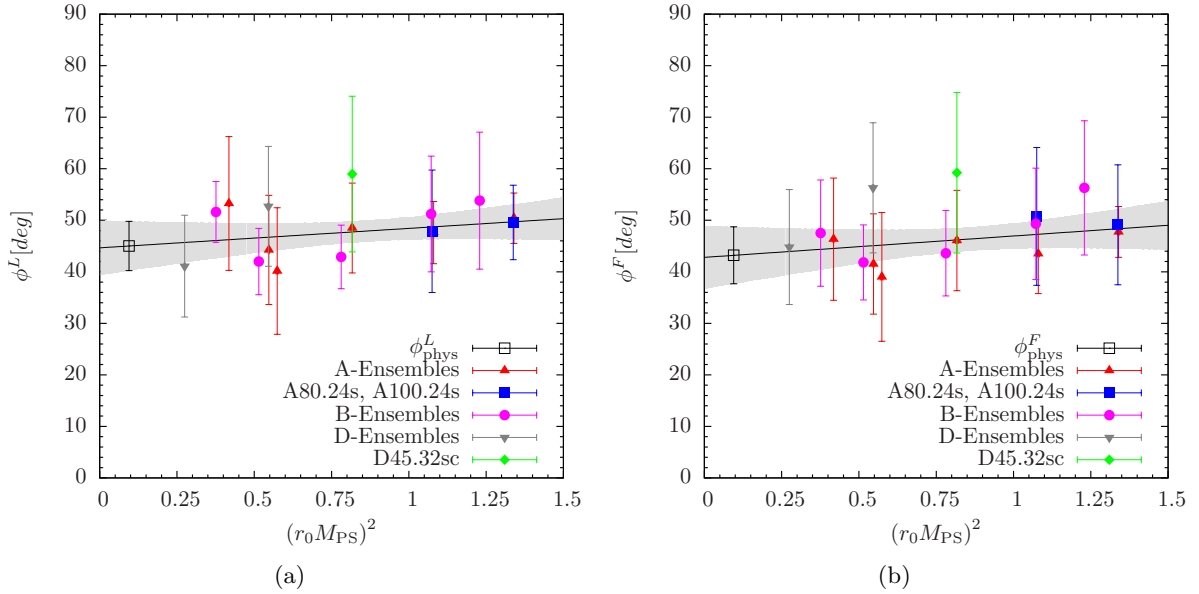$$\phi = 44(5)^\circ_{\text{stat}} . \tag{3.22}$$

Figure 3.16: (a) mixing angle $\phi^L$ from local amplitudes of a $4 \times 4$ matrix (no charm quark). (b) mixing angle $\phi^F$ from fuzzed amplitudes of $6 \times 6$ matrix (including charm quark)

Due to the very large statistical errors we refrain from giving any numerical estimate of possible systematic effects. However, we have checked that our determination of the mixing angle is not affected by the uncertainty on the ratio of renormalization constants $Z$. To this end we varied $Z$ in a large range from 0.4 to 1.0, which did not affect the extraction of the mixing angles at all. An example for this is shown in the left panel of figure 3.17, where we plotted the dependence of $\phi^L$ on $Z$ for ensemble $D15.48$. It is clear from this plot that the variation introduced by $Z$ is by far smaller than the statistical uncertainty. We remark that this statement still holds even for the much smaller errors on the mixing angles obtained from using the excited state removal method, which will be discussed below. The same behavior is observed for the other ensembles, hence we conclude that our evaluation of the mixing angle is not affected by systematic uncertainties stemming from the $Z$ ratio within our statistical errors.

In the right panel of figure 3.17 we show the results for the mixing angle $\phi$ from the improved analysis method using a $2 \times 2$ correlation function matrix built from local operators only (c.f. table 3.8) as a function of $(r_0 M_{\mathrm{PS}})^2$. A comparison with figure 3.16 reveals that the data from the standard and the improved method appear to be compatible, although the large statistical errors resulting from the standard method render a definite statement difficult. Concerning systematic effects introduced by scaling artifacts and mistuned values of the strange quark mass, we remark that still no clear picture arises albeit that the errors are decreased by roughly one order of magnitude compared to the standard approach. The situation is similar to the one we observed for the mass of the $\eta'$: considering the data for the two sets of ensembles ($A80.24$, $A80.24s$) and ($A100.24$, $A100.24s$) it appears that the value of the strange quark mass may have some influence but this may depend on the value of the light quark mass and the lattice spacing
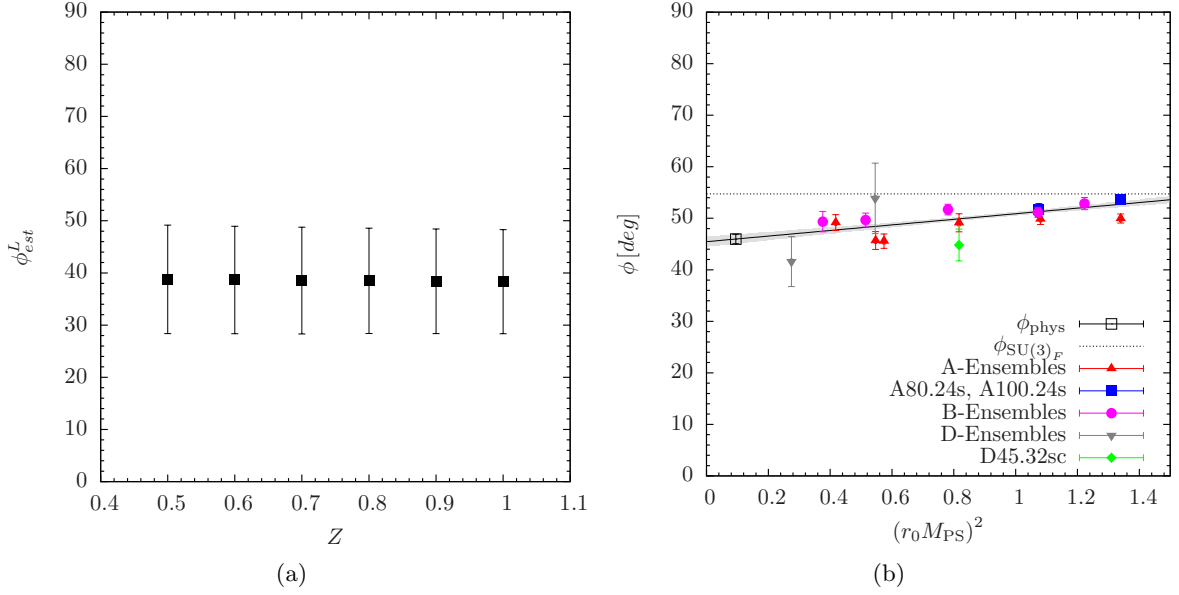
Figure 3.17: (a) $Z$-dependence of the mixing angle $\phi$ from a $4 \times 4$ correlation function matrix using local amplitudes for $D15.48$. (b) Mixing angle $\phi$ from local amplitudes of a $2 \times 2$ matrix with excited states removed.

such that it is not possible to disentangle these effects with the available data. In particular, at smaller values of the light quark mass the data for $A$- and $B$-ensembles agree again well within errors, although these sets of ensembles have different strange quark mass. However, with respect to the mass dependence of the mixing angle it is worthwhile to mention that our data is consistent with the SU (3) flavor symmetry requirement $\phi_{\mathrm{SU}(3)_F} = \arctan \sqrt{2}$ which is indicated by the dotted, horizontal line the left panel of figure 3.17. In addition, we remark that finite size effects appear to be negligible, the data for the two ensembles $A40.24$ and $A40.32$ agree very well within errors. Since it is not possible to further disentangle the systematic effects (e.g. resolve a strange quark mass dependence), we employ the same procedure as discussed in section 3.4, i.e. we fit each the data at each lattice spacing separately to obtain an estimate for the systematic uncertainties. The data is again compatible with a linear fit in $(r_0 M_{\mathrm{PS}})^2$ and at the physical value of the pion mass we have

$$\phi = 46.0(0.9)_{\mathrm{stat}} (2.7)^\circ_{\mathrm{sys}} , \tag{3.23}$$

which is our final result for the mixing angle in the quark flavor basis using pseudoscalar matrix elements.

Besides the mixing angle $\phi$, we consider the angles $\phi_l$, $\phi_s$ which are relevant to cross-check the assumptions entering our mixing scheme. The results for $\phi_l$ and $\phi_s$ have been plotted in the left and right panel of figure 3.18, respectively. Again, we have performed linear fits in $(r_0 M_{\mathrm{PS}})^2$, which are also shown in the plots together with the results at the physical pion mass that are given by

$$\phi_l = 47.7(1.2)_{\mathrm{stat}} (4.1)^\circ_{\mathrm{sys}} , \qquad \phi_s = 44.3(0.9)_{\mathrm{stat}} (3.0)^\circ_{\mathrm{sys}} , \tag{3.24}$$
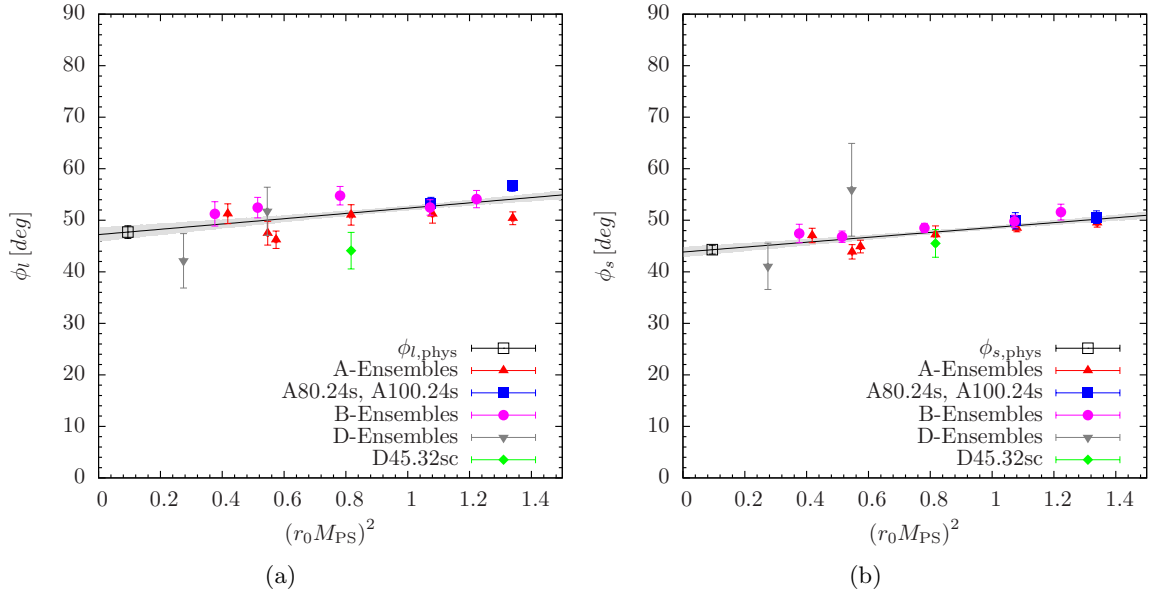
Figure 3.18: (a) Mixing angle $\phi_l$ and (b) mixing angle $\phi_s$; both from local amplitudes of a $2 \times 2$ matrix with excited states removed.

where the systematic uncertainties have been determined in the same way as for the angle $\phi$ itself. The results are compatible within errors, although it is interesting to note that the values and the extrapolated result for $\phi_l$ exhibit slightly larger statistical and systematical errors. Notably, for $\phi_s$ there is very good agreement for the results within each of the two set ($A80.24$, $A80.24s$) and ($A100.24$, $A100.24s$), indicating that the influence of the strange quark is smaller for this quantity and in general more of the data points lie within the error band of the linear fit. Moreover, we can also perform a direct linear extrapolation of the difference $\Delta\phi_{ls} = \phi_l - \phi_s$, which yields

$$\Delta\phi_{ls} = 2.8(1.1)_{\text{stat}}(2.6)^{\circ}_{\text{sys}},\tag{3.25}$$

compatible with zero within errors.

As discussed in the previous subsection, the application of the excited state removal method allows also for an extraction of the decay constant parameters $f_l$ and $f_s$ to a rather high statistical precision. We have plotted the results for $f_l$ and $f_s$ as a function of $(r_0 M_{\text{PS}})^2$ in the upper left and right panels of figure 3.19, respectively. Visual inspection of the data for $f_l$ exhibits a rather nonlinear curvature and may a non-trivial dependence on the value of the strange quark mass as well as significant scaling artifacts, although the somewhat diverse results at the finest lattice spacing do not allow for a definite statement. Furthermore, these effects seem not to be small compared to the statistical errors. Therefore, one should not expect a simple, linear fit to allow for a good description of the data. For $f_s$ one observes a very clear dependence on the value of the strange quark mass, although from the data for ($A80.24$, $A80.24s$) and ($A100.24$, $A100.24s$) this dependence does not necessarily appear to be constant with respect to the value of the light quark mass. Considering the results at the finest lattice spacing there may also exist a more

subtle interplay between quark mass dependence and scaling artifacts.

For these reasons it seems necessary to rather study suitable ratios quantities which cancel at least some of the aforementioned effects instead of performing direct extrapolations of the decay constant parameters themselves. Indeed, it turns out that this is possible by considering the ratios $f_l/f_{\mathrm{PS}}$ and $f_s/f_K$ using our lattice data for $f_{\mathrm{PS}}$ and $f_K$ as given in table 3.4. The latter choice may be considered motivated on the grounds that a similar approach using $M_K$ has already been shown to work very well for the case of the $\eta$ mass. The results for these ratios are shown in the lower two panels of figure 3.19 again as a function of $(r_0 M_{\mathrm{PS}})^2$. First of all, it is apparent that for the case of $f_l/f_{\mathrm{PS}}$ some of the light quark mass dependence cancels and the resulting curvature for each lattice spacing seems less severe and rather compatible with a linear fit. The linear extrapolation using all available data is also shown in the plot and at the physical value of the pion mass we have

$$f_l/f_{\mathrm{PS}} = 0.859(7)_{\mathrm{stat}}(64)_{\mathrm{sys}} .\tag{3.26}$$

However, from the plot it appears that there is still a rather sizable dependence on the lattice spacing present while the strange quark mass dependence seems to cancel in ratio as all $A$-ensembles fall on one single curve. In fact, the systematic error estimated from fitting the data at each value of the lattice spacing separately is one order of magnitude larger than the statistical error and there is clear trend towards larger values of $f_l/f_{\mathrm{PS}}$ extrapolated to the physical pion mass for increasing value of the lattice spacing. Therefore, we additionally quote the result of a linear fit restricted to the data at the finest lattice spacing, which yields $(f_l/f_{\mathrm{PS}})^D = 0.924(22)_{\mathrm{stat}}$.

For the ratio $f_s/f_K$ most of the strange quark mass dependence is canceled and the data seems almost perfectly linear in the light quark mass, exhibiting only a moderate slope. Moreover, for this case there are no discernible scaling artifacts within errors and the data is well described by a linear fit which gives

$$f_s/f_K = 1.166(11)_{\mathrm{stat}}(31)_{\mathrm{sys}} ,\tag{3.27}$$

at the physical value of the pion mass. Clearly, the systematic error is significantly smaller than the one obtained for the physical value of $f_l/f_{\mathrm{PS}}$, confirming the smallness of any residual lattice artifacts or strange quark mass dependence for $f_s/f_K$.

### 3.5.2  Discussion of results

In this section we have computed the relevant mixing parameters of the $\eta$–$\eta'$ system in the quark flavor basis using pseudoscalar matrix elements for light and strange degrees of freedom as discussed in detail in subsection 1.1.5. Using the standard method it is only feasible to extract the single mixing angle $\phi$ as the statistical and systematic uncertainties for all further quantities are too large. Nonetheless, the result in Eq. (3.22) turns out to be in good agreement with the one obtained from the excited state removal method in Eq. (3.23) and both are compatible with most lattice determinations, i.e. an old UKQCD work [158] and more recent results by RBC/UKQCD [7] as well as HSC [8, 157], which all quote values in between 40° and 50°.
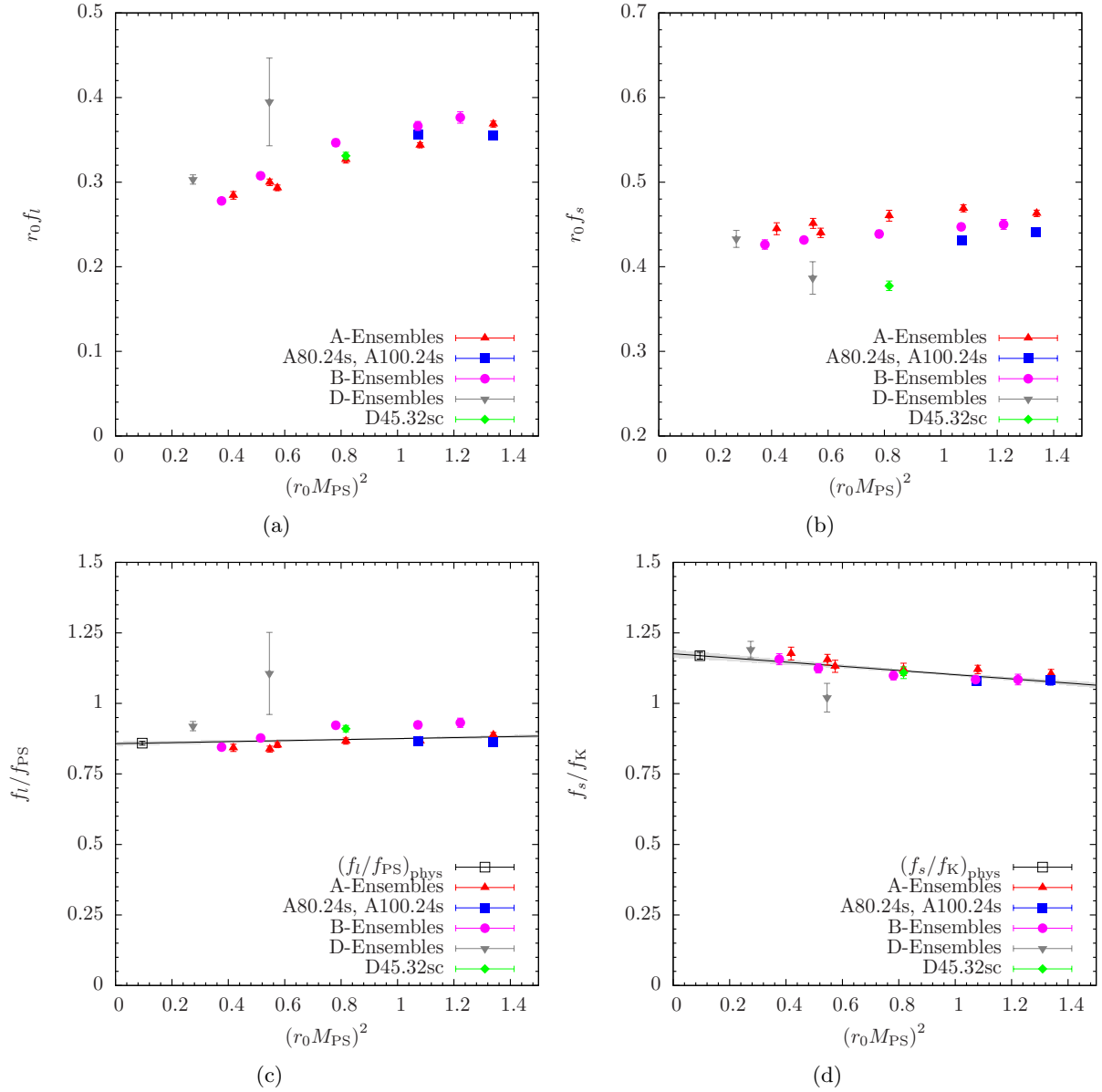
Figure 3.19: (a) Quark flavor basis decay constant parameter $r_0 f_l$ as function of $(r_0 M_{PS})^2$. (b) The same as in the left panel but for $r_0 f_s$. (c) Decay constant ratio $f_l/f_{PS}$ and (d) similar ratio for $f_s$ using kaon decay constant $f_K$ instead of $f_{PS}$.

However, the recent UKQCD investigation using staggered quarks [9] favors a smaller value of $34(3)^\circ$. Our result indicates that the $\eta$ exhibits a large flavor octet component while the $\eta'$ is dominantly a flavor singlet state.

Comparing our result to experimental and phenomenological results [9,40,159] we find agreement

with results from radiative decays and glueball mixing ($\sim 42°$), while results from photon fusion and charm-$\eta$ production favor a value of $\sim 33°$. However, our final result for $\phi$ is slightly larger than the average estimate from phenomenology [40]. Moreover, we remark that within the statistical errors from the standard method no significant influence of the charm quark could be observed, which is also expected on phenomenological grounds [40]. In fact, including the charm operators in the correlation function matrix leads to almost identical values for the mixing with slightly increased error due to additional noise introduced by the corresponding correlators.

Another issue that we are able to address concerns the validity of the assumptions that enter the derivation of the single angle mixing scheme in the quark flavor basis, i.e. the smallness of the OZI corrections and further, higher order terms that have been dropped due to the application of $\chi$PT in order to use pseudoscalar matrix elements instead of axial vector ones. For this purpose we computed the angles $\phi_l$ and $\phi_l$ using the excited state removal method, which – unlike the standard method – yields sufficiently small errors to allow for a meaningful check. As discussed previously, these angles are not well defined quantities to the given order in chiral perturbation theory, however, their values should be very similar if the assumptions are valid to a reasonable level. Indeed our physical results for $\phi_l$ and $\phi_l$ in Eq. (3.24) are compatible within errors and the direct extrapolation of the difference in Eq. (3.25) agrees well with the phenomenological estimate $|\phi_l - \phi_s| < 5°$ given in [40]. These results confirm the validity of the assumption that the aforementioned OZI corrections are small and that the quark flavor basis indeed allows to a good approximation for a description in terms of a mixing scheme involving only one instead of two angles.

In addition we have performed the first lattice calculation of the decay constant parameters $f_l$ and $f_s$ completing the set of parameters of the mixing scheme. For the extrapolation to the physical point we considered the ratios $f_l/f_{\mathrm{PS}}$ and $f_s/f_K$ using our lattice data on $f_{\mathrm{PS}}$ and $f_K$ in order to decrease systematic effects. For the case of $f_l/f_{\mathrm{PS}}$ we still observe significant scaling artifacts and the result in Eq. (3.26) is very likely to be underestimated. Indeed, the average phenomenological estimate given in [40] is far off and lies not even within our rather large estimate for the systematic error, which only covers the difference up to the result obtained at the finest value of the lattice spacing, i.e. $(f_l/f_{\mathrm{PS}})^D = 0.924(22)_{\mathrm{stat}}$. Clearly, additional data at the finest value of lattice spacing would be desirable to perform a more reliable analysis, as well as input from W$\chi$PT which would allow for a more sophisticated fitting ansatz. For $f_s/f_K$ the cancellation of the strange quark mass dependence seem to work very well and scaling artifacts are negligible. The physical value in Eq. (3.27) is in excellent agreement with the average phenomenological value in [40]. Moreover, even the combined statistical and systematic error on our result is smaller than the error quoted for the phenomenological estimate.

## 3.6   Determination of low-energy constants of W$\chi$PT

In this final section we present the results of our W$\chi$PT-based analysis concerning the mass splittings in Eqs. (1.221) and (1.220). The central part of this analysis is again performed in the Wilson twisted mass setup with $N_f = 2 + 1 + 1$ dynamical quark flavors and a major part

of our efforts concerns the estimation of the systematic effects entering our determinations of the LECs. In a second step we will vary the details of the lattice action in order to explore the qualitative changes resulting for the values of the LECs. For this purpose we change the number of dynamical quark flavors using $N_f = 2$ flavors of Wilson twisted mass fermions and replace the Iwasaki gauge action by the tree-level Symanzik improved gauge action [77, 85, 136]. In addition, we will study effects arising from smearing the gauge links in the covariant derivatives entering Eq. (1.151). To this end, we consider data obtained from *stout smearing* [160], which is analytic in the un-smeared link variables and hence suitable for numerical simulations using the hybrid Monte Carlo algorithm. Finally, we consider results obtained from the inclusion of the Sheikholeslami-Wohlert term as given in Eq. (1.161). All the results presented in this section have been previously published in [2].

### 3.6.1 $N_f = 2 + 1 + 1$ WtmLQCD with Iwasaki gauge action

For the details of the setup used in our study involving $N_f = 2 + 1 + 1$ dynamical quark flavors in the Wilson twisted mass formulation we refer to section 3.1 and in particular table 3.1 as it involves the same ensembles and sets of gauge configurations that have been employed in the $\eta, \eta'$ related investigations. The relevant values of the pseudoscalar meson masses for the $N_f = 2 + 1 + 1$ ensembles are collected in tables 3.4 and 3.5.

In figure 3.20 we show the mass splittings defined in Eqs. (1.221, (1.220) that are directly proportional to $W_8'$ and $W_6'$, respectively. From these two plots it is apparent that the lattice data fulfill the conditions $W_8' < 0$ and $W_6' > 0$ which is in agreement with bounds that have been calculated in [107, 112, 125]. In the following we will address the systematic effects introduced by lattice artifacts, the quark mass dependence and finite size effects to allow for meaningful a determination of the values for the LECs $W_6'$ and $W_8'$.

First of all, we remark that in the "large cut-off effects" power counting and at leading order in the W$\chi$PT Lagrangian, the mass splittings as given in Eqs. (1.221), (1.220) are expected to be independent of the lattice spacing and the light quark mass. Therefore, any presence of such effects might hint at effects entering at higher orders in the chiral expansion. Unfortunately, the corresponding NLO expressions for the mass splittings are not available in the literature, hence we rely on a separate study to estimate the systematic error. For this we consider the continuum limit of the mass splittings at fixed light quark mass and perform a comparison of constant and linear extrapolations in $(r_0 M_{PS})^2$. Concerning the continuum limit of the mass splittings, we observe from the two plots in figure 3.20 that data exhibiting similar values of $(M_{PS} r_0)^2$ but differing in the value of the lattice spacing seem rather compatible. In particular, this holds for the larger lattice sizes, which in the plots are represented by filled symbols.

In the left panel of figure 3.21 we show the lattice spacing dependence of the two aforementioned mass splittings at a common reference mass $(M_{PS} r_0)^2 \approx 0.55$. For this purpose we have only considered the largest lattice sizes $L$. Although the physical size of the lattice slightly changes for different values of $\beta$, our lattices all satisfy $L \gtrsim 2.5\,\mathrm{fm}$ and $M_{PS} L \gtrsim 4$. Therefore, one should not expect a large effect from the small mismatch in the physical volume. The plot in the

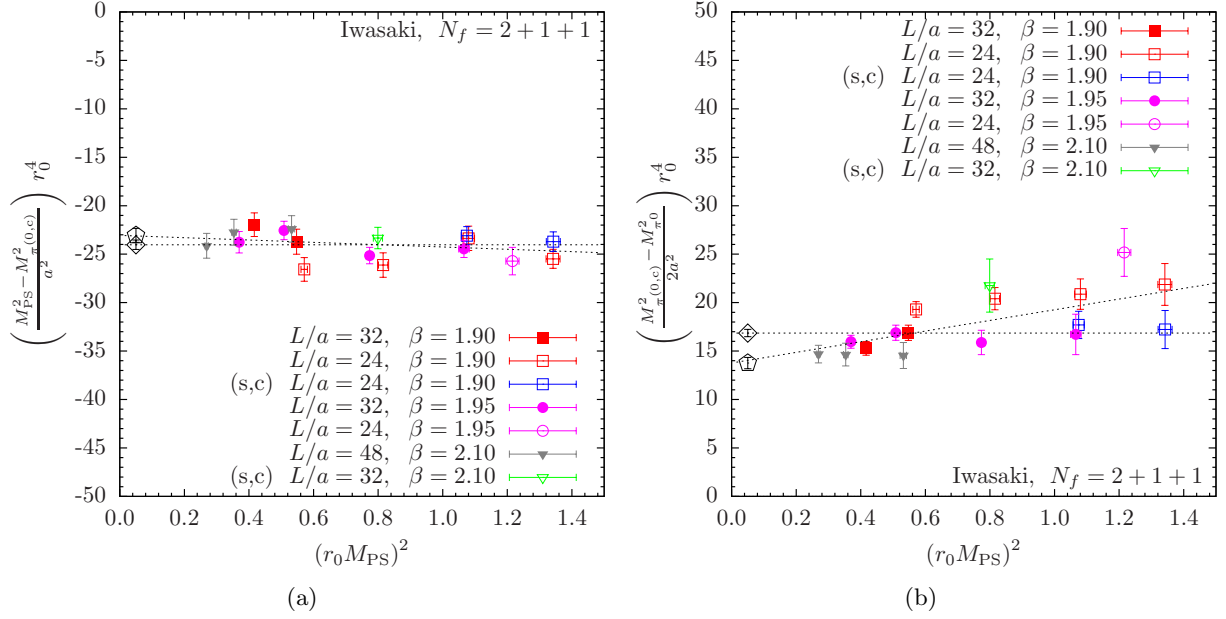Figure 3.20: Results for the mass splittings (a) $(M_{\mathrm{PS}}^2 - M_{\pi^0,c}^2)/a^2$ in Eq. (1.220) and (b) $(M_{\pi^0,c}^2 - M_{\pi^0}^2)/2a^2$ in Eq. (1.221) in units of $r_0$ as a function of $(r_0 M_{\mathrm{PS}})^2$. The results are obtained from $N_f = 2 + 1 + 1$ flavors of Wilson twisted mass fermions and the Iwasaki gauge action. The mass splittings are directly related to the Wilson LECs $W_8'$ and $W_6'$. Filled and empty symbols denote different lattice sizes. The label "(s,c)" identifies ensembles with a different values of the strange and charm quark masses in the sea. In addition, the results of a chiral extrapolation from a constant and a linear fit in $(r_0 M_{\mathrm{PS}})^2$ have been included. The difference between these two extrapolations enters the systematic error analysis.

left panel of figure 3.21 clearly suggest that the residual effects of different values of the lattice spacing are small. At this point we recall that these lattice artifacts are of subleading order in the chiral expansion. In order to give an estimate of these effects, we include in the systematic error of our analysis the difference between the values of the mass splittings obtained from the two finest lattice spacings.

Concerning the light-quark mass dependence one may expect the mass terms appearing at NLO to contain a linear term in $M_{\mathrm{PS}}^2$. Moreover, a chiral logarithm of the form $M_{\mathrm{PS}}^2 \log(M_{\mathrm{PS}}^2)$ may be present. Indeed, it was shown in [130] that such terms occur in the NLO W$\chi$PT expression of the mass splitting between the charged and neutral pion masses. Since the exact form of these logarithmic terms is yet unknown for the mass splittings in question, we restrict ourselves to a linear chiral extrapolation in $M_{\mathrm{PS}}^2$. Besides, our data is not precise enough to allow us to disentangle possible logarithmic contributions anyway. We use the result of the linear extrapolation as the central value and estimate the systematic error introduced by the light quark mass dependence from the difference to the results from the constant extrapolation.

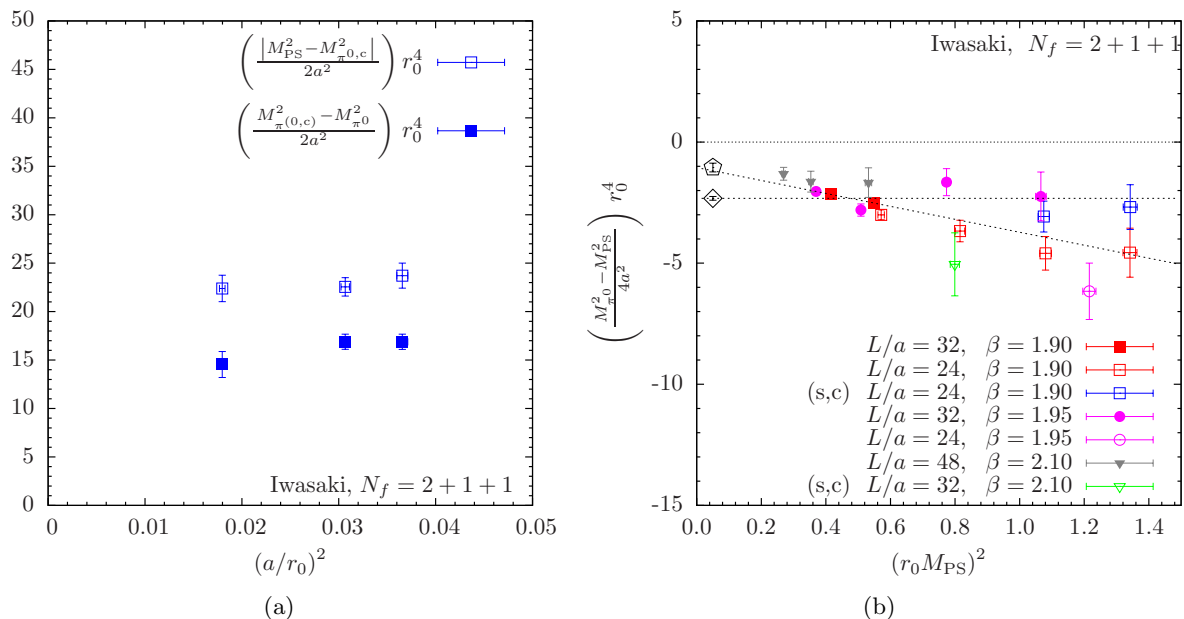Finally, we take finite volume effects into account by considering the two ensembles A40.24

Figure 3.21: (a) Lattice spacing dependence of the mass splittings $|M_{\text{PS}}^2 - M_{\pi^0,c}^2|/a^2$ (open symbols) – and $(M_{\pi^0,c}^2 - M_{\pi^0}^2)/2a^2$ (filled symbols) at a common reference mass $(M_{\text{PS}} r_0)^2 \approx 0.55$ for the setup $N_f = 2 + 1 + 1$ dynamical flavors of Wilson twisted mass fermions and the Iwasaki gauge action. For the sake of visibility, the absolute value of the mass splitting is given for $|M_{\text{PS}}^2 - M_{\pi^0,c}^2|/a^2$. (b) Pion mass-splitting, $(M_{\pi^0}^2 - M_{\text{PS}}^2)/a^2$, normalized according to Eq. (1.223) in order to relate it to the combination of W$\chi$PT LECs $c_2$. We show chiral extrapolations corresponding to a constant and a linear fit in $M_{\text{PS}}^2$.

and A40.32 which differ only by their respective lattice sizes, i.e. $L \approx 2.1\,\text{fm}$ and $2.8\,\text{fm}$. The difference between the values of the mass splittings from these two ensembles is added to the systematic error. We expect this to be a conservative choice as these two ensembles exhibit a rather small value of the light quark mass, hence finite size effects may be non-negligible. Moreover, they belong to the set of ensembles employing the coarsest lattice spacing, for which possible finite size effects induced by the neutral pion mass should be larger.

In subsection 1.3.5 it has been been pointed out that the determination of the W$\chi$PT LECs from lattice data with $N_f = 2 + 1 + 1$ flavors assumes that the heavy sea quarks decouple sufficiently from the light quark dynamics governing the pion sector. The residual heavy quark mass dependence that enters $W_6'$ and $W_8'$ can be revealed by considering different values for the strange and charm quark masses around their physical values. The effect of varying these masses is shown in figure 3.20 by the points which are labeled "(s,c)". In order to estimate the resulting systematic effect we determine the difference between the mass splittings from ensembles $A80.24$ and $A80.24s$. We expect this to be a conservative choice for three reasons. First, for the ensemble $A80.24s$ the strange quark mass is very close to the physical point. Secondly, the change in the strange quark mass is largest for the two ensembles $A80.24$ and $A80.24s$. Finally, the effect of

|        | $w_8' \, r_0^4$ | $w_8'$ | $W_8' \, (r_0^6 W_0^2)$ |
|--------|------------------|---------|--------------------------|
| sys.   | $-2.9(4)$        | $-[571(32)\,\mathrm{MeV}]^4$ | $-0.0138(22)$ |
|        | $w_6' \, r_0^4$ | $w_6'$ | $W_6' \, (r_0^6 W_0^2)$ |
| sys.   | $+1.7(7)$        | $+[502(58)\,\mathrm{MeV}]^4$ | $+0.0082(34)$ |
|        | $c_2 \, r_0^4$  | $c_2$  | $-2\,(2W_6' + W_8')\,(r_0^6 W_0^2)$ |
| lin.   | $-1.1(2)$        | $-[444(28)\,\mathrm{MeV}]^4$ | $-0.0050(10)$ |
| cst.   | $-2.3(1)$        | $-[541(24)\,\mathrm{MeV}]^4$ | $-0.0111(10)$ |

Table 3.9: Results the W$\chi$PT LECs $W_{6,8}'$ ($w_{6,8}'$) and $c_2$ from the $N_f = 2+1+1$ setup with Wtm fermions and the Iwasaki gauge action. For the conversion to physical units $r_0 = 0.45(2)$ fm has been used. The values in the last column are derived from Eq. (1.219) using $r_0 f = 0.276(12)$ from [79]. For $W_{6,8}'$ the systematic error analysis (see text) has been incorporated in the overall uncertainty indicated by the label "sys." in the table. In the last two lines we give the results of a constant and a linear chiral extrapolation of $c_2$ in $M_{\mathrm{PS}}^2$ with purely statistical errors; see also the right panel of figure 3.21.

the strange sea quarks should be larger than that of the corresponding charm quarks.

In order to give an estimate for the systematic error induced by the previously discussed systematic effects, we combine them in quadrature. This procedure leads to the following values for the mass splittings in the Wilson twisted mass setup with $N_f = 2+1+1$ dynamical quark flavors and the Iwasaki gauge action

$$\left( \frac{M_{\mathrm{PS}}^2 - M_{\pi^0,c}^2}{a^2} \right) r_0^4 = -23.0\,(0.7)_{\mathrm{stat}}\,(3.0)_{\mathrm{sys}} \,, \tag{3.28}$$

$$\left( \frac{M_{\pi^0,c}^2 - M_{\pi^0}^2}{2a^2} \right) r_0^4 = +13.8\,(0.6)_{\mathrm{stat}}\,(5.6)_{\mathrm{sys}} \,. \tag{3.29}$$

The corresponding values of the Wilson LECs are collected in table 3.9. Note that the results for $w_6'$ and $w_8'$ are indeed precise enough to give a definite sign for these LECs.

In addition, the combination of LECs $c_2$, has been calculated directly the mass splitting $M_{\pi^0}^2 - M_{\mathrm{PS}}^2$ as given in Eq. (1.223). The results for this mass splitting are shown in the right panel of figure 3.21 together with chiral extrapolations from a constant and a linear fit in $M_{\mathrm{PS}}^2$. In table 3.9 we have listed the results from both extrapolations and quote only a statistical error on these two numbers. The values arising from both extrapolations clearly favor a negative a sign of $c_2$. Furthermore, we remark that the NLO W$\chi$PT expressions for $c_2$ have been given in [130]. Besides the Wilson LECs appearing already at leading order and the usual Gasser-Leutwyler LECs, further parameters are encountered at NLO. However, a determination of these additional parameters is beyond the scope of our study. Such an analysis should also include the decay constants in addition to the pion masses and will be subject to future work. Earlier results for the Gasser-Leutwyler LECs have been given from studies in [79, 151], where fits based on continuum $\chi$PT have been directly applied to the lattice data.

| $\beta$ | $L/a$ | $a\mu_l$ | $aM_{\mathrm{PS}}$ | $aM_{\pi^0,c}$ | $aM_{\pi^0}$ | $r_0/a$ |
|---|---|---|---|---|---|---|
| 3.90 | 32 | 0.0040 | 0.1338(02) | 0.2080(30) | 0.1100(080) | 5.35(4) |
| 3.90 | 24 | 0.0040 | 0.1362(07) | 0.2120(30) | 0.1090(070) | 5.35(4) |
| 3.90 | 16 | 0.0040 | 0.1596(30) | 0.2226(95) | N/A | 5.35(4) |
| 3.90 | 24 | 0.0064 | 0.1694(04) | N/A | 0.1340(100) | 5.35(4) |
| 3.90 | 16 | 0.0085 | 0.1940(05) | N/A | 0.1690(110) | 5.35(4) |
| 3.90 | 16 | 0.0074 | 0.1963(17) | 0.2541(55) | N/A | 5.35(4) |
| 4.05 | 32 | 0.0030 | 0.1038(06) | 0.1500(30) | 0.0900(060) | 6.71(4) |
| 4.05 | 20 | 0.0030 | 0.1191(41) | 0.1571(62) | N/A | 6.71(4) |
| 4.05 | 32 | 0.0060 | 0.1432(06) | 0.1800(20) | 0.1230(060) | 6.71(4) |
| 4.20 | 24 | 0.0020 | 0.0941(31) | 0.1157(61) | N/A | 8.36(6) |

Table 3.10: Results for the charged $M_{\mathrm{PS}}$, neutral connected $M_{\pi^0,c}$ and neutral $M_{\pi^0}$ pion masses from ETMC simulations with $N_f = 2$ flavors of Wilson twisted mass fermions at maximal twist and the tree-level Symanzik improved gauge action [77]. In addition the values for the Sommer scale $r_0$ in the chiral limit is given for each value of the lattice spacing [78].

Finally, we note that extensions of the analytical expressions to SU (3) W$\chi$PT are currently not available in the literature. In principle, the knowledge of the corresponding formulas would allow for an inclusion of our data for the kaon sector, which would be very beneficial with respect to the statistical errors on the derived quantities due to the absence of quark disconnected diagrams for the relevant correlation functions.

### 3.6.2  $N_f = 2$ WtmLQCD with tree-level Symanzik improved gauge action

In this subsection, we again aim at a determination of the LECs $W'_6$ and $W'_8$. However, now we consider the case of $N_f = 2$ dynamical flavors of Wilson twisted mass fermions and the tree-level Symanzik improved (tlSym) gauge action. The relevant results for this setup (i.e. the masses in the pion sector) have been given in [77,85,136]. Note that the available data set for this setup is significantly smaller then the one we analyzed for the $N_f = 2+1+1$ case, such that this study may suffer from an insufficient control of systematic effects. Nonetheless, it seems worthwhile to try to perform at least a qualitative comparison with the $N_f = 2+1+1$ case in order to obtain some information on the the size of cutoff effects in different lattice setups.

The lattice simulations that we considered in this work [77,161] were again performed at three values of the lattice spacing $a \approx 0.08\,\mathrm{fm}$, $0.07\,\mathrm{fm}$ and $0.05\,\mathrm{fm}$ corresponding to values of the gauge coupling $\beta = 3.90$, $4.05$ and $\beta = 4.20$, respectively. The charged pion mass $M_{\mathrm{PS}}$ in these simulations covers a range from $\sim 310\,\mathrm{MeV}$ to $\sim 460\,\mathrm{MeV}$. The physical spatial lattice volumes range from $(1.3\,\mathrm{fm})^3$ to $(2.6\,\mathrm{fm})^3$ and it is again possible to study possible finite size effects in the desired quantities from ensembles which differ only by the lattice size. In table 3.10 we have collected the values of the pseudoscalar meson masses for the $N_f = 2$ ensembles [77]. The resulting mass splitting derived from Eqs. (1.221)-(1.220) are illustrated in figure 3.22.
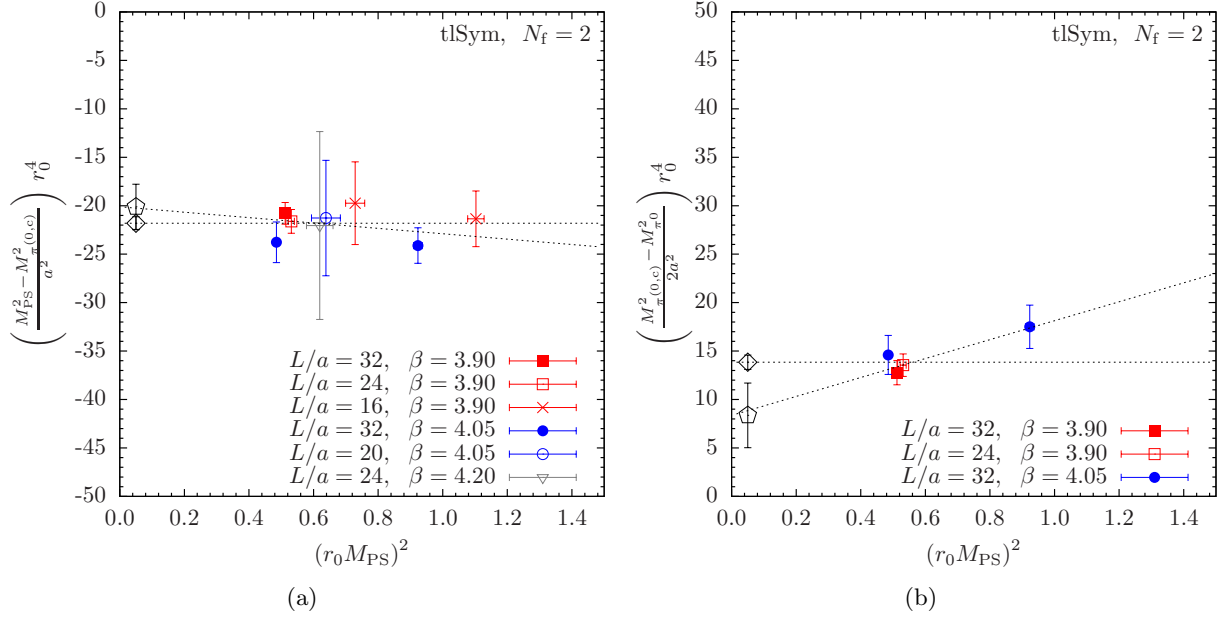
Figure 3.22: Results for the mass splittings from the lattice setup with $N_f = 2$ flavors of Wilson twisted mass fermions and the tlSym gauge action. (a) $(M_{\mathrm{PS}}^2 - M_{\pi^0,c}^2)/a^2$ in Eq. (1.221) and (b) $(M_{\pi^0,c}^2 - M_{\pi^0}^2)/2a^2$ in Eq. (1.220) as a function of $M_{\mathrm{PS}}^2$. The mass splittings are directly related to the Wilson LECs $W_8'$ and $W_6'$. Open and filled symbols refer to a change in the lattice size.

Similar to the previous analysis we want to explore the systematic effects that may affect these determinations. To this end, we proceed in the same way as for the $N_f = 2 + 1 + 1$ case. Again, we can estimate possible finite size effects from ensembles which differ only by the physical volume. For the coarsest lattice spacing corresponding to $\beta = 3.90$, a set of three ensembles with $L/a = 16$, 24 and 32 is available for the case of $(M_{\mathrm{PS}}^2 - M_{\pi^0,c}^2)/a^2$. The corresponding results are illustrated in the left panel of figure. 3.23. From this plot it is apparent that within the current statistical uncertainties, no clear signs of finite size effects are visible in the data. Moreover, we observe that data obtained at two different values of the lattice spacings (corresponding to $\beta = 3.90$ and 4.05) agree within errors. This may be seen as an indication that there are no large lattice artifacts present in these mass splittings.

Unfortunately, due to lack of sufficient data it is not possible to investigate the quark mass dependence of the mass splitting $(M_{\pi^0,c}^2 - M_{\pi^0}^2)/a^2$ in a systematic way. Similar to the $N_f = 2 + 1 + 1$ case, we incorporate the deviation between a constant and a linear extrapolation in $M_{\mathrm{PS}}^2$ in the estimate of the systematic uncertainties. Again, we use the results of the linear fit as our central value. This leads to the following values for the mass splittings

$$\left( \frac{M_{\mathrm{PS}}^2 - M_{\pi^0,c}^2}{a^2} \right) r_0^4 = -20.1\,(2.3)_{\mathrm{stat}}\,(1.7)_{\mathrm{sys}} \,, \tag{3.30}$$

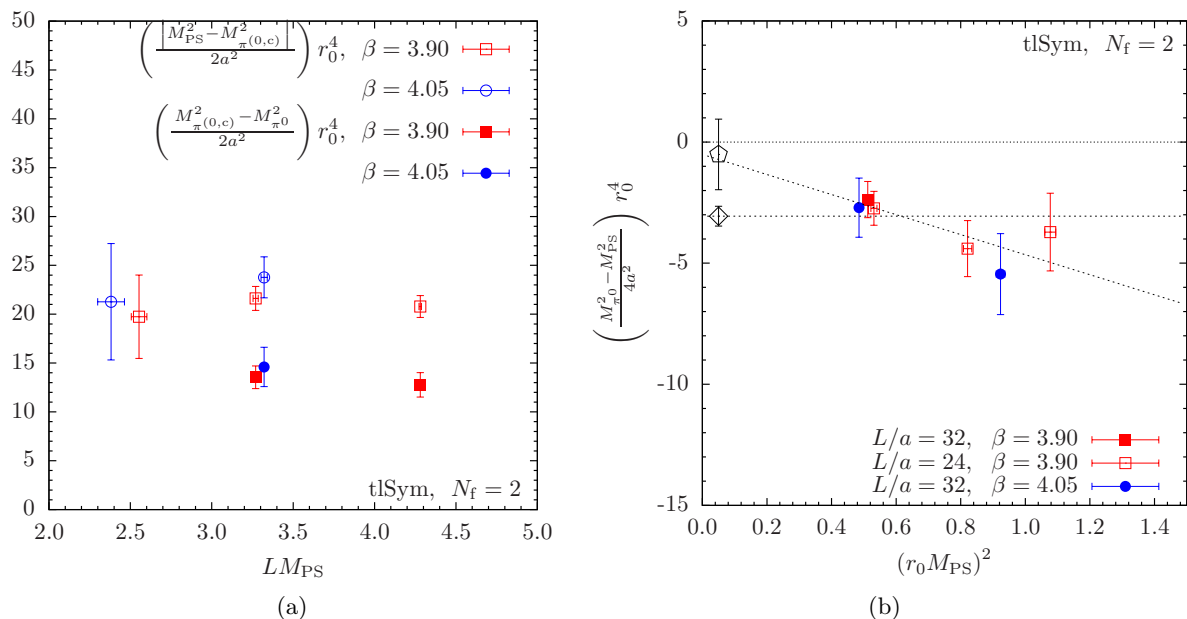Figure 3.23: (a) Finite volume effects for the mass splittings $|M_{\rm PS}^2 - M_{\pi^0,c}^2|/a^2$ (open symbols) and $(M_{\pi^0,c}^2 - M_{\pi^0}^2)/2a^2$ (filled symbols). Note that the absolute value of the mass-splitting is used in the case of empty symbols. (b) Results for $(M_{\pi^0}^2 - M_{\rm PS}^2)/a^2$ normalized according to Eq. (1.223) in order to relate it to $c_2$. In addition, we show a chiral extrapolation from a constant and a linear fit in $M_{\rm PS}^2$ is also shown. Results are obtained from the lattice setup with the $N_f = 2$ flavors of Wilson twisted mass fermions and the tlSym gauge action.

$$\left( \frac{M_{\pi^0,c}^2 - M_{\pi^0}^2}{2a^2} \right) r_0^4 = +8.4\,(3.3) \pm (5.5) \; , \tag{3.31}$$

The corresponding values of the Wilson LECs are collected in Tab. 3.11. We remark, that $W_8'$ has recently been determined from a mixed action involving the same $N_f = 2$ lattice action in the sea sector as used in our study, but with Neuberger overlap valence quarks [124]. The value quoted in in this investigation $W_8'\,(r_0^6 W_0^2) = -0.0064(24)$, differs from our estimate in table 3.11 at the $2\sigma$ level. However, concerning this possible issue it should be stressed again that our estimate does not include a complete estimate of the systematic error.

In the right panel of figure 3.23 we show the results for $c_2$ determined in the $N_f = 2$ setup. Again, more data would be required in order to explore the residual quark mass dependence of $c_2$. Therefore, we quote separately the results of a constant and a linear chiral extrapolation in $M_{\rm PS}^2$

$$c_2\,r_0^4\,[\,\mathrm{cst.}\,] = -3.1(0.4)_{\rm stat} \; , \tag{3.32}$$

$$c_2\,r_0^4\,[\,\mathrm{lin.}\,] = -0.5(1.5)_{\rm stat} \; . \tag{3.33}$$

Note that these values are consistent with those obtained from the results for the pseudoscalar

| $w'_8 \, r_0^4$ | $w'_8$ | $W'_8 \, (r_0^6 W_0^2)$ |
|---|---|---|
| -2.5(4) | $-[552(025)\,\mathrm{MeV}]^4$ | -0.0119(17) |
| $w'_6 \, r_0^4$ | $w'_6$ | $W'_6 \, (r_0^6 W_0^2)$ |
| +1.0(8) | $+[443(138)\,\mathrm{MeV}]^4$ | +0.0049(38) |

Table 3.11: Results for the W$\chi$PT LECs $W'_{6,8}$ ($w'_{6,8}$) from the $N_f = 2$ setup using Wtm fermions and the tree-level Symanzik improved gauge action. For the conversion to physical units again $r_0 = 0.45(2)$ fm has been used. The values for $W'_{6,8}$ have been derived from Eq. (1.219), using $r_0 f = 0.275(6)$ from [77] as input.

meson masses in [77]. Moreover, they are also very similar to the ones obtained in [129] for $K = -4c_2$ from an investigation of finite volume effects in the twisted mass formulation. We stress that all the lattice measurements favor a negative sign of $c_2$.

### 3.6.3    Discussion of results

Before closing this section, we address some additional details and issues regarding our analysis of the W$\chi$PT LECs. First, we remark that two out of three quantities (i.e. $W'_6$ and $c_2$) depend on the neutral pion mass $M_{\pi^0}$, which receives large contributions from quark disconnected diagrams. These diagrams clearly dominate the statistical error for $W'_6$ and $c_2$. In this context it is interesting to note that the results for the neutral pion mass in table 3.5 indicate that the relative error does not depend on the light quark mass, whereas it decreases when increasing the lattice volume. For our simulations this actually implies that one obtains $M_{\pi^0}$ with smaller relative statistical errors for ensembles at smaller light quark mass, because these ensembles tend to have larger volumes.

Apart from this effect, the statistical errors do not allow us to perform a meaningful study of the light quark mass dependence for the mass splittings related to the $W'_6$ and $c_2$, as can be inferred from the corresponding plots in the right panels of figures 3.20 and 3.21. In principle, such a mass dependence is expected to appear at NLO in the chiral expansion of W$\chi$PT, however, we do neither see a clear trend towards such an dependence from our data nor can we exclude that it is negligible within our errors. Nevertheless, it has to be pointed out that the possibility of such a dependence is particularly relevant for the combination of LECs $c_2 \sim -(2w'_6 + w'_8)$ which allows for a partial cancellation of the effects stemming from $w'_6$ and $w'_8$. The issue of NLO terms affecting the determination $c_2$ have also been discussed in [121]. As it has been previously mentioned in subsection 1.3.5, the sign of $c_2$ indicates whether either the Aoki ($c_2 > 0$) or the Sharpe-Singleton ($c_2 < 0$) scenario is realized concerning the phase structure of Wilson fermions. Still, our lattice data seems to be in favor of the latter scenario.

Concerning a possible dependence of the LECs $W'_{6,8}$ and $c_2$ on the lattice setup, we can compare our results for $N_f = 2 + 1 + 1$ flavors of Wilson twisted mass fermions and the Iwasaki gauge action with those obtained in the $N_f = 2$ setup with the tlSym gauge action. This comparison
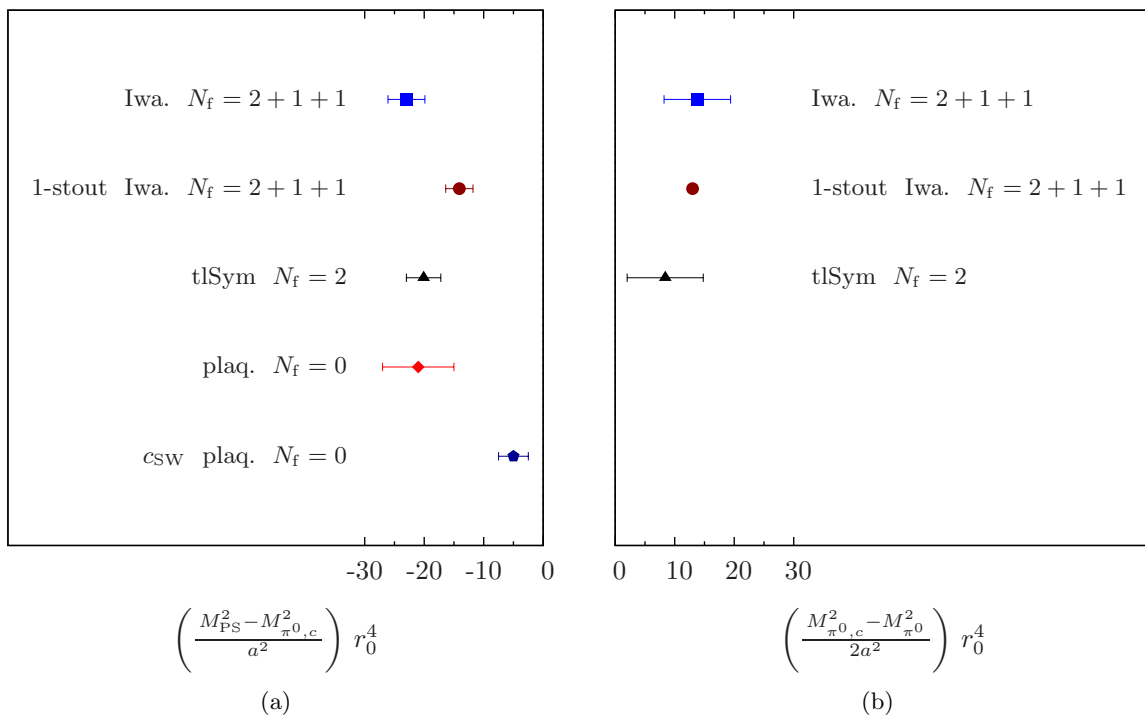
Figure 3.24: Comparison of the values of the mass splittings (a) $(M_{\mathrm{PS}}^2 - M_{\pi^0,c}^2)/a^2$ and (b) $(M_{\pi^0,c}^2 - M_{\pi^0}^2)/2a^2$ from different lattice setups. Results from stout smearing are labeled 1-stout and the result from quenched simulations involving the clover term is denoted by $c_{\mathrm{SW}}$ to distinguish from the plain quenched setup; see text for further details.

does not reveal any significant difference between the two setups. Moreover, we can extend such an comparison for the case of the mass splittings to further lattice actions, although we point out that for most of these results a study of the full systematic uncertainties is not available. Therefore, such an comparison has necessarily to remain at a qualitative level. In [79] a lattice setup with $N_f = 2 + 1 + 1$ Wilson twisted mass fermions and the Iwasaki gauge action has been considered, but in this case also one iteration of stout smearing was included. The mass splittings obtained in this setup are compared to our results in figure 3.24. From this comparison it appears that stout smearing reduces the size of the mass splitting $(M_{\mathrm{PS}}^2 - M_{\pi^0,c}^2)/a^2$, while $(M_{\pi^0,c}^2 - M_{\pi^0}^2)/a^2$ remains unaffected within the statistical uncertainties. However, it should be stressed that for the results in the setup involving stout smearing only a single ensemble has been considered.

In the left panel of figure 3.24 we have included further estimates of the mass splitting $(M_{\mathrm{PS}}^2 - M_{\pi^0,c}^2)/a^2$ from two different types of quenched simulations, which differ only by the absence or presence of the clover term. for both quenched setups Wilson twisted mass fermions and the plain plaquette gauge action have been used. For the case without a clover term, the corresponding results were taken from [162] and we have used results from different lattice spacings and quark

masses to estimate the systematic uncertainties entering $(M_{\mathrm{PS}}^2 - M_{\pi^0,c}^2)/a^2$. For the quenched simulations in which the Sheikholeslami-Wohlert term is included, we follow [163], where the non-perturbative determination of $c_{\mathrm{SW}}$ was used. Considering the setups which do neither include stout-smearing nor the clover term, it appears that the value of the mass splitting $(M_{\mathrm{PS}}^2 - M_{\pi^0,c}^2)/a^2$ is not affected by a simultaneous change of the gauge action and the number of dynamical quark flavors. However, from the current data it is not possible to rule out that changing only the number of flavors or the gauge action might still have a non-zero effect. To this end, it would be required to include further actions and also increase the statistical precision of the results.

Finally, we remark that the introduction of the clover term in the quenched setup leads to a reduction of $\mathcal{O}\left(a^2\right)$ effects, which can be seen in the left panel of figure 3.24 for the mass splitting $(M_{\mathrm{PS}}^2 - M_{\pi^0,c}^2)/a^2$. This result motivates the inclusion of a clover term in simulations with dynamical quarks, an activity which at the time of writing this thesis has already been started by the ETMC for the case of a degenerate doublet. Moreover, it would be interesting to investigate if also the splitting $(M_{\pi^0,c}^2 - M_{\pi^0}^2)/2a^2$ is reduced for such a setup.

# Summary and outlook

In this work we have performed the first study of the $\eta$–$\eta'$ system from $N_f = 2+1+1$ dynamical quark flavors using the Wilson twisted mass formulation. For this study we employed three values of the lattice spacing and values of the light quark mass corresponding to charged pion masses ranging from $\sim 230$ to $\sim 500\,\mathrm{MeV}$. In addition, we investigated two dedicated pairs of ensembles for which the value of the strange quark mass has been varied, whilst keeping the remaining physical parameters fixed. Besides covering a large range of quark masses, the gauge ensembles used in this work feature three values for the lattice spacing as well as many different lattice volumes. The data set generated for this study more than triples the available world data from lattice simulations involving three or more dynamical quark flavors.

These prerequisites allowed for an extrapolation of the mass of the $\eta$ with well controlled systematics. Residual effects of lattice artifacts have been determined to be small from scaling tests performed at two different values of the light quark mass. The difference between a constant and a linear fit in $(r_0 M_{\mathrm{PS}})^2$ has been used to assign a systematic error to the final result from the extrapolation to physical values of the charged pion mass. In addition, we have accounted for mistuned values of the strange quark mass by calculating the derivative of $(r_0 M_\eta)^2$ with respect to $(r_0 M_K)^2$ to correct all our data by means of the procedure discussed in subsection 3.3.1. Besides, finite size effect have been shown to be negligible within the available statistical precision. Having estimated all systematic effects regarding the $\eta$ meson, we finally presented a continuum value for $M_\eta$ which fully agrees with experimental data.

In case of the mass of the $\eta'$ meson we observed significantly larger gauge noise and also notable effects of autocorrelation, resulting in much larger statistical errors. In fact, the values determined using the standard method (i.e. solving a GEVP directly for the full correlation function matrix) can only serve as an upper bound on the mass. However, a significant improvement has been achieved employing an analysis method which is based on the subtraction of the excited states in the connected pieces of the correlation functions. This allowed for an even more precise study of the $\eta$ mass as well as for a meaningful calculation of the $\eta'$ mass. Additionally, it allows to perform a chiral extrapolation in the light quark mass also for the mass of the $\eta'$. The final results for the masses of both states are listed in in table 3.12, which includes an overview on all our final, physical results for the $\eta$, $\eta'$ study. The resulting masses are both in excellent agreement with experimental data, demonstrating that QCD does indeed account for the observed large mass splitting between $\eta$ and $\eta'$. Moreover, the present work has been the first study of the $\eta$–$\eta'$ system including at least three dynamical quark flavors in which control over systematic

| | | | |
|---|---|---|---|
| $M_\eta$ | $= 551(8)_{\text{stat}}(6)_{\text{sys}}$ MeV | $M_{\eta'}$ | $= 1006(54)_{\text{stat}}(38)_{\text{sys}}(+61)_{\text{ex}}$ MeV |
| $\phi$ | $= 46.0(0.9)_{\text{stat}}(2.7)^\circ_{\text{sys}}$ | $\Delta\phi_{ls}$ | $= 2.8(1.1)_{\text{stat}}(2.6)^\circ_{\text{sys}}$ |
| $f_l/f_{\text{PS}}$ | $= 0.859(7)_{\text{stat}}(64)_{\text{sys}}$ | $f_s/f_K$ | $= 1.166(11)_{\text{stat}}(31)_{\text{sys}}$ |

Table 3.12: Collection of the final results of this work. Masses and mixing parameters are extrapolated to the physical value of the charged pion mass. The quoted values all refer to the improved analysis method. The third error on the $\eta'$ mass refers to our method. Note that the result for $f_l/f_{\text{PS}}$ is likely to be affected by significant lattice artifacts and hence too small.

effects has been achieved, e.g. regarding effects of different values of the quark masses and the lattice spacing.

Furthermore, we have studied mixing parameters in the quark flavor basis for the flavor singlet sector from pseudoscalar matrix elements. The final, physical results of this study are also included in table 3.12. For the mixing angle $\phi$ we found good agreement with most other lattice determinations and we observed only very moderate systematic uncertainties from scaling artifacts or residual effects of the strange quark mass. Our final result for $\phi$ indicates that the $\eta$ is mainly an octet state while the $\eta'$ is indeed dominated by the flavor singlet component. Possible contributions form the charm sector turned out to be compatible with zero for both states.

The removal of excited states in the connected part of the correlation functions provided significant improvement regarding the statistical error and it was only through this method that the extraction of the remaining decay constant parameters became feasible as well. In order to account for lattice artifacts and the dependence on the value of the strange quark mass we have not extrapolated $f_l$ and $f_s$ directly but rather considered the ratios $f_l/f_{\text{PS}}$ and $f_s/f_K$ expecting to cancel some of the effects. For $f_s/f_K$ this worked well as most of the strange quark mass dependence disappeared in the ratio and no sizable lattice artifacts have been observed. The extrapolation to the physical value of the charged pion mass lead to a value that is in excellent agreement with phenomenological studies within its very small statistical and systematic errors. For the ratio $f_l/f_{\text{PS}}$ we still observed significant lattice artifacts which is also reflected by the larger systematic error on this quantity compared to the one obtained for $f_s/f_K$. Looking at our lattice data for this quantity, the actual effects of scaling artifacts appear not to be entirely covered by this error, hence our estimate at the physical value of the charged pion mass should be considered a lower bound rather than a definite result. However, regarding the dependence on the lattice spacing, there is a clear trend in the data for $f_l/f_{\text{PS}}$ pointing towards larger values at decreasing values of the lattice spacing which is expected from phenomenology. Finally, it should again be stressed that using pseudoscalar matrix elements instead of axial vector ones requires some additional input from chiral perturbation theory. The resulting mixing parameters are related to the ones defined from axial vector matrix elements only up to corrections stemming from higher order terms in the standard chiral expansion and higher orders in $1/N_C$. It is due to the anomaly that the mixing parameters defined from axial vector currents are not directly related to the ones defined from pseudoscalar currents.

Future investigations in the $N_f = 2+1+1$ setup concerning the light pseudoscalar flavor singlet mesons may address the following issues and extensions which some of them will be addressed in more detail below:

- Inclusion of gluonic operators.

- Further methods of variance reduction.

- Use of the stochastic distillation technique [164] to increase the operator basis.

- Inclusion of further ensembles with different values of the strange quark mass but fixed physical parameters otherwise.

- Explicit test of the Veneziano-Witten formula combining our results for meson masses with additional results from suitable quenched simulations.

- Simulation at the physical point.

The implementation of additional gluonic operators would in principle allow to study possible gluonic contributions to the $\eta$ and $\eta'$ states, using an extended mixing scheme as discussed in [40]. However, this is very demanding from both the computational and theoretical point of view. Such an extension involves the calculation of correlations between quark loops on the one hand and purely gluonic contributions on the other hand, which is expected to give an extremely noisy signal for the resulting correlation function. Besides, it is not clear how to define a local, purely gluonic operator and using a non-local interpolating operator would cause additional issues regarding renormalization.

In principle, it is also still possible to consider further methods of variance reduction. For instance, in the heavy quark sector we cannot apply the one-end trick for the evaluation of the quark disconnected diagrams as it is the case for the light sector. One possibility to tackle this issue, would be the use of point-to-point correlators [140]. Such an improved variance reduction might finally allow one to add axial vector operators in addition to the pseudoscalar ones, which would be very desirable with respect to the study of the mixing parameters. However, this approach would also introduce some additional model dependence. Attempts to generalize the method used in the light sector to a non-degenerate doublet have so far not been successful, because there is no simple relations between elements of the Dirac operator in flavor space and the resulting propagators. At this point we remark that one might also consider to carry out the entire analysis in a different lattice setup, employing a flavor diagonal action in the heavy quark sector as well, which will be discussed below.

Using stochastic distillation to construct suitable interpolating fields instead of considering only local (and fuzzed) operators would allow to systematically increase the operator basis. This is expected to help reducing the excited state contamination in the lowest lying states, hence allowing for fits to the principal correlators at smaller times, which might also significantly reduce the statistical errors. Compared to the excited state removal method used in this work, this would have the advantage that one does not rely on any additional assumption concerning the

quark disconnected diagrams. Moreover, this would also allow for a more systematic approach concerning the identification of further states, e.g. possible multi-particle states in the spectrum.

In case of the $\eta'$ we observed that it was not feasible to disentangle effects stemming from possible scaling artifacts an different values of the strange quark mass. In fact, it is not obvious from the data if there is a large effect contributing from any of the these sources, although some hints on scaling artifacts are present. In order to be able to assess such systematics one would clearly require additional simulations with different values of the strange quark mass, whilst keeping the remaining physical parameters fixed. Ideally, this should even be done at more than one lattice spacing.

Another – computationally very demanding – approach regarding the issue of quark mass dependence would be based on simulations performed at the physical point. This should allow to carry out a more direct computation of the desired quantities, eliminating the need for chiral extrapolations. Consequently, one would obtain even better control over systematic effects related to finite values of the lattice spacing or finite size effects. Recently, the ETMC has started the generation of corresponding gauge configurations in the $N_f = 2$ setup and it is expected that these efforts will be extended to the $N_f = 2 + 1 + 1$ setup in the future, which would be required for a study of $\eta$ and $\eta'$ mesons.

Finally, it is also possible to study $\eta$ and $\eta'$ mesons in a mixed action setup. In principle, such an approach would allow to avoid the issues related to explicit flavor symmetry violation in the heavy valence quark sector, leading to much simpler correlation functions and possibly allowing for the use of more sophisticated methods of variance reduction. Nonetheless, in such a setup one needs to perform a careful matching of valence quark masses and should proceed with caution regarding the continuum limit, as this kind of setup violates unitarity and involves partial quenching, which may pose a problem for the particular case of the $\eta,\eta'$ system, as mentioned in subsection 1.2.1. Such a study is currently in progress employing the Osterwalder-Seiler action and first results look promising considering possible issues of taking the continuum limit [165].

In addition to our analysis of the light pseudoscalar flavor singlet sector we have determined the W$\chi$PT LECs $W_6'$, $W_8'$ and $c_2$, which parametrize the size of $O(a^2)$ lattice artifacts. For this investigation we have again employed $N_f = 2 + 1 + 1$ flavors of Wilson twisted mass fermions together with the Iwasaki gauge action. This allowed us to give a rather complete estimate of the systematic uncertainties on our results for $W_6'$ and $W_8'$. The lattice data was found to satisfy the recently derived bounds $W_8' < 0$ and $W_6' > 0$ [107, 112, 125].

Furthermore, we have studied the dependence of the mass splittings $\left(M_{\mathrm{PS}}^2 - M_{\pi^0,c}^2\right)/a^2$ and $(M_{\pi^0,c}^2 - M_{\pi^0}^2)/2a^2$ on the choice of the lattice action. Keeping in mind the qualitative nature of this comparison, it is still tempting to propose an improved lattice action which should lead to a reduced mass splitting $\left(M_{\mathrm{PS}}^2 - M_{\pi^0,c}^2\right)/a^2$. Considering the outcome of our comparison of actions, such an improved action based on dynamical twisted mass fermions should involve in addition the Sheikholeslami-Wohlert term and smearing. However, further studies are required to obtain a definite statement on this point and also to extend it to the case of

$\left(M^2_{\pi^0,c} - M^2_{\pi^0}\right)/2a^2$. Note, that any partial cancellation of contributions from $W'_6$ and $W'_8$ to $c_2$ implies that the residual mass dependence of $c_2$ becomes more sensitive to terms of higher order in the chiral expansion. While this potential reduction of $c_2$ would certainly be desirable, it not possible to determine its value from the currently available lattice data.

The determination of the W$\chi$PT LECs is essential to make a quantitative statement about the impact of O($a^2$) terms on physical quantities calculated from a given lattice action. In principle, the knowledge of these LECs can be used to design a lattice action which exhibits smaller lattice artifacts. This would allow to approach the continuum limit in a more controlled way. For this purpose it would still be desirable to obtain the relevant LECs with higher statistical precision. Moreover, an independent calculation of the Wilson W$\chi$PT LECs, as it has been presented in this work, can be useful for $\chi$PT fits of light meson observables by constraining these fits to lattice data. Therefore, the results of our study using full and connected-only neutral pion masses together with charged pion masses may also be useful for other collaborations working with Wilson-type fermions.

In summary, this thesis has demonstrated that Wilson twisted mass fermions at maximal twist are very suitable to study the $\eta$-$\eta'$ system, since they allow – through special noise reduction techniques – for precise calculations of the masses and mixing parameters. The results of this study are overall in very good agreement with results from experiment and phenomenology, confirming that QCD accounts for the observed properties of these mesons. In addition, we were able to determine a set of low energy constants of W$\chi$PT using our results for masses in the pion sector, which may lead to better control simulations with twisted mass fermions. Finally, results of this study have indicated that adding a clover term to the Wilson twisted mass action may allow to carry out simulations at the physical point. In fact, corresponding activities have already been started for the case of $N_f = 2$ dynamical quark flavors.

# Appendix A

# Conventions and definitions

## A.1  Index conventions

Throughout this work Greek letters $\alpha$, $\beta$, ... are used to denote Dirac indices running from 0 to 3. Similarly for Euclidean (and Lorentz) indices Greek letters are employed, but starting from $\mu$, $\nu$, ... and again running from 0 to 3, whereas spatial vector components carry Latin indices $k$, $l$, ... that run from 1 to 3. Group indices of the fundamental representations of SU $(N_c)$ and (S)U $(N_f)$ are labeled by $A$, $B$, ... and $i$, $j$, ..., respectively. Indices of the adjoint representations are denoted by $a$, $b$, ... in both cases, but it will be clear from the context to which group we are actually referring to. Repeated indices within one expression are always assumed to be summed over, unless stated otherwise.

## A.2  Pauli matrices

We choose the following representation for the generators $\frac{\tau^a}{2}$ of $SU(2)$

$$\tau^1 = \begin{pmatrix} 0 & 1 \\ 1 & 0 \end{pmatrix}, \qquad \tau^2 = \begin{pmatrix} 0 & -i \\ i & 0 \end{pmatrix}, \qquad \tau^3 = \begin{pmatrix} 1 & 0 \\ 0 & -1 \end{pmatrix}, \qquad . \tag{A.1}$$

They satisfy the usual (anti-)commutation relations

$$\left[\tau^a, \tau^b\right] = 2i\epsilon^{abc}\tau^c, \qquad \left\{\tau^a, \tau^b\right\} = 2\delta^{ab} \, . \tag{A.2}$$

The normalization is chosen such that

$$\mathrm{tr}[\tau^a\tau^b] = 2\delta^{ab} \, . \tag{A.3}$$

Additionally, we define

$$\tau^0 = \mathbb{1}_{2\times 2} \, , \tag{A.4}$$

which also satisfies the above normalization condition.

## A.3  Gell-Mann matrices

For the case of $SU(3)$, a representation of the traceless generators $T^a = \frac{\lambda^a}{2}$ is given by the Gell-Mann matrices $\lambda^a$, which have the following form

$$
\lambda^1 = \begin{pmatrix} 0 & 1 & 0 \\ 1 & 0 & 0 \\ 0 & 0 & 0 \end{pmatrix}, \ \lambda^2 = \begin{pmatrix} 0 & -i & 0 \\ i & 0 & 0 \\ 0 & 0 & 0 \end{pmatrix}, \ \lambda^3 = \begin{pmatrix} 1 & 0 & 0 \\ 0 & -1 & 0 \\ 0 & 0 & 0 \end{pmatrix}, \ \lambda^4 = \begin{pmatrix} 0 & 0 & 1 \\ 0 & 0 & 0 \\ 1 & 0 & 0 \end{pmatrix},
$$

$$
\lambda^5 = \begin{pmatrix} 0 & 0 & -i \\ 0 & 0 & 0 \\ i & 0 & 0 \end{pmatrix}, \ \lambda^6 = \begin{pmatrix} 0 & 0 & 0 \\ 0 & 0 & 1 \\ 0 & 1 & 0 \end{pmatrix}, \ \lambda^7 = \begin{pmatrix} 0 & 0 & 0 \\ 0 & 0 & -i \\ 0 & i & 0 \end{pmatrix}, \ \lambda^8 = \frac{1}{\sqrt{3}} \begin{pmatrix} 1 & 0 & 0 \\ 0 & 1 & 0 \\ 0 & 0 & -2 \end{pmatrix}.
$$

$$(A.5)$$

The generators satisfy the commutation relations

$$
[T^a, T^b] = i f^{abc} T^c \,, \tag{A.6}
$$

where $f^{abc}$ denotes the structure constants of $SU(3)$. The normalization is chosen such that

$$
\mathrm{tr}[\lambda^a \lambda^b] = 4 \, \mathrm{tr}[T^a T^b] = 2 \, \delta^{ab} \,. \tag{A.7}
$$

## A.4  Dirac matrices

In Euclidean spacetime we work with the following chiral representation of the Dirac matrices

$$
\gamma_\mu = \begin{pmatrix} 0 & \sigma_\mu \\ \sigma_\mu^\dagger & 0 \end{pmatrix} \,, \tag{A.8}
$$

where $\sigma_k = -i\tau^k$ for $k = 1,2,3$ and $\sigma_0 = -\tau^0 = -\mathbb{1}_{2\times 2}$. They fulfill the standard anti-commutation relation

$$
\{\gamma_\mu, \gamma_\nu\} = 2\delta_{\mu\nu} \,. \tag{A.9}
$$

In addition we define

$$
\gamma_5 = \gamma_1 \gamma_2 \gamma_3 \gamma_0 \,, \tag{A.10}
$$

which implies the following properties

$$
\gamma_5^\dagger = \gamma_5 \,, \qquad \gamma_5^2 = 1 \,. \tag{A.11}
$$

In this chiral representation the projection operators on states of left- and right-handed chirality are given by

$$
P_{L/R} = \frac{1}{2} \left(1 \mp \gamma_5\right) \,. \tag{A.12}
$$

The corresponding representation of the Dirac matrices in Minkowski space is given by the replacements

$$
\gamma_0 \to \gamma_0 \,, \qquad \gamma_k \to i\gamma_k \,, \quad \delta_{\mu\nu} \to g_{\mu\nu} \,, \tag{A.13}
$$

where the signature of $g_{\mu\nu}$ is given by $(+,-,-,-)$.

# Appendix B

# Correlation function matrices

This appendix contains a list of the (unrenormalized) correlation function matrix elements for the neutral pion and $\eta$, $\eta'$ mesons in the twisted basis, which have been implemented and used for this work. The correlation functions for the charged pion and the kaon are excluded as they consist only of a single, connected piece and thus do neither exhibit any relative factors or signs nor a complicated flavor structure as it is the case for the strange and charm contributions to $\eta$ and $\eta'$ mesons.

We give the explicit, analytic expressions in terms of quark flavor dependent propagators and $\gamma$-matrix combinations. We exploit all relevant symmetries to reduce the number of terms in the final result and to reveal additional restrictions, e.g. contributions being explicitly real, imaginary or zero. However, keep in mind that one still needs to carefully match these expressions with the actual conventions of the codes that perform the contractions numerically. In practice those may differ from the analytical factors and signs that are given in this appendix.

Moreover, all correlation function matrices are symmetric by definition, hence we could in principal restrict ourselves to calculate the diagonal elements and e.g. the upper triangle matrix. However, it turns out that using all elements explicitly, gives a slightly better signal as the symmetric elements are not always numerically identical if they involve connected contributions. This becomes particularly relevant for $\eta$ and $\eta'$ as the corresponding correlation functions involve much more terms than those for the other pseudoscalar mesons considered in this work. The reason for this can be traced back to the non-trivial behavior of the spin, flavor and time index structure for connected pieces belonging to off-diagonal matrix elements under an exchange of operators at source and sink. Therefore we include the analytic expressions of all matrix elements as they have been used in the actual implementation. This also applies to their respective Dirac structure, i.e. we do keep the $\gamma_5$-matrices stemming from the application of the $\gamma_5$-trick which is explicitly used by the code.

We use the following notations (c.f. sections 2.1, 2.2):

1. Correlation function matrix elements are functions of Euclidean time $t$ and are denoted by $\mathcal{C}^P_{\mathcal{O}_i \mathcal{O}_j}(t)$, where $\mathcal{O}_i$, $\mathcal{O}_j$ refer to the fermionic bilinears (operators) at source and sink,

respectively.  In the present context we always refer to operators in the twisted basis for labeling correlation functions and drop corresponding superscripts.  Moreover, the superscript $P$ denotes the relevant particle(s) that occur as states in the spectrum of the correlation function matrix.

2. Operators are denoted corresponding to their respective Dirac structure in the twisted basis and obtain an additional index $l$, $h$ that refers to light and heavy quark sector, respectively.

3. Propagators are denoted by $G_{f_i f_j}^{xy}$, where the flavor indices $f_i$ and $f_j$ refer to the flavor of the quark field at spacetime positions $x$, $y$, respectively.

## B.1   Correlation functions for the neutral pion

For the neutral pion, one obtains the following correlation functions

$$\mathcal{C}_{\mathcal{S}_l^0 \mathcal{S}_l^0}^{\pi^0}(t) = a^3 \sum_{\vec{x}} \left( -\mathrm{Re}\,\mathrm{tr}\left[\gamma_5 \left(G_{dd}^{0x}\right)^\dagger \gamma_5\, G_{uu}^{0x}\right] + 2\,\mathrm{Re}\,\mathrm{tr}\left[G_{uu}^{00}\right] \mathrm{Re}\,\mathrm{tr}\left[G_{uu}^{xx}\right] \right), \tag{B.1}$$

$$\mathcal{C}_{\mathcal{S}_l^0 \mathcal{A}_l^3}^{\pi^0}(t) = a^3 \sum_{\vec{x}} \left( -\mathrm{Re}\,\mathrm{tr}\left[\gamma_5 \left(G_{dd}^{0x}\right)^\dagger \gamma_5\, G_{uu}^{0x}\, i\gamma_0\gamma_5\right] + 2\,\mathrm{Re}\,\mathrm{tr}\left[G_{uu}^{00}\right] \mathrm{Re}\,\mathrm{tr}\left[G_{uu}^{xx}\, i\gamma_0\gamma_5\right] \right), \tag{B.2}$$

$$\mathcal{C}_{\mathcal{A}_l^3 \mathcal{S}_l^0}^{\pi^0}(t) = a^3 \sum_{\vec{x}} \left( -\mathrm{Re}\,\mathrm{tr}\left[\gamma_5 \left(G_{dd}^{0x}\right)^\dagger \gamma_5\, i\gamma_0\gamma_5\, G_{uu}^{0x}\right] + 2\,\mathrm{Re}\,\mathrm{tr}\left[G_{uu}^{00}\, i\gamma_0\gamma_5\right] \mathrm{Re}\,\mathrm{tr}\left[G_{uu}^{xx}\right] \right), \tag{B.3}$$

$$\mathcal{C}_{\mathcal{A}_l^3 \mathcal{A}_l^3}^{\pi^0}(t) = a^3 \sum_{\vec{x}} \left( -\mathrm{Re}\,\mathrm{tr}\left[\gamma_5 \left(G_{dd}^{0x}\right)^\dagger \gamma_5\, i\gamma_0\gamma_5\, G_{uu}^{0x}\, i\gamma_0\gamma_5\right] + 2\,\mathrm{Re}\,\mathrm{tr}\left[G_{uu}^{00}\, i\gamma_0\gamma_5\right] \mathrm{Re}\,\mathrm{tr}\left[G_{uu}^{xx}\, i\gamma_0\gamma_5\right] \right), \tag{B.4}$$

where $\mathcal{S}_l^0$, $\mathcal{A}_l^3$ are the scalar and axial vector operators for the $\pi^0$ as defined in Eqs. (2.8),(2.9). We remark that the disconnected loops stemming from the axial vector current

$$\mathrm{Re}\,\mathrm{tr}\left[G_{uu}^{yy}\, i\gamma_0\gamma_5\right] = \mathrm{tr}\left[\left(G_{uu}^{yy} - G_{dd}^{yy}\right) i\gamma_0\gamma_5\right], \quad y = 0, x, \tag{B.5}$$

can be implemented using efficient variance reduction via the one-end trick as discussed in subsection 2.2.1. From the transformation behavior of the relevant currents under twisted symmetries in table (2.1) one can read off that the cross-correlators for the neutral pion behave sinh-like.

## B.2   Correlation functions for $\eta$, $\eta'$

For the $\eta$–$\eta'$ system the correlation functions are treated in the rotated twisted basis as given in Eqs. (2.30),(2.31), such that the scalar and pseudoscalar contributions to operators in the heavy

sector are disentangled. The relevant operators $\mathcal{S}_l^3$, $\mathcal{S}_h^3$ and $\mathcal{P}_h^0$ are defined in Eqs. (2.26), (2.32) and (2.33) respectively, leading to

$$\mathcal{C}_{\mathcal{S}_l^3 \mathcal{S}_l^3}^{\eta,\eta'}(t) = a^3 \sum_{\vec{x}} \left( -\operatorname{Re} \operatorname{tr}\left[\gamma_5 \left(G_{dd}^{0x}\right)^\dagger \gamma_5 \, G_{uu}^{0x}\right] - 2 \operatorname{Im} \operatorname{tr}\left[G_{uu}^{00}\right] \operatorname{Im} \operatorname{tr}\left[G_{uu}^{xx}\right] \right), \tag{B.6}$$

$$\mathcal{C}_{\mathcal{S}_l^3 \mathcal{S}_h^3}^{\eta,\eta'}(t) = a^3 \sum_{\vec{x}} \left( +2 \operatorname{Im} \operatorname{tr}\left[G_{uu}^{00}\right] \operatorname{Im} \operatorname{tr}\left[G_{sc}^{xx}\right] \right), \tag{B.7}$$

$$\mathcal{C}_{\mathcal{S}_l^3 \mathcal{P}_h^0}^{\eta,\eta'}(t) = a^3 \sum_{\vec{x}} \left( +\operatorname{Im} \operatorname{tr}\left[G_{uu}^{00}\right] \operatorname{Im} \operatorname{tr}\left[\left(G_{cc}^{xx} - G_{ss}^{xx}\right) i\gamma_5\right] \right), \tag{B.8}$$

$$\mathcal{C}_{\mathcal{S}_h^3 \mathcal{S}_l^3}^{\eta,\eta'}(t) = a^3 \sum_{\vec{x}} \left( +2 \operatorname{Im} \operatorname{tr}\left[G_{sc}^{00}\right] \operatorname{Im} \operatorname{tr}\left[G_{uu}^{xx}\right] \right), \tag{B.9}$$

$$\begin{aligned}
\mathcal{C}_{\mathcal{S}_h^3 \mathcal{S}_h^3}^{\eta,\eta'}(t) = \frac{a^3}{2} \sum_{\vec{x}} \Big( &+\operatorname{Re} \operatorname{tr}\left[\gamma_5 \left(G_{cs}^{0x}\right)^\dagger \gamma_5 \, G_{sc}^{0x}\right] - \operatorname{Re} \operatorname{tr}\left[\gamma_5 \left(G_{cc}^{0x}\right)^\dagger \gamma_5 \, G_{ss}^{0x}\right] \\
&-\operatorname{Re} \operatorname{tr}\left[\gamma_5 \left(G_{ss}^{0x}\right)^\dagger \gamma_5 \, G_{cc}^{0x}\right] + \operatorname{Re} \operatorname{tr}\left[\gamma_5 \left(G_{sc}^{0x}\right)^\dagger \gamma_5 \, G_{cs}^{0x}\right] \\
&-4 \operatorname{Im} \operatorname{tr}\left[G_{sc}^{00}\right] \operatorname{Im} \operatorname{tr}\left[G_{sc}^{xx}\right] \Big),
\end{aligned} \tag{B.10}$$

$$\begin{aligned}
\mathcal{C}_{\mathcal{S}_h^3 \mathcal{P}_h^0}^{\eta,\eta'}(t) = \frac{a^3}{2} \sum_{\vec{x}} \Big( &-\operatorname{Re} \operatorname{tr}\left[\gamma_5 \left(G_{cc}^{0x}\right)^\dagger \gamma_5 \, G_{sc}^{0x}\right] - \operatorname{Re} \operatorname{tr}\left[\gamma_5 \left(G_{cs}^{0x}\right)^\dagger \gamma_5 \, G_{ss}^{0x}\right] \\
&+\operatorname{Re} \operatorname{tr}\left[\gamma_5 \left(G_{sc}^{0x}\right)^\dagger \gamma_5 \, G_{cc}^{0x}\right] + \operatorname{Re} \operatorname{tr}\left[\gamma_5 \left(G_{ss}^{0x}\right)^\dagger \gamma_5 \, G_{cs}^{0x}\right] \\
&-4 \operatorname{Im} \operatorname{tr}\left[G_{sc}^{00}\right] \operatorname{Im} \operatorname{tr}\left[\left(G_{cc}^{xx} - G_{ss}^{xx}\right)\right] \Big),
\end{aligned} \tag{B.11}$$

$$\mathcal{C}_{\mathcal{P}_h^0 \mathcal{S}_l^3}^{\eta,\eta'}(t) = a^3 \sum_{\vec{x}} \left( +\operatorname{Im} \operatorname{tr}\left[G_{uu}^{00}\right] \operatorname{Im} \operatorname{tr}\left[\left(G_{cc}^{xx} - G_{ss}^{xx}\right) i\gamma_5\right] \right), \tag{B.12}$$

$$\begin{aligned}
\mathcal{C}_{\mathcal{P}_h^0 \mathcal{S}_h^3}^{\eta,\eta'}(t) = \frac{a^3}{2} \sum_{\vec{x}} \Big( &+\operatorname{Re} \operatorname{tr}\left[\gamma_5 \left(G_{cs}^{0x}\right)^\dagger \gamma_5 \, G_{cc}^{0x}\right] - \operatorname{Re} \operatorname{tr}\left[\gamma_5 \left(G_{cc}^{0x}\right)^\dagger \gamma_5 \, G_{cs}^{0x}\right] \\
&+\operatorname{Re} \operatorname{tr}\left[\gamma_5 \left(G_{ss}^{0x}\right)^\dagger \gamma_5 \, G_{sc}^{0x}\right] - \operatorname{Re} \operatorname{tr}\left[\gamma_5 \left(G_{sc}^{0x}\right)^\dagger \gamma_5 \, G_{ss}^{0x}\right] \\
&-4 \operatorname{Im} \operatorname{tr}\left[\left(G_{cc}^{00} - G_{ss}^{00}\right)\right] \operatorname{Im} \operatorname{tr}\left[G_{sc}^{xx}\right] \Big),
\end{aligned} \tag{B.13}$$

$$\begin{aligned}
\mathcal{C}_{\mathcal{P}_h^0 \mathcal{P}_h^0}^{\eta,\eta'}(t) = \frac{a^3}{2} \sum_{\vec{x}} \Big( &-\operatorname{Re} \operatorname{tr}\left[\gamma_5 \left(G_{cc}^{0x}\right)^\dagger \gamma_5 \, G_{cc}^{0x}\right] - \operatorname{Re} \operatorname{tr}\left[\gamma_5 \left(G_{cs}^{0x}\right)^\dagger \gamma_5 \, G_{cs}^{0x}\right] \\
&-\operatorname{Re} \operatorname{tr}\left[\gamma_5 \left(G_{sc}^{0x}\right)^\dagger \gamma_5 \, G_{sc}^{0x}\right] - \operatorname{Re} \operatorname{tr}\left[\gamma_5 \left(G_{ss}^{0x}\right)^\dagger \gamma_5 \, G_{ss}^{0x}\right] \\
&-4 \operatorname{Im} \operatorname{tr}\left[\left(G_{cc}^{00} - G_{ss}^{00}\right)\right] \operatorname{Im} \operatorname{tr}\left[\left(G_{cc}^{xx} - G_{ss}^{xx}\right)\right] \Big).
\end{aligned} \tag{B.14}$$

The loops related to the light scalar current in twisted basis

$$\operatorname{Im} \operatorname{tr}\left[G_{uu\ s}^{yy}\right] = \operatorname{tr}\left[\left(G_{uu}^{yy} - G_{dd}^{yy}\right) i\gamma_0\gamma_5\right], \quad y = 0, x, \tag{B.15}$$

can be calculated using the one-end trick, similar to the axial vector ones for the neutral pion. The cross-correlators involving only pseudoscalar operators in the physical basis are always

*cosh*-like. However, if we had included the physical axial vector current, the cross-correlators between physical pseudoscalar and axial vector would be sinh-like, although the cross-correlators within the axial vector sector itself are again cosh-like. Furthermore it should be noted that the cross-correlators consisting purely of disconnected contributions are still positive definite correlation functions, whereas the disconnected terms in all other matrix elements for $\eta$ and $\eta'$ yield a negative contribution to the respective correlation functions.

# Appendix C

# Fitting details

## C.1 Parameters for GEVP

In this appendix we give the details of our analysis of masses, decay constants and mixing angles for which we employed the GEVP in Eq. (2.67). This requires a suitable choice of three parameters for each state that we want to fit. Let us first consider the case of standard correlation function matrices, i.e. without subtraction of excited states in the connected correlators for $\eta$, $\eta'$. The parameters for the corresponding analysis are listed in Tab. (C.1) for $\eta$, $\eta'$ and in Tab. (C.2) for the other octet mesons. For $\eta$, $\eta'$ also the resulting uncorrelated $\chi^2/$dof values have been included. Many analysis details have already been included in Ref. [1] and most of the following discussion is based on this paper.

The first parameter is the value of $t_0/a$, which determines the correlation function matrix $\mathcal{C}(t_0)$ on the right-hand side of Eq. (2.67) and that has some impact on corrections due to higher states [144]. In general it is advantageous to choose $t_0/a$ large, but in practice the actual choice is constrained by the exponentially increasing noise that enters $\mathcal{C}(t_0)$ for larger values $t_0/a$. This is particularly a problem if dealing with quantities involving disconnected diagrams such as $\eta$, $\eta'$ or the $\pi^0$. Especially for the $\eta'$ there are in some cases only very few data points available, such that it is necessary to choose a smaller value of $t_0/a$ as the value that one can choose for the $\eta$. Besides the fact that we list parameters for multiple mesons in the same table, this is why we replace $t_0/a$ by $t_0^n/a$, such that the additional superscript labels the corresponding states. On the other hand, for ground state quantities involving only connected diagrams such as the charged pion or the kaon one can work at rather large $t/a$ for the extraction of masses due to the absence of disconnected diagrams, hence it turns out that one does not need particularly large values of $t_0/a$ in these cases either, e.g. for the kaon one can safely choose $t_0^K/a = 1$

The remaining two parameters $t_1^n/a$ and $t_2^n/a$ simply determine the interval in $t/a$ for which we perform a fit to the corresponding eigenvalues $\lambda^{(n)}(t_0, t)$. Due to the rather large difference in the signal-to-noise ratio between the two lowest lying states in the $\eta$–$\eta'$ system, we employ two different approaches to deal with fits to the ground state and the first excited state:

| ensemble | $t_0^\eta/a$ | $t_1^\eta/a$ | $t_2^\eta/a$ | $\left(\chi^2\right)^\eta/$dof | $t_0^{\eta'}/a$ | $t_1^{\eta'}/a$ | $t_2^{\eta'}/a$ | $\left(\chi^2\right)^{\eta'}/$dof |
|---|---|---|---|---|---|---|---|---|
| A30.32 | 2 | 7 | 17 | 0.205 | 1 | 2 | 11 | 0.277 |
| A40.24 | 2 | 7 | 16 | 0.135 | 1 | 2 | 10 | 0.185 |
| A40.32 | 2 | 7 | 15 | 0.092 | 1 | 2 | 10 | 0.130 |
| A60.24 | 2 | 7 | 15 | 0.137 | 1 | 2 | 10 | 0.296 |
| A80.24 | 2 | 7 | 16 | 0.108 | 1 | 2 | 10 | 0.137 |
| A100.24 | 2 | 7 | 15 | 0.214 | 1 | 2 | 11 | 0.137 |
| A80.24s | 2 | 7 | 17 | 0.230 | 1 | 2 | 11 | 0.440 |
| A100.24s | 2 | 7 | 16 | 0.086 | 1 | 2 | 10 | 0.116 |
| B25.32 | 3 | 6 | 11 | 0.222 | 1 | 2 | 11 | 0.463 |
| B35.32 | 2 | 8 | 17 | 0.110 | 1 | 2 | 10 | 0.433 |
| B55.32 | 2 | 8 | 18 | 0.167 | 1 | 2 | 11 | 0.366 |
| B75.32 | 2 | 8 | 14 | 0.301 | 1 | 2 | 10 | 0.338 |
| B85.24 | 2 | 8 | 16 | 0.106 | 1 | 2 | 10 | 0.127 |
| D15.48 | 3 | 8 | 16 | 0.190 | 2 | 3 | 12 | 0.114 |
| D30.48 | 3 | 8 | 16 | 0.207 | 2 | 3 | 12 | 0.143 |
| D45.32sc | 3 | 8 | 19 | 0.174 | 2 | 3 | 18 | 0.105 |

Table C.1: Parameters of the GEVP applied to the $6 \times 6$ matrix from local and fuzzed operators. Note that the ensemble $D20.48$ has been excluded from this table due to bad plateaux in both principal correlators rendering a reliable fit unfeasible.

1. For the ground states (i.e. $n = \eta, \pi^\pm, \pi^0, K$ and the connected-only quantities $n = \pi_{\mathrm{conn}}^0, \eta_{\mathrm{conn}}^s$) we fit a single cosh in a region $[t_1^n/a, t_2^n/a]$ to our data for $\lambda^\eta(t, t_0)$. The lower bound of the fit-range $t_1^n/a$ for any state $n$ is chosen by visual inspection of the effective mass plot to lie at the beginning of the plateau and also such that further increasing $t_1^n/a$ does not change the value of the resulting mass within errors. The latter statement similarly holds for the choice of the starting value $t_0^n/a$ in Eq. (2.67). As mentioned before, choosing larger values of $t_0/a$ leads to improved (i.e. smaller) masses, though due to noise it is only possible to moderately increase $t_0^n/a$ until the error becomes too large and dominates over any possible improvement.

2. For the first excited state (i.e. $\eta'$) we perform a three state cosh-fit to the data of $\lambda^{\eta'}(t, t_0)$, starting from the lowest $t_1^{\eta'}/a$ possible, i.e. $t_1^{\eta'}/a = t_0^{\eta'}/a + 1$ in order to use as many points as possible. This is necessary because for many ensembles there is no clear plateau in the effective masses reached before the signal is lost in noise. Therefore, this procedure is a major source of systematic error for the determination of $\eta'$ masses, at least for those cases where only few points are available. Only for the $D$ ensembles it turns out to be possible to choose $t_0^{\eta'}/a > 1$, for all other ensembles we had to use $t_0^{\eta'}/a = 1$. Note that this procedure does not allow to extract the corresponding physical amplitudes of the $\eta'$-state, which we determined separately from a factorizing fit model; see next section.

| ensemble | $t_0^{\rm PS}/a$ | $t_1^{\rm PS}/a$ | $t_2^{\rm PS}/a$ | $t_0^{\pi^0}/a$ | $t_1^{\pi^0}/a$ | $t_2^{\pi^0}/a$ | $t_0^K/a$ | $t_1^K/a$ | $t_2^K/a$ |
|---|---|---|---|---|---|---|---|---|---|
| A30.32 | 2 | 10 | 31 | 2 | 10 | 20 | 1 | 15 | 31 |
| A40.24 | 2 | 10 | 23 | 2 | 10 | 15 | 1 | 12 | 23 |
| A40.32 | 2 | 10 | 31 | 2 | 10 | 20 | 1 | 15 | 31 |
| A60.24 | 2 | 10 | 23 | 2 | 10 | 15 | 1 | 12 | 23 |
| A80.24 | 2 | 10 | 23 | 2 | 10 | 15 | 1 | 12 | 23 |
| A100.24 | 2 | 10 | 23 | 2 | 10 | 15 | 1 | 12 | 23 |
| A80.24s | 2 | 10 | 23 | 2 | 10 | 15 | 1 | 12 | 23 |
| A100.24s | 2 | 10 | 23 | 2 | 10 | 15 | 1 | 12 | 23 |
| B25.32 | 3 | 10 | 31 | 2 | 10 | 20 | 1 | 15 | 31 |
| B35.32 | 3 | 10 | 31 | 2 | 10 | 20 | 1 | 15 | 31 |
| B55.32 | 3 | 10 | 31 | 2 | 10 | 20 | 1 | 15 | 31 |
| B75.32 | 3 | 10 | 31 | 2 | 10 | 20 | 1 | 15 | 31 |
| B85.24 | 2 | 10 | 23 | 2 | 10 | 15 | 1 | 12 | 23 |
| D15.48 | 3 | 10 | 47 | 3 | 10 | 20 | 1 | 15 | 47 |
| D20.48 | 3 | 10 | 47 | 3 | 10 | 20 | 1 | 15 | 47 |
| D30.48 | 3 | 10 | 47 | 3 | 10 | 20 | 1 | 15 | 47 |
| D45.32sc | 3 | 10 | 31 | 3 | 10 | 20 | 1 | 12 | 31 |

Table C.2: Parameters of the GEVP applied to the correlation function matrices from local and fuzzed operators for the pions and the kaon. For the pions and the kaon we employ $4 \times 4$- and $8 \times 8$-matrices, respectively. The parameters for the $\pi^0_{\rm conn}$ are identical to the ones of the charged pion

The upper bound of the fit range $t_2^n/a$ is independently determined for every state $n$ by the last eigenvalue $\lambda^{(n)}(t_2, t_0)$ distinguishable from noise. In practice this implies that we have $t_2/a = t_{\max}/a = (T/a)/2 - 1$ for quantities that receive only connected contributions, because of the excellent signal-to-noise ration in these cases. Moreover, the value of $t_2^n/a$ is not very important for the fit, as eigenvalues at large $t/a$ have typically large errors and therefore do not contribute much to the fit.

Finally, we consider the case of correlation function matrices with subtracted excited states in the connected contributions. This approach only applies to the $\eta$–$\eta'$ system and it is again necessary to choose different fit parameters for $\eta$ and $\eta'$. However, one needs only a single cosh fit in both cases and it turns out that the corresponding fit ranges can be chosen identical for all ensembles, regardless of lattice size, lattice spacing and light quark mass. This simplification is possible for two reasons:

First of all, the mass of the $\eta$ shows an almost perfect, constant plateau over a large part of the $t/a$-range, as can be seen in the right panel Fig. (3.9). Nonetheless a small bias is observed if one takes the very first point at $t/a = 2$ into account, hence we use $t_1^\eta/a = 3$, which resolves this issue. This bias is most likely due to some residual excited state pollution. The choice of $t_0/a$

does not affect the results, besides decreasing the signal quality for larger values, thus we can use $t_0 = 1/a$ for both states. For the mass of the $\eta'$ we do not see any bias depending on the point at $t/a = 2$ within its larger errors, hence we set $t_1^{\eta'}/a = 2$ for this case to obtain a better signal.

The second reason is again given by the fact that eigenvalues at larger $t/a$ do not give any significant contribution, hence we choose $t_2^\eta/a = 8$ and $t^{\eta'}/a = 4$ for the upper bounds of the fit ranges. In many cases one could actually use (much) more points but this does neither change the result within errors, nor give any improvement of the errors themselves.

Besides these parameters that are significant to the actual GEVP analysis, the approach of removing the excited states at the level of correlation functions requires an additional fit to the ground state of the connected correlators as discussed in section 3.4. The corresponding fit range $[t_1/a, t_2/a]$ is again chosen in a similar manner as for the GEVP, i.e. by visual inspection of the data such that it clearly lies within the linear domain of the logarithmic correlation function. It turns out that one can choose the lower bound safely to be $t_1/a = 10$ for all ensembles, whereas the upper bound is adjusted depending on the lattice size, leading to $t_2/a(L/a = 24) = 20$, $t_2/a(L/a = 32) = 25$ and $t_2/a(L/a = 24) = 30$. In principal one could also choose $t_2/a = t_{\max}/a$, but this only results in slightly larger errors and does not lead to any significant change of the fit result at all.

## C.2  Parameters for factorizing fit

The factorizing fit model as detailed in Eq. (2.101) has only been used for the determination of mixing angles from the original, full correlation function matrix without prior subtraction of excited states in the connected correlators. In all other applications based on amplitudes (i.e. $f_{\mathrm{PS}}$, $f_K$ and $\eta,\eta'$-mixing parameters from correlation function matrices with subtracted excited states in the connected contributions) we use amplitudes calculated directly from the GEVP as discussed in subsection 2.2.2 and using the parameters listed in the preceding section, such that the entire analysis is consistently performed from the GEVP only. The reason for using a factorizing fit instead of the GEVP in the first mentioned case is tied to the $\eta'$-state which we extract from a three state cosh fit. Although this procedure allows to extract a mass without reaching an actual plateau in the effective mass plot, it is not sufficient to determine the corresponding physical amplitudes.

We apply the factorizing fit model directly to the renormalized matrix in the original twisted basis in Eq. (2.88) and limit ourselves to $n = 2$ in Eq. (2.101), i.e. a two state fit. As discussed before, the ratio of renormalization constants $Z = Z_P/Z_S$ does not affect masses and angles, but only amplitudes and the decay constants $f_l$, $f_s$. For the results of the angles we used the values summarized in table 3.3. They have been obtained by matching a mixed action to the unitary action and extrapolating to the chiral limit, see ref. [133]. These values agree well with the RI-MOM determination of ETMC [153], and the method we discussed in the text.

Since we have already determined the masses from the GEVP, we use those together with their

| ensemble | $t_1/a$ | $t_2/a$ | $\chi^2_{4\times4}$ | $\chi^2_{6\times6}$ |
|----------|---------|---------|---------------------|---------------------|
| A30.32 | 6 | 18 | 0.252 | 0.561 |
| A40.24 | 6 | 14 | 0.144 | 0.626 |
| A40.32 | 6 | 15 | 0.466 | 0.628 |
| A60.24 | 6 | 14 | 0.229 | 0.470 |
| A80.24 | 6 | 14 | 0.204 | 0.545 |
| A100.24 | 6 | 13 | 0.165 | 0.395 |
| A80.24s | 6 | 17 | 0.803 | 0.986 |
| A100.24s | 6 | 13 | 0.063 | 0.293 |
| B25.32 | 6 | 16 | 0.326 | 0.857 |
| B35.32 | 6 | 15 | 0.283 | 0.694 |
| B55.32 | 6 | 16 | 0.836 | 0.774 |
| B75.32 | 6 | 12 | 0.449 | 0.636 |
| B85.24 | 6 | 14 | 0.172 | 0.469 |
| D15.48 | 7 | 17 | 0.328 | 0.567 |
| D30.48 | 7 | 15 | 0.423 | 0.491 |
| D45.32sc | 7 | 15 | 0.388 | 0.686 |

Table C.3: Parameters for the factorizing fit.

errors (see table 3.5) as priors to our factorizing fit. This leads to a more stable fit, but we have checked that it does not affect the result. In our fits we always minimize an uncorrelated $\chi^2$ function, because the correlation matrix is too noisy and we want to avoid additional model independence, e.g. using a singular value decomposition and applying some cut to the resulting spectrum. Table C.3 lists the input parameters and the resulting, uncorrelated $\chi^2/\mathrm{dof}$ for the fits to the $4 \times 4$ (light and strange degrees of freedom, local and fuzzed operators) and $6 \times 6$ (light, strange, charm degrees of freedom and local and fuzzed operators) correlation function matrix. The results quoted in the main text for the angles were determined using the $4 \times 4$ matrix, because the charm does not contribute. However, with the $6 \times 6$ matrix we obtain almost identical results.

The values for the lower bound of the fit range $t_1/a$ are chosen to be constant for every value of the lattice spacing, whereas the upper bound $t_2/a$ is determined by the requirement that $\chi^2/\mathrm{dof} < 1$, and such that it is close to the $t_2^\eta/a$ used for the GEVP analysis.

# Danksagung

und Geduld für mich aufbrachte.

# Bibliography

[1] Konstantin Ottnad et al. $\eta$ and $\eta'$ mesons from Nf=2+1+1 twisted mass lattice QCD. *JHEP*, 1211:048, 2012, 1206.6719.

[2] Gregorio Herdoiza, Karl Jansen, Chris Michael, Konstantin Ottnad, and Carsten Urbach. Determination of Low-Energy Constants of Wilson Chiral Perturbation Theory. *JHEP*, 1305:038, 2013, 1303.3516.

[3] Chris Michael, Konstantin Ottnad, and Carsten Urbach. $\eta$ and $\eta'$ mixing from Lattice QCD. *Phys. Rev. Lett. 111*, 181602, 2013, 1310.1207.

[4] Konstantin Ottnad, Carsten Urbach, Chris Michael, and Siebren Reker. Eta and eta' meson masses from Nf=2+1+1 twisted mass lattice QCD. *PoS*, LATTICE2011:336, 2011, 1111.3596.

[5] Krzysztof Cichy, Vincent Drach, Elena Garcia Ramos, Karl Jansen, Chris Michael, et al. Properties of pseudoscalar flavour-singlet mesons from 2+1+1 twisted mass lattice QCD. *PoS*, LATTICE2012:151, 2012, 1211.4497.

[6] Chris Michael, Konstantin Ottnad, and Carsten Urbach. $\eta$ and $\eta'$ masses and decay constants from lattice QCD with 2+1+1 quark flavours. 2013, 1311.5490.

[7] N.H. Christ, C. Dawson, T. Izubuchi, C. Jung, Q. Liu, et al. The $\eta$ and $\eta'$ mesons from Lattice QCD. *Phys.Rev.Lett.*, 105:241601, 2010, 1002.2999.

[8] Jozef J. Dudek, Robert G. Edwards, Balint Joo, Michael J. Peardon, David G. Richards, et al. Isoscalar meson spectroscopy from lattice QCD. *Phys.Rev.*, D83:111502, 2011, 1102.4299.

[9] Eric B. Gregory, Alan C. Irving, Christopher M. Richards, and Craig McNeile. A study of the eta and eta' mesons with improved staggered fermions. *Phys.Rev.*, D86:014504, 2012, 1112.4384.

[10] D.J. Gross and Frank Wilczek. Ultraviolet Behavior of Nonabelian Gauge Theories. *Phys.Rev.Lett.*, 30:1343–1346, 1973.

[11] H. Fritzsch, M. Gell-Mann, and H. Leutwyler. Advantages of the color octet gluon picture. *Phys. Lett.*, B47:365–368, 1973.

[12] S. Weinberg. Nonabelian gauge theories of the strong interactions. *Phys. Rev. Lett.*, 31:494–497, 1973.

[13] D.J. Gross and Frank Wilczek. Asymptotically Free Gauge Theories. 1. *Phys.Rev.*, D8:3633–3652, 1973.

[14] D.J. Gross and Frank Wilczek. Asymptotically Free Gauge Theories. 2. *Phys.Rev.*, D9:980–993, 1974.

[15] Karl Jansen, Felix Karbstein, Attila Nagy, and Marc Wagner. $\Lambda_{\bar{M}S}$ from the static potential for QCD with $n_f = 2$ dynamical quark flavors. *JHEP*, 1201:025, 2012, 1110.6859.

[16] Patrick Fritzsch, Francesco Knechtli, Bjorn Leder, Marina Marinkovic, Stefan Schaefer, et al. The strange quark mass and Lambda parameter of two flavor QCD. *Nucl.Phys.*, B865:397–429, 2012, 1205.5380.

[17] J. Beringer et al. Review of Particle Physics (RPP). *Phys.Rev.*, D86:010001, 2012.

[18] C. A. Baker et al. An improved experimental limit on the electric dipole moment of the neutron. *Phys. Rev. Lett.*, 97:131801, 2006, hep-ex/0602020.

[19] K. Ottnad, B. Kubis, U.-G. Meissner, and F.-K. Guo. New insights into the neutron electric dipole moment. *Phys.Lett.*, B687:42–47, 2010, 0911.3981.

[20] Stephen L. Adler. Axial vector vertex in spinor electrodynamics. *Phys.Rev.*, 177:2426–2438, 1969.

[21] J.S. Bell and R. Jackiw. A PCAC puzzle: $\pi^0 \to \gamma\gamma$ in the $\sigma$-model. *Nuovo Cim.*, A60:47–61, 1969.

[22] Kazuo Fujikawa. Path Integral for Gauge Theories with Fermions. *Phys. Rev.*, D21:2848, 1980.

[23] Gerard 't Hooft. Computation of the Quantum Effects Due to a Four-Dimensional Pseudoparticle. *Phys.Rev.*, D14:3432–3450, 1976.

[24] G. 't Hooft. Erratum: Computation of the quantum effects due to a four-dimensional pseudoparticle. *Phys. Rev. D*, 18:2199–2200, Sep 1978.

[25] Gerard 't Hooft. How Instantons Solve the U(1) Problem. *Phys.Rept.*, 142:357–387, 1986.

[26] Gerard 't Hooft. A planar diagram theory for strong interactions. *Nucl. Phys.*, B72:461, 1974.

[27] Edward Witten. Current Algebra Theorems for the U(1) Goldstone Boson. *Nucl. Phys.*, B156:269, 1979.

[28] Edward Witten. Large N Chiral Dynamics. *Annals Phys.*, 128:363, 1980.

[29] J. Gasser and H. Leutwyler. Chiral Perturbation Theory to One Loop. *Ann. Phys.*, 158:142, 1984.

[30] J. Gasser and H. Leutwyler. Chiral Perturbation Theory: Expansions in the Mass of the Strange Quark. *Nucl. Phys.*, B250:465, 1985.

[31] Sidney R. Coleman, J. Wess, and Bruno Zumino. Structure of phenomenological Lagrangians. 1. *Phys. Rev.*, 177:2239–2247, 1969.

[32] Jr. Callan, Curtis G., Sidney R. Coleman, J. Wess, and Bruno Zumino. Structure of phenomenological Lagrangians. 2. *Phys. Rev.*, 177:2247–2250, 1969.

[33] Aneesh V. Manohar. Effective field theories. 1996, hep-ph/9606222.

[34] Steven Weinberg. Phenomenological Lagrangians. *Physica*, A96:327, 1979.

[35] C. Rosenzweig, J. Schechter, and C.G. Trahern. Is the Effective Lagrangian for QCD a Sigma Model? *Phys.Rev.*, D21:3388, 1980.

[36] P. Di Vecchia and G. Veneziano. Chiral Dynamics in the Large n Limit. *Nucl.Phys.*, B171:253, 1980.

[37] Roland Kaiser and H. Leutwyler. Pseudoscalar decay constants at large N(c). 1998, hep-ph/9806336.

[38] H. Leutwyler. Bounds on the light quark masses. *Phys. Lett.*, B374:163–168, 1996, hep-ph/9601234.

[39] H. Leutwyler. On the 1/N expansion in chiral perturbation theory. *Nucl.Phys.Proc.Suppl.*, 64:223–231, 1998, hep-ph/9709408.

[40] Thorsten Feldmann. Quark structure of pseudoscalar mesons. *Int.J.Mod.Phys.*, A15:159–207, 2000, hep-ph/9907491.

[41] G. Veneziano. U(1) Without Instantons. *Nucl.Phys.*, B159:213–224, 1979.

[42] T. Feldmann, P. Kroll, and B. Stech. Mixing and decay constants of pseudoscalar mesons: The Sequel. *Phys.Lett.*, B449:339–346, 1999, hep-ph/9812269.

[43] T. Feldmann, P. Kroll, and B. Stech. Mixing and decay constants of pseudoscalar mesons. *Phys.Rev.*, D58:114006, 1998, hep-ph/9802409.

[44] Jonathan L. Rosner and Sheldon Stone. Leptonic decays of charged pseudoscalar mesons - 2012. 2012, 1201.2401.

[45] Kenneth G. Wilson. Confinement of Quarks. *Phys.Rev.*, D10:2445–2459, 1974.

[46] Thomas DeGrand and Carleton E. Detar. Lattice methods for quantum chromodynamics. 2006.

[47] I. Montvay and G. Munster. Quantum fields on a lattice. 1994.

[48] H.J. Rothe. Lattice gauge theories: An Introduction. *World Sci.Lect.Notes Phys.*, 43:1–381, 1992.

[49] Konrad Osterwalder and Robert Schrader. AXIOMS FOR EUCLIDEAN GREEN'S FUNCTIONS. *Commun.Math.Phys.*, 31:83–112, 1973.

[50] Konrad Osterwalder and Robert Schrader. Axioms for Euclidean Green's Functions. 2. *Commun.Math.Phys.*, 42:281, 1975.

[51] M. Luscher. Construction of a Selfadjoint, Strictly Positive Transfer Matrix for Euclidean Lattice Gauge Theories. *Commun.Math.Phys.*, 54:283, 1977.

[52] K. Symanzik. Some topics in quantum field theory. In R. Schrader et al., editor, *Mathematical problems in theoretical physics*, volume 153, pages 47–58, 1981. Presented at 6th Int. Conf. on Mathematical Physics, Berlin, West Germany.

[53] K. Symanzik. Continuum limit and improved action in lattice theories. 1. principles and phi**4 theory. *Nucl. Phys.*, B226:187, 1983.

[54] K. Symanzik. Continuum limit and improved action in lattice theories. 2. o(n) nonlinear sigma model in perturbation theory. *Nucl. Phys.*, B226:205, 1983.

[55] B. Sheikholeslami and R. Wohlert. Improved continuum limit lattice action for qcd with Wilson fermions. *Nucl. Phys.*, B259:572, 1985.

[56] M. Lüscher, S. Sint, R. Sommer, and P. Weisz. Chiral symmetry and O(a) improvement in lattice QCD. *Nucl. Phys.*, B478:365–400, 1996, hep-lat/9605038.

[57] P. Weisz. Continuum Limit Improved Lattice Action for Pure Yang-Mills Theory. 1. *Nucl.Phys.*, B212:1, 1983.

[58] P. Weisz and R. Wohlert. Continuum limit improved lattice action for pure Yang-Mills theory. 2. *Nucl. Phys.*, B236:397, 1984.

[59] Y. Iwasaki. Renormalization group analysis of lattice theories and improved lattice action: two-dimensional nonlinear o(n) sigma model. *Nucl. Phys.*, B258:141–156, 1985.

[60] Y. Iwasaki, K. Kanaya, T. Kaneko, and T. Yoshie. Scaling in SU(3) pure gauge theory with a renormalization group improved action. *Phys. Rev.*, D56:151–160, 1997, hep-lat/9610023.

[61] Y. Iwasaki. Renormalization Group Analysis of Lattice Theories and Improved Lattice Action. II – four-dimensional non-abelian SU(N) gauge model. 2011, 1111.7054.

[62] H. B. Nielsen and M. Ninomiya. Absence of neutrinos on a lattice. 1. proof by homotopy theory. *Nucl. Phys.*, B185:20, 1981.

[63] H. B. Nielsen and M. Ninomiya. No go theorem for regularizing chiral fermions. *Phys. Lett.*, B105:219, 1981.

[64] H. B. Nielsen and M. Ninomiya. Absence of neutrinos on a lattice. 2. intuitive topological proof. *Nucl. Phys.*, B193:173, 1981.

[65] P. H. Ginsparg and K. G. Wilson. A remnant of chiral symmetry on the lattice. *Phys. Rev.*, D25:2649, 1982.

[66] H. Neuberger. Exactly massless quarks on the lattice. *Phys. Lett.*, B417:141–144, 1998, hep-lat/9707022.

[67] H. Neuberger. More about exactly massless quarks on the lattice. *Phys. Lett.*, B427:353–355, 1998, hep-lat/9801031.

[68] D. B. Kaplan. A method for simulating chiral fermions on the lattice. *Phys. Lett.*, B288:342–347, 1992, hep-lat/9206013.

[69] L. H. Karsten and J. Smit. Lattice fermions: species doubling, chiral invariance, and the triangle anomaly. *Nucl. Phys.*, B183:103, 1981.

[70] T. Reisz and H.J. Rothe. Chiral symmetry restoration and axial vector renormalization for Wilson fermions. *Phys.Rev.*, D62:014504, 2000, hep-lat/0003003.

[71] Andrea Shindler. Twisted mass lattice QCD. *Phys.Rept.*, 461:37–110, 2008, 0707.4093.

[72] R. Frezzotti, P. A. Grassi, S. Sint, and P. Weisz. Lattice QCD with a chirally twisted mass term. *JHEP*, 08:058, 2001, hep-lat/0101001.

[73] R. Frezzotti, P. A. Grassi, S. Sint, and P. Weisz. A local formulation of lattice QCD without unphysical fermion zero modes. *Nucl. Phys. Proc. Suppl.*, 83:941–946, 2000, hep-lat/9909003.

[74] R. Frezzotti and G. C. Rossi. Chirally improving Wilson fermions. I: O(a) improvement. *JHEP*, 08:007, 2004, hep-lat/0306014.

[75] Karl Jansen, Andrea Shindler, Carsten Urbach, and Ines Wetzorke. Scaling test for Wilson twisted mass QCD. *Phys.Lett.*, B586:432–438, 2004, hep-lat/0312013.

[76] K. Jansen, M. Papinutto, A. Shindler, C. Urbach, and I. Wetzorke. Quenched scaling of Wilson twisted mass fermions. *JHEP*, 0509:071, 2005, hep-lat/0507010.

[77] Remi Baron et al. Light Meson Physics from Maximally Twisted Mass Lattice QCD. *JHEP*, 1008:097, 2010, 0911.5061.

[78] B. Blossier et al. Average up/down, strange and charm quark masses with Nf=2 twisted mass lattice QCD. *Phys.Rev.*, D82:114513, 2010, 1010.3659.

[79] R. Baron et al. Light hadrons from lattice QCD with light (u,d), strange and charm dynamical quarks. *JHEP*, 06:111, 2010, 1004.5284.

[80] T. Chiarappa et al. Numerical simulation of QCD with u, d, s and c quarks in the twisted-mass Wilson formulation. *Eur. Phys. J.*, C50:373–383, 2007, hep-lat/0606011.

[81] R. Frezzotti and S. Sint. Some remarks on O(a) improved twisted mass QCD. *Nucl. Phys. Proc. Suppl.*, 106:814–816, 2002, hep-lat/0110140.

[82] M. Della Morte, R. Frezzotti, and J. Heitger. Quenched twisted mass QCD at small quark masses and in large volume. *Nucl. Phys. Proc. Suppl.*, 106:260–262, 2002, hep-lat/0110166.

[83] R. Frezzotti and G. C. Rossi. Twisted-mass lattice QCD with mass non-degenerate quarks. *Nucl. Phys. Proc. Suppl.*, 128:193–202, 2004, hep-lat/0311008.

[84] L. Del Debbio, L. Giusti, M. Lüscher, R. Petronzio, and N. Tantalo. QCD with light Wilson quarks on fine lattices. I: First experiences and physics results. *JHEP*, 02:056, 2007, hep-lat/0610059.

[85] Ph. Boucaud et al. Dynamical twisted mass fermions with light quarks. *Phys. Lett.*, B650:304–311, 2007, hep-lat/0701012.

[86] Huey-Wen Lin et al. First results from 2+1 dynamical quark flavors on an anisotropic lattice: Light-hadron spectroscopy and setting the strange-quark mass. *Phys.Rev.*, D79:034502, 2009, 0810.3588.

[87] S. Dürr, Z. Fodor, J. Frison, C. Hoelbling, R. Hoffmann, et al. Ab-Initio Determination of Light Hadron Masses. *Science*, 322:1224–1227, 2008, 0906.3599.

[88] S. Aoki et al. Physical Point Simulation in 2+1 Flavor Lattice QCD. *Phys.Rev.*, D81:074503, 2010, 0911.2561.

[89] S. Dürr, Z. Fodor, C. Hoelbling, S.D. Katz, S. Krieg, et al. Lattice QCD at the physical point: Simulation and analysis details. *JHEP*, 1108:148, 2011, 1011.2711.

[90] W. Bietenholz, V. Bornyakov, M. Gockeler, R. Horsley, W.G. Lockhart, et al. Flavour blindness and patterns of flavour symmetry breaking in lattice simulations of up, down and strange quarks. *Phys.Rev.*, D84:054509, 2011, 1102.5300.

[91] S. R. Sharpe and Jr. Singleton, R. Spontaneous flavor and parity breaking with Wilson fermions. *Phys. Rev.*, D58:074501, 1998, hep-lat/9804028.

[92] Maarten Golterman. Applications of chiral perturbation theory to lattice QCD. pages 423–515, 2009, 0912.4042.

[93] Oliver Bär, Gautam Rupak, and Noam Shoresh. Chiral perturbation theory at O(a**2) for lattice QCD. *Phys. Rev.*, D70:034508, 2004, hep-lat/0306021.

[94] Sinya Aoki. New Phase Structure for Lattice QCD with Wilson Fermions. *Phys.Rev.*, D30:2653, 1984.

[95] Michael Creutz. Wilson fermions at finite temperature. 1996, hep-lat/9608024.

[96] S. Aoki and A. Gocksch. Spontaneous breaking of flavor symmetry and parity in lattice QCD with Wilson fermions. *Phys.Rev.*, D45:3845–3853, 1992.

[97] Tom Blum et al. Qcd thermodynamics with wilson quarks at large kappa. *Phys. Rev.*, D50:3377–3381, 1994, hep-lat/9404006.

[98] S. Aoki. On the phase structure of QCD with Wilson fermions. *Prog. Theor. Phys. Suppl.*, 122:179–186, 1996, hep-lat/9509008.

[99] Sinya Aoki, Tomoyuki Kaneda, and Akira Ukawa. Structure of critical lines in quenched lattice QCD with the Wilson quark action. *Phys.Rev.*, D56:1808–1811, 1997, hep-lat/9612019.

[100] S. Aoki et al. Non-trivial phase structure of N(f) = 3 QCD with O(a)- improved Wilson fermion at zero temperature. *Nucl. Phys. Proc. Suppl.*, 106:263–265, 2002, hep-lat/0110088.

[101] E.-M. Ilgenfritz, W. Kerler, M. Müller-Preußker, A. Sternbeck, and H. Stüben. A numerical reinvestigation of the Aoki phase with N(f) = 2 Wilson fermions at zero temperature. *Phys. Rev.*, D69:074511, 2004, hep-lat/0309057.

[102] S. Aoki et al. Bulk first-order phase transition in three-flavor lattice QCD with O(a)- improved Wilson fermion action at zero temperature. *Phys.Rev.*, D72:054510, 2005, hep-lat/0409016.

[103] F. Farchioni et al. Twisted mass quarks and the phase structure of lattice QCD. *Eur. Phys. J.*, C39:421–433, 2005, hep-lat/0406039.

[104] F. Farchioni et al. The phase structure of lattice QCD with Wilson quarks and renormalization group improved gluons. *Eur. Phys. J.*, C42:73–87, 2005, hep-lat/0410031.

[105] F. Farchioni et al. Lattice spacing dependence of the first order phase transition for dynamical twisted mass fermions. *Phys. Lett.*, B624:324–333, 2005, hep-lat/0506025.

[106] F. Farchioni et al. Numerical simulations with two flavours of twisted-mass wilson quarks and dbw2 gauge action. *Eur. Phys. J.*, C47:453–472, 2006, hep-lat/0512017.

[107] P.H. Damgaard, K. Splittorff, and J.J.M. Verbaarschot. Microscopic Spectrum of the Wilson Dirac Operator. *Phys.Rev.Lett.*, 105:162002, 2010, 1001.2937.

[108] G. Akemann, P.H. Damgaard, K. Splittorff, and J.J.M. Verbaarschot. Spectrum of the Wilson Dirac Operator at Finite Lattice Spacings. *Phys.Rev.*, D83:085014, 2011, 1012.0752.

[109] K. Splittorff and J.J.M. Verbaarschot. The Wilson Dirac Spectrum for QCD with Dynamical Quarks. *Phys.Rev.*, D84:065031, 2011, 1105.6229.

[110] K. Splittorff and J.J.M. Verbaarschot. Progress on the Microscopic Spectrum of the Dirac Operator for QCD with Wilson Fermions. *PoS*, LATTICE2011:113, 2011, 1112.0377.

[111] K. Splittorff and J.J.M. Verbaarschot. The Microscopic Twisted Mass Dirac Spectrum. *Phys.Rev.*, D85:105008, 2012, 1201.1361.

[112] M. Kieburg, K. Splittorff, and J.J.M. Verbaarschot. The Realization of the Sharpe-Singleton Scenario. *Phys.Rev.*, D85:094011, 2012, 1202.0620.

[113] P.H. Damgaard, U.M. Heller, and K. Splittorff. New Ways to Determine Low-Energy Constants with Wilson Fermions. 2012, 1206.4786.

[114] Albert Deuzeman, Urs Wenger, and Jair Wuilloud. Spectral properties of the Wilson Dirac operator in the $\epsilon$-regime. 2011, 1110.4002.

[115] P.H. Damgaard, U.M. Heller, and K. Splittorff. Finite-Volume Scaling of the Wilson-Dirac Operator Spectrum. 2011, 1110.2851.

[116] Poul H. Damgaard, Urs M. Heller, and Kim Splittorff. Wilson chiral perturbation theory, Wilson-Dirac operator eigenvalues and clover improvement. 2013, 1301.3099.

[117] Silvia Necco and Andrea Shindler. Spectral density of the Hermitean Wilson Dirac operator: a NLO computation in chiral perturbation theory. *JHEP*, 1104:031, 2011, 1101.1778.

[118] S. Necco and A. Shindler. On the spectral density of the Wilson operator. *PoS*, LAT-TICE2011:250, 2011, 1108.1950.

[119] S. Necco and A. Shindler. Corrections to the Banks-Casher relation with Wilson quarks. PoS:056 (2012), CD12, 1302.5595.

[120] Sinya Aoki, Oliver Bär, and Benedikt Biedermann. Pion scattering in Wilson chiral perturbation theory. *Phys.Rev.*, D78:114501, 2008, 0806.4863.

[121] Fabio Bernardoni, John Bulava, and Rainer Sommer. Determination of the Wilson ChPT low energy constant $c_2$. *PoS*, LATTICE2011:095, 2011, 1111.4351.

[122] Maxwell T. Hansen and Stephen R. Sharpe. Determining low-energy constants in partially quenched Wilson chiral perturbation theory. *Phys.Rev.*, D85:054504, 2012, 1112.3998.

[123] Oliver Bär, Gautam Rupak, and Noam Shoresh. Simulations with different lattice Dirac operators for valence and sea quarks. *Phys. Rev.*, D67:114505, 2003, hep-lat/0210050.

[124] K. Cichy, V. Drach, E. Garcia-Ramos, G. Herdoiza, and K. Jansen. Overlap valence quarks on a twisted mass sea: a case study for mixed action Lattice QCD. *Nucl.Phys.*, B869:131–163, 2013, 1211.1605.

[125] Maxwell T. Hansen and Stephen R. Sharpe. Constraint on the Low Energy Constants of Wilson Chiral Perturbation Theory. *Phys.Rev.*, D85:014503, 2012, 1111.2404.

[126] G. Münster. On the phase structure of twisted mass lattice QCD. *JHEP*, 09:035, 2004, hep-lat/0407006.

[127] L. Scorzato. Pion mass splitting and phase structure in twisted mass QCD. *Eur. Phys. J.*, C37:445–455, 2004, hep-lat/0407023.

[128] S. R. Sharpe and J. M. S. Wu. The phase diagram of twisted mass lattice QCD. *Phys. Rev.*, D70:094029, 2004, hep-lat/0407025.

[129] Gilberto Colangelo, Urs Wenger, and Jackson M.S. Wu. Twisted Mass Finite Volume Effects. *Phys.Rev.*, D82:034502, 2010, 1003.0847.

[130] Oliver Bar. Chiral logs in twisted mass lattice QCD with large isospin breaking. *Phys.Rev.*, D82:094505, 2010, 1008.0784.

[131] Satoru Ueda and Sinya Aoki. Chiral perturbation theory for twisted mass QCD at small quark mass. 2011, 1109.0073.

[132] Gernot Münster and Tobias Sudmann. Twisted mass chiral perturbation theory for 2+1+1 quark flavours. *JHEP*, 1104:116, 2011, 1103.1494.

[133] Federico Farchioni, Gregorio Herdoiza, Karl Jansen, Andreas Nube, Marcus Petschlies, et al. Pseudoscalar decay constants from $N_f$=2+1+1 twisted mass lattice QCD. *PoS*, LATTICE2010:128, 2010, 1012.0200.

[134] Remi Baron et al. Computing K and D meson masses with $N_f = 2+1+1$ twisted mass lattice QCD. *Comput.Phys.Commun.*, 182:299–316, 2011, 1005.2042.

[135] P. Lacock, A. McKerrell, C. Michael, I. M. Stopher, and P. W. Stephenson. Efficient hadronic operators in lattice gauge theory. *Phys. Rev.*, D51:6403–6410, 1995, hep-lat/9412079.

[136] Philippe Boucaud et al. Dynamical Twisted Mass Fermions with Light Quarks: Simulation and Analysis Details. *Comput.Phys.Commun.*, 179:695–715, 2008, 0803.0224.

[137] K. Jansen and C. Urbach. tmLQCD: A Program suite to simulate Wilson Twisted mass Lattice QCD. *Comput.Phys.Commun.*, 180:2717–2738, 2009, 0905.3331.

[138] M. Foster and C. Michael. Quark mass dependence of hadron masses from lattice QCD. *Phys. Rev.*, D59:074503, 1999, hep-lat/9810021.

[139] C. McNeile and C. Michael. Decay width of light quark hybrid meson from the lattice. *Phys. Rev.*, D73:074506, 2006, hep-lat/0603007.

[140] K. Jansen, Christopher Michael, and C. Urbach. The eta-prime meson from lattice QCD. *Eur.Phys.J.*, C58:261–269, 2008, 0804.3871.

[141] Craig McNeile and Chris Michael. Mixing of scalar glueballs and flavour-singlet scalar mesons. *Phys. Rev.*, D63:114503, 2001, hep-lat/0010019.

[142] Christopher Michael and I. Teasdale. EXTRACTING GLUEBALL MASSES FROM LATTICE QCD. *Nucl.Phys.*, B215:433, 1983.

[143] M. Lüscher and U. Wolff. HOW TO CALCULATE THE ELASTIC SCATTERING MATRIX IN TWO-DIMENSIONAL QUANTUM FIELD THEORIES BY NUMERICAL SIMULATION. *Nucl.Phys.*, B339:222–252, 1990.

[144] Benoit Blossier, Michele Della Morte, Georg von Hippel, Tereza Mendes, and Rainer Sommer. On the generalized eigenvalue method for energies and matrix elements in lattice field theory. *JHEP*, 0904:094, 2009, 0902.1265.

[145] A. Skouroupathis and H. Panagopoulos. Two-loop renormalization of scalar and pseudoscalar fermion bilinears on the lattice. *Phys.Rev.*, D76:094514, 2007, 0707.2906.

[146] R. Sommer. A New way to set the energy scale in lattice gauge theories and its applications to the static force and alpha-s in SU(2) Yang-Mills theory. *Nucl.Phys.*, B411:839–854, 1994, hep-lat/9310022.

[147] J. Gasser and H. Leutwyler. Light quarks at low temperatures. *Phys. Lett.*, B184:83, 1987.

[148] Gilberto Colangelo, Stephan Dürr, and Christoph Haefeli. Finite volume effects for meson masses and decay constants. *Nucl. Phys.*, B721:136–174, 2005, hep-lat/0503014.

[149] N. Madras and A. D. Sokal. The pivot algorithm: a highly efficient monte carlo method for selfavoiding walk. *J. Statist. Phys.*, 50:109–186, 1988.

[150] U. Wolff. Monte carlo errors with less errors. *Comput. Phys. Commun.*, 156:143–153, 2004, hep-lat/0306017.

[151] R. Baron et al. Light hadrons from Nf=2+1+1 dynamical twisted mass fermions. *PoS*, LATTICE2010:123, 2010, 1101.0518.

[152] Gilberto Colangelo, Stephan Durr, Andreas Juttner, Laurent Lellouch, Heinrich Leutwyler, et al. Review of lattice results concerning low energy particle physics. *Eur.Phys.J.*, C71:1695, 2011, 1011.4408.

[153] B. Blossier et al. Renormalisation constants of quark bilinears in lattice QCD with four dynamical Wilson quarks. 2011, 1112.1540.

[154] C. Urbach, K. Jansen, A. Shindler, and U. Wenger. HMC algorithm with multiple time scale integration and mass preconditioning. *Comput.Phys.Commun.*, 174:87–98, 2006, hep-lat/0506011.

[155] H. Neff, N. Eicker, T. Lippert, John W. Negele, and K. Schilling. On the low fermionic eigenmode dominance in QCD on the lattice. *Phys.Rev.*, D64:114509, 2001, hep-lat/0106016.

[156] T. Kaneko et al. Flavor-singlet mesons in N(f) = 2+1 QCD with dynamical overlap quarks. *PoS*, LAT2009:107, 2009, 0910.4648.

[157] Jozef J. Dudek, Robert G. Edwards, Peng Guo, and Christopher E. Thomas. Toward the excited isoscalar meson spectrum from lattice QCD. 2013, 1309.2608.

[158] C. McNeile and Christopher Michael. The eta and eta-prime mesons in QCD. *Phys.Lett.*, B491:123–129, 2000, hep-lat/0006020.

[159] Camilla Di Donato, Giulia Ricciardi, and Ikaros Bigi. $\eta - \eta'$ Mixing - From electromagnetic transitions to weak decays of charm and beauty hadrons. *Phys.Rev.*, D85:013016, 2012, 1105.3557.

[160] Colin Morningstar and Mike J. Peardon. Analytic smearing of SU(3) link variables in lattice QCD. *Phys. Rev.*, D69:054501, 2004, hep-lat/0311018.

[161] Krzysztof Cichy, Gregorio Herdoiza, and Karl Jansen. Continuum Limit of Overlap Valence Quarks on a Twisted Mass Sea. *Nucl.Phys.*, B847:179–196, 2011, 1012.4412.

[162] K. Jansen et al. Flavour breaking effects of Wilson twisted mass fermions. *Phys. Lett.*, B624:334–341, 2005, hep-lat/0507032.

[163] P. Dimopoulos, H. Simma, and A. Vladikas. Quenched B(K)-parameter from Osterwalder-Seiler tmQCD quarks and mass-splitting discretization effects. *JHEP*, 0907:007, 2009, 0902.1074.

[164] Colin Morningstar, John Bulava, Justin Foley, Keisuke J. Juge, David Lenkner, et al. Improved stochastic estimation of quark propagation with Laplacian Heaviside smearing in lattice QCD. *Phys.Rev.*, D83:114505, 2011, 1104.3870.

[165] Konstantin Ottnad, Carsten Urbach, and Falk Zimmermann. Investigating a mixed action approach for $\eta$ and $\eta'$ mesons in Nf=2+1+1 lattice QCD. 2013, 1311.7015.

[166] T. P. Cheng and L. F. Li. *Gauge Theory of Elementary Particle Physics*. Oxford Science Publications, 1984.

[167] J.F. Donoghue, E. Golowich, and Barry R. Holstein. Dynamics of the standard model. *Camb.Monogr.Part.Phys.Nucl.Phys.Cosmol.*, 2:1–540, 1992.

[168] M. Galassi et al. *GNU Scientific Library Reference Manual (3rd Ed.)*.

[169] R Development Core Team. *R: A language and environment for statistical computing*. R Foundation for Statistical Computing, Vienna, Austria, 2005. ISBN 3-900051-07-0.